UNDERSTANDING MODERN AND ANCIENT HYDROGEOLOGIC FEATURES: SPRINGS IN THE NGORONGORO VOLCANIC HIGHLAND AND GLOBAL WETLAND FACIES

By

MONICA KELLY NORTON

A thesis to be submitted to the

School of Graduate Studies

Rutgers, The State University of New Jersey

In partial fulfillment of the requirements

For the degree of

Master of Science

Graduate Program in Geological Sciences

Written under the direction of

Dr. Gail M. Ashley

And approved by

_____

_____

_____

New Brunswick, New Jersey

October, 2019

ABSTRACT OF THE THESIS

Understanding Modern and Ancient Hydrogeologic Features:
Springs in the Ngorongoro Volcanic Highland and
Global Wetland Facies

By MONICA KELLY NORTON

Thesis Director:

Dr. Gail M. Ashley

Groundwater is an important component of the hydrologic cycle and a crucial resource of fresh water for people and animals, as well as crop irrigation. In the subsurface, groundwater is protected from evaporation and climate fluctuations, thereby ensuring persistence and longevity. Surface expression of groundwater discharge (e.g., seeps, spring, and wetlands) supports plants and animals creating ecological niches that leave permanent sedimentary records that vary with biome. Springs and wetlands form under a variety of physical, chemical, and biological conditions. These complexities make understanding how modern systems form as well as interpreting ancient systems in the geologic record a challenge.

Precipitation on the Ngorongoro Volcanic Highland (NVH), a ~3000 m high massif of volcanoes situated at the southern bifurcation of the Gregory Rift (the eastern branch of the East African Rift System), provides the water source for several springs surrounding the NVH. Despite the heavy reliance on these springs as a source of year-round fresh drinking water for the many people and animals residing in this region, there have been

virtually no studies on the sustainability or longevity of these springs. Insufficient data make groundwater modeling in the region problematic. Therefore, as a step toward generating accurate quantitative groundwater models in this region, a reconnaissance-level, qualitative study was undertaken in Chapter One in which the physical framework of the groundwater basin as well as hydrologic inputs were described by examining nine springs and regional rainfall data. Field and laboratory methods (i.e., site observations of springs, water sample analysis, river flow rate analysis, regional rainfall analysis, and geologic cross-section generation) were used to quantify temporal and spatial rainfall patterns for the study area as well as to generate schematic conceptual models typifying regional modes of spring formation. An analysis of the rainfall data shows that two monsoon-driven wet seasons (October-November "short rains" and March-May "long rains") occur on a yearly basis; peaks in rainfall occur nearly every 5 years and can be partially explained by El Niño and Indian Ocean Dipole events, but other oceanographic factors yet to be determined may also play a role in the interannual variability in rainfall; and the orography of the study area highly impacts the spatial distribution of rainfall (more rain on the NVH than the neighboring plains and rift valley below). Extreme episodic rainfall events, such as the biannual monsoons and interannual years of abundant rainfall seen at the study region, are known to be important for recharging aquifers.

Based on geological, geomorphological, hydrological, and geochemical data collected, three schematic conceptual models were developed to capture modes of spring formation for the study region: (1) Groundwater intersects the surface at local base level;

(2) Permeable rock (aquifer) intersects surface along slope; and (3) Artesian flow under hydraulic head. These spring settings provide the physical framework for understanding the mechanisms of groundwater supply in the region and a model for what may be occurring in similar rift valley regions.

Currently, there is no consensus on a facies model for paleowetlands. Wetlands have yet to be included as depositional environments in classic facies model textbooks. The hypothesis that wetlands have distinct facies in the geologic record and that their facies can be even further distinguished by the mean annual precipitation (MAP) and mean annual temperature (MAT) of their environment is tested in Chapter Two. Modern wetland deposits in the literature from each of the terrestrial biomes of the world, representing varying levels of MAT and MAP, were explored to determine if distinguishing characteristics found in the geologic record set deposits from these biomes apart. While this study determines that there are distinct similarities among wetland deposits across the world, a novel facies model that categorizes wetland deposits into three types by climate (i.e., Tundra/Taiga, Desert, and Grassland/Forest Wetlands) is proposed herein. An improved understanding and identification of the records left by wetlands is crucial for anticipating the future of these diverse yet fragile environments.

ACKNOWLEDGEMENTS

First, I will take this opportunity to thank Dr. Gail Ashley not only for her endless guidance and wisdom, but also for inspiring me throughout my time knowing her. I am quite lucky to be her last (39th!!) thesis mentee! I also thank my committee members, Dr. Ying Fan Reinfelder and Dr. Christopher Lepre for their support, inspiration, and guidance throughout my time in graduate school.

Special thanks to Dr. Jeremy Delaney for his knowledge and assistance (and quick wit!) both in the field and out. Thank you to Dr. Martha Withjack for her help with my cross-sections and for letting me borrow her protractor for an extended period; to Dr. Linda Godfrey and Dr. James Wright for sharing their isotope geochemistry wisdom with me; to Dr. Myla Aronson for guiding me in the unfamiliar territory of wetland ecology and providing a unique perspective; and to Dr. Karen Bemis for sharing her knowledge on the Ngorongoro Volcanic Highlands and for the insightful discussions.

Thanks are due to Dr. Yair Rosenthal, Dr. Robert Sherrell, and Kaixuan "Ryan" Bu of the Rutgers Inorganic Analytical Laboratory for running the major cation analyses; to Dr. Nathan Lee and Yuwei "Cindy" Wang of the Rutgers Department of Environmental Sciences Laboratory for running the major anion analyses; and to Dr. Emily Beverly, Dr. Naomi Levin, and Phoebe Aron for running the stable isotope analyses at the University of Michigan Department of Earth and Environmental Sciences (Ann Arbor) Laboratory.

Thank you to the folks at the Ngorongoro Conservation Area Authority including Joshua Mwankunda, Andrew Lowassa, Hillary Mushi, Saningo Kimirei, and Zainabu Suleiman. Thanks to all of you for taking the time to meet and provide necessary

information to conduct research. Additionally, thanks are due to the Tanzanian locals including and others who aided in the data collection: Joseph Masoy for guiding us throughout the country and helping us reach our research objectives; Isaiah OleMoita for being our local guide and helping us find springs ("chemchem"); Father Albano, our gracious host at the Catholic Mission and knowledge-source for the town of Endulen; Chris and Nani Schmeling for providing the impressive self-collected Kisima Ngeda rainfall records; Magreth Kaisoe for leading us to the Garusi River DIVER by memory and inviting us over for some delicious "Nyama Choma". Also thanks to Charles Musiba; Godfrey OleMoita; John Ombeni Mdee; Simon Matero (now deceased); and Doris Barboni. Asante sana to you all.

Much thanks to Dr. Mark Cuthbert of the Cardiff University for the very important and insightful discussions which helped shape and guide much of my research as well as to his student, Jessica Macha, for sharing research on rainfall patterns at the Ngorongoro region.

Special thanks to the Coastal Climate Risk and Resilience (C2R2) program, particularly the program leaders (Dr. Carrie Ferraro, Dr. Robert Kopp, and Dr. Rebecca Jordan), for encouraging me to expand my graduate education across disciplines. I am also extremely appreciative of the other fellow graduate students in the C2R2 program who broadened my perspective and provided support and encouragement throughout our time together at Rutgers.

I acknowledge the Rutgers Graduate School for the Off-Campus Dissertation Development Award which enabled me to conduct field work in Tanzania, Africa. I also

acknowledge the Kenneth N. Weaver Student Travel Award Program from the Northeastern Section of the Geological Society of America (GSA) for granting the necessary funds to travel and share my research at the 2018 GSA Meeting in Indianapolis. I also thank the Earth and Planetary Sciences Department for providing funds to travel to and share my research at the 2018 American Geophysical Union Meeting in Washington D.C. Additionally, I acknowledge National Science Foundation Award (SGP ACACIA 1349651) to G.M. Ashley and J.S. Delaney which enabled the field work in Tanzania.

Thank you to all the professors and graduate students from the Earth and Planetary Sciences Department. Everyone I met in the department has taught me something new and helped shaped my character. My fellow graduate students have provided support, encouragement, and of course, laughter, throughout all the trials and tribulations we experienced as graduate students.

Last, but certainly not least, a million thanks to my friends and, of course, my family. Thank you for providing infinite love and support throughout my entire time in graduate school. Your patience is much appreciated as I know it has often been tested. You are all the rock behind this geologist.

I am so very grateful for all of you.

TABLE OF CONTENTS

LIST OF FIGURES

CHAPTER ONE

CHAPTER TWO

LIST OF TABLES

CHAPTER ONE

CHAPTER TWO

LIST OF APPENDICES

CHAPTER ONE

CHAPTER TWO

THESIS INTRODUCTION

Springs and wetlands are hydrogeological features that are found world-wide. They exist at the surface of the Earth where they can be easily seen, yet the processes involved in forming them often occur below the surface, hidden from view. They provide a plethora of services to society and the environment including providing a source of fresh drinking water, improving water quality, attenuating flood waters, serving as refugia for biodiversity, creating recreation space, regulating carbon and nutrient cycling, and many more (LePage et al., 2012). Not only are they important at present, but they have also proven to be paramount to human survival throughout history (Ashley et al., 2009) and will continue to be valued through time. However, these systems have notoriously been difficult to understand and interpret. Springs and wetlands exist at the interface of a variety of physical, chemical, and biological processes which makes understanding modern systems and identifying ancient systems in the geologic record difficult (Tooth and McCarthy, 2007). The two chapters of this thesis aim to shrink this knowledge gap by examining modern springs on a small scale (Chapter One) and creating a facies model for modern and ancient wetlands at a global scale (Chapter Two).

Chapter One focuses on the formation of modern springs in the Ngorongoro Volcanic Highland (NVH) region in northern Tanzania. Such springs provide a year-round supply of drinkable water to local people, animals, and tourists in an otherwise arid environment. Yet, the nature of the groundwater system supplying these springs as well as the spatiotemporal availability of water in the region is not well known. There are many reasons why these systems are poorly understood including: a lack of geological

(borehole) data for the region; poor record-keeping and archiving of precipitation data and well-pumping records; a paucity of infiltration parameters/groundwater recharge data; and a lack of publicly accessible data on local or regional aquifers. Without these data, the physical framework and the hydrological inputs of the groundwater system (two categories of data that are essential for making meaningful numerical groundwater models) cannot be accurately described (Kumar, 2015). Groundwater models are only as good as the data put into them. Therefore, as a step toward generating accurate quantitative groundwater models in this region, Chapter One undertakes a qualitative study to describe the physical framework and hydrological inputs of the groundwater system. The following data collected/generated for this study include: observations from nine springs visited in Summer 2018; water samples from each spring analyzed for water quality, major cations/anions, and stable isotopes; Garusi River flow rate; longitudinal profiles and geologic cross-sections connecting the recharge area to discharge area for each spring; and schematic conceptual models of geologic contexts of the springs.

In Chapter Two, the research focuses on wetland deposits in the geologic record on a global scale. Despite the fact that wetlands provide numerous ecosystem services and are studied by many scientists, little is known about them from a geological perspective (Tooth and McCarthy, 2007). Wetland deposits (facies) offer clues to better understand wetlands as depositional environments by providing an account of what is preserved in the geologic record. Such inferences are important to properly identify paleowetlands in sedimentary deposits which can be used to interpret the past environment, as well as to constrain models which predict how wetlands may change in

the future (LePage et al., 2012). However, there is currently no consensus among geologists as to what features from the geologic record are characteristic of paleowetlands (i.e., a facies model for wetlands). In fact, classic facies model textbooks have yet to include wetlands as an environment of deposition (e.g., Walker, 1984; James and Dalrymple, 2010). Chapter Two makes an attempt at characterizing wetland deposits in the lithologic record, determining if a unique set of characteristics can be attributed to wetland deposits (distinguishing them from all other depositional environments). Wetlands deposits from different terrestrial biomes of the world are also compared to one another to see if they can be even further distinguished by basic parameters of climate (mean annual temperature and precipitation). These objectives are addressed by gathering data from published documents of modern and ancient wetland deposits across the world.

REFERENCES FOR THESIS INTRODUCTION

Ashley, G.M., Tactikos, J.C., and Owen, R.B., 2009, Hominin use of springs and wetlands: paleoclimate and archaeological records from Olduvai Gorge (~1.79-1.74 Ma): Palaeogeography, Palaeoclimatology, Palaeoecology, v. 272, p. 1–16, doi:10.1016/j.palaeo.2008.10.016.

James, N.P., and Dalrymple, R.W., 2010, Facies models 4: Geological Association of Canada, 3–18 p.

Kumar, C.P., 2015, Modelling of groundwater flow and data requirements: International Journal of Modern Sciences and Engineering Technology, v. 2, p. 18–27.

LePage, B.A., Jacobs, B.F., and Williams, C.J., 2012, Insights from paleohistory illuminate future climate change effects on wetlands, *in* Global Change and the Function and Distribution of Wetlands, p. 1–151, doi:10.1007/978-94-007-4494-3.

Tooth, S., and McCarthy, T.S., 2007, Wetlands in drylands: geomorphological and sedimentological characteristics, with emphasis on examples from southern Africa: Progress in Physical Geography, v. 31, p. 3–41, doi:10.1177/0309133307073879.

Walker, R.G., 1984, Facies Models: St. Johns, Geological Association of Canada, Business and Economic Service, 317 p.

CHAPTER ONE

A HYDROGEOLOGIC FRAMEWORK FOR SPRING FORMATION IN THE NGORONGORO VOLCANIC HIGHLAND REGION

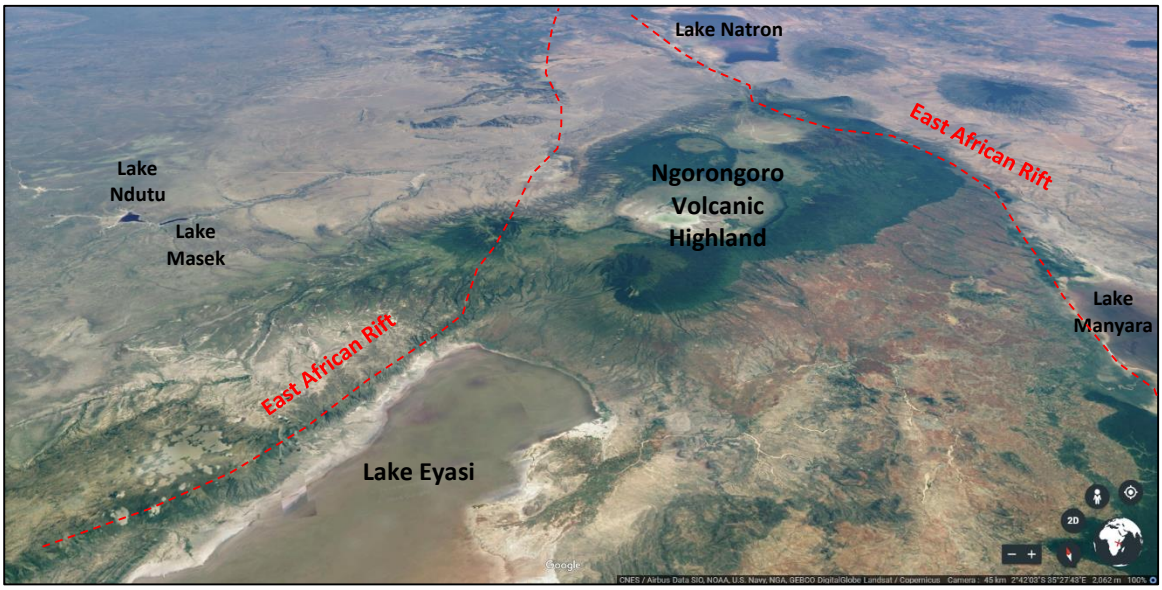

Figure 0. 3-Dimensional image of Study Area (GoogleMaps© Landsat/Copernicus).

ABSTRACT

Rainfall on the Plio-Pleistocene volcanoes of the Ngorongoro Volcanic Highland (NVH) in northern Tanzania provides the source of groundwater for the Ngorongoro Conservation Area (NCA), a national park that includes two designated Natural Heritage sites: Olduvai Gorge and Laetoli Footprint Site. The ~3300 m high NVH captures moisture from semi-annual monsoonal rains (~915 mm/yr) from the southeast trade winds casting a dramatic rain shadow on the Serengeti Plain to the west and rift lowlands below. With evaporation (~2500 mm/yr) exceeding annual rainfall, the hydrologic budget is moisture-limited and surface runoff is seasonal. Groundwater is shielded from evaporation and discharges into topographic lows or fault conduits to the surface. The water supply is buffered from seasonal variability in rainfall. Regional groundwater systems are critical to the local people, animals, and tourists and the demand for fresh water from springs and wells is growing exponentially. However, there are virtually no hydrogeological studies that examine the sustainability or longevity of these spring systems. Insufficient data make groundwater modeling in the region problematic since groundwater models are only as good as the data used to constrain them.

Therefore, as a step toward generating quantitative groundwater models in this region, a qualitative, reconnaissance-level study was undertaken in which the physical framework and hydrological inputs of the groundwater system were described by examining nine springs and regional rainfall data. Field and laboratory methods were used to generate the following data: site descriptions; water sampling and analysis for water quality, major anion/cations, and stable isotopes; precipitation data and analysis; river

flow rate data and analysis; longitudinal profiles and geologic cross-sections extending from each spring recharge to discharge area; and schematic conceptual models of springs in geologic contexts. Moreover, a novel method was introduced for measuring relative stream stage.

Distinct temporal and spatial rainfall patterns were determined for the study region which shed critical light on generating groundwater recharge estimates. On a yearly basis, there are two wet seasons (October-November “short rains” and March-May “long rains”); On an interannual basis, peak rainfall years occur nearly every 5 years and can be partially explained by El Niño and Indian Ocean Dipole events, but other oceanographic factors yet to be determined may also play a role in the interannual variability in rainfall; and the orography of the study area highly impacts the spatial distribution of rainfall creating a distinct rain shadow from east to west. Extreme episodic rainfall events, such as the biannual monsoons and interannual years of abundant rainfall seen at the study region, are known to be important for recharging aquifers.

Based on geological, geomorphological, hydrological, and geochemical data collected, three schematic conceptual models were developed to determine modes of spring formation in this mountainous terrane: (1) Groundwater intersects the surface at local base level; (2) Permeable rock (aquifer) intersects surface along slope; and (3) Artesian flow under hydraulic head. Additionally, of the volcanic units which comprise the study region, unfractured basalt units appear to have lower permeabilities than tuff units based on the field-based observation of the regular occurrence of groundwater seeps and springs in associated tuffs. Therefore, the tuff layers are interpreted to be the primary

local aquifers. These spring settings provide the framework for understanding the mechanisms of groundwater supply in the region and a model for what may be occurring in rift valley settings elsewhere.

While groundwater modeling was beyond the scope of this study, it is the goal to provide as much of a geologic and hydrologic framework as possible in a region where information is sparse to nonexistent to lead to a more quantitative understanding of the hydrogeology of the region. Such an understanding is crucial, especially as the global environment changes and impacts these groundwater systems which will in turn impact the lives of so many people and animals that depend on them.

INTRODUCTION

Hundreds of active springs have been observed to occur within the East African Rift System (EARS) (Cuthbert et al., 2017) (**Figure 1A**). Such springs provide fresh and potable water year-round to a countless number of people and animals in places where surface water is otherwise only available seasonally. Yet, the nature of these groundwater systems and the spatiotemporal availability of water in East Africa are poorly understood.

One such example within the EARS where numerous springs exist and are heavily relied on by people and animals is the area near the Ngorongoro Volcanic Highland (NVH) in northern Tanzania. The NVH is a complex of volcanoes situated at the southern bifurcation of the Gregory Rift (the eastern branch of the EARS) (**Figure 1**). The NVH is a topographically high area that towers ~2000 m over plains to the west and ~3300 m over the rift valley below (Hay, 1976; Mollel and Swisher, 2012; Mana et al., 2014). To the west of the NVH, numerous springs persist year-round despite the fact that the environment there is moisture-limited. This study focuses on the groundwater system and rainfall patterns of this region including the southern portion of the NVH and the lowlands to the south and west of this area where springs occur (**Figure 1B**).

The majority of the study area is within the bounds of the Ngorongoro Conservation Area (NCA) (**Figure 1B**). The NCA is a UNESCO-designated World Heritage Site and Cultural World Heritage Site located in northern Tanzania (Ikanda and Packer, 2008; Melita and Mendlinger, 2013). The 8292 km^2 NCA contains two designated National Heritage archaeological sites (i.e., Olduvai Gorge and Laetoli Footprint Site) as well as the 250 km^2 Ngorongoro Crater, a volcanic caldera designated a core wildlife reserve (Ikanda

and Packer, 2008; Mollel and Swisher, 2012). The NCA is home to ~70,000 Maasai people (Melita and Mendlinger, 2013), a few million animals (Akyoo and Nkwame; Melita and Mendlinger, 2013; Kisoki, 2018), and is visited by over 600,000 tourists annually (Qorro, 2018).

The NCA receives on average ~915 mm of rainfall a year (Tanania Meteorological Agency, 2019), which is exceeded by the yearly evaporation of ~2500 mm (Renaut et al., 2017), making the region a moisture-limited environment with only seasonal surface runoff. All of the people and animals of the NCA, therefore, must turn to the groundwater as a source of fresh, potable water in order to live.

The NVH is presumed to significantly impact the rainfall distribution and the recharge of groundwater for the region. Large-scale shifts in wind direction caused by the twice-a-year migration of the Intertropical Convergence Zone (ITCZ) drives the East African Monsoon system which delivers semi-annual rains to the study region (Camberlin, 2018). During the monsoon-driven wet seasons, moisture from the Indian Ocean (~500 km away) is carried by southeast trade winds to the NVH. As air rises over the highland, moisture condenses and precipitates out as rainfall, casting a dramatic rain shadow on the plains and rift lowlands below. The rain that infiltrates the NVH recharges the groundwater and is shielded from evaporation. The groundwater discharges into topographic lows or fault conduits to the surface and is thus buffered from seasonal variability in rainfall (**Figure 1B**). While this process is assumed for the region, it has yet to be clearly supported by data (Wolanski and Gereta, 2001; Olago et al., 2009).

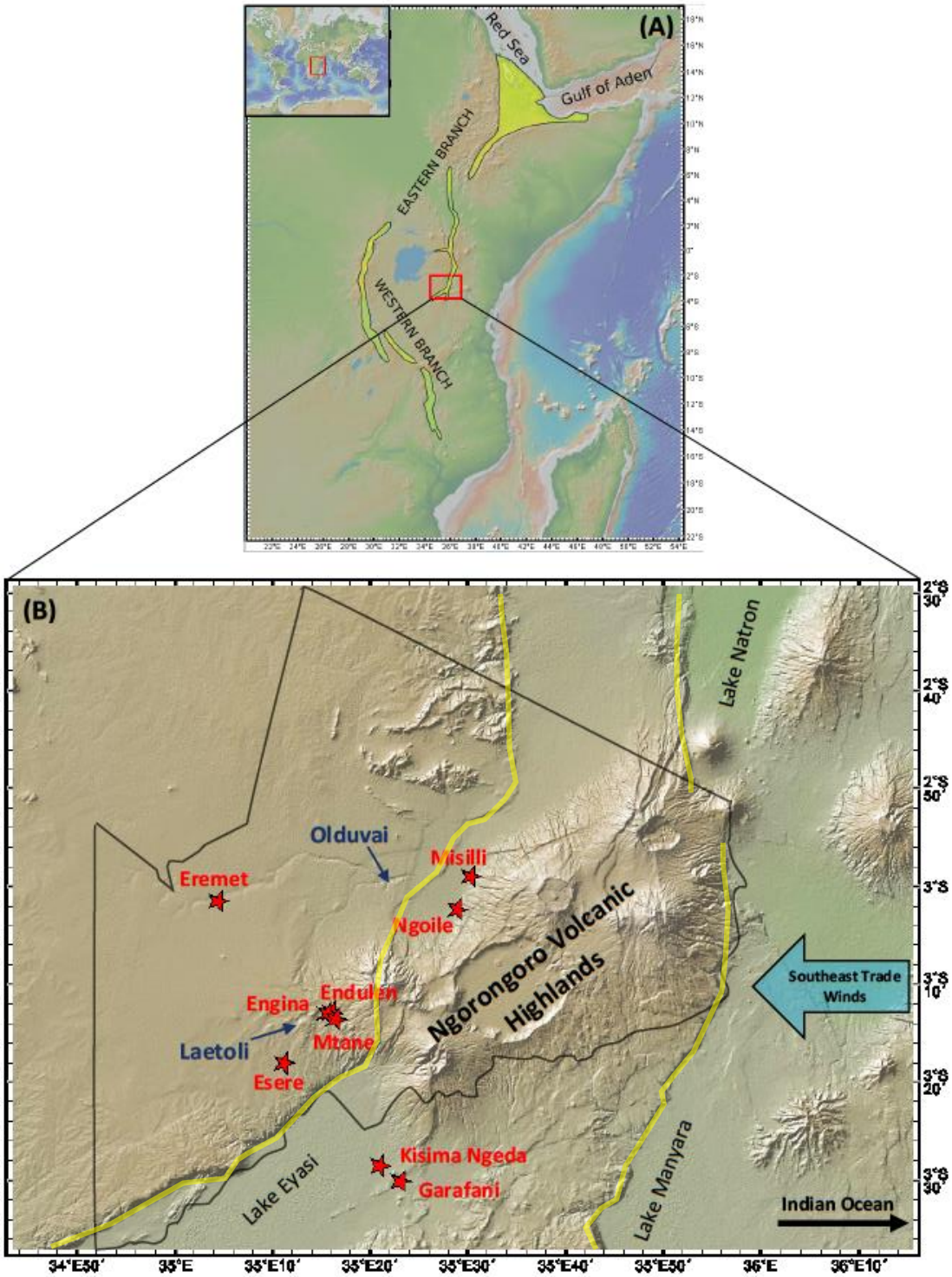

Figure 1. Study Area Context. **(A)** The East African Rift System (EARS) located in eastern Africa. Rift valleys are highlighted in yellow. The study area is boxed in red. **(B)** Map of the study area. The EARS bifurcates into two separate rifts (traced in yellow) around the Ngorongoro Volcanic Highland (NVH). The Ngorongoro Conservation Area (NCA) is outlined in black. Red stars indicate locations of the springs studied. The two National Heritage Archaeological Sites are depicted in blue. Southeast trade winds carry moisture from the Indian Ocean and from local lakes to the NVH, supplying water for the springs. Base map from Ryan et al. (2009; http://www.geomapapp.org).

Groundwater in the study area is accessed naturally via groundwater discharge areas (i.e., spring, wetlands, rivers) or is pumped from the ground via wells with impunity (Kashaigili, 2010; NCAA, 2016). Not only do groundwater discharge areas of the study area play an important role in the survival of people, flora, and fauna today, but they also play an important role during periods of extended drought.

Despite the importance of this groundwater supply to people and animals (domestic and wild), little research has been done to quantify and determine how sustainable these systems are. Insufficient data make groundwater modeling in the region problematic as groundwater models are only as good as the data used to constrain them. Therefore, as a step toward generating accurate quantitative groundwater models in this region, a qualitative, reconnaissance-level study is undertaken in which the physical framework and hydrological inputs of the groundwater system (two categories of data that are essential in making meaningful groundwater models) are described (Kumar, 2015). It is noted that groundwater modeling is beyond the scope of this thesis.

The objectives of this study are to: (1) contribute to understanding the physical framework of the groundwater basin by generating schematic conceptual models of spring formation for nine springs visited; and (2) contribute to understanding the hydrological inputs of the system by examining spatial and temporal rainfall patterns across the study region. These contributions will provide the necessary framework for future hydrogeological studies and groundwater modeling.

BACKGROUND

Geology

The East African Rift System

The EARS is one of the few active intracontinental rift systems that exists on Earth today. The EARS extends roughly 4000 km north-south in East Africa, from the Red Sea and Gulf of Aden in the north (Triple Afar Junction) to the Zambezi River and Mozambique in the south (**Figure 1A**). The EARS represents the boundary where the African Plate is separating into two new tectonic plates, the Somali Plate (to the west of the rift) and the Nubian Plate (to the east of the rift). It is the consensus that faulting along the EARS began in the Oligocene as hot rising asthenosphere material uplifted the lithosphere sourced from mantle plumes. This resulted in a thinning of the lithosphere and various phases of volcanism along the rift. Fault-related volcanism along the rift ranges from below sea level vents in the Danakil Depression of Ethiopia to the 6000 m high Kilimanjaro mountain in northern Tanzania (Ebinger et al., 1997; Foster et al., 1997; Le Gall et al., 2008; Mollel et al., 2008; Mollel and Swisher, 2012; Mana et al., 2014; Macgregor, 2015; Scoon, 2018).

The Ngorongoro Volcanic Highlands

There are two branches of the EARS: the Eastern Branch (known as the Gregory Rift) and the Western Branch (**Figure 1A**). The NVH is located at the southern bifurcation of the Gregory Rift (**Figures 1A and 2**). The NVH is composed of several mainly basaltic shield volcanoes characterized by a widening of the EARS at about 3 degrees South. At least eight main extinct volcanoes or vents make up the NVH (i.e., Lemagurut, Satiman,

Oldeani, Ngorongoro, Olmoti, Loolmalasin, Embagai, and Kerimasi) and one active volcano (i.e., Oldoinyo Lengai).

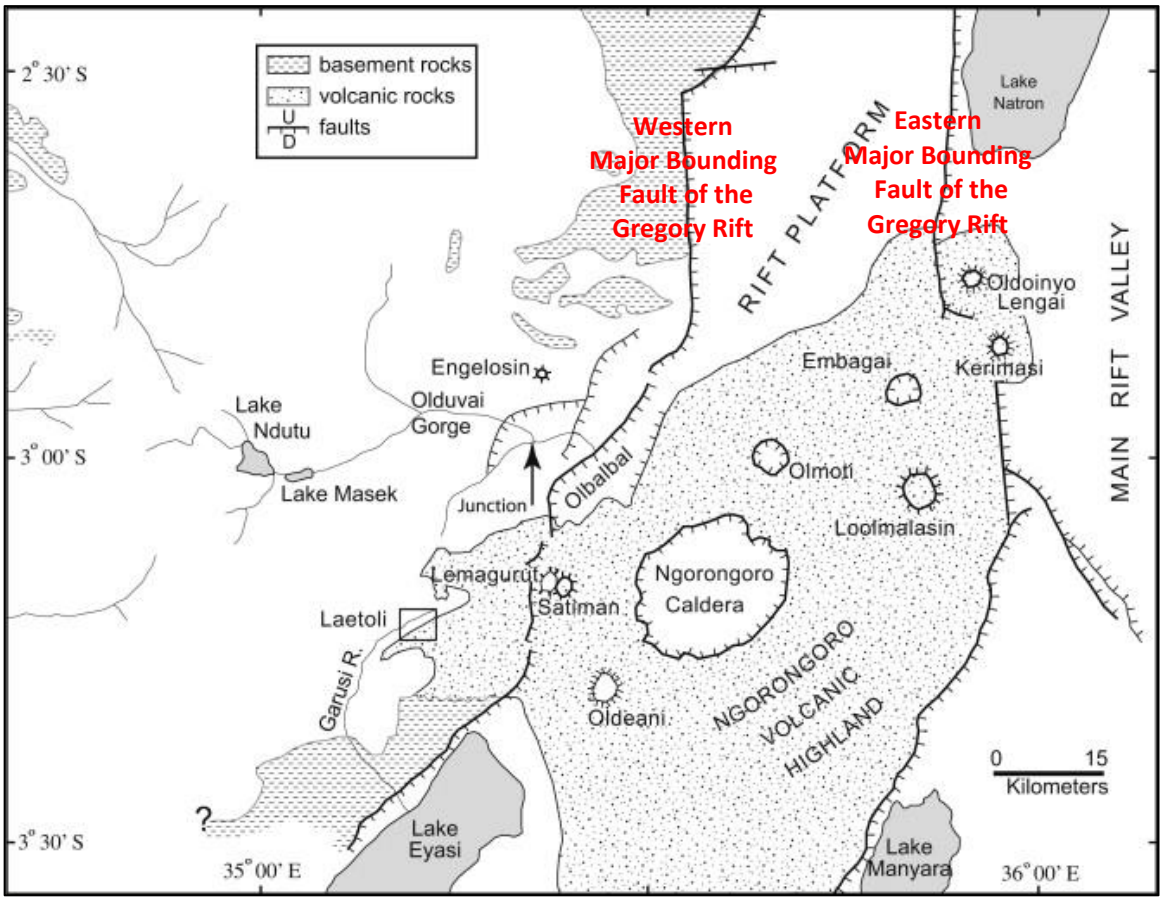

Figure 2. The volcanoes which comprise the Ngorongoro Volcanic Highland (NVH). Modified from Hay (1976).

The volcanoes of the NVH are composed of various igneous compositions ranging from basalts to rhyolite, silica-undersaturated lavas, and carbonatites (**Figure 3** and **Table 1**), and range in age from late Miocene to present (**Table 1**). The NVH spans about 80 km from the southernmost Oldeani volcano to the active Oldoinyo Lengai in the north (Ebinger et al., 1997; Foster et al., 1997; Le Gall et al., 2008; Mollel et al., 2008; Mollel and Swisher, 2012; Mana et al., 2014; Macgregor, 2015).

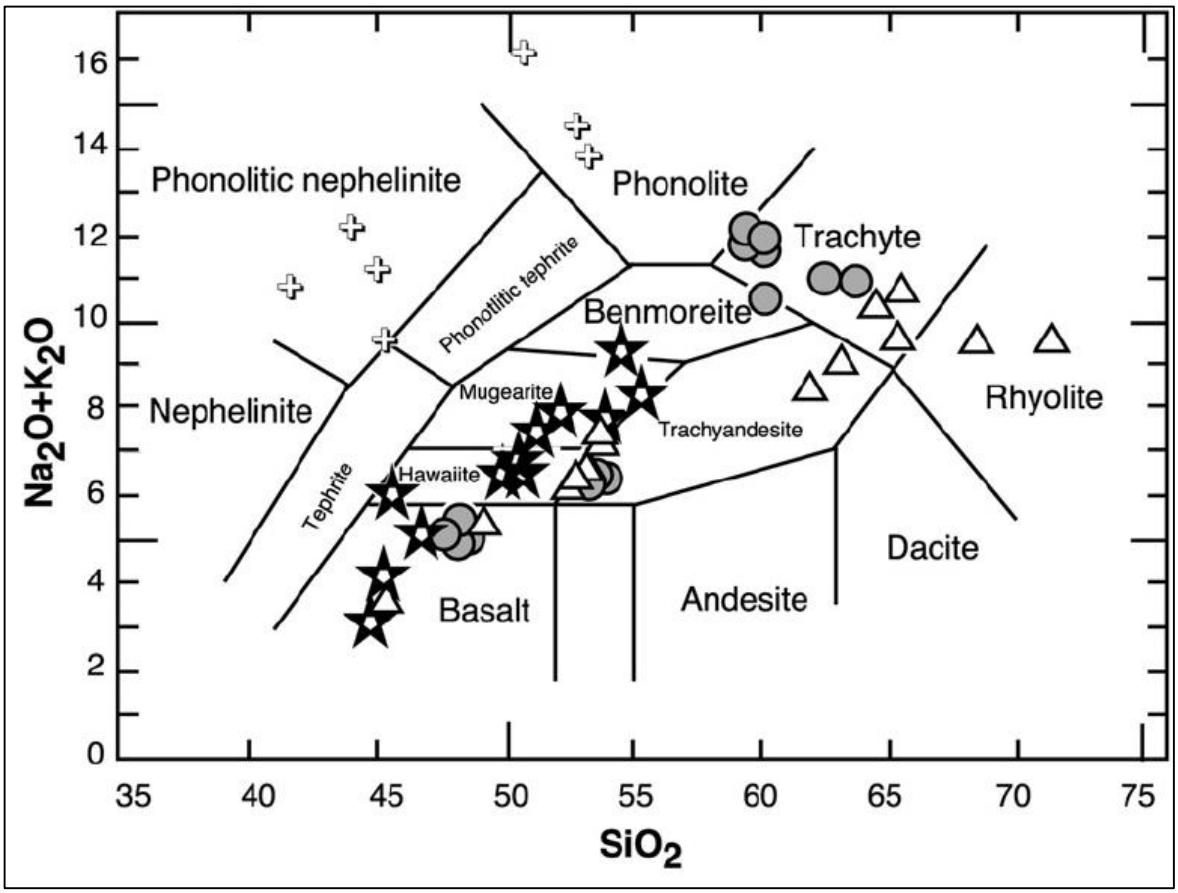

Figure 3. Composition of sampled lavas from the Ngorongoro Volcanic Highland. **Circles**=Olmoti caldera lava; **Triangles**=Ngorongoro caldera lava; **Pluses**=Satiman volcano lava; **Stars**=Lemagurut volcano lava. Data from Mollel and Swisher (2012). Figure 16 from Stollhofen et al. (2008).

In the Plio-Pleistocene volcanism was extensive along the Gregory Rift, with the eruption of alkali basalt-trachyte-phonolite lavas building the Satiman, Lemagurut, Ngorongoro, Olmoti, Embagai, Loolmalasin, Oldeani, Oldonyo Sambu, Terosero, Kitumbeine, Gelai, Meru, and Kilimanjaro mountains. After ~1.2 Ma there was a faulting event associated with another phase of volcanic activity (Mollel and Swisher, 2012). These lavas (forming ultra-basic to ultra-alkaline phonolites and feldspathoidal syenites) were not as large in volume and were more explosive than the previous volcanism and are thought to have built the pyroclastic cones of Meru, Monduli, Oldonyo Lengai, and Kerimasi. At Oldonyo Lengai and Kerimasi, however, carbonatite lavas, nephelinites, and

phonolites have been documented (Dawson, 2008; Mollel et al., 2008; Mollel and Swisher, 2012; Mana et al., 2014).

Table 1. Summary of the type, age, and composition of the main volcanoes comprising the NVH. Ages were determined using either $^{40}Ar/^{39}Ar$ or K-Ar dating (Dawson 2008[a]; Mollel and Swisher 2012[b]).

Volcano Name	Type[a]	~Age[b] (Ma)	Primary Compositions[a,b]
Oldoinyo Lengai	Stratovolcano	150 ka – Present	Carbonatite; Nephelinitic and phonolitic tuffs and agglomerates
Kerimasi	Stratovolcano	1.1	Carbonatite; Nephelinitic pyroclasts, carbonatitic limestone, agglomerate, and agglomeratic tuffs
Embagai	Shield	1.2 – 0.6;	Porphyritic nephelinite, foidite, occasional glassy lava
Loolmalasin	Shield	N/A	Basanite, basalt, trachyte
Oldeani	Shield	1.6 - 1.5	Basalt and trachyandesite
Olmoti	Shield	2.0 – 1.8	Lavas and other pyroclastics ranging from basalt through trachyte
Ngorongoro	Shield	2.3 – 2.2	Lavas range from basalt to rhyolite and includes ignimbrites and agglomerates
Lemagurut	Shield	2.4 – 2.2	Phaneritic basalt through hawaiite, mugearite, and benmorite
Satiman	Stratovolcano	4.6 – 3.5	Porphyritic foidite to phonolite

Study Area

The volcanoes of the NVH associated with the study area include Oldeani, Satiman, Lemagurut, Ngorongoro, and Olmoti (**Figure 1B**). The nine springs examined as a part of this study are believed to be recharged from moisture intercepted by these volcanoes, located in the southern portion of the NVH. All volcanoes are shield volcanoes, except for Satiman which is a stratovolcano (Dawson, 2008). These volcanoes formed during the Plio-Pleistocene, more specifically between 4.6 and 1.5 Ma, and are composed of alkali basalt-trachyte-phonolites (**Table 1**) (Dawson, 2008; Mollel et al., 2008; Mollel and Swisher, 2012; Mana et al., 2014).

Surficial geological information of the study area is obtained via geologic maps (Geological Survey of Tanzania, 1958, 1961, 1964, 1965) which are provided in **Appendix I**. To summarize, a stitching of the geologic maps relevant to the study area is provided below as **Figure 4**. The subsurface geology of the study area cannot be accurately described here because very little geologic borehole records are available; therefore, the geologic description is limited to observations of surficial geology and exposed outcrops. In general, the oldest surficial geologic units are Precambrian-aged bedrock consisting of gneisses, quartzites, schists, granodiorite, granite, and cataclasites which are found at and surrounding the escarpment bordering the west of Lake Eyasi as well as at a number of smaller outcrops exposed among the calcareous tuffs and localized carbonate deposits in the western portion of the study area. Lying above these units are Pleistocene-aged extrusive units consisting of tuffs and basalts which cap the volcano summits. Units associated with Satiman, Ngorongoro, Lemagurut, and Oldeani include basalt, olivine basalts, trachyte, undifferentiated basaltic lavas, tuffs and agglomerates, nephelinites, volcanic conglomerate, and phonolite. At higher elevations, near the volcano summits, are Recent red soils and red brown earthy tuffs. Additionally, alluvium occurs at the base of the mountains at the margin of Lake Eyasi, Lake Olbalbal, and Lake Masek (Geological Survey of Tanzania, 1958, 1961, 1964, 1965).

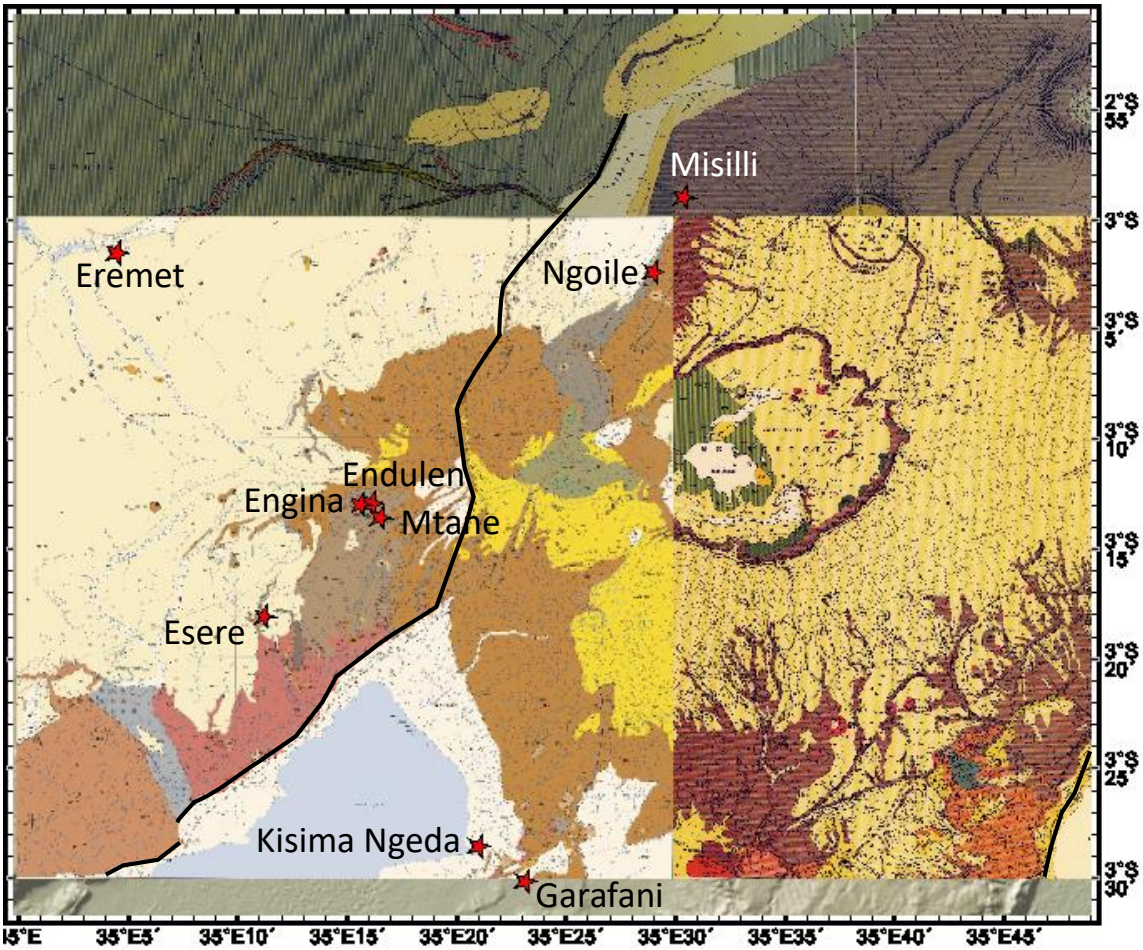

Figure 4. A stitching of four geologic maps that cover the study region. The maps were made at different times, therefore, colors and names of geologic units vary from one map to another. Stars indicate locations of springs studied. Black lines follow approximate location of major bounding fault of the EARS that cuts through the study region. Detailed Quarter-Degree Sheets (Geological Survey of Tanzania, 1958, 1961, 1964, 1965) are provided in **Appendix I**.

Climate

The climate in East Africa is complex in that it is controlled by many factors: from large-scale tropical atmospheric factors such as convergence zones, jet streams, and monsoons to regional terrestrial factors such as topography, lakes, and maritime influence such as sea-surface temperature variability (**Figure 5**). In most of the region, there are two wet seasons which occur when the East African Monsoon brings moisture from the Indian Ocean to the East African region. The shifts in wind direction that result

in the semi-annual rains of the East African Monsoon are caused by the twice-a-year migration of the ITCZ (Camberlin, 2018). Variability in wet seasons is evidenced to be strongly linked to El Niño-Southern Oscillation (ENSO) events, where years with more rainfall are associated with ENSO years (Indeje et al., 2000; Nicholson, 2017). Additionally, on multidecadal timescales, the Indian Ocean Dipole (IOD) (Kijazi and Reason, 2009; Tierney et al., 2013) as well as the North Atlantic Oscillation (NAO) (Lechleitner et al., 2017) have been shown to enhance East African rainfall variability. Furthermore, the complex interactions between ENSO and IOD can result in intense rainfall events which have been shown to drive groundwater recharge in the region (Taylor et al., 2012).

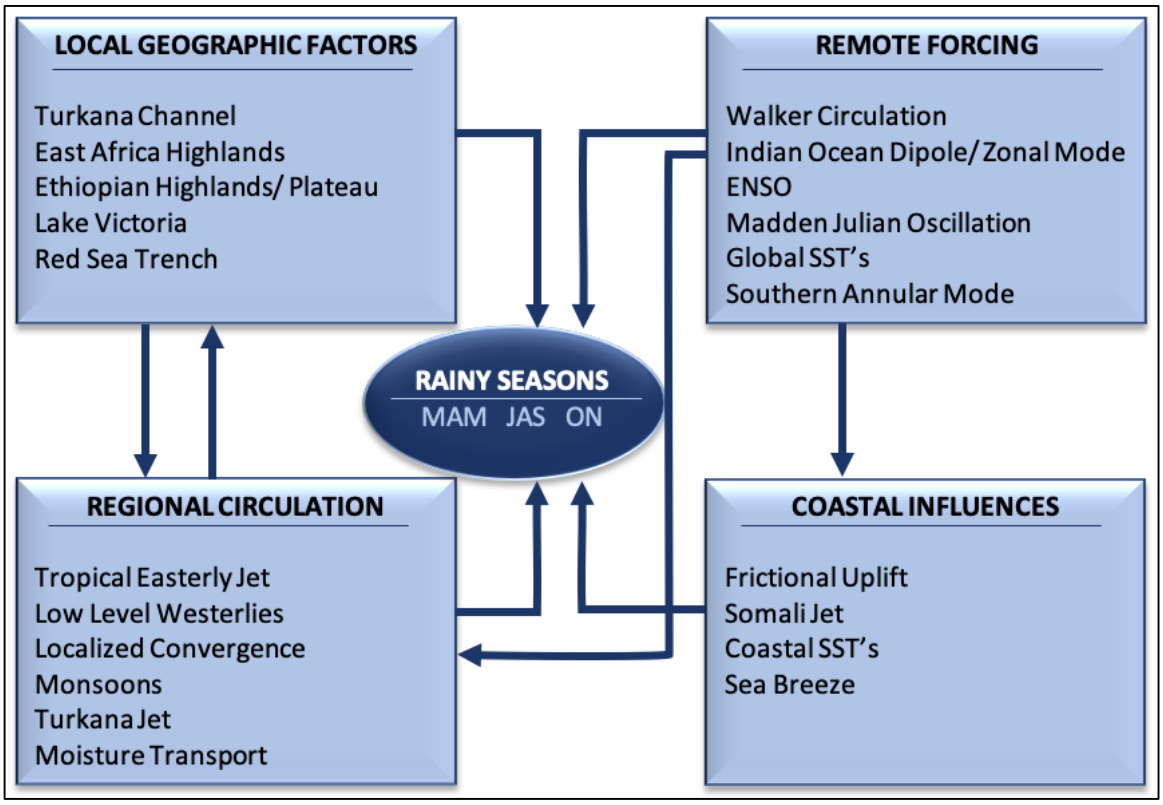

Figure 5. Factors that influence rainy seasons (**MAM**=March through May; **JAS**=July through September; **ON**=October through November) in East Africa and the interrelationships among the factors. Figure modified from Nicholson (2017).

Various studies have supported the idea that long-term wet/dry cycles in the East African region are driven by precession orbital cycles. Diatomite beds in the Central Kenyan Rift, indicative of periods of freshwater lake development during the Late Cenozoic, are spaced at ~23 thousand year intervals, correlating with precession-driven orbital cycles (Deino et al., 2006). At Olduvai Gorge in Tanzania, paleolake expansion and contraction during the Pliocene-Pleistocene boundary was interpreted to be linked to precession-controlled cyclicity by a high-resolution tuff-defined stratigraphic record (Ashley, 2007). Carbon-isotopic signatures of organic matter preserved in lake sediments at Olduvai Gorge from ~2 Ma were observed to correlate primarily with precession-controlled cycles (Magill et al., 2013; Colcord et al., 2018). Furthermore, authigenic clay geochemical analysis of mudstone samples at Olduvai Gorge indicated that the Pleistocene lake salinity levels at this locality were controlled by precession cycles (Deocampo et al., 2017). Also at Olduvai Gorge, groundwater modeling and paleogeological reconstruction done by Cuthbert and Ashley (2014) suggests that the Olduvai groundwater system would likely have provided a freshwater resource throughout the precession cycle, even during long droughts occurring on decadal to multicentennial timescales (Cuthbert and Ashley, 2014).

Hydrology

Precipitation

Annual rainfall is bimodal in most of the region: the main wet season is from March to May (MAM) and the short wet season is from October to November (ON) each

year. The twice-a-year migration of the ITCZ, accompanied by shifting wind directions, drives the semi-annual rainfall pattern (Camberlin, 2018). During the MAM wet season, also referred to as “masika”, rains are typically longer and heavier. The ON wet season, referred to as “vuli”, is typically shorter and less reliable than the MAM wet season. Most interannual variability is, therefore, associated with the ON rains (Nicholson, 2017).

Surface Hydrology

Rainfall on the NVH is quickly transported via ephemeral streams downslope toward the nearest base levels (**Figure 6**). Base levels include the surrounding rift lakes (i.e., Lake Eyasi to the southwest, Lake Manyara to the southeast, and Lake Natron to the north of the NVH) as well as Lake Olbalbal and Lake Masek to the west of the NVH (**Figures 1B**, **2**, and **6**). Surface water also collects seasonally within the calderas of NVH volcanoes, such as Lake Magadi in the caldera of Ngorongoro Crater and Lake Empakat in the caldera of Embagai Crater. Additionally, surface water feeds wetlands that are scattered throughout the area (Geological Survey of Tanzania, 1958, 1961, 1964, 1965).

Groundwater

While numerous springs and groundwater-fed wetlands occur throughout the NCA and are critical for wildlife, tourism, industry, and people living in the NCA, the hydrogeology of the region has not been thoroughly studied (Deocampo and Ashley, 1999; Kashaigili, 2010; Cuthbert et al., 2017). Very limited geological borehole data are available and usually these data are only privy to private Hydrogeological Surveying firms or Environmental/ Engineer/ Construction firms (ex: Sawere 2015).

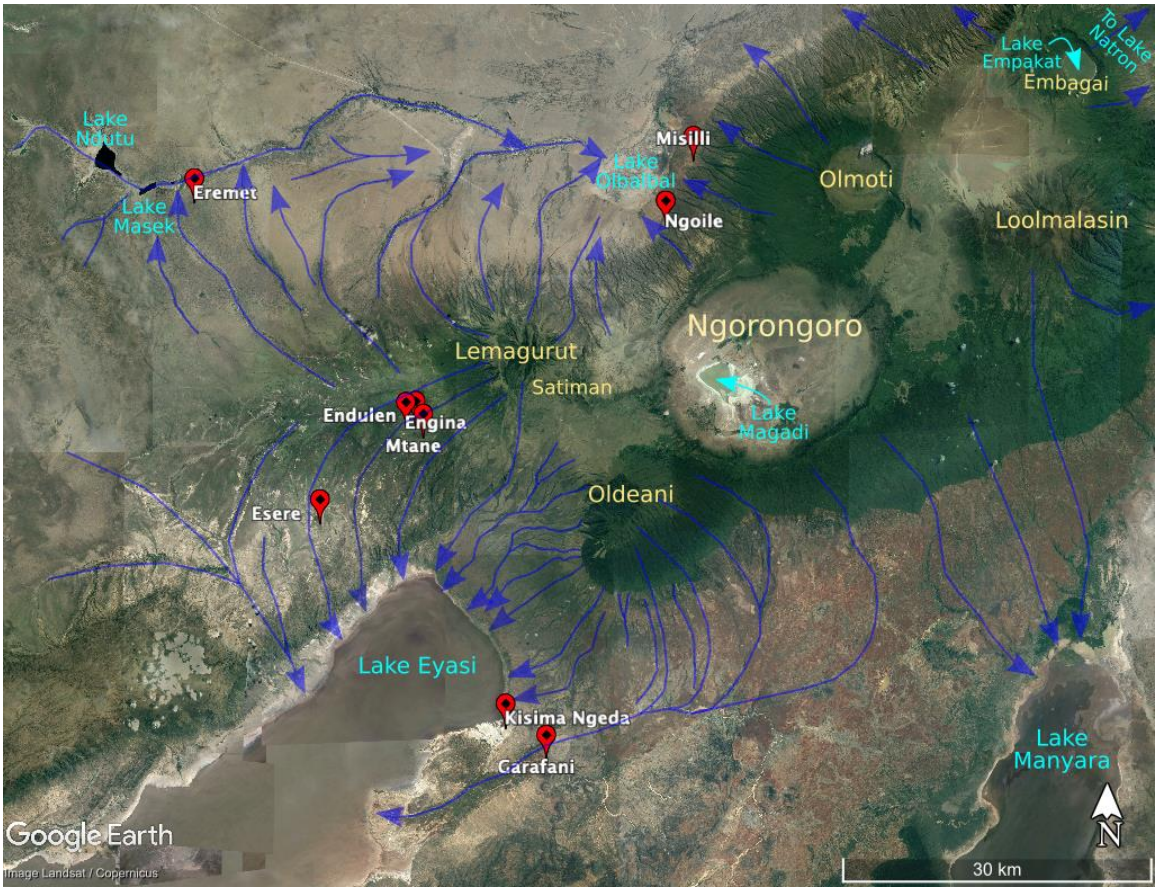

Figure 6. Surface water drainage pattern for the study region. Most streams are ephemeral. Surface water travels from NVH to the nearest base level. Spring names are labeled in white; volcanoes are labeled in yellow; and lakes are labeled in blue (GoogleEarth© Image Landsat/Copernicus).

Geomorphology

The NVH spans a distance of ~90 km from the Eyasi half graben in the southwest to the steep Natron Basin boundary fault escarpment in the northeast (**Figure 2**). At least nine main extinct volcanoes or vents make up the NVH and one active volcano (**Table 2**). Some of the volcanoes contain large craters (i.e., Ngorongoro, Olmoti, and Embagai), but most do not. The elevation of the volcanoes range from 2380 m (Ngorongoro) to 3648 m (Loolmalasin) and the diameters range from 6 km (Satiman) to 35 km (Ngorongoro). The NVH rises as much as 2900 m (Loolmalasin) to 700 m (Satiman) over the plains and rift valleys adjacent to the west. The NVH sits at the southern bifurcation of the Gregory Rift

where the rift diverges into two rifts bounded by major faults. The western major bounding fault runs N-S through the study area, cutting through Lemagurut and continuing along the western border of Lake Eyasi. The eastern major bounding fault runs N-S through the study area, cutting through the NVH in the northwest by Oldoinyo Lengai and continuing along the eastern boundary of the NVH/ western boundary of Lake Manyara (**Figure 2**) (Dawson, 2008; Mollel and Swisher, 2012).

Table 2. NVH Geomorphology (Dawson, 2008; Mollel and Swisher, 2012).

Volcano Name	Elevation (m)	Relief over Adjacent Rift Valley or Plain (m)	Diameter (km)	Crater Diameter (km)	Crater Lake
Oldoinyo Lengai	3188	2300	12		
Kerimasi	2575	1700	13		
Embagai	3235	2300	30	6.3 x 7.8	Lake Empakat
Loolmalasin	3648	2900	25		
Olmoti	3101	1800	30	6	
Ngorongoro	2380	1300	35	19 x 22	Lake Magadi
Lemagurut	3135	1500	20		
Satiman	2870	700	6		
Oldeani	3219	2200	20	5	

Various processes take place at the surface of the study area to create the features and forms described above. Endogenic processes such as volcanism and rifting and exogenic processes such as alluvial, colluvial, and even aeolian processes are the main processes controlling the shape of the landscape (Ritter et al., 2011). The following sections summarize these surface processes and their relation to the study area.

Endogenic Processes

Volcanism

The volcanoes which make up the NVH are classified as shield volcanoes and stratovolcanoes (including carbonatite volcanoes) (**Table 1**). Samples of lava from Satiman, Lemagurut, Ngorongoro, and Olmoti were analyzed and their compositions are

summarized as **Figure 3** (Stollhofen et al., 2008; Mollel and Swisher, 2012). The volcanoes are mainly composed of basalts and trachy-andesites which are associated with effusive lava flows typical of shield volcanoes. However, some lava flows are more alkaline, indicating more explosive viscous lava flows containing more water and gas, typical of stratovolcanoes (McHenry et al., 2008; Stollhofen et al., 2008; Ritter et al., 2011; Mollel and Swisher, 2012). The two youngest volcanoes of the NVH, Oldoinyo Lengai and Kerimasi, are both carbonatite stratovolcanoes which are composed of very fluid and highly weatherable carbonatite ash. Over time, weathering and erosion processes modify and smooth the rugged terrain built up by volcanic processes and redistribute material from higher to lower elevations (Dawson, 2008; Ritter et al., 2011; Mollel and Swisher, 2012; Ashley, 2014). While many volcanoes make up the NVH, all are dormant, except for the carbonatite volcano Oldoinyo Lengai located in the northeast of the NVH (**Table 1**). In fact, Oldoinyo Lengai is the only carbonatite volcano in the world that is actively erupting. Oldoinyo Lengai, referred to as the "Mountain of God", continues to build up the landscape. Its latest eruption was recorded to occur between 2007-2008, where significant ash was deposited; however, updates since then of effusive carbonatite lava flows inside the pit crater starting in 2017 and continuing through present day have been observed (Global Volcanism Program, 2019).

Rifting

The EARS is presently active and undergoing extensive continental extension (**Figure 1B**). As a consequence of the rifting, a series of half grabens have formed along the EARS where linear valleys are bordered by regional escarpments. In the study region,

two major normal bounding faults (part of the Gregory Rift) run N-S through the NVH and form the Eyasi Basin in the southwest and the Natron-Manyara Basin in the east (**Figure 7**). The western border fault of Lake Eyasi can be traced northward dissecting Mt. Lemagurut (**Figure 7**, yellow highlight) and continues on to Lake Natron. This indicates that the normal fault is younger than Mt. Lemagurut (faulting occurred at least <2.2 Ma) (**Table 1**). Additionally, the normal fault provides a direct conduit for surface water to enter the groundwater system supplying the Endulen area. These sedimentary basins are half-grabens occupied by shallow seasonal lakes (Lake Eyasi, Lake Natron, and Lake Manyara). Between the Eyasi and Manyara faults is the Mbulu plateau which contains several internal faults (**Figure 7**). These two major escarpments have drastically impacted the regional topography and thus the regional drainage patterns (Le Gall et al., 2008; Ritter et al., 2011; Scoon, 2018).

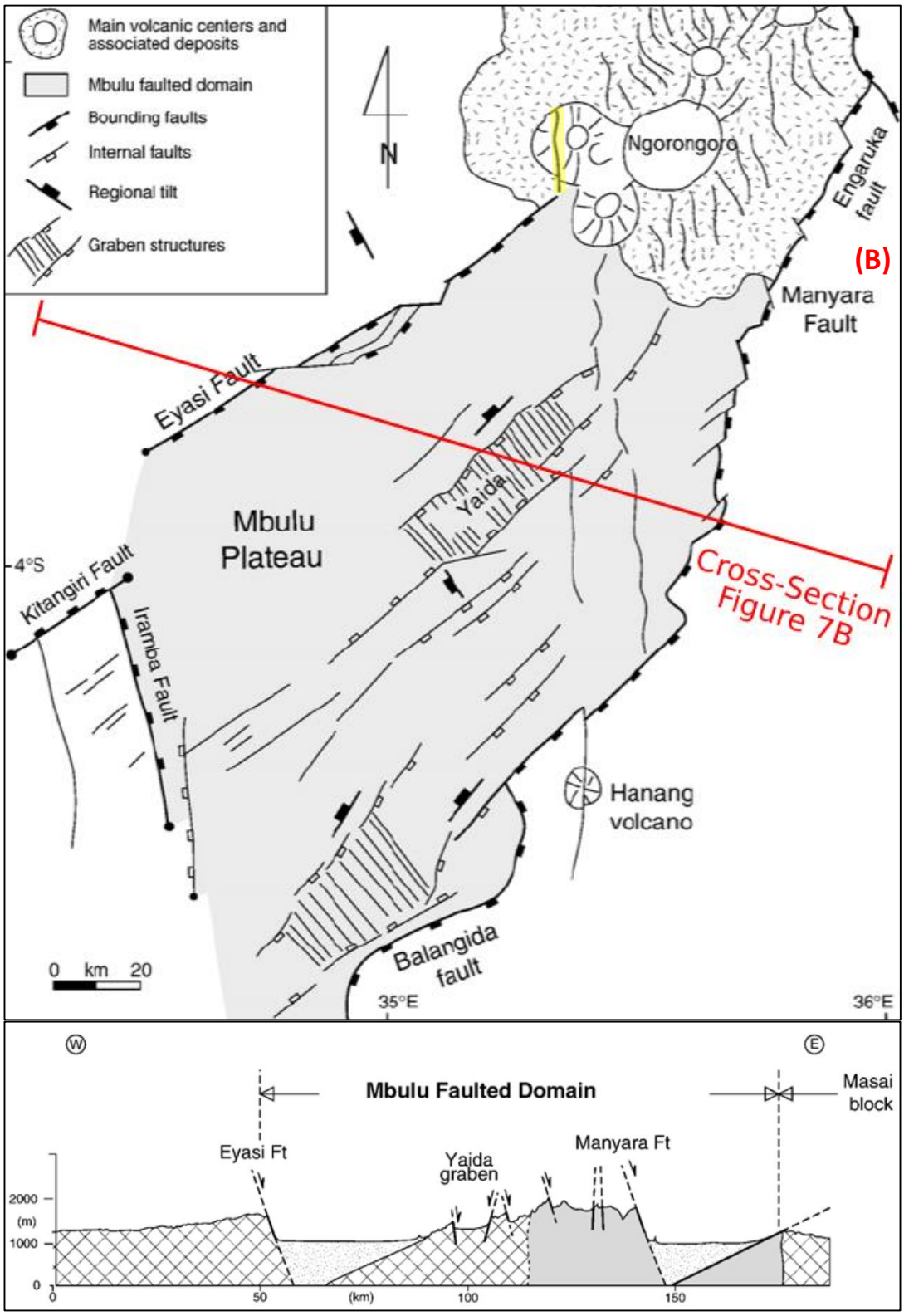

Figure 7. Fault distribution within the study region. **(A)** 2-Dimensional map of faults located in the Mbulu plateau between Eyasi and Manyara. Yellow highlight indicates where major bounding fault dissects Mt. Lemagurut. **(B)** Structural cross-section in the Mbulu plateau (Vertical Exaggeration is ~10). Modified from Le Gall et al. (2008).

Exogenic Processes

While volcanism builds up the landscape and rifting causes local subsidence and faulting, exogenic processes (i.e., colluvial, alluvial, and aeolian processes) work to level out the topography by redistributing material and reshaping the landscape.

Tropical weathering of volcanic rocks of the NVH under semi-arid and arid climate has created a cover of soil and unconsolidated sediment that is moved by colluvial (gravity-driven), alluvial (running water) (**Figure 8**), and aeolian (wind) processes in areas of sparse vegetation. The western drier slopes of the study region, where poor grazing practices by Maasai locals have seriously reduced vegetation, are highly vulnerable to these exogenic processes.

Figure 8. Pictures of a flash-flood in action in Olduvai Gorge in 2011, photographed by Dr. Gail Ashley. Debris captured by the river can be observed in the right pictures.

STUDY AREA

Spring Study Sites and DIVER Locations

Nine springs located in the environs of the NVH were chosen for study: Endulen, Engina, Mtane, Misilli, Ngoile, Kisima Ngeda, Garafani, Esere, and Eremet. The springs were selected because they had history of persistent flow based on verbal reports from community leaders and/or their locations were on geologic or topographic maps produced in the ~1960's indicating longevity of at least 60 years (Geological Survey of Tanzania, 1958, 1961, 1964, 1965). Endulen, Engina, and Mtane springs are located along the western slope of Mt. Lemagurut/ Mt. Satiman; the Misilli and Ngoile springs are located at the base of Mt. Olmoti's western slope; the Kisima Ngeda and Garafani springs are located to the south of Mt. Oldeani, on the northeast shore of Lake Eyasi; the Esere spring is located to the southwest of Mt. Lemagurut/ Mt. Satiman; and the Eremet spring is located to the northwest of Mt. Lemagurut, to the east of Lake Masek (in the Olduvai drainage). Spring locations are depicted in **Figure 1B**, **3**, and **6**.

In addition to these springs, some data were collected on surface runoff in the Garusi River. Two pressure transducers (DIVERS; discussed in methods section) installed in the channel of the Garusi River were recovered to measure seasonal discharge: one in the upper watershed of the river and one in the middle watershed (near the Laetoli footprint site). In addition, a DIVER was recovered from the Endulen Hospital office to measure local air pressure changes. The locations of the recovered DIVERS and an image of the instrument are depicted in **Figure 9**.

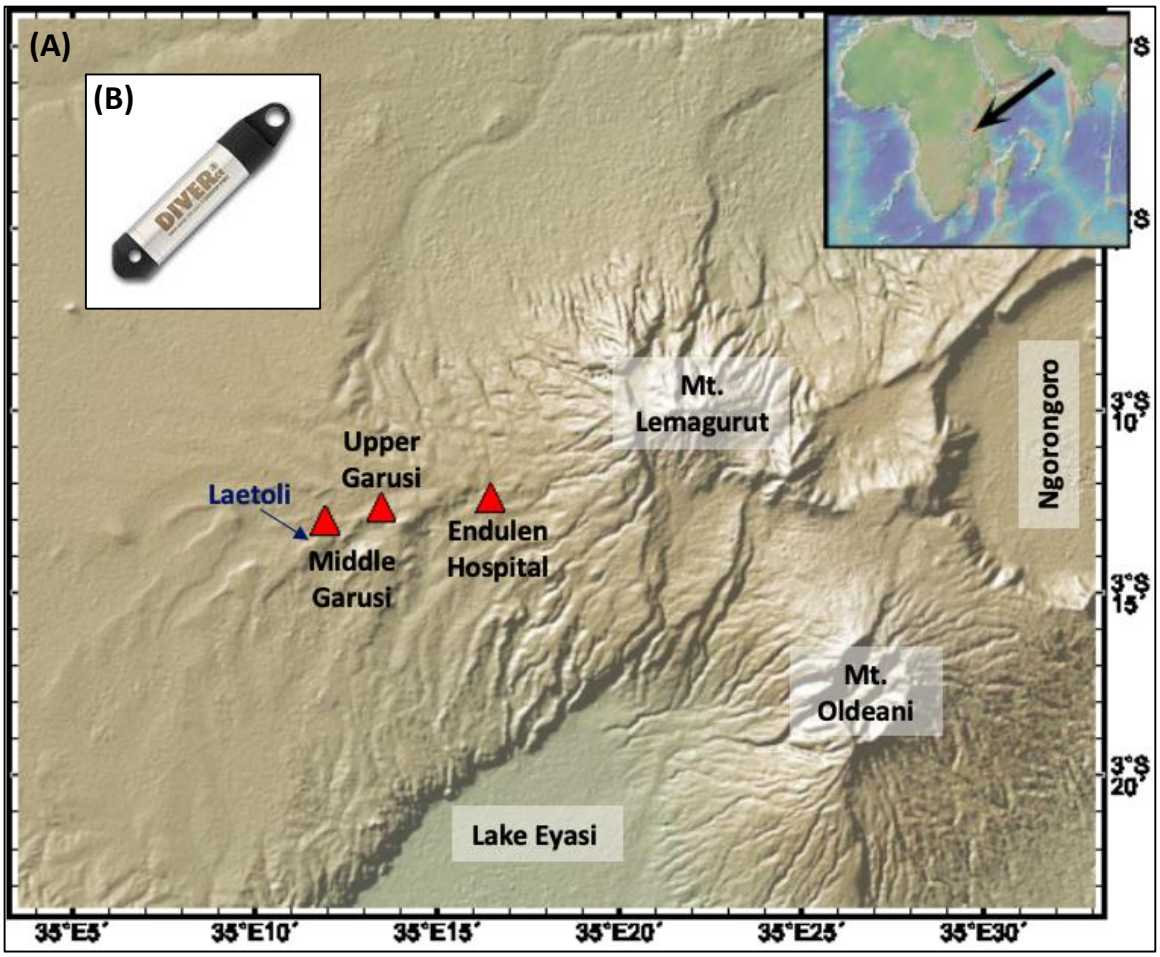

Figure 9. DIVER. **(A)** Recovered DIVER locations indicated by red triangles. Two DIVERS were recovered from the Garusi River and one atmospheric DIVER was recovered from the Endulen Hospital. The Laetoli Footprints site is indicated in blue. Base map from Ryan et al. (2009; http://www.geomapapp.org). **(B)** Image of DIVER instrument (~9 cm long) (Van Essen Instruments B.V., 2017).

METHODS

Data were collected in the field and laboratory. In order to gain an understanding of the groundwater system, nine springs located within the rain shadow of the NVH (**Figure 1B**) were visited and data including GPS position, site descriptions of local geomorphology and geology, and water samples were collected in July 2018. Laboratory methods included geochemical analysis of groundwater samples, preliminary analysis of the Garusi River seasonal discharge recorded by DIVERS, analysis of spatial and temporal variability of regional rainfall data, the creation of geologic cross-sections from spring recharge to discharge, and schematic conceptual models of groundwater flow and spring formation.

Field Methods

Site Descriptions

At each spring location, the following information was collected when possible: geomorphic setting, local surficial geology, locals' knowledge on groundwater and water supply, reports, photographs, GPS points, and any other miscellaneous observations such as possible sources of local pollution of water.

Water Sampling

All water sampling was done at or as close to the spring orifice as possible to get the most representative measurements of the groundwater at each spring locality. Water quality data including pH, temperature, and conductivity were collected using the Oakton PC 10 portable water quality probe. The probe was calibrated before use. Alkalinity measurements of the water samples were collected using the HANNA H1775 Checker HC

Handheld Colorimeter. Water for major cation analyses were collected at each spring in 25 mL Nalgene bottles (pre-washed with acid) with screw caps and filtered in the field using 0.2 micron filters. Water for major anion analyses were collected at each spring in 25 mL Nalgene bottles (rinsed with deionized distilled water) with screw caps and filtered using 0.4 micron filters. Water for stable isotope analyses were collected at each spring in glass vials which were prepared on purchase for isotope sample collection. Additionally, water for isotope analyses were collected from a few additional spring locations in the Serengeti to the west for comparison purposes.

DIVER Collection

As part of an ongoing modern hydrology and ecology study of the Ngorongoro region by Dr. Mark Cuthbert and Dr. Gail Ashley, pressure transducers (DIVERS) were placed at various locations within the study region between 2015-2018 to record river discharge during the fall and spring rainy seasons of 2015-2018 and any short term rain events that may occur throughout the year. Eight DIVERS were installed in summer 2015; however, only three DIVERS were recovered in summer 2016. The remaining five DIVERS could not be located and were presumed to have been a casualty of erosion. Data from the three recovered DIVERS were downloaded and the DIVERS were re-installed in summer 2016. Only two of the three reinstalled DIVERS were recovered in summer 2018. A summary of all installed DIVERS is provided as **Table 3**.

Two DIVERS from the Garusi River channel were recovered: one installed in the upper watershed of the channel (installed 2015, recovered 2016) and one installed in the

middle watershed of the channel (installed 2016, recovered 2018). DIVERS were attached to trees or buried under boulders within the channel of the river.

Additionally, a DIVER stored at the Endulen Hospital office to measure local air pressure changes was recovered (installed 2015, recovered and re-installed 2016, recovered 2018). The location of the recovered DIVER from the Endulen Hospital office is also depicted in **Figure 9**.

Table 3. Location and status of the eight installed DIVERS. "X" indicates DIVER was lost and data were not recovered.

#	DIVER ID	DIVER Location	Recovered Data
1	C7277	Main Gorge Olduvai (weir dam)	X
2	F0799	Side Gorge Olduvai (weir dam)	X
3	F0906	Endulen spring (weir)	X
4	G1090	Middle Garusi River (channel)	X
5	D8282	Lower Garusi River (channel)	X
6	F0790	Upper Garusi River (channel)	2015-2016
7	F0346	Endulen (indoor - hospital)	2015-2018
8	F1228	Middle Garusi River (channel)	2016-2018

Laboratory Methods

Geochemical Analysis

Major cation analyses of the water samples were performed on a high resolution Inductively Coupled Plasma Mass Spectrometer (ICP-MS), model Element XR (Thermo, Germany), at the Rutgers Inorganic Analytical Laboratory (RIAL) directed by Yair Rosenthal and Robert Sherrell from the Department of Marine and Coastal Sciences. Samples were run by Kaixuan "Ryan" Bu, RIAL Manager/ Research Associate. Samples were analyzed for the following cations: Calcium, Manganese, Sodium, Magnesium, and Potassium.

Major anion analyses of the water samples were performed on a Dionex™ Aquion™ Ion Chromatography (IC) System at the Rutgers Department of Environmental Sciences directed by Nathan Yee. Samples were run by Research Assistant Yuwei "Cindy"

Wang. Samples were analyzed for the following anions: Fluoride, Chloride, Bromide, Nitrate, and Sulfate.

Stable isotopes of the water samples were performed on a Picarro L2130-i cavity ringdown spectrometer with an A0211 high-precision vaporizer and attached autosampler at the University of Michigan Department of Earth and Environmental Sciences (Ann Arbor). The samples were run by Phoebe Aron, a graduate student at University of Michigan. The Picarro ChemCorrect software was used to monitor samples for organic contamination. Precision was better than 0.1‰ and 0.3‰ for $\delta^{18}O$ and δD, respectively.

Precipitation Analysis

Monthly rainfall data collected at 23 sites during varying time periods within the NCA were provided by the Ngorongoro Conservation Area Authority (NCAA) for analysis. Rainfall data were analyzed to determine temporal and spatial trends. Additionally, rainfall data at Kisima Ngeda were collected from 1995 to 2015 by Chris Schmeling. ENSO (Jan Null, 2019) and IOD (Australian Government Bureau of Meteorology, 2019) data were also analyzed in conjunction with the rainfall data.

Additionally, an unpublished poster (Macha, 2019), which used the same rainfall data from the NCAA to determine rainfall patterns for the NCA, was included as a part of this analysis.

River Flow Rate Analysis

The DIVER is a submersible datalogger designed to measure water pressure and temperature when submerged at a fixed level under the water surface as a proxy for

discharge. The data are stored for up to 2½ years and the instrument has a 10-year battery life (Van Essen Instruments B.V., 2017). The data from the three retrieved DIVERS (i.e., Upper Garusi River, Middle Garusi River, and the Endulen Hospital office) (**Figure 9**) were downloaded to a computer (the data cannot be accessed remotely) and analyzed as a part of the flow rate analysis.

A groundwater model was created in 2012 by Rutgers undergraduate student Elizabeth Miller using the MODFLOW program produced by the USGS (a modular finite-difference flow model that solves the groundwater flow equation) to estimate the rate of groundwater flow into wetlands surrounding Lake Eyasi. Findings from this report are included as a part of the flow rate analysis.

Geologic Cross-Sections

Based on the collected field and laboratory data as well as additional resources such as geologic and topographic maps, GeoMappApp, and Google Earth Pro, five geologic cross-sections were made from the presumed spring recharge locations (volcano summits) to the spring discharge locations.

Spring Schematic Conceptual Models

Based on the integration of the geological, geomorphological, hydrological, and geochemical data collected, three schematic conceptual models were developed to determine modes of spring formation for the nine springs examined in the study region.

RESULTS & INTERPRETATIONS

Site Descriptions

Detailed descriptions of the sites visited during summer 2018 are provided below and summarized as **Table 4**. Dr. Gail Ashley of Rutgers University and Dr. Mark Cuthbert of Cardiff University have visited most of these springs on various occasions; however, only information from the reconnaissance in July 2018 is reported herein.

Endulen

The Endulen spring (**Figure 10A**) was visited on June 21st, 2018. Site elevation at GPS coordinates 03°12’56”S, 35°16’8.5”E was 1813 m. The spring is composed of the combined flow from multiple groundwater seeps into rills and small channels at the headwaters of the Endulen River. Whereas the discharge points were not directly observable, water pooled naturally in depressions in the river channel and behind weirs built by local residents. The geologic setting appears to be an alluvial/ colluvial fan. The surficial geology surrounding the river was covered with soil and vegetation; the river bed contained large basalt clasts ranging in size from pebbles to boulders. Fig trees were situated along the bank of the river. Water samples were collected roughly 30-50 m away from the seepage points where the river water was flowing. The Endulen spring is the main water source for the village of Endulen and is used for drinking water, domestic use, and watering livestock. Annotated photos of the Endulen spring site are provided as **Appendix II**.

Figure 10A. Endulen spring photograph. View of spring seepage area at headwaters of stream. Fig tree situated on the left. More photographs of the Endulen spring are included in **Appendix II**.

Engina

The Engina spring (**Figure 10B**) was visited on June 23, 2018. Site elevation at GPS coordinates 03°12’59.5”S, 35°15’38.5”E was 1771 m. Isaiah Olemoita, a local of the town of Endulen, was guide. A small spring pool surrounded by lush, tall vegetation is presumed to be fed by numerous groundwater seeps. Water from the spring pool flowed into a man-made cement structure which dammed the water to keep it clean and allow for easy access by locals. The geologic setting was interpreted to be an alluvial fan. Surficial geology was unobservable due to cover by soils and vegetation. Water samples were collected adjacent to the spring pool where the water was flowing into the cement structure. The spring flows year-round and has been a dependable water source for many years, perhaps decades (Isaiah Olemoita, personal communication, July 2018). The water

is used for drinking, washing, and watering livestock. Annotated photos of the Engina spring site are provided as **Appendix II**.

Figure 10B. Engina spring photograph. View of flowing water coming from highly vegetated spring seepage area. Water is flowing toward photographer. More photographs of the Engina spring are included in **Appendix II**.

Mtane

The Mtane spring (**Figure 10C**) was visited on June 23, 2018. Site elevation at GPS coordinates 03°13’35”S, 35°16’33”E was 1710 m. Once again, Isaiah Olemoita, a local of the town of Endulen, was guide. Groundwater discharged under weak hydraulic head from riverbed sediments at the headwaters of the Mtane River and flow rapidly downstream. The surficial geology surrounding the river was covered with soil and vegetation; the river bed contained large lava clasts ranging in size from pebbles to boulders. The geologic setting appeared to be an alluvial fan. Holes dug into the river bed no larger than a meter in diameter were explained to be locations where locals extracted

groundwater (Isaiah Olemoita, personal communication, July 2018). Yellow Fever trees were situated along the banks of the river. Water samples were collected at the spring orifice. The spring flows year-round (Isaiah Olemoita, personal communication, July 2018). Annotated photos of the Mtane spring site are provided as **Appendix II**.

Figure 10C. Mtane spring photograph. View of the river headwaters where groundwater is seeping out. More photographs of the Mtane spring are included in **Appendix II**.

Misilli

The Misilli spring site was not visited due to the inability to obtain a permit from officials during the visit. In the spring area, a well was enclosed in a building to protect the quality of the water and deter pilferers. A pipe carried water from the well downhill to the local village where it was stored in a tank and dispensed to villages (**Figure 10D**); the water sample was taken directly from the pipe coming from the well. Site elevation

at GPS coordinates 02°59’0.48”S, 35°30’23.74”E was recorded as 1335 m where the water was collected on June 18, 2018.

Figure 10D. Misilli photograph. View of the storage container filled with water from the Misilli spring area. Locals use faucet on container to fill up their buckets with water.

Ngoile

Similarly to Misilli, the Ngoile spring was not visited due to the inability to obtain a permit because of time constraints. In the spring area, a well was enclosed in a building to protect the quality of the water and deter pilferers. A pipe carried water from the well downhill to the local village where it filled a man-made cement structure for easy access and hygienic purposes (**Figure 10E**). Water was collected once again directly from the pipe coming from the well. Site elevation at GPS coordinates 03°02’22.88”S, 35°29’0.13”E was recorded as 1341 m where the water was collected on June 18, 2018.

Figure 10E. Ngoile photograph. View of the man-made cement structure trough filled with water conveyed via pipe from the Ngoile spring area.

Kisima Ngeda

The Kisima Ngeda spring area (**Figure 10F**) was visited on June 26, 2018. Site elevation at GPS coordinates 03°28’32.8”S, 35°21’1”E was 1032 m. Several large spring pools were identified adjacent to and downslope from a ~15 m tall outcrop of vesicular basalt (volcanic neck). The spring pools fed into an expansive wetland system bordering Lake Eyasi. The geologic setting appeared to be an alluvial fan with localized outcrops of vesicular basalt. The entire area was surrounded by tall, lush vegetation whereas only a mile or so upslope from the springs, savannah vegetation dominated and Baobab trees occur. The Kisima Ngeda Tented Camp is located in the vicinity and frequented with

tourists. Local Chris Schmeling, owner of the tented camps, was interviewed. Daily rainfall measurements are collected by Chris Schmeling, showing that Kisima Ngeda received ~400 mm of rain in the past year of 2018. Rainfall measurements collected by him for the last 20 years were shared with the research team and are discussed in the precipitation analysis. Groundwater was collected in 2013 from the wetland area adjacent to the basalt outcrop. Annotated photos of the Kisima Ngeda spring site are provided as **Appendix II**.

Figure 10F. Kisima Ngeda spring photograph. View of small portion of extensive wetland system at Kisima Ngeda. More photographs of the Kisima Ngeda springs are included in **Appendix II**.

Garafani

The Garafani spring area (**Figure 10G**) was visited on June 27, 2018. Site elevation at GPS coordinates 03°30’8.4”S, 35°23’9.1”E was 1090 m. These springs were located to the southeast of Kisima Ngeda. Groundwater seeps out of and around an outcrop of volcanic rock and collects downslope into large pools bordered by lush wetland. Water

samples were collected at a spring orifice where water seeped out of volcanic rock. Yellow Fever and Ficus trees were situated adjacent to the spring pool. Approximately 50 locals occur by the spring pool collecting water into five-gallon buckets. Annotated photos of the Garafani spring site are in **Appendix II**.

Figure 10G. Garafani spring photograph. View of spring pool and surrounding wetland vegetation. More photographs of the Garafani spring are included in **Appendix II**.

Esere

The Esere spring area (**Figure 10H**) was visited on June 22, 2018. Site elevation at GPS coordinates 03°18’5”S, 35°11’14.2”E was 1591 m. While the spring discharge points were not directly observable, they were interpreted to exist at multiple points where water pooled at the surface and fed a large wetland. The bedrock is fractured basement rocks. The surficial geology was exposed throughout most of the area and consisted of

highly fractured/ faulted tuff. Additionally, mounds of tufa deposits (i.e., mounds of sandy-silty gray carbonate) were observed throughout the area. Areas surrounding the springs consisted of lush wetland vegetation; however, the remainder of the site contained very little if any vegetation. The water is used for drinking, washing, and watering livestock. Water samples were collected from a well located within the spring/ wetland area since no spring orifice or flowing water was observable. Annotated photos of the Esere spring site are in **Appendix II**.

Figure 10H. Esere spring photograph. View wetland vegetation surrounding spring area. More photographs of the Esere spring are included in **Appendix II**.

Eremet

The Eremet spring area (**Figure 10I**) was visited on June 24, 2018. Site elevation at GPS coordinates 03°01’35”S, 35°04’29.7”E was 1594 m. The site is located ~3.5 km east of Lake Masek. Groundwater discharges at the base of the slope in a seep-line extending

~1 km in the east-west direction. Water seeps out of silty-sand volcaniclastic-altered tuff into a depression which appears by its geomorphology to be a paleo lake basin. Water collects into pools and drains toward the center of the basin where it flows generally downslope to the east. Water samples were collected where groundwater was seeping out of the tuff and collecting in a pool directly below the orifice. Surficial geology consisted of fractured carbonate-cemented tufaceous silt, posited to have been deposited in a high-stage lake environment. Lush wetland vegetation immediately surrounded the spring pools and continued along the entire rim of the paleo lake basin. Annotated photos of the Eremet spring site are provided as **Appendix II**.

Figure 10I. Eremet spring photograph. View looking into pale lake basin where springs discharge, looking west. More photographs of the Eremet spring are included in **Appendix II**.

Garusi River

The Middle Garusi River was visited on June 22, 2018. Site elevation at GPS coordinates 03°12’37.3”, 035°12.5’57.6” was recorded as 1779 m. The Upper Garusi River was visited on June 25, 2018. Site elevation at GPS coordinates 03°12’36.4”S, 35°12’58.4”E was recorded as 1782. The river bed at both locations was dry and channel depth was estimated to be ~3 m below the ground surface. The river bed contained alluvial deposits consisting of sand, silt, and large clasts ranging in size from pebbles to boulder. Two DIVERS were installed in the Garusi River in 2016; only one was retrieved at the time of the site visit (Middle Garusi DIVER). The recovered instrument was found attached to the root of a tree located on the bank of the river (**Figure 10J**). Annotated photos from the Middle and Upper Garusi River are provided as **Appendix II**.

Figure 10J. Middle Garusi River photograph. Retrieved DIVER from river by Joseph Masoy and Gail Ashley. DIVER was secured to root of tree with cable ties and buried under boulders on July 2, 2016. More photographs of the Garusi River are included in **Appendix II**.

Table 4. Site Descriptions Summary.

Site Name	Coordinates	Elevation (m)	Type	Geologic Setting	Sample Location
Endulen	03°12’56”S 35°16’8.5”E	1813	Seepage springs feeding river	Alluvial fan; volcaniclastics	30-50 m downstream from orifice
Engina	03°12’59.5”S 35°15’38.5”E	1771	Seepage spring feeding small Spring pool and wetland	Alluvial fan; volcaniclastics	Flowing water adjacent to spring pool
Mtane	03°13’35”S 35°16’33”E	1710	Seepage springs feeding river	Alluvial fan; volcaniclastics	Spring seep from rock at headwater of river
Misilli	02°59’0.48”S 35°30’23.74”E	1335	Seeping springs at base of slope	Alluvial fan	Water conveyed by pipe to village from upslope well
Ngoile	03°02’22.88”S 35°29’0.13”E	1341	Seeping springs at base of slope	Alluvial fan	Water conveyed by pipe to village from upslope well
Kisima Ngeda	03°28’32.8”S 35°21’1”E	1032	Large spring pools feeding expansive wetland system	Alluvium; upslope basalt outcrop	No sample taken
Garafani	03°30’8.4”S 35°23’9.1”E	1090	Seepage springs feeding spring pool and large wetland	Associated with basalt outcrop	Spring seep from rock into pool
Esere	03°18’5”S 35°11’14.2”E	1591	Artesian flow feeding large wetland	Highly fracture tuff; tufa deposits	Well in wetland
Eremet	03°01’35”S 35°04’29.7”E	1594	Seepage springs feeding large wetland	Volcaniclastic altered tuff; paleolake sediments	Spring seep from rock
Garusi River			River bed	Dry channel, alluvial deposits	Instrument secured to tree root on channel bank
Middle	03°12’37.3”, 035°12.5’57.6”	1779			
Upper	03°12’36.4”S 35°12’58.4”E	1782			

Water Chemistry Analysis

Dr. Gail Ashley of Rutgers University and Dr. Mark Cuthbert of Cardiff University have collected water quality data on most of these springs for several years; however, only data analyses of the water samples collected in July 2018 are reported herein.

Water Quality Measurements

Results

Water quality measurements, water temperature, pH, conductivity, and alkalinity, for each spring are listed in **Table 5**. Groundwater temperatures ranged from 19.9 to 26.8°C with the average being 23°C. The spring water of Esere and Eremet were both >26°C, Misilli and Ngoile spring waters were between 23°C and 26°C, and all other spring waters were between 19°C and 23°C. The pH ranged from 7.19 to 8.62 with the average being 7.7. The spring water of Esere and Eremet had more alkaline readings of 8.1 and 8.62 whereas all other springs had more neutral readings. Conductivities ranged between 246 µS and 464,000 µS. The highest conductivity reading (464,000 µS) was recorded at Eremet followed by Kisima Ngeda (1398 µS), Esere (892 µS), and Mtane (702 µS). The remaining spring conductivities were between ~200 µS and 400 µS. Alkalinity readings ranged between 84 ppm and >500 ppm. The highest alkalinity was recorded at Eremet (>500 ppm), followed by Esere (346 ppm) and Mtane (316 ppm). The remaining alkalinity readings were between ~80 ppm and 200 ppm.

Table 5. Water quality measurements collected for the nine springs visited.

Spring Name	pH	Temperature (°C)	Conductivity (µS)	Alkalinity (ppm)
Endulen	7.86	19.9	397	198
Engina	7.26	20.7	407	207
Mtane	7.19	22.2	702	316
Misilli	7.64	25.4	246	112
Ngoile	7.78	23.9	211	84
Kisima Ngeda	7.79	20.7	1398	-
Garafani	7.77	21.1	259	123
Esere	8.62	29	892	346
Eremet	8.1	26.8	464000	>500

Interpretation

At Misilli and Ngoile, the spring water traveled through a pipe for ~1600 m before being measured, which can explain the elevated water temperatures at these two locations. The high spring water temperature at Esere could be explained by a deep groundwater flow path: it is plausible that as the groundwater traveled deep underground, geothermal processes raised the water temperature prior to the groundwater being brought to the surface via fractures under artesian pressure. Additionally, spring water at Eremet likely traveled in a shallow aquifer, accounting for the elevated temperature.

Very high conductivity and alkalinity readings at Eremet support the idea that the region used to be a lake basin and that the local "bedrock" and soils are paleolake deposits. The lake would have likely been saline and alkaline, similar to modern Lake Masek and Lake Ndutu, and have existed during a former wetter period when there were overall higher lake levels. The paleo lake, located at a higher elevation than Lake Masek and Ndutu, would have likely been the first to dry up as the climate changed, yet the alkalinity would be preserved in the sediments. Water traveling through paleo lake sediment would acquire cations and anions left behind from the alkaline lake which would account for the high conductivity/ alkalinity values of the groundwater (**Table 5**).

The Esere spring also has high conductivity and alkalinity readings, which is posited to be related to the high temperature, and thus more reactive, groundwater. The two

parameters, temperature and alkalinity, are often positively correlated (Barron and Ashton, 2007).

Groundwater associated with the EARS has been observed to be typically alkaline with high pH values (Kashaigili, 2010). This is consistent particularly with Esere and Eremet locations.

Major Cation and Anion Analysis

Results

Major cations and anion results of the water samples at each spring are provided in **Table 6**. Samples were analyzed for the following cations and anions: Calcium, Manganese, Sodium, Magnesium, Potassium, Fluoride, Chloride, Bromide, Nitrate, and Sulfate. Ion concentrations of the spring waters were compared to the United States Environmental Protection Agency (USPEA) drinking water standards. Of the analyzed ions regulated by the USEPA, only Fluoride (at Esere and Eremet springs) and Nitrate (at Mtane spring) concentrations exceeded the USEPA Maximum Contaminant Level (MCL). Additionally, Fluoride (at Mtane spring, Lake Olbalbal, and the Eyasi Lodge Well) and Chloride (at Eremet spring) exceeded the USEPA Secondary Maximum Contaminant Level (SMCL). The MCL levels represent the legal threshold a contaminant is allowed in USA public water systems and SMCL represents non-mandatory water quality standards that are set in the USA for aesthetic consideration (such as taste, color, and odor) (USEPA, 2018).

Table 6. Major anion and cation results compared to United States Environmental Protection Agency (USEPA) drinking water standards.

Spring Name	**Concentration (ppm)**									
	Ca^+	**Mn^+**	**Na^+**	**Mg^+**	**K^+**	**F^-**	**Cl^-**	**Br^-**	**NO_3^-**	**SO_4^-**
Mtane Spring	**80.9**	0.0014	55.5	16.4	11.8	2.01	17.78	0.11	33.04	3.91
Misilli Spring	22.5	0.0006	24.5	3.15	7.21	1.08	2.58	0.03	5.01	5.62
Ngoile Spring	8.54	0.0089	40.9	1.19	11.4	0.97	5.86	0.04	5.23	10.04
Endulen Spring	-	-	-	-	-	-	6.45	0.04	3.16	3.17
Esere Spring	5.61	0.0025	201	4.43	**17.2**	4.95	68.90	0.19	1.06	17.06
Olbalbal Lake	12.6	**0.0249**	149	0.49	5.48	7.91	15.88	0.12	0.09	21.39
Engina Spring	42.7	0.0005	36.5	11.2	4.27	0.94	5.87	0.04	5.49	1.68
Eyasi Lodge Well	25.3	0.0003	165	18.6	6.33	5.31	52.78	0.80	3.11	24.79
Eremet Spring	7.66	0.0133	**1127**	3.80	39.5	38.66	482.28	4.53	7.47	232.79
Garafani Spring	22.4	0.0007	19.1	9.79	1.83	-	-	-	-	-
USEPA MCL	None	None	None	None	None	4	None	None	10	None
USEPA SMCL	None	0.05	None	None	None	2	250	None	None	250

Notes:
ppm = parts per million
Red = concentration exceeds **USEPA** 2018 **MCL** standards for drinking water
Purple = concentration exceeds **USEPA** 2018 **SMCL** standards for drinking water
USPEA = United States Environmental Protection Agency
MCL = Maximum Contaminant Level; legal threshold that is allowed in US public water systems
SMCL = Secondary Maximum Contaminated Level; non-mandatory water quality standards set for aesthetic considerations in US

Interpretation

In general, the water quality at these sites is acceptable for drinking (according to USEPA drinking standards), with the exception of the high Fluoride concentrations at a few of the locations and high Nitrate at one of the locations. These results align with other groundwater quality reports for Tanzania (Kashaigili, 2010).

Groundwater from the volcanic terrains of Tanzania have been reported to have high Fluoride concentrations. This is attributed to lavas, intrusions, and ashes associated with the EARS which contain abundant fluorine-rich minerals (Kashaigili, 2010). Additionally, Fluoride concentrations in major depressions occurs through extreme evaporation of lake water and thus infiltration into shallow aquifers (Kashaigili, 2010). The

high Fluoride concentrations at Esere and Eremet can support the notion that groundwater at these localities has traveled through rock longer (increasing water-rock interaction). Nitrate concentrations have been reported to impact groundwater quality in some parts of Tanzania and is attributed to pollution from sewage effluents (Kashaigili, 2010). Relatively high Sodium concentrations have also been reported in the groundwater of the EARS (Kashaigili, 2010). High Chloride (salinity) concentrations are considered a problem in central Tanzania where there is high evaporation and poor drainage (Kashaigili, 2010). This may be the case for Esere and Eremet which both have higher Chloride concentrations compared to the other locations. Also, the water temperatures at Esere and Eremet are higher than the other springs which makes the water more reactive and provides an explanation for the for the high ion concentrations at these springs.

Stable Isotope Analysis

Results

Stable isotope results of the water samples at each spring are provided in **Appendix III**. The results are summarized as **Figure 11** below. Based on these data, the Local Meteoric Water Line (LMWL) has the equation $y = 8x + 18$ and is positioned above the Global Meteoric Water Line (GMWL), which has the equation $y = 8x + 10$. The best fit line for all of the samples, except for Esere, Eremet, and Lake Olbalbal, has the equation $y = 3.3x – 4.5$.

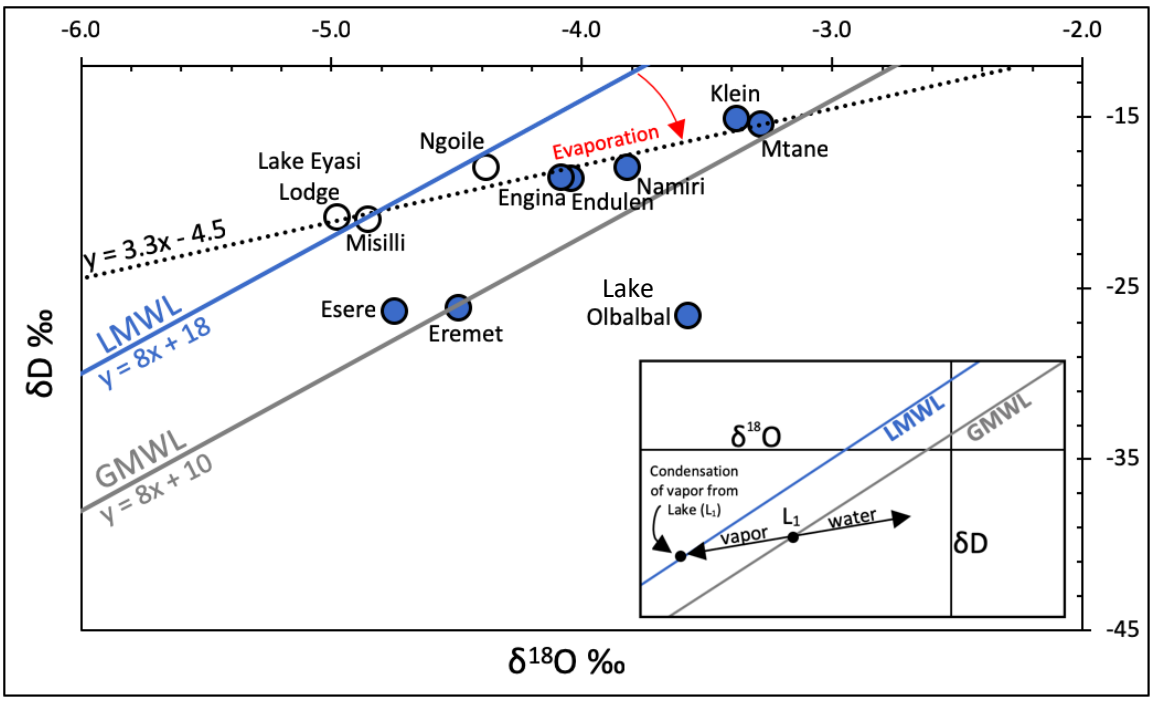

Figure 11. Stable isotope plot for water samples. Water samples collected from wells, representing conditions less likely to be subjected to evaporation, are indicated by open circles. Water samples collected on the surface, representing conditions more likely to be subjected to evaporation, are indicated by closed circles. The Global Meteoric Water Line (GMWL) is depicted in gray. The Local Meteoric Water Line (LMWL) is depicted in blue. The best fit line for the data samples (excluding Esere, Eremet, and Lake Olbalbal) is dashed in blue.

Interpretations

The positioning of the LMWL above the GMWL (**Figure 11**) indicates that the local atmosphere is more arid compared to the global atmosphere. It can be presumed that as water in the atmosphere travels from the Indian Ocean, the $\delta^{18}O$ and δD of the precipitation decreases. In addition, the rift lakes surrounding the NVH (e.g. Lake Manyara and Lake Eyasi) can be presumed to further contribute to the local atmosphere having more negative compositions than the global average. This process is illustrated as **Figure 12** below.

Spring samples that fall below the LMWL (such as Engina, Endulen, Namiri, Klein, and Mtane) are represented by the dashed line in **Figure 11**. This deviation from the LMWL is presumed to be caused by evaporative loss associated with the sampling procedure. Springs sampled directly from the ground (i.e., from wells), represented by open circles in **Figure 11**, were less likely to be subjected to evaporation and have isotopic concentrations closest to the local meteoric compositions. However, springs sampled from the surface (i.e., subaerial), represented by closed circles in **Figure 11**, were more likely to have be subjected to some evaporation, altering the isotopic compositions of those samples to deviate from the LMWL. Additionally, the isotopic compositions of water from the Esere spring, Eremet spring, and Lake Olbalbal deviated from the LMWL. Lake Olbalbal is spring-fed from Olmoti, but receives river water from the Olduvai River which could account for the deviation in isotopic concentrations from the others. As for Esere and Eremet, while it is uncertain as to why they do not fall on the LMWL, it does suggest

there is something about these springs that is inherently different (in terms of geologic setting and/or hydrologic history) from the others.

The local hydrology of the region (i.e., evaporation from surrounding rift lakes) plays an important role in explaining differences between the isotopic composition of the local meteoric water and the global. Rietti-Shati et al. (2000) come to a similar conclusion in that the isotopic composition of high-altitude fresh-waters on Mt. Kenya in equatorial East Africa is influenced by local hydrological factors resulting also in more negative compositions of local meteoric water compared to global.

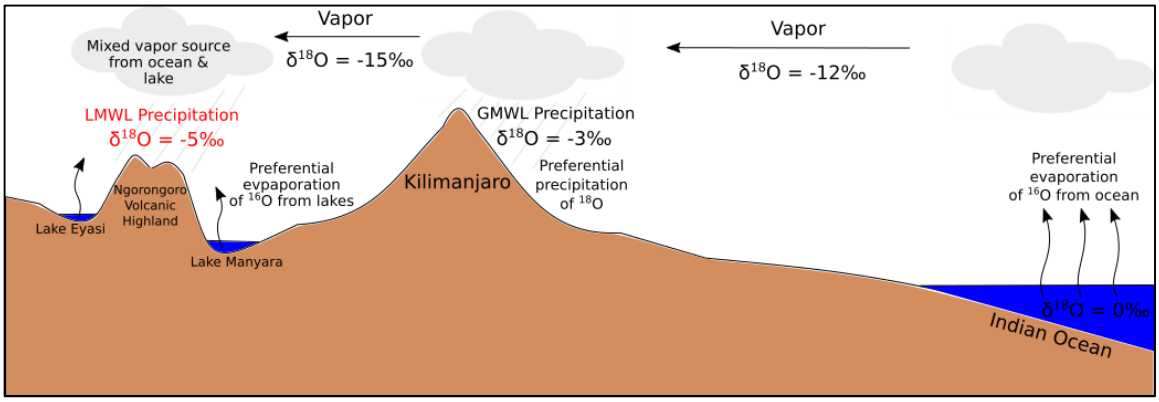

Figure 12. Conceptual diagram of the isotopic fractionation occurring at the study site. As water in the atmosphere travels from the Indian Ocean toward the NVH, $\delta^{18}O$ decreases. Water evaporated from rift lakes (i.e., Lake Eyasi and Lake Manyara) surrounding the NVH enriches the local atmosphere in ^{16}O. Both processes result in a lower isotopic composition of spring water at the study site than the global average.

Precipitation Analysis

The NCAA records monthly rainfall data at 23 sites within the NCA (**Figure 13**). Available rainfall records at each location were provided by the NCAA and are included in **Appendix IV**. Additionally, rainfall data at Kisima Ngeda (**Figure 13**) were collected by Chris Schmeling from 1995 to 2015 and are also provided in **Appendix IV**.

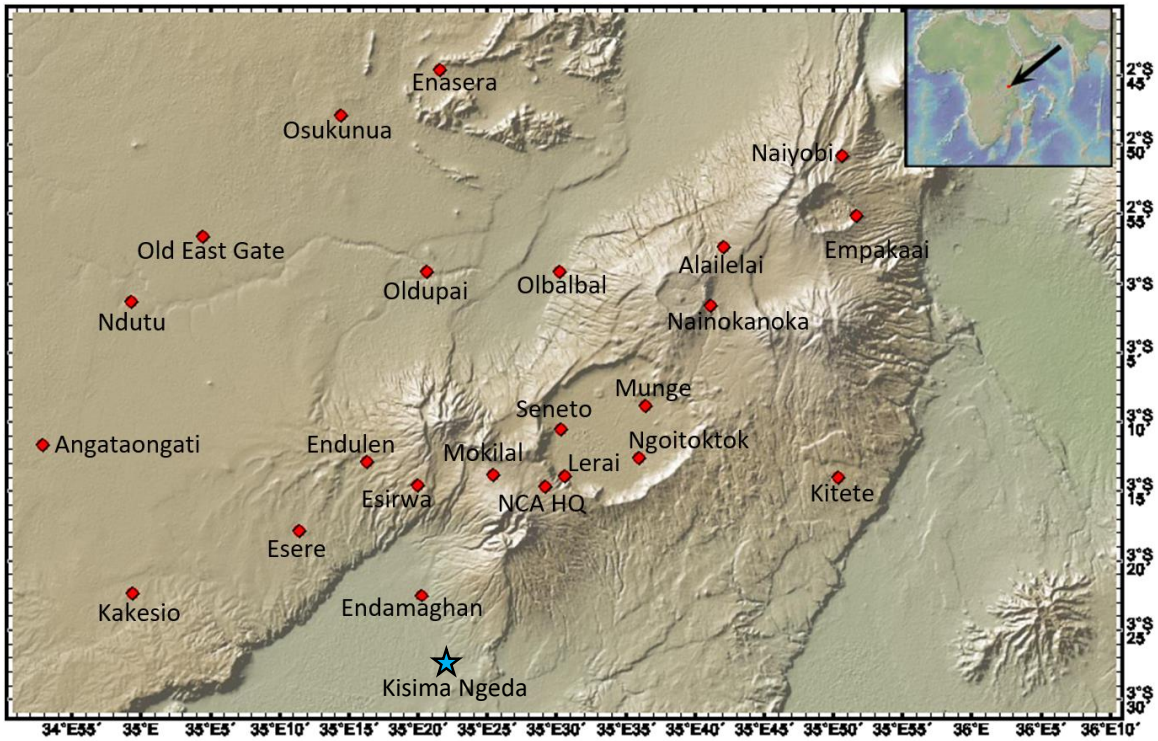

Figure 13. NCA rainfall gauge locations maintained by the NCAA (indicated by red diamonds); Kisima Ngeda rainfall gauge maintained by Chris Schmeling (indicated by blue star). Base map from Ryan et al. (2009; http://www.geomapapp.org).

Temporal Analysis

Results

Rainfall data from the NCA HQ gauge and the Kisima Ngeda gauge (**Figure 13**) were analyzed for temporal patterns. Yearly rainfall data at NCA HQ and Kisima Ngeda locations over the 19-year time period between 1995 and 2014 are depicted in **Figure 14A**. Monthly and mean annual rainfall at both locations varied greatly during this time period. NCA HQ received on average 912 mm of rain a year, with the highest recorded yearly rainfall measured at 1705 mm in 1997 and lowest yearly rainfall measured at 296 mm in 1995. Kisima Ngeda received on average 459 mm of rain a year, with the highest recorded yearly rainfall measured at 780 mm in 2006 and lowest yearly rainfall measured at 198 mm in 2003.

Additionally, 3-4 peaks in rainfall can be identified during the 19-year period occurring circa 1997, 2002, 2006-07, and 2011-13(?) at NCA HQ and Kisima Ngeda (**Figure 14**). When compared to El Niño years (Jan Null, 2019), which are known to bring wet conditions to East Africa (Kijazi and Reason, 2009; Tierney et al., 2013), the 1997 and 2002 peak rainfall years match up with El Niño years; however, the remaining peak rainfall years do not follow suit (**Figure 14**). In fact, the peak rainfall year occurring circa 2006-07 actually occurs counter-intuitively during a La Niña year. When compared to positive IOD years (Australian Government Bureau of Meteorology, 2019), which are also known to bring wet conditions to East Africa (Owor et al., 2009; Taylor et al., 2012; Taylor and Jasechko, 2015), the 1997 peak matches up with a positive IOD year as does the 2007 peak (**Figure 14**). The positive IOD year in 2007 can help to explain why the study region received more rain that year despite it being a La Niña year.

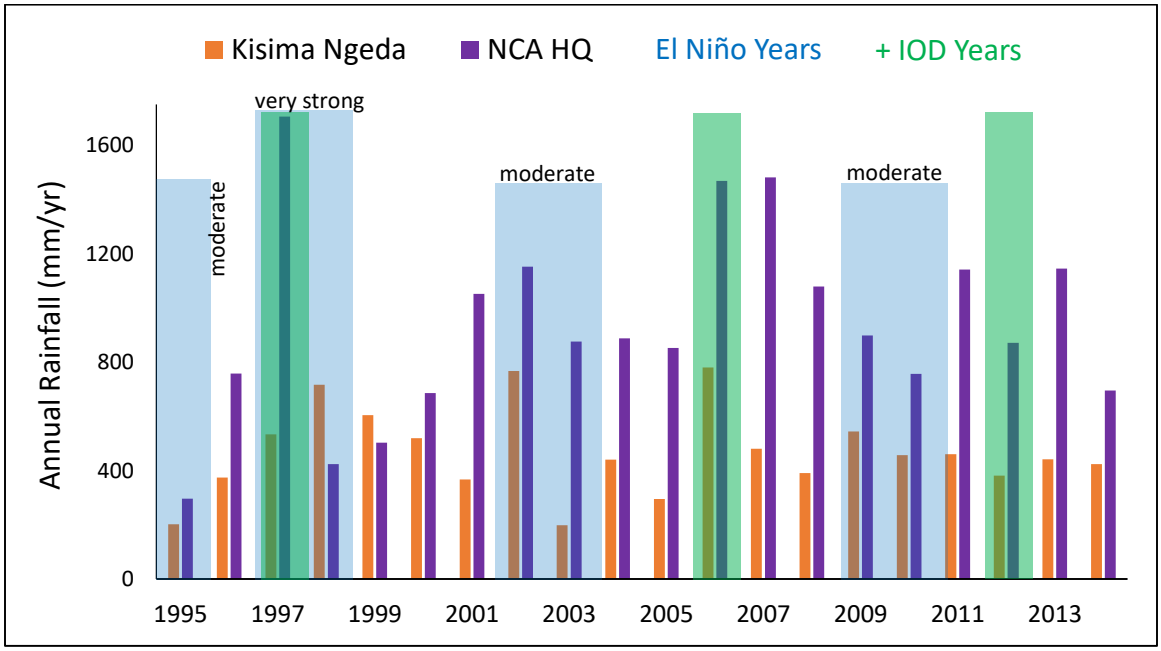

Figure 14. Annual Rainfall at the NCA HQ and Kisima Ngeda from 1995 to 2014 (**Appendix IV**). Kisima Ngeda received ~half the amount of rain that NCA HQ received during this time frame. El Niño years are highlighted in blue and positive Indian Ocean Dipole (IOD) years are highlighted in green.

Monthly rainfall data from rain gauges located at NCA HQ and Kisima Ngeda over the 4-year period between 2010 and 2014 are depicted as **Figure 15**. At both locations, monthly rainfall varies semi-annually in that two wet seasons occur every year: the March-May (MAM) "long rains" and the October-November (ON) "short rains". Between the 2010 and 2014, NCA HQ received an average 456 mm of rain over the long rain season (March-May) and 52 mm of rain over the short rain season (October-November).

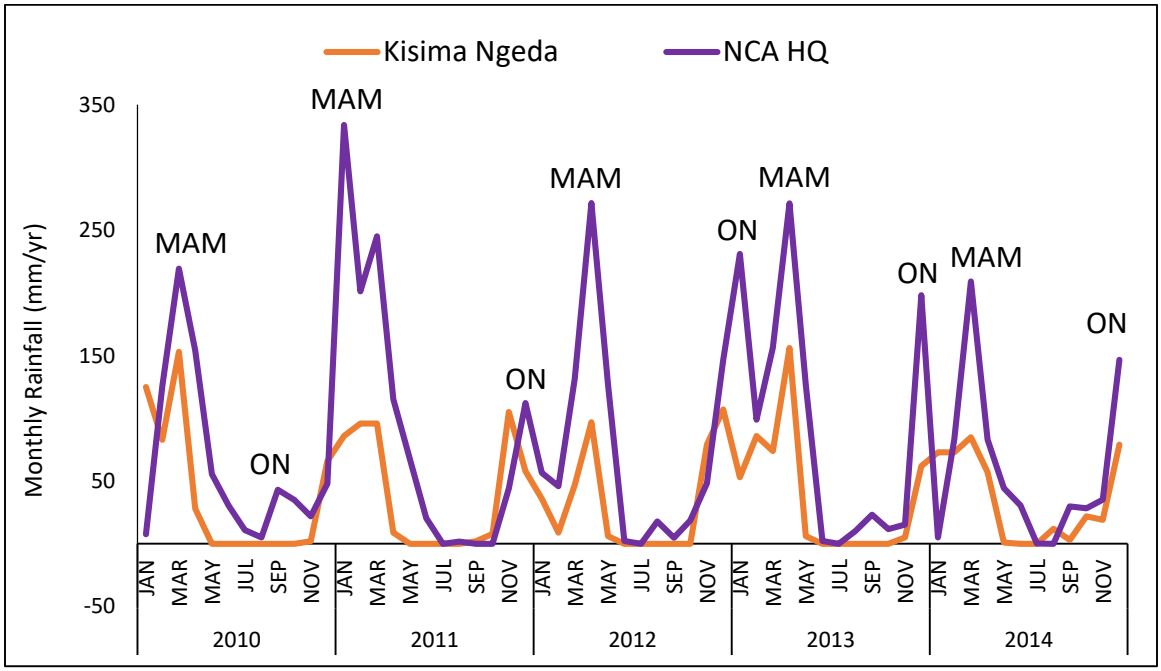

Figure 15. Monthly Rainfall Analysis. Monthly rainfall at NCA HQ and Kisima Ngeda from 2010-2014 (**Appendix IV**). Bimodal annual rainfall cycles exist at both locations: a long wet season from March to May (MAM) and a short wet season from October to November (ON).

Interpretations

Based on these data, there are two temporal patterns. The first temporal pattern occurs on an interannual basis in which peak rainfall years occur nearly every 5 years (**Figure 14**). The cyclicity in rainfall can be partially explained by ENSO and IOD; however, other oceanographic factors yet to be determined may also play a role in the interannual variability in rainfall at the study region. The second temporal pattern occurs on a yearly

basis in which two peaks in rainfall occur each year at the study region: one from March to May (MAM) and one from October to November (ON). Although the amount and duration of rainfall observed at the study region vary each year, the pattern of two wet seasons occurring roughly during these time frames appears to be predictable. These two wet seasons can be attributed to the seasonal migration of the ITCZ which drives the twice-a-year East African Monsoon to deliver rainfall to the study region (Nicholson, 2017). Extreme, episodic rainfall events, such as the biannual monsoons and interannual peak rainfall years seen at the study region, are known to be important for recharging aquifers in East Africa and the same can be assumed for the study region (Owor et al., 2009; Taylor et al., 2012; Taylor and Jasechko, 2015).

Spatial Analysis

Results

A distinct difference in amount of rainfall between the two rain stations occurs during the 19-year time frame (**Figure 14**) as well as over the 4-year time frame (**Figure 15**). On average, NCA HQ (located at ~2380 m) received ~50% more rain than Kisima Ngeda (located at ~1032 m). Between 1995 and 2014, the NCA headquarters received an average of 936 mm of rainfall a year while Kisima Ngeda received an average of only 469 mm of rainfall a year.

The same precipitation data from the NCAA were used to come to a similar conclusion (Macha, 2019). By averaging the precipitation data from the 23 rain gauges at the NCA over ~two decades, a clear spatial pattern is observed across the study region: the highlands receive more rain than the lowlands (**Figure 16**). Based on these results,

Macha (2019) suggests that the local orography appears to drive rainfall distribution across the NCA (**Figure 16**).

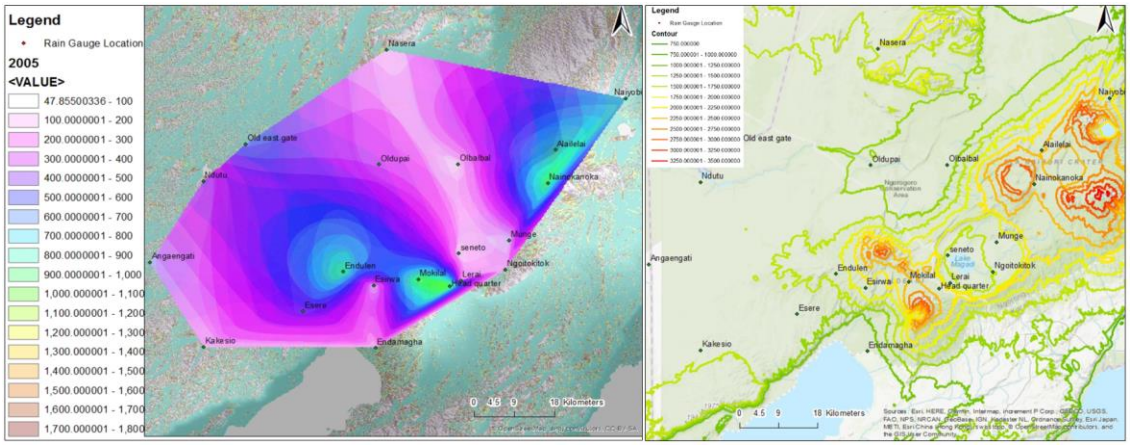

Figure 16. Spatial distribution of average annual rainfall (mm) across the study region (left) compared to regional topography (right). Rain gauge locations are indicated (Macha, 2019).

Interpretation

Based on these rainfall analyses, it is concluded that orography highly impacts the rainfall distribution across the study region. Localities at higher elevations (i.e., NVH) typically receive more rainfall than lowlands localities. These data can provide the basis for better understanding where groundwater recharge likely occurs for future groundwater modeling.

Flow Rate Analysis

<u>DIVER Analysis</u>

Pressure data extracted from the Endulen Hospital DIVER (F0346), Upper Garusi River DIVER (F0790), and the Middle Garusi River DIVER (F1228) (**Figure 9**) were analyzed. Relative stream stage was calculated for the Upper and Middle Garusi River locations (**Figure 17**) by subtracting the barometric pressure recorded at the Endulen Hospital location from the total pressure for each Garusi River DIVER. The barometric

measurements were taken at a different location than the stream bed loggers which adds some complications in interpreting these data, however large flow events appear to have been recorded. There is a baseline stage value at around 50 cm for the Upper Garusi River (**Figure 17A**) and at around 60 cm for the Middle Garusi River (**Figure 17B**) that represents dry conditions at the river. Big peaks above the baseline are interpreted to as flow events. Values below the baseline are interpreted to be artefacts of very dry or hot ambient conditions.

Comparing relative stream stage to local rainfall was not possible at this point due to the unavailability of Endulen rainfall data during the time frame of the stage measurements (2015-2018). However, doing such analyses in the future could aid in understanding the relationship between rainfall events and river flow events and could lead to better groundwater recharge estimates. Recharge for the region is not known, yet it is an essential variable to consider in making groundwater models. However, this method proves to be a relatively cheap and easy way to obtain river stage data when such data is incredibly sparse or nonexistent for the region.

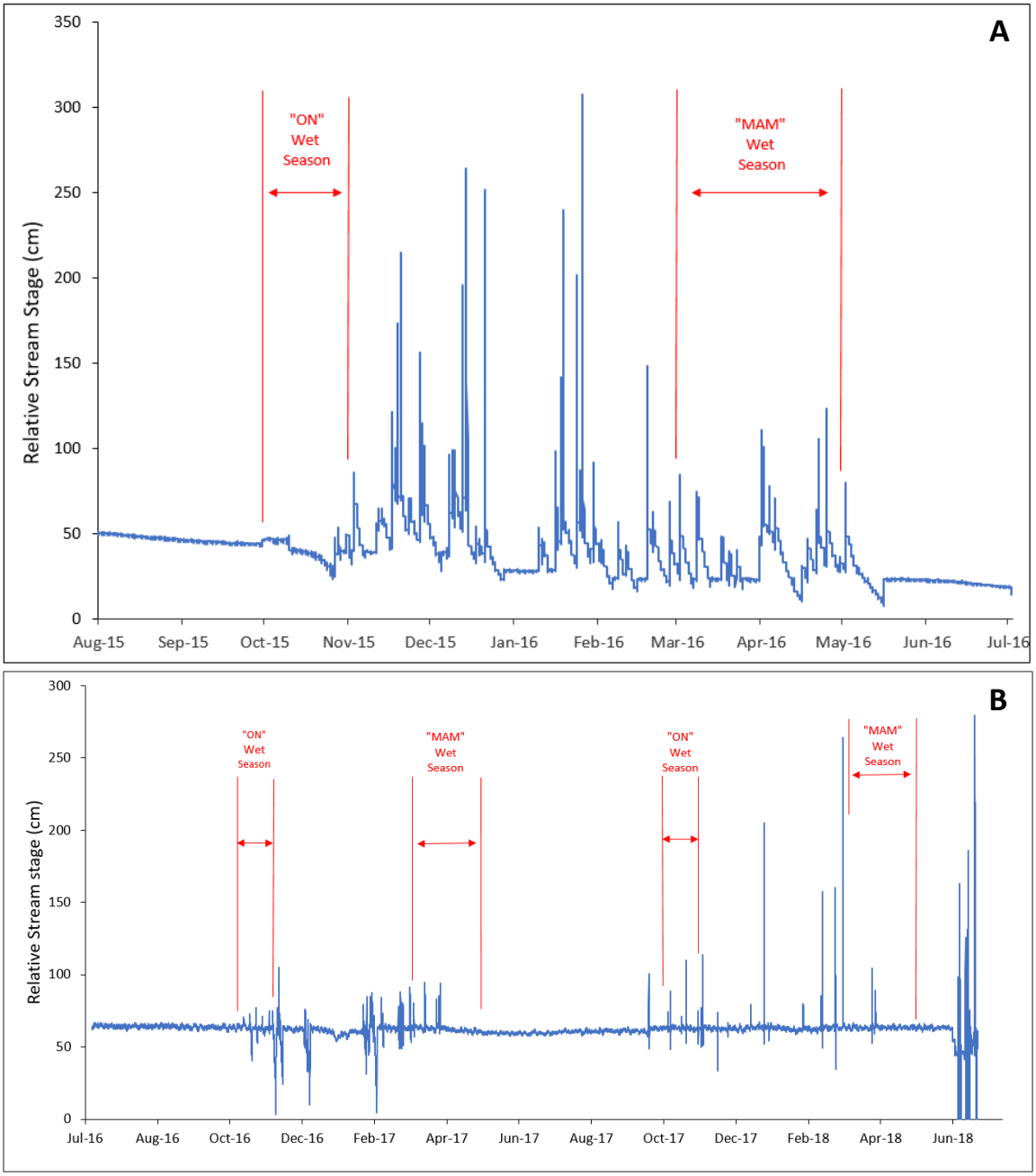

Figure 17. DIVER data used to calculate hourly relative stream stage at two locations along the Garusi River. Relative stream stage was calculated by subtracting the atmospheric pressure recorded at the Endulen Hospital (F0346) DIVER from the total pressure at each Garusi River DIVER. The two yearly wet seasons, ON and MAM, are depicted in red. **(A)** Upper Garusi River (F0790) hourly relative stream stage measurements from August 2015 to July 2016. **(B)** Middle Garusi River (F1228) hourly relative stream stage measurements from July 2016 to July 2018.

Groundwater Modeling in the Lake Eyasi Basin, Tanzania, Africa by Elizabeth Miller

In 2012, Elizabeth Miller generated a groundwater model to estimate the rate of groundwater flow into the wetlands surrounding Lake Eyasi using the MODFLOW program produced by the USGS (a modular finite-difference flow model that solves the groundwater flow equation). Groundwater flow from Mt. Oldeani (~3000 m) to the Kisima Ngeda wetlands (~1000 m), over a 25 km distance, was estimated to take between 1100 to 700 years on average, with differing water table recharge values (**Figure 6**). However, there were several limitations to this model, including a very coarse grid, limited data to calibrate to model (i.e., wells and cores), and an uncertain recharge value. Additionally, there are no precipitation data for Mt. Oldeani; the closest rain gauge is at the NCA park headquarters (**Figure 13**). The report is provided in **Appendix V.**

Longitudinal Profiles

Nine longitudinal profiles (one per spring) were generated using Google Earth Pro (**Appendix VI**). Each longitudinal profile was constructed with assumed recharge at the higher elevation and the spring location at the lower elevation. A summary of the longitudinal profile characteristics is provided in **Table 7**. Endulen, Engina, Mtane, Misilli, and Ngoile are located closest to their respective assumed recharge areas (between 12.4-18.8 km away) and have the highest average slopes (between 8.56-10.38%). Eremet is the farthest from its assumed recharge area (36.3 km) and has the lowest average slope (4.13%). Kisima Ngeda, Garafani, and Esere are located around 25 km from their respective assumed recharge areas and have average slopes between ~6-8%. Endulen, Engina, and Mtane have the smallest hydraulic heads (between 1287-1304 m) and Kisima

Ngeda and Garafani have the largest hydraulic heads (1973 m and 1922 m, respectively). Misilli, Ngoile, Esere, and Eremet have more moderate hydraulic heads (between 1499-1610 m).

Table 7. Longitudinal profile characteristics for the nine springs visited.

Spring Name	Assumed Recharge Area	Recharge Elevation (m)	Spring Elevation (m)	Recharge minus discharge (head, m)	Distance from Recharge to Spring (km)	Average Slope
Endulen	Lemagurut	3102	1815	1287	12.4	10.38%
Engina	Lemagurut	3110	1783	1327	13.4	9.90%
Mtane	Lemagurut	3100	1796	1304	12.4	10.52%
Misilli	Olmoti	2913	1335	1578	16.5	9.56%
Ngoile	Olmoti	2955	1345	1610	18.8	8.56%
Kisima Ngeda	Oldeani	3010	1037	1973	24.9	7.92%
Garafani	Oldeani	3013	1091	1922	25.8	7.45%
Esere	Lemagurut	3101	1592	1509	25.3	5.96%
Eremet	Lemagurut	3096	1597	1499	36.3	4.13%

Geologic Cross-Sections

Geologic cross-sections for most springs were generated based on geologic and topographic data and are provided in **Appendix VII**. Only surficial geology depicted in the cross-sections is known with confidence; assumptions made for unit thicknesses and dips are indicated by dashed lines. Dips of geological units were approximated based on few identified dip measurements provided by the geologic maps (**Appendix I**)**.** Additionally, posited groundwater flow paths are indicated by a blue arrow for each cross-section.

Endulen

The Endulen cross-section stretches ~15 km from Mt. Lemagurut's summit in the northeast, through the town of Endulen (near the Endulen, Engina, and Mtane springs), to ~1 km southwest of Endulen (**Appendix VII**). Rainfall is assumed to primarily infiltrate the surface via the N-S normal fault that cuts through Lemagurut to the west of its summit

(**Figures 2** and **7**). The geologic map indicates the fault is in basalt. It is presumed that groundwater would preferentially flow downslope through the older tuff layer located beneath the younger basalt layer. Based on field properties of the volcanic materials, the tuff is assumed to be more permeable than the basalt. Tuffs in the field were poorly welded together and basalts were solid and massive and, although layered, did not contain extensive jointing. As the literature suggests, poorly welded tuffs can have very high permeabilities, rivaling even fractured basalts (Freeze and Cherry, 1979; Geldon, 2004; Smyth and Sharp, 2006). Upon reaching Endulen, a change in surficial geology from basalt to tuff is presumed to be the factor driving spring formation in the Endulen region. At the Endulen and Mtane springs, groundwater exits into the headwaters of a river channel which has previously been carved out by ephemeral surface waters (**Figure 18**). At the Engina spring, water emanates at a low point in the local topography forming a small spring pool and wetland (**Figure 18**).

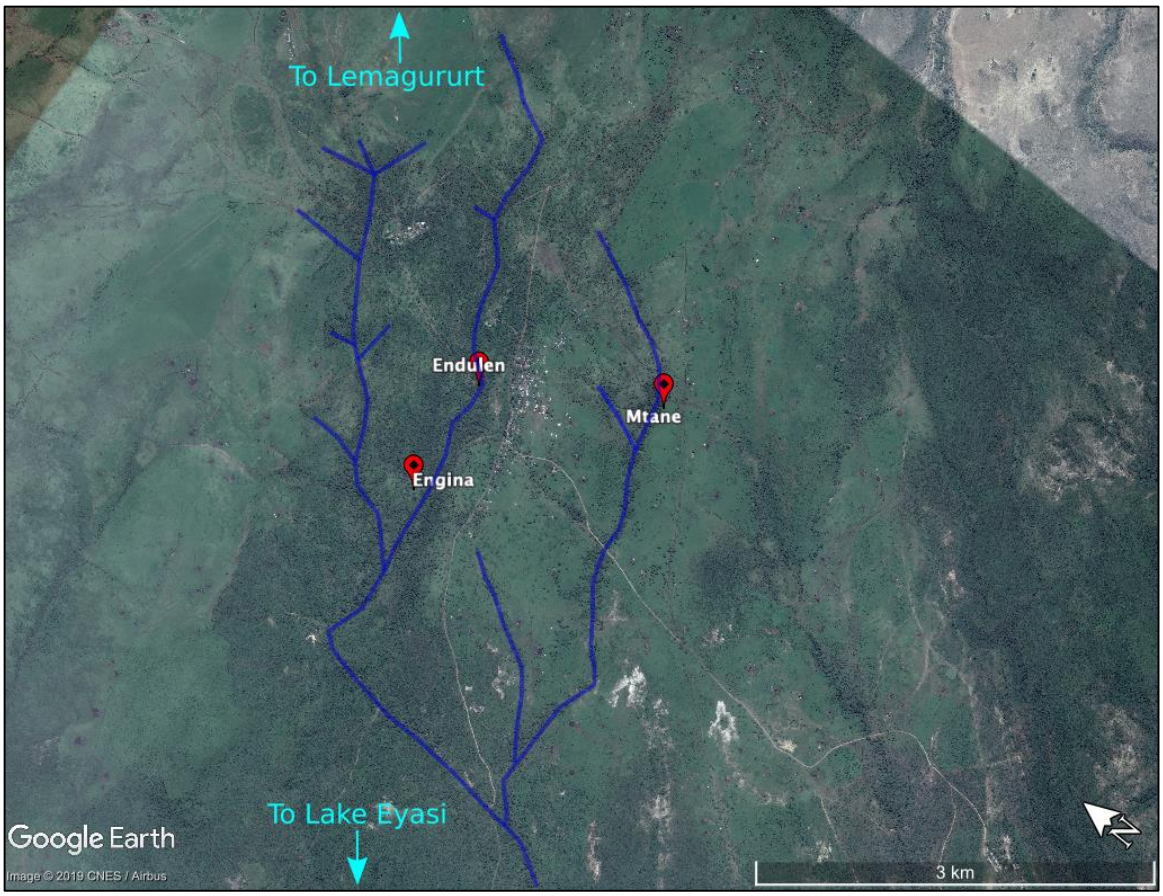

Figure 18. Presumed surface drainage pattern (dark blue tracings) around Endulen, Mtane, and Engina springs inferred from image. Endulen and Mtane springs appear to emanate along first-order ephemeral streams which coalesce into one stream further down slope. Engina emanates in a vegetated area, adjacent to a first-order stream (GoogleEarth Image©2019 CNES / Airbus).

Misilli

The Misilli cross-section extends ~16 km from Mt. Olmoti's crater to the Misilli spring located to the northwest (**Appendix VII**). Rainfall at the summit of Olmoti is assumed to infiltrate the basalt unit at the crater summit and slowly move downslope through this unit. Groundwater is likely to continue to flow through this layer until the topography levels out and the water table intersects the more permeable alluvium. The Ngoile spring is located ~6.5 km to the south of Misilli and based on the similarity in surficial geology and topography, water feeding this spring is assumed to follow a similar path.

Kisima Ngeda

The Kisima Ngeda cross-section extends ~25 km from Mt. Oldeani's summit to the Kisima Ngeda springs located to the southwest (**Appendix VII**). Rainfall sourcing the Kisima Ngeda spring occurs on the 3000 m high Oldeani summit. A portion infiltrates the alluvial fan deposits upslope of Kisima Ngeda springs and wetland complex. Once reaching these more permeable sediments, water is assumed to enter the groundwater system and discharge at local base level along the fringes of Lake Eyasi where it feeds expansive wetlands. At Kisima Ngeda, there is a large (~50 m) basaltic outcrop (plug) directly upslope from the springs which appears to be a key factor controlling groundwater discharge at the Kisima Ngeda location. The basaltic outcrop may affect groundwater flow very locally, impeding flow and creating somewhat of a bottleneck; groundwater quickly flows to the surface around and directly downslope of the basalt. A similar groundwater flow path is presumed to explain the Garafani spring system, located ~5 km southeast of Kisima Ngeda as similar surficial geology and topography exits at the Garafani location.

Esere

The Esere cross-section extends ~29 km from Mt. Lemagurut's summit to the Esere springs located to the southwest (**Appendix VII**). Similarly to the Endulen cross-section, rainfall feeding the Esere springs is assumed to infiltrate the surface via the N-S normal fault that cuts through Lemagurut to the west of its summit. Once again, it is presumed that groundwater reaching the sub-surface would preferentially flow downslope through the older tuff layer located beneath the younger basalt layer because the tuff is assumed to be more permeable than the basalt. However, water feeding the

Esere springs probably flows deeper than water feeding the Endulen springs. Based on the field observations including tufa deposits and highly fractured tuffs at Esere as well as the high temperature, alkalinity, and ion concentrations of the Esere groundwater, springs here are interpreted to be artesian and flow through fractures in the tuff and likely Precambrian basement rock beneath (the tuffs appear to be windblown pyroclastic silts cemented with carbonate that likely form a thin layer above Precambrian basement rock). It is posited that groundwater flows deeply underground until it reaches subsurface fractures which act as conduits to the surface.

Eremet

The Eremet cross-section extends ~40.5 km from Mt. Lemagurut's summit to the Eremet springs located to the southwest (**Appendix VII**). Unlike Endulen or Esere, the older tuff unit is not present at the surface. It is posited that rainfall at the Mt. Lemagurut summit flows over the less permeable basalt layer until it reaches the younger brown and calcareous tuff layer which is presumed to be more permeable allowing the surface water to infiltrate. Groundwater most likely flows close to the surface through the tuff unit until it reaches the Eremet springs region. The relatively warm groundwater temperature (26.8°C) supports this. Based on field observations as well as water conductivity values at Eremet, it appears that an alkaline lake occupied a wide shallow basin where the modern spring-fed wetland is now located (**Figure 19**). Given this information, it is assumed that this area used to be and most likely still acts as a local base level where surface and groundwater have preferential paths to flow toward. Springs emanate from the walls of the presumed pale lake basin and feed an extensive wetland system.

Figure 19. Aerial image of neighboring alkaline lakes (Ndutu and Masek) and the presumed (ephemeral) surface drainage pattern (blue tracings) surrounding the Eremet spring. Eremet Springs discharges along the margin of what is interpreted to be a paleolake basin. The paleolake is presumed to be associated with the other two lakes; the elevation of the paleolake is higher than the elevation at both Lake Masek and Lake Ndutu. Groundwater is presumed to travel to Eremet spring from the southeast (recharged at Mt. Lemagurut) (GoogleEarth Image©2019 CNES / Airbus).

Schematic Conceptual Models of Springs

Based on the integration of the geological, geomorphological, hydrological, and geochemical data collected, three schematic conceptual models (**Figure 20A-C**) were developed to determine modes of spring formation for the nine spring examined in the study region.

(A) Groundwater intersects the surface at local base level

In this scenario, groundwater travels downslope until the topography shallows and the water table intersects the surface and springs form (**Figure 20A**). This typically occurs where the topography shallows out (slope gradient decreases). Alluvium is usually present providing a more permeable layer for groundwater intersecting the surface to discharge from. The springs located along the eastern fringes of Lake Eyasi, including Kisima Ngeda and Garafani, are in this category. Some artesian springs in the vicinity of Kisima Ngeda (Shilling, 2013) would likely fall within this category too. The Misilli and Ngoile springs also are likely to form under similar mechanisms. Even though Misilli and Ngoile are located much closer to their assumed recharge area, the way in which the slope shallows out forming a local base level is considered to be a large driving factor in causing springs to form there. Additionally, the Eremet springs fall under this category. Even though the Eremet springs are nearly double the distance away from their posited recharge source than the other springs in this group, the main driving force here is base level. Eremet is interpreted to be a paleo lake basin, making the area a local base level the main control on discharge (**Figure 19**).

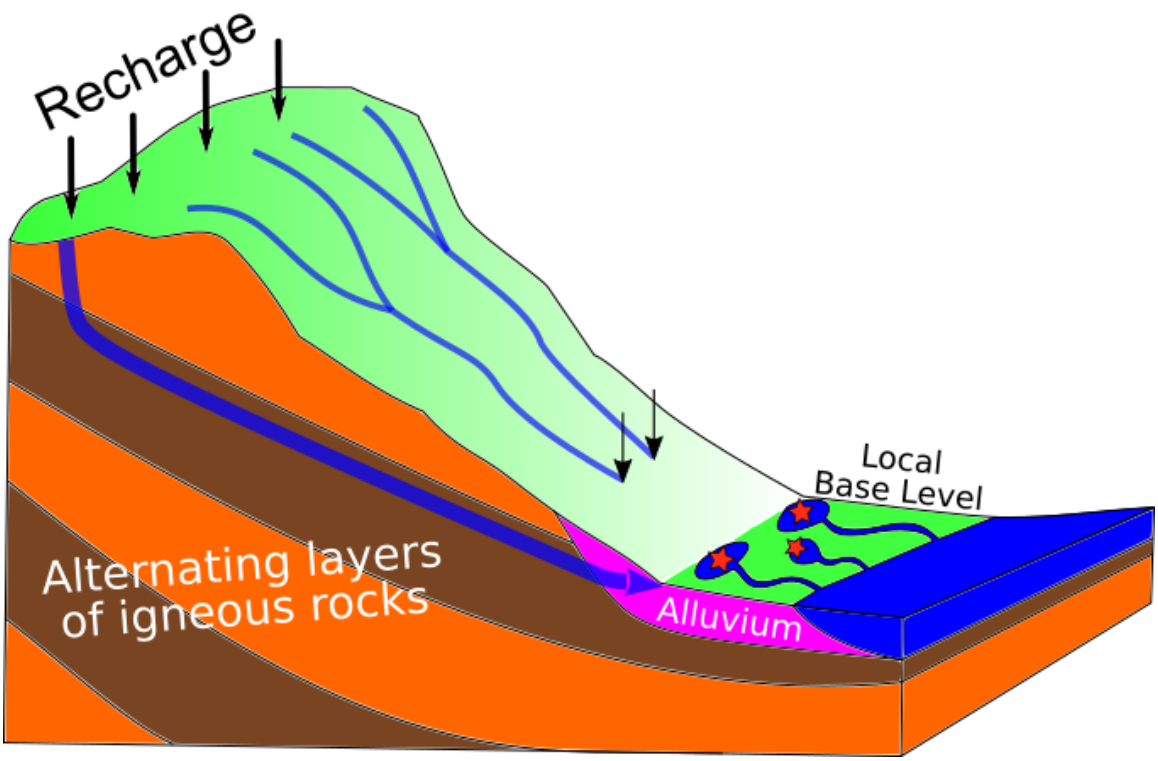

Figure 20A. Spring Schematic Conceptual Model A: Groundwater intersects the surface at local base level. Groundwater recharge, indicated by black arrows, occurs either at the NVH summit or farther downslope where surface water loses to unconsolidated sediments. Groundwater discharges as springs where the slope shallows at the local base level, indicated by red stars.

(B) Permeable rock (aquifer) intersects surface along slope

In some cases, springs discharge along the slope of the volcanoes (**Figure 20B**). Rather than local base level controlling spring formation as in scenario **A**, here the local geology is presumed to be the key factor in spring formation. As more permeable rock (tuff) serving as the local aquifer intersects the surface, groundwater flowing through this unit can discharge to the surface. This is the case for the Endulen springs including Endulen, Mtane, and Engina.

In this region, a basalt unit outcrops upslope. A tuff unit which underlies the basalt unit is assumed to be more permeable and acts as the local aquifer. Further down slope, the tuff is exposed at the surface allowing for groundwater to discharge onto the surface.

Additionally, local factors, such as previously carved out river bed channels by ephemeral surface waters as well as microtopography also plays an important part in spring formation here (**Figure 18**) (Cuthbert et al., 2016).

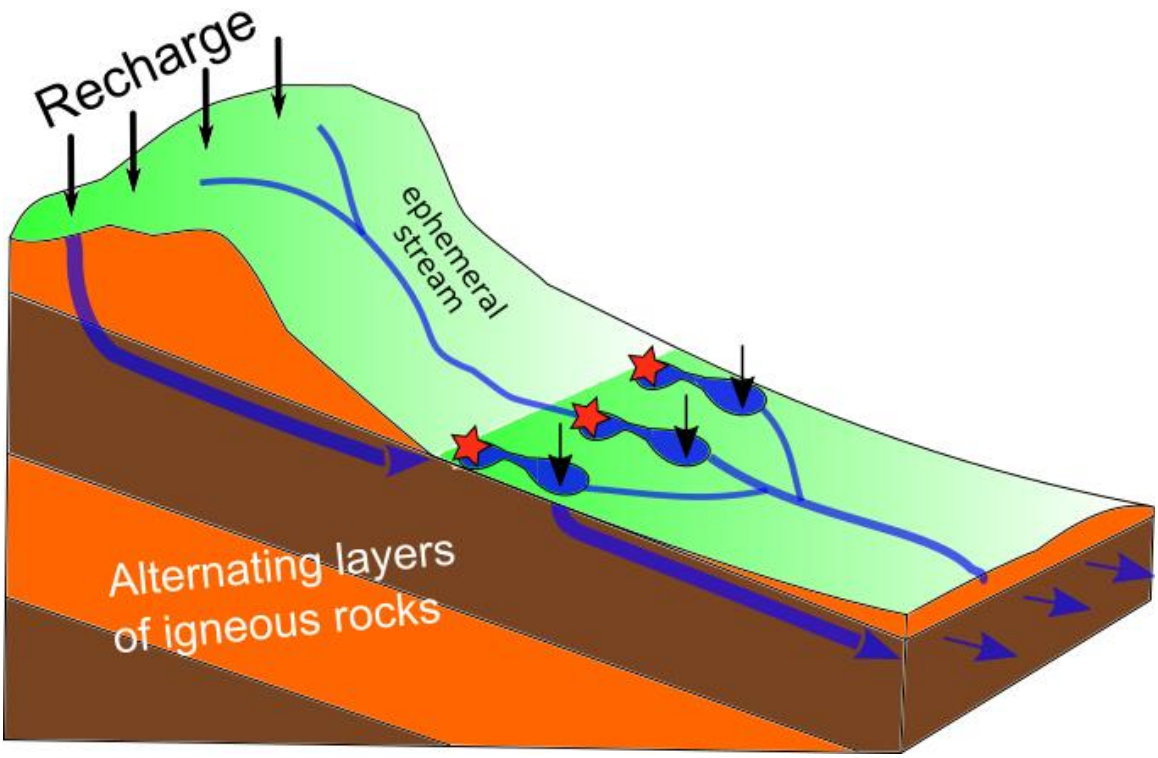

Figure 20B. Spring Schematic Conceptual Model B: Permeable rock (aquifer) intersects surface along slope. Groundwater recharge, indicated by black arrows, occurs either at the NVH summit or where permeable rock (indicated by brown layer) is no longer exposed at the surface. Groundwater discharges as springs along the slope as a seepline where the permeable unit (acting as the local aquifer) intersects the surface, indicated by red stars.

(C) <u>Artesian flow up fractures under hydraulic head</u>

The final scenario in which springs form in this region is groundwater discharge associated with fractured bedrock resulting in artesian flow (**Figure 20C**). In this scenario, where water is under hydraulic head, fractures in rock play an important role in spring formation. This mechanism appears to occur at the Esere spring site. Highly fractured tuffs, paleo tufa mound deposits, unusually warm water temperatures, and high water

conductivity/ alkalinity all support the interpretation of geochemically active groundwater and local rock system.

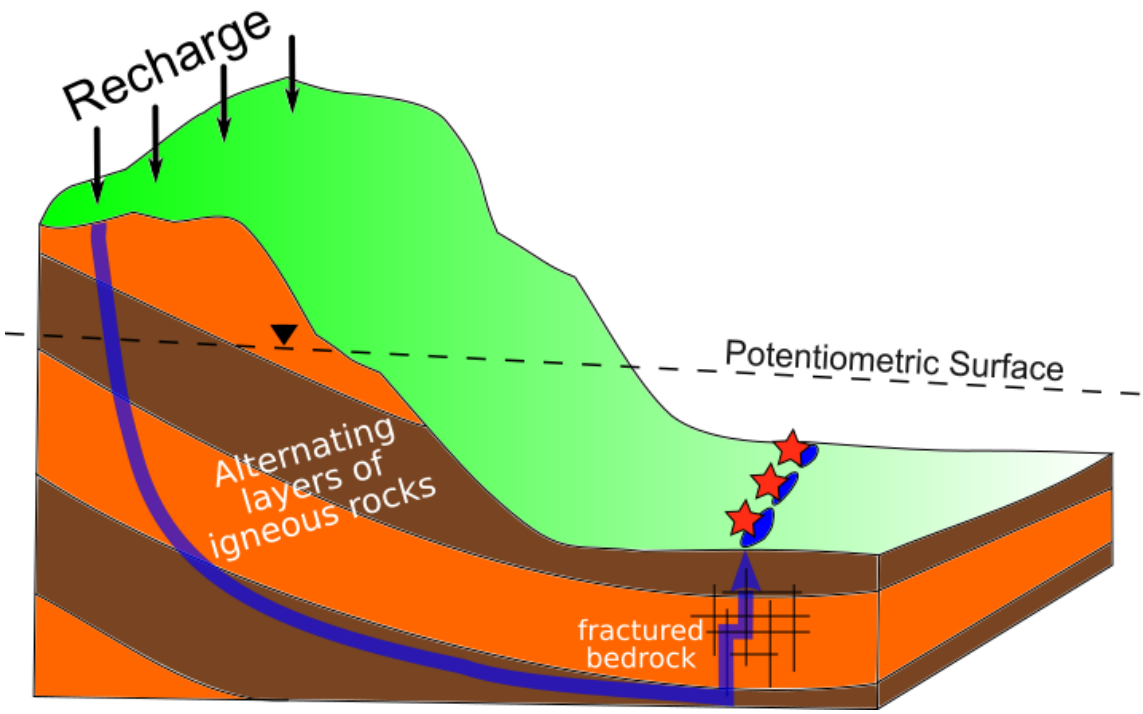

Figure 20C. Spring Schematic Conceptual Model C: Artesian flow up fractures under hydraulic head. Groundwater recharge, indicated by black arrows, occurs at the NVH summit. Groundwater travels deeply until it reaches fractured rock where it flows to the surface under hydraulic pressure and discharges as springs, indicated by the red stars.

DISCUSSION

Very few studies have examined the hydrogeology of Tanzania, let alone of the NVH study area. Studies that are done by consultants or local communities are not available to the public. The lack of geologic (structural and stratigraphic) and hydrologic (recharge or discharge data) for Tanzania in general makes understanding groundwater systems a great challenge. Nevertheless, these systems are heavily relied on for fresh, potable drinking water by thousands of people and millions of animals with little idea as to how long the resources will persist. Even more challenging is the uncertainty that will arise as the global climate changes and impacts these systems (Cuthbert et al., 2017).

The objectives of this study were to present a reconnaissance-level, qualitative description of the physical framework and hydrological inputs of the study region's groundwater system in order to lay the groundwork for future quantitative hydrogeological studies and groundwater modelling. The main goals were to: (1) contribute to understanding the physical framework of the groundwater basin by generating schematic conceptual models of spring formation for nine springs visited; and (2) contribute to understanding the hydrological inputs of the system by examining spatial and temporal rainfall patterns across the study region.

Rainfall Analysis

Rainfall data were analyzed and it was concluded that rain in the study region has distinct temporal and spatial patterns. Two wet seasons, caused by the seasonal migration of the ITCZ driving East African Monsoons, occur in the study region on a yearly basis (ON and MAM), much like most of the East African region (Nicholson, 2017) (**Figure**

15). The MAM wet season was almost always longer and more intense than the ON wet season during any given year and the amount of rainfall produced each year varied significantly. In addition to the seasonal rainfall pattern, an interannual rainfall pattern was observed at the study region in which peak rainfall years occurred nearly every 5 years (**Figure 14**). Based on this analysis, ENSO and IOD can partially explain the interannual variability in rainfall; however, other oceanographic factors not yet determined may also play a role. ENSO and IOD are two climate processes have been credited with maintaining water security of groundwater-dependent communities in Tanzania by recharging the aquifer during multiannual recessions in groundwater levels (Taylor et al., 2012). However, extreme, episodic rainfall events, such as the biannual monsoons and interannual peak rainfall years seen at the study region, are known to be important for recharging aquifers in East Africa and the same can be assumed for the study region (Owor et al., 2009; Taylor et al., 2012; Taylor and Jasechko, 2015).

The orography of the study region was also shown to highly impact the spatial distribution of rainfall in that higher elevations of the NVH received more yearly rainfall on average compared to lower elevations located in the rain shadow of the NVH. Using the same precipitation data, Macha (2019) reported a similar conclusion that local orography appears to drive rainfall distribution across the NCA. Nicholson (2017) has noted topography to be a factor influencing the general precipitation of East African climatology as well. Recharge for the study region likely occurs at topographic highs such as the NVH region.

Surface water and groundwater are both integral parts of the hydrologic cycle. As part of a reconnaissance study of ephemeral streams in the NVH, a novel method was introduced for measuring relative stream stage that can be continued in the future to aid in constraining recharge values. The DIVER program was of limited success but yield some records of discharge in the Garusi River.

The rainfall analysis provided a better understanding of the hydrological inputs of the study region by using novel rainfall data and technologies. Other than the study conducted by Macha (2019), regional rainfall data have not been analyzed or made accessible to the public. Without such data, groundwater recharge, a highly important parameter used in groundwater modeling, is impossible to accurately estimate.

Spring Schematic Conceptual Models

Based on the geological, geomorphological, hydrological, and geochemical data collected, three schematic conceptual models were developed to depict modes of spring formation for the nine springs. The irregular topography of the mountains massif of the NVH, as well as the stratified volcanos results in a variety of modes of spring formation. A commonality that existed was that the source of water for the springs was presumed to be the intercepted moisture transported by east trade winds from the Indian Ocean as well as from evaporation of nearby rift lakes. The major bounding (normal) fault on the west side of Lake Eyasi that cuts through Mt. Lemagurut provides a direct path for precipitation to infiltrate into the subsurface (**Figures 2 and 7A**). Of the volcanic units which comprise the study region, the basalt flows are presumed to have lower

permeabilities than tuff units, which led to the interpretation of tuff layers acting as aquifers. This interpretation was based on field observations of the tuffs and basalts in which tuffs appeared to weakly welded and basalts appeared to be solid and massive. Although basalts are layered, they are not extensively fractured. As the literature suggests, poorly welded tuffs can have very high permeabilities, rivaling even fractured basalts (Freeze and Cherry, 1979; Geldon, 2004; Smyth and Sharp, 2006). Groundwater in this region discharged as springs via a few different mechanisms: (A) where the water table intersects the surface at local base level; (B) where an aquifer is exposed at the surface; and (C) where groundwater moves to the surface under hydraulic head through (locally) fractured rock.

These conceptual models represent a few mechanisms in which groundwater discharges onto the surface as seeps, groundwater-fed rivers, and artesian springs. They can provide a baseline to compare to similar regions around the world. As Burg et al. (2016) point out, parallels in spring formation can be drawn for hydrogeological systems associated with other saline lakes such as the Dead Sea in Israel, the Great Salt Lake in the United States, Lake Asal in Djibuti, Africa, Lake Frome in Australia, and Lake Magadi in Kenya, Africa. The spring complex located along the shore of the Dead Sea is similar to Kisima Ngeda, Garafani, and Eremet in that their formation is primarily controlled by the local base level which contains a saline lake (Burg et al., 2016). Changes in local base level, therefore, will greatly impact these groundwater resources as is being seen with the Dead Sea spring complex (Burg et al., 2016). Developing schematic conceptual models for the study region springs can allow for such parallels to be made and insights to be drawn.

Spring conceptual models developed for the study region are also not unique from previously classified spring conceptual models. Springer and Stevens (2009) developed 12 “Spheres of Discharge” to capture the varying types of springs. Schematic conceptual model A (water table intersects the surface at local base level) would most likely be considered a “Helocrene” spring as this type of spring emerges low gradient wetlands where indistinct or multiple sources of seeping come from shallow, unconfined aquifers. Schematic conceptual model B (aquifer is exposed at the surface) would likely be considered a “Limnocrene” spring as this type of spring emergences from a confined or unconfined aquifer in pool(s). Schematic conceptual model C (fractured material moved groundwater to the surface) would likely be considered a “Mound form” spring as this spring type forms from a mineralized (usually carbonate) mound and is frequently found at magmatic or fault systems (Springer and Stevens, 2009).

Assuming that subsurface geology is similar among volcanoes, it is reasonable to assume that groundwater discharging at the middle of a slope has the shortest residence times whereas groundwater discharging tens of kilometers away at the base of the slope or via fractures have longer residence times. Elizabeth Miller estimated residence times of groundwater flow from Mt. Oldeani to the wetlands along the fringe of Lake Eyasi to take between ~700-1100 (**Appendix V** and **Figure 6**). Preliminary groundwater modeling by Cuthbert and Ashley (2014) suggest spring flows can persist 100s to 1000s of years after groundwater recharge.

Spring settings provide the physical framework for understanding the mechanisms of groundwater supply in the region and mountainous terrains elsewhere. The first

necessary step of any groundwater model requires conceptual qualitative thinking which, for the study region, has not been done before this study. These spring settings lay the groundwork for a more quantitative understanding of the hydrogeology of this region in the future.

CONCLUSIONS

Insufficient data of the groundwater system of the Ngorongoro Volcanic Highland (NVH) region in northern Tanzania makes quantitative groundwater modeling for the region a challenge. Therefore, a reconnaissance-level, qualitative study was undertaken as a primary step in which the physical framework and hydrological inputs of the NVH groundwater system (two categories of data that are essential in making meaningful groundwater models) were described (Kumar, 2015). The contributions to these two categories of data include the following:

1. Analyses of precipitation data indicated that both temporal and spatial rainfall patterns exist for the study region. Other than the study conducted by Macha (2019), regional rainfall data have not been analyzed or made accessible to the public. Without such data, groundwater recharge, a highly important parameter used in groundwater modeling, is impossible to accurately estimate. Conclusions from this analysis include the following:
    a. On an interannual basis, peak rainfall years occur nearly every 5 years. Between 1995 and 2014, there were ~4 years in which the annual rainfall at NCA HQ peaked above the average annual rainfall amount of 912 mm. ENSO and the IOD can partially explain the interannual variability in rainfall at the study region; however other oceanographic features not yet determined may also play a role;
    b. On a yearly basis, the migration of the ITCZ driving East African Monsoons results in two wet seasons to occur: long rains (spring) and short rains

(fall). Between the 2010 and 2014, the NCA headquarters received an average 456 mm of rain over the long rain season (March-May) and 52 mm of rain over the short rain season (October-November).

- Extreme, episodic rainfall events, such as the biannual monsoons and interannual peak rainfall years seen at the study region, are known to be important for recharging aquifers in East Africa and the same can be assumed for the study region (Owor et al., 2009; Taylor et al., 2012; Taylor and Jasechko, 2015).;

c. The variation in the amount of rainfall received across the study region is attributed to its orography: higher elevations such as the NVH receive more rainfall than lower elevations which are located in the rain shadow of the NVH. Between 1995 and 2014, the NCA headquarters received an average of 936 mm of rainfall a year while Kisima Ngeda, situated within the rain shadow of the NVH, received an average of only 469 mm of rainfall a year. Additionally, using rainfall data from 23 rain gauges scattered across the NCA, Macha (2019) determined that local orography appears to drive rainfall distribution across the NCA;

- These spatial and temporal rainfall patterns provide the basis for better understanding where groundwater recharge likely occurs for future groundwater modeling.

2. Water quality of the springs visited were acceptable for drinking based on USEPA drinking standards, with the exception of fluoride concentrations. Esere and Eremet

tended to have higher ion concentrations, temperatures, alkalinities, conductivities, and pH than the other springs.

3. Stable isotope analyses of the groundwater support the idea that springs are sourced by atmospheric moisture coming from the Indian Ocean, but also some recycling from the adjacent rift lakes. Most of the spring water samples fall on the same LMWL, with the exception of Esere and Eremet which are affected by the local geological setting. The LMWL is positioned above the GMWL indicating that the local atmosphere is more arid compared to the global atmosphere, which was found to be common in other regions of East Africa.
4. A novel approach of measuring river stage was used at the Garusi River using DIVERS. Pressure data collected from the Garusi River and local atmosphere were used to determine relative stream stage of the river in which large flow events could be identified. These river stage measurements could not be compared to local rainfall data due to inaccessibility to local rainfall data for relevant years (2015-2018); however, this methodology provides a novel way to make such analyses in the future.
5. Geologic cross-sections indicating surficial geology between several springs (points of discharge) and their assumed recharge areas on topographic high points depict the likely groundwater flow paths for each individual spring. The cross-sections provide the basis for the construction of the spring conceptual models. A commonality that existed was that the source of water for the springs was presumed to be the intercepted moisture transported by east trade winds from both the Indian Ocean as well as from evaporation of nearby rift lakes. The major bounding (normal) fault on

the west side of Lake Eyasi that cuts through Lemagurut provides a direct path for precipitation to infiltrate into the subsurface. Of the volcanic units which comprise the study region, unfractured basalt units appear to have lower permeabilities than tuff units based on the field-based observation of the regular occurrence of groundwater seeps and springs in associated tuffs. The tuff layers are interpreted to be the primary local aquifers.

6. Based on the integration of the geological, geomorphological, hydrological, and geochemical data presented above, three schematic conceptual models of spring formation for the nine springs:
    a. Groundwater intersects the surface at local base level;
    b. Permeable rock (aquifer) intersects surface along slope; and
    c. Artesian flow up fractures under hydraulic head.
7. These spring settings provide the framework for understanding the mechanisms of groundwater supply in the region in the region and mountainous terrains elsewhere. The first necessary step of any groundwater model requires conceptual qualitative thinking which, for the study region, has not been done before this study. The interpretation of geological context of the nine spring settings lay the groundwork for a more quantitative understanding of the hydrogeology of this region in the future.

REFERENCES FOR CHAPTER ONE

Akyoo, B.A., and Nkwame, M. Ngorongoro: A priceless asset: Ngorongoro Conservation Area Authority, p. 3, http://www.ngorongorocrater.org/craters.html (accessed February 2019).

Ashley, G.M., 2014, Geology and geomorphology on northern Tanzania, *in* Museo de la Evolucion Humana ed., The Cradle of Humankind, Burgois, Spain, p. 298–300.

Ashley, G.M., 2007, Orbital rhythms, monsoons, and playa lake response, Olduvai Basin, equatorial East Africa (ca. 1.85-1.74 Ma): Geology, v. 35, p. 1091–1094, doi:10.1130/G24163A.1.

Australian Government Bureau of Meteorology, 2019, Indian Ocean influences on Australian climate: Commonwealth of Australia Bureau of Meteorology, http://www.bom.gov.au/climate/iod/.

Barron, J.J., and Ashton, C., 2007, The effect of temperature on conductivity measurement: a Reagecon technical paper: Reagecon, p. 1–5, www.reagecon.com.

Burg, A., Yechieli, Y., and Galili, U., 2016, Response of a coastal hydrogeological system to a rapid decline in sea level; the case of Zuqim springs - The largest discharge area along the Dead Sea coast: Journal of Hydrology, v. 536, p. 222–235, doi:10.1016/j.jhydrol.2016.02.039.

Camberlin, P., 2018, Climate of Eastern Africa: Oxford University Press USA, 1–52 p., doi:10.1093/acrefore/9780190228620.013.512.

Colcord, D.E., Shilling, A.M., Sauer, P.E., Freeman, K.H., Njau, J.K., Stanistreet, I.G., Stollhofen, H., Schick, K.D., Toth, N., and Brassell, S.C., 2018, Sub-Milankovitch paleoclimatic and paleoenvironmental variability in East Africa recorded by Pleistocene lacustrine sediments from Olduvai Gorge, Tanzania: Palaeogeography, Palaeoclimatology, Palaeoecology, v. 495, p. 284–291, doi:10.1016/j.palaeo.2018.01.023.

Cuthbert, M.O., Acworth, R.I., Andersen, M.S., Larsen, J.R., McCallum, A.M., Rau, G.C., and Tellam, J.H., 2016, Understanding and quantifying focused, indirect groundwater recharge from ephemeral streams using water table fluctuations: American Geophysical Union, v. 51, p. 9127–9140, doi:10.1002/2014WR016259.

Cuthbert, M.O., and Ashley, G.M., 2014, A spring forward for hominin evolution in East Africa: PLoS ONE, v. 9, p. 9, doi:10.1371/journal.pone.0107358.

Cuthbert, M.O., Gleeson, T., Reynolds, S.C., Bennett, M.R., Newton, A.C., Mccormack, C.J., and Ashley, G.M., 2017, Modelling the role of groundwater hydro-refugia in East African hominin evolution and dispersal: Nature Communications, v. 8, p. 1–11, doi:10.1038/ncomms15696.

Dawson, J.B., 2008, The Gregory Rift Valley and Neogene - recent volcanoes of northern Tanzania: London, Geological Society, 102 p.

Deino, A.L., Kingston, J.D., Glen, J.M., Edgar, R.K., and Hill, A., 2006, Precessional forcing of lacustrine sedimentation in the late Cenozoic Chemeron Basin, Central Kenya Rift, and calibration of the Gauss/Matuyama boundary: Earth and Planetary Science Letters, v. 247, p. 41–60, doi:10.1016/j.epsl.2006.04.009.

Deocampo, D.M., and Ashley, G.M., 1999, Siliceous islands in a carbonate sea; modern and Pleistocene spring-fed wetlands in Ngorongoro Crater and Oldupai Gorge, Tanzania: Journal of Sedimentary Research, v. 69, p. 974–979, doi:10.2110/jsr.69.974.

Deocampo, D.M., Berry, P.A., Beverly, E.J., Ashley, G.M., and Jarrett, R.E., 2017, Whole-rock geochemistry tracks precessional control of Pleistocene lake salinity at Olduvai Gorge, Tanzania: A record of authigenic clays: Geology, v. 45, p. 683–686, doi:10.1130/G38950.1.

Ebinger, C., Djomani, Y.P., Mbede, E., Foster, A., and Dawson, J.B., 1997, Rifting Archaean lithosphere : the Eyasi – Manyara – Natron rifts, East Africa: Journal of the Geological Society, London, v. 154, p. 947–960.

Van Essen Instruments B.V., 2017, Micro-Diver:, https://www.vanessen.com/products/water-level/micro-diver.

Foster, A., Ebinger, C., Mbede, E., Rex, D., and Victoria, L., 1997, Tectonic development of the northern Tanzanian sector of the East African Rift System: v. 154, p. 689–700.

Freeze, R.A., and Cherry, J.A., 1979, Groundwater (C. Brenn & K. McNeilt, Eds.): Englewood Cliffs, N.J., Prentice-Hall, Inc.

Le Gall, B., Nonnotte, P., Rolet, J., Benoit, M., and Guillou, H., 2008, Rift propagation at craton margin. Distribution of faulting and volcanism in the North Tanzanian Divergence (East Africa) during Neogene times: Tectonophysics, v. 448, p. 1–19, doi:10.1016/j.tecto.2007.11.005.

Geldon, A.L., 2004, Hydraulic tests of Miocene volcanic rocks at Yucca Mountain and Pahute Mesa and implications for groundwater flow in the southwest Nevada volcanic field, Nevada and California: Geological Society of America, v. 381, doi:http://doi.org/10.1130/SPE381.

Geological Survey of Tanzania, 1961, Angata Salei, Quarter Degree Sheet 39.

Geological Survey of Tanzania, 1964, Endulen, Quarter Degree Sheet 52.

Geological Survey of Tanzania, 1965, Ngorongoro, Quarter Degree Sheet 53.

Geological Survey of Tanzania, 1958, Oldoinyo Ogol, Quarter Degree Sheet 12 S.W.

Global Volcanism Program, 2019, Ol Doinyo Lengai: Smithsonian Institution, http://volcano.si.edu/volcano.cfm?vn=261080.

Hay, R.L., 1976, Geology of the Olduvai Gorge: a study of sedimentation in a semiarid basin: University of California Press, 203 p.

Ikanda, D., and Packer, C., 2008, Ritual vs. retaliatory killing of African lions in the Ngorongoro Conservation Area, Tanzania: Endangered Species Research, v. 6, p. 67–74, doi:10.3354/esr00120.

Indeje, M., Semazzi, F.H.M., and Ogallo, L.J., 2000, ENSO signals in East African rainfall seasons: International Jounrnal of Climatology, v. 20, p. 19–46, papers2://publication/uuid/31B98E48-E7D0-4739-944E-63E6E64DAFFA.

Jan Null, 2019, El Niño and La Niña Years and Intensities: Based on Oceanic Niño Index (ONI): Golden Gate Weather Services, https://ggweather.com/enso/oni.htm (accessed April 2019).

Kashaigili, J.J., 2010, Assessment of groundwater availability and its current and potential use and impacts in Tanzania.

Kijazi, A.L., and Reason, C.J.C., 2009, Analysis of the 2006 floods over northern Tanzania: International Journal of Climatology, p. 955–970, doi:10.1002/joc.

Kisoki, L., 2018, personal commnunication.

Kumar, C.P., 2015, Modelling of groundwater flow and data requirements: International Journal of Modern Sciences and Engineering Technology, v. 2, p. 18–27.

Lechleitner, F.A., Breitenbach, S.F.M., Rehfeld, K., Ridley, H.E., Asmerom, Y., Prufer, K.M., Marwan, N., Goswami, B., Kennett, D.J., Aquino, V.V., Polyak, V., Haug, G.H., Eglinton, T.I., and Baldini, J.U.L., 2017, Tropical rainfall over the last two millennia: Evidence for a low-latitude hydrologic seesaw: Scientific Reports, v. 7, p. 1–9, doi:10.1038/srep45809.

Macgregor, D., 2015, History of the development of the East African Rift System: A series of interpreted maps through time: Journal of African Earth Sciences, v. 101, p. 232–252, doi:10.1016/j.jafrearsci.2014.09.016.

Macha, J., 2019, El Nino Southern Oscillation impacts on rainfall in Ngorongoro Conservation Area.

Magill, C.R., Ashley, G.M., and Freeman, K.H., 2013, Ecosystem variability and early human habitats in eastern Africa: Proceedings of the National Academy of Sciences, v. 110, p. 1167–1174, doi:10.1073/pnas.1206276110.

Mana, S., Furman, T., Turrin, B.D., Feigenson, M.D., and Swisher, C.C., 2014, Magmatic activity across the East African North Tanzanian Divergence Zone: Journal of the Geological Society, v. 172, p. 368–389, doi:10.1144/jgs2014-072.

McHenry, L.J., Mollel, G.F., and Swisher, C.C., 2008, Compositional and textural correlations between Olduvai Gorge Bed I tephra and volcanic sources in the Ngorongoro Volcanic Highlands, Tanzania: Quaternary International, v. 178, p. 306–319, doi:10.1016/j.quaint.2007.01.004.

Melita, A.W., and Mendlinger, S., 2013, The Impact of tourism revenue on the local communities' livelihood: a case study of Ngorongoro Conservation Area, Tanzania: Journal of Service Science and Management, v. 06, p. 117–126, doi:10.4236/jssm.2013.61012.

Mollel, G.F., and Swisher, C.C., 2012, The Ngorongoro Volcanic Highland and its relationships to volcanic deposits at Olduvai Gorge and East African Rift volcanism: Journal of Human Evolution, v. 63, p. 274–283, doi:10.1016/j.jhevol.2011.09.001.

Mollel, G.F., Swisher, C.C., Feigenson, M.D., and Carr, M.J., 2008, Geochemical evolution of Ngorongoro Caldera, Northern Tanzania: Implications for crust-magma interaction: Earth and Planetary Science Letters, v. 271, p. 337–347, doi:10.1016/j.epsl.2008.04.014.

NCAA, 2016, Water resource investigation stage 1.

Nicholson, S.E., 2017, Climate and climatic variability of rainfall over eastern Africa: American Geophysical Union, p. 590–635, doi:10.1002/2016RG000549.

Olago, D., Opere, A., and Barongo, J., 2009, Holocene palaeohydrology, groundwater and climate change in the lake basins of the Central Kenya Rift: Hydrological Sciences Journal, v. 54, p. 765–780, doi:10.1623/hysj.54.4.765.

Owor, M., Taylor, R.G., Tindimugaya, C., and Mwesigwa, D., 2009, Rainfall intensity and groundwater recharge: Empirical evidence from the Upper Nile Basin: Environmental Research Letters, v. 4, doi:10.1088/1748-9326/4/3/035009.

Qorro, E., 2018, Ngorongoro attracts more than 6000 tourists in year: IPPMedia.com, https://www.ippmedia.com/en/news/ngorongoro-attracts-more-600000-tourists-year.

Renaut, R.W., Owen, R.B., and Ego, J.K., 2017, Geothermal activity and hydrothermal mineral deposits at southern Lake Bogoria, Kenya Rift Valley: Impact of lake level changes: Journal of African Earth Sciences, v. 129, p. 623–646, doi:10.1016/j.jafrearsci.2017.01.012.

Rietti-Shati, M., Yam, R., Karlen, W., and Shemesh, A., 2000, Stable isotope composition of tropical high-attitude fresh-waters on Mt. Kenya, Equatorial East Africa: Chemical Geology, v. 166, p. 341–350, doi:10.1016/S0009-2541(99)00233-8.

Ritter, D.F., Kochel, R.C., and Miller, J.R., 2011, Process geomorphology: Long Grove, Illinois, Waveland Press, Inc., 652 p.

Ryan, W.B.F., Carbotte, S.M., Coplan, J.O., O'Hara, S., Melkonian, A., Arko, R., Weissel, R.A., Ferrini, V., Goodwillie, A., Nitsche, F., Bonczkowski, J., and Zemsky, R., 2009, Global multi-resolution topography synthesis, Geochem. Geophys. Geosyst.:, doi:10.1029/2008GC002332.

Sawere, P.C., 2015, Report on hydrogeological and geo-electrical survey for selection of potential sites for borehole drilling for provision of water supply to Laetoli Hominin Footprints Museum.

Scoon, R.N., 2018, Geology of national parks of central/southern Kenya and Northern Tanzania: Cham, Springer International Publishing, doi:10.1007/978-3-319-73785-0.

Shilling, A.M., 2013, Characterization of groundwater discharge sites using remote sensing and wetland cores, Lake Eyasi Basin, Tanzania, Unpublished MS Thesis: Rutgers The State University of New Jersey - New Brunswick, doi:1535926.

Smyth, R.C., and Sharp, J.M., 2006, The hydrology of tuffs: Geological Society of America Special Paper 408, p. 91–111, doi:10.1130/2006.2408(4.1).

Springer, A.E., and Stevens, L.E., 2009, Spheres of discharge of springs: Hydrogeology Journal, v. 17, p. 83–93, doi:10.1007/s10040-008-0341-y.

Stollhofen, H., Stanistreet, I.G., McHenry, L.J., Mollel, G.F., Blumenschine, R.J., and Masao, F.T., 2008, Fingerprinting facies of the Tuff IF marker, with implications for early hominin palaeoecology, Olduvai Gorge, Tanzania: Palaeogeography, Palaeoclimatology, Palaeoecology, v. 259, p. 382–409, doi:10.1016/j.palaeo.2007.09.024.

Tanzania Meteorological Agency, 2019, United Republic of Tanzania; Tanzania Meteorological Agency; ISO 9001:2015 Certified Aviation Meteorological Services:, http://www.meteo.go.tz/ (accessed February 2019).

Taylor, R.G., and Jasechko, S., 2015, Intensive rainfall recharges tropical groundwaters: Environmental Research Letters, v. 10, p. 124015, doi:10.1088/1748-9326/10/12/124015.

Taylor, R.G., Todd, M.C., Maurice, L., Nahozya, E., Sanga, H., and MacDonald, A.M., 2012, Evidence of the dependence of groundwater resources on extreme rainfall in East Africa: Nature Climate Change, p. 1–11, doi:10.1038/nclimate1731.

Tierney, J.E., Smerdon, J.E., Anchukaitis, K.J., and Seager, R., 2013, Multidecadal variability in East African hydroclimate controlled by the Indian Ocean: Nature, v. 493, p. 389–392, doi:10.1038/nature11785.

USEPA, 2018, 2018 Edition of the Drinking Water Standards and Health Advisories:, doi:EPA 822-S-12-001.

Wolanski, E., and Gereta, E., 2001, Water quantity and quality as the factors driving the Serengeti ecosystem, Tanzania: Hydrobiologia, v. 458, p. 169–180, doi:10.1023/A:1013125321838.

CHAPTER TWO

WETLAND FACIES ACROSS BIOMES OF THE WORLD

ABSTRACT

Wetlands cover approximately 8.6 percent of the Earth's land surface and are found on every continent except Antarctica and in every climate, from the tropics to the arctic. However, wetland processes and their deposits are poorly understood; they are a relatively new field of research among geologists. There is no consensus on a facies model for paleowetlands. This may be due to the fact that biological and sedimentological processes vary by biome and thus wetland deposits differ worldwide.

This research tests the hypothesis that wetlands have distinct facies in the geologic record and that their facies can be even further distinguished by the mean annual temperature (MAT) and mean annual precipitation (MAP) of their environment. Modern wetland deposits from each of the eight terrestrial biomes of the world (i.e. tundra, subarctic taiga, temperate forest, temperate grassland, temperate desert, tropical rain forest, tropical savanna, and tropical desert), representing varying MAT and MAP, were explored to determine if characteristics (i.e., sediments, flora/fauna fossils, paleosols, physical and geochemical features such as sedimentary structures, color, texture, redoximorphic- features, etc.) can distinguish these biomes. Holocene paleowetlands records provide the data to group deposits into their representative biomes. Analyzing wetland deposits across biomes allows for general summaries of the depositional environment (i.e., a facies model) to be proposed which is useful for: interpreting the system it represents, providing a norm for comparison purposes, predicting new geological situations, and teaching and learning about environments.

While this study determines that there are distinct similarities among wetland deposits across the world, a novel facies model that categorizes wetland deposits into three types by climate (i.e., Tundra/Taiga, Desert, and Grassland/Forest Wetlands) is proposed. An improved understanding and identification of the sedimentary records by wetlands is crucial for anticipating the future of these diverse yet fragile environments.

INTRODUCTION

Wetlands exist in land areas that are saturated with water for all or at least part of the year, occupying a transitional environment between terrestrial and aquatic ecosystems (National Research Council, 1995; Tooth and McCarthy, 2007). They perform several critical functions from regulating water, energy, carbon and nutrient cycling to attenuating flood water, improving water quality, creating recreation space, and serving as refugia for biodiversity (LePage et al., 2012). Although the values of wetlands are highly recognized and appreciated today, they have not always been identified as such until more recently and are a relatively new field of study, especially among geologists (Mitsch and Gosselink, 2007). In fact, classic facies model textbooks (i.e., James and Dalrymple, 2010) have yet to mention wetlands as environments of deposition.

The eclectic benefits wetlands provide for society and nature make wetland research interdisciplinary. Ecologists, biologists, and hydrologists are some of the main contributors to wetland research and while their contributions provide unique perspectives on wetlands, their focus is primarily on their present function and formation, whereas little attention has been given to the long-term geological perspective on wetlands (Tooth and McCarthy, 2007). Furthermore, wetland processes occur in the "Critical Zone", Earth's permeable near-surface layer where rock, soil, water, air, and living organisms interact involving a plethora of processes (CZO, 2012). Because wetlands exist in a such a complex setting where many processes are at work, such as atmospheric processes from above and water-saturation processes from below, the geologic deposits are complex, making interpretation of the deposits difficult (Ashley et al., 2013).

Wetlands currently cover approximately 8.6% of the Earth's land surface (LePage et al., 2012) including swamps, bogs, marshes, mires, fens, and other wet environments (Mitsch and Gosselink, 2007). Since wetlands are land drainage features and exist wherever there is a locally positive near-surface water balance at least seasonally (Tooth and McCarthy, 2007), they occur worldwide (**Figure 1**). In fact, they exist on every continent, except Antarctica, and in every climate from the tropics to the arctic (Mitsch and Gosselink, 2007). However, as the global climate inevitably changes, the extent and locations of wetlands across the planet will also change. Before one can begin to predict how wetlands may respond to global climate change, a better understanding of these systems is needed.

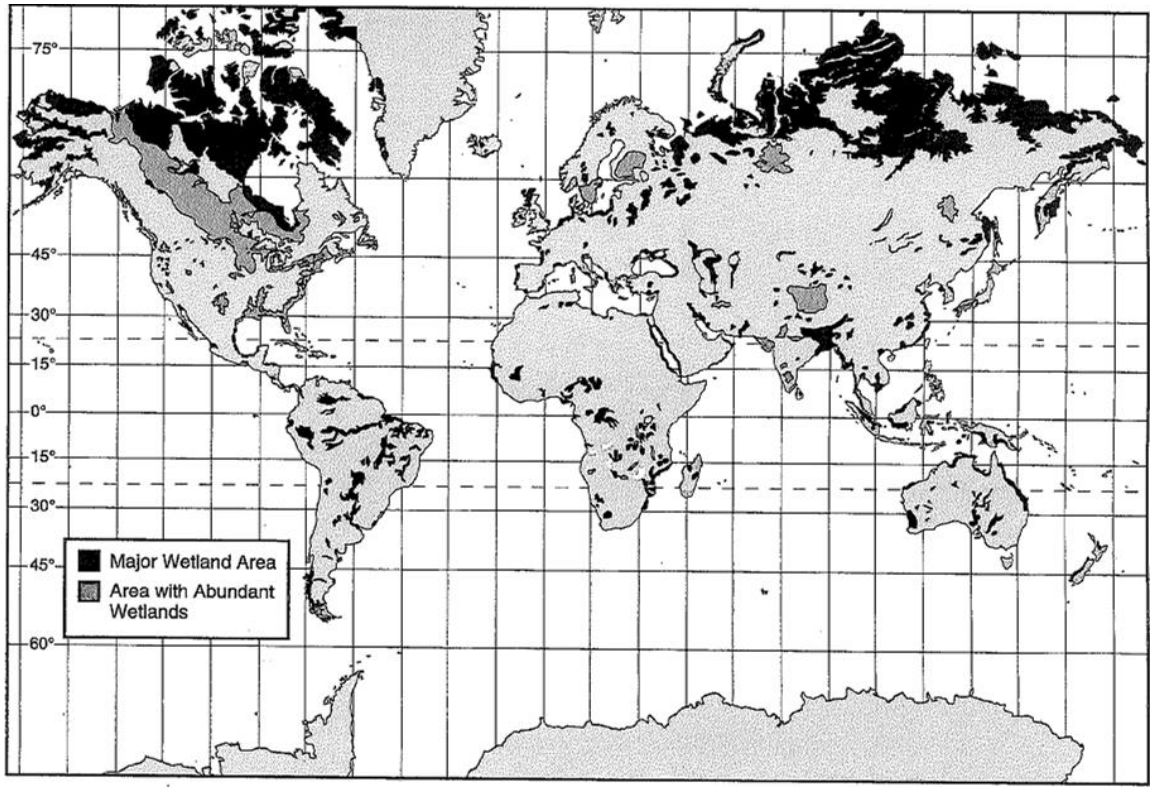

Figure 1. Distribution of the world's wetlands. Modified from Mitsch and Gosselink (2007).

Scientists cannot peak into a crystal ball to see how wetlands will change in the future; however, they are able to generate models for the future that can be constrained with wetland observations from the present and past. How close these models will be to reality is a function of the limited wetland data and observations that have been collected over the past few hundred years (LePage et al., 2012; Ashley et al., 2013). There is a need to better understand the past through more observational research in order to make more meaningful predictions for the future.

The geological record is an archive of minerals and organic matter/ plant and animal remains which act as proxies providing clues to reconstructing past environments. Some proxies (such as organic matter, fossils, ash layers, etc.) can be dated, allowing for the time of deposition to be determined as well. Through the examination of fossils of flora/fauna and paleosol physical and geochemical features in paleowetland deposits, distinguishing characteristics of wetlands can be defined (LePage et al., 2012). However, there is currently no consensus among geologists as to what features from the geologic record are characteristic of paleowetlands. Fortunately, since wetlands exist worldwide and can be found in deposits from every biome, representing environments in terms of temperature and precipitation (**Figure 2**), these deposits can be examined for distinguishing characteristics across biomes.

The objectives of this paper are to: (1) characterize modern wetland deposits in the lithologic record; (2) determine if a unique set of characteristics can be attributed to wetland deposits distinguishing them from all other depositional environments; and (3)

compare and contrast wetland deposits from different terrestrial biomes of the world to see if wetland deposits can be even further distinguished by MAT and MAP.

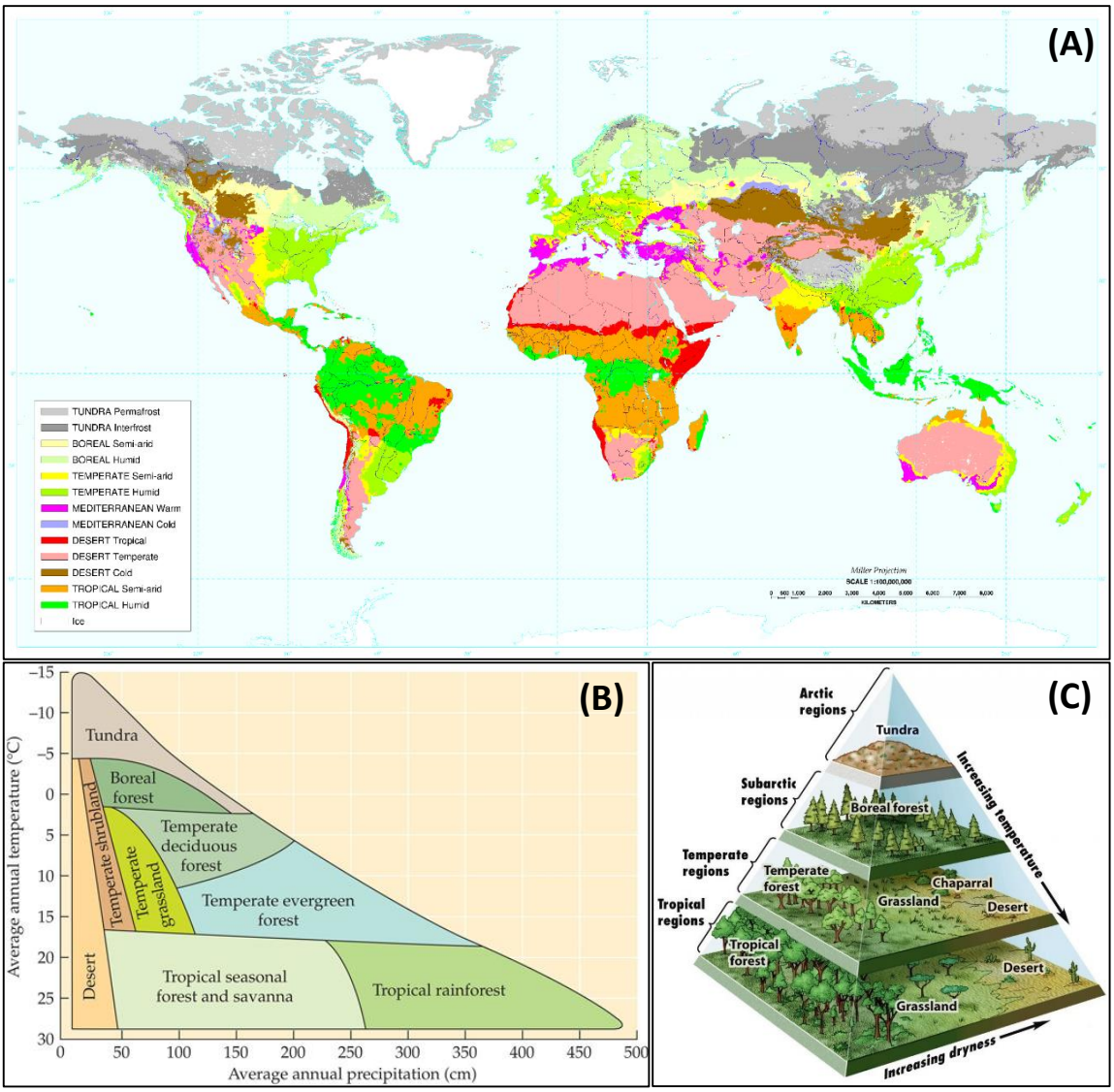

Figure 2. Biomes. (**A**) Map showing the distribution of the world's biomes (USDA, 2003). (**B**) Graph showing MAP (centimeters) versus MAT (degrees Celsius) for the biomes of the world (Cain et al., 2014). (**C**) Conceptual model of biomes in relation to temperature and dryness (Vnaya, 2016).

BACKGROUND

Facies Models

Sedimentary successions exposed in outcrop or obtained by coring have physical and, biological, and chemical features (i.e., typical sedimentary structures, texture, or type of fossil) which can be interpreted to infer the processes which created them and thus the environment of deposition in which the deposit was formed. This technique is termed facies analysis and is commonly used as an effective method to tease information out of the sedimentary record. Over the years, it has become apparent that certain environments can be associated with particular assemblages of facies (Walker, 1984). Such realizations have enabled sedimentary geologists to generate facies models, or general summaries of depositional environments, which can be used for several purposes: (1) to interpret the system it represents; (2) to provide a norm for comparison purposes; (3) to act as a framework and guide for further observations; (4) to predict new geological situations; and (5) to aid in teaching and learning about environments (**Figure 3**) (James and Dalrymple, 2010).

The processes leading to the creation of a facies model are depicted as **Figure 3.** In general, creating a facies model involves the subjective assessment of commonalities that can be found among all modern and ancient case studies of a certain environment, with less regard to local details and more of a focus to the overarching general characteristics of the system (James and Dalrymple, 2010).

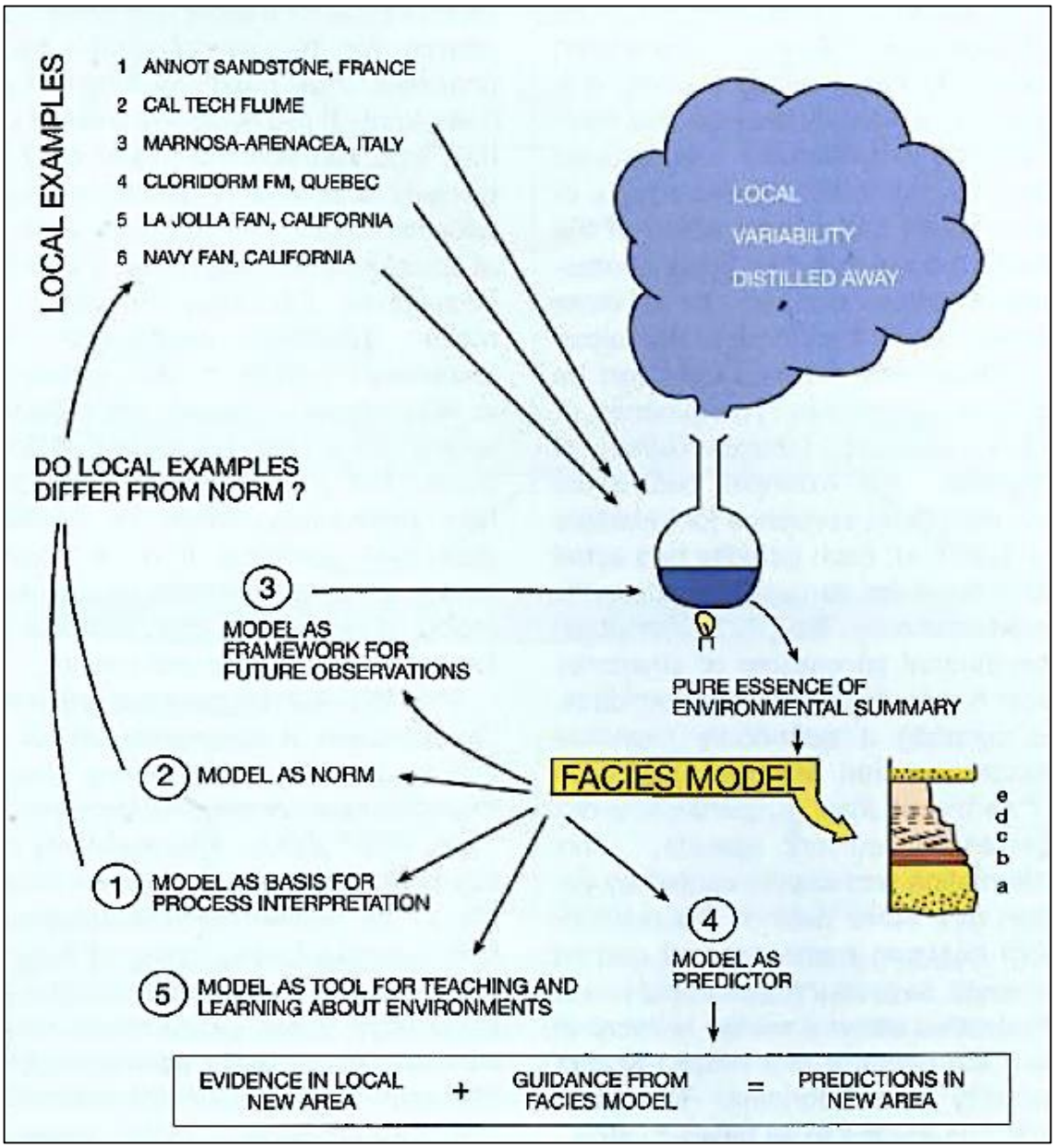

Figure 3. Distillation processes involved in generating a facies model and the uses of a facies model. Modified from Walker (1984).

Wetland Characterizations

During the last few decades there has been a growing realization in the geological community that wetlands are an important environment on modern landscapes. Four studies summarized below reveal previous geological wetland characterizations.

(1) Fossil Spring Deposits in the Southern Great Basin and their Implications for Changes in Water-Table Levels near Yucca Mountain, Nevada, during Quaternary Time (Quade et al., 1995)

Quade et al. (1995) were the first to identify evidence of the water table (i.e., springs, wetlands) in the geologic record. They focused on Quaternary deposits at the Yucca Mountains in Nevada which were previously misinterpreted as lacustrine in origin. By examining the deposits and mollusk fauna found within them, they identified many characteristics to support the idea that these deposits represent a spring/ wet environment. They identified deposits associated with a high water table as the "phreatophyte flat" as consisting of mainly pale brown sand-silt entrapped by dense stands of phreatophytes covering valley bottoms. Deposits associated with springs discharge and wetlands were identified to consist of pale green to white muds, containing a mix of aquatic, semiaquatic, and moist terrestrial mollusks (Quade et al., 1995). While they did not refer to these deposit descriptions as "facies model" for spring or wetland environments, they did make the association between common characteristics in the sedimentary record and environment of deposition, paving the way for future facies models. They are credited to be the first to identify this whole new class of sediments which prior published literature failed to recognize or misinterpreted as lacustrine.

(2) Wetlands in Drylands: Geomorphological and Sedimentological Characteristics, with Emphasis on Examples from Southern Africa (Tooth and McCarthy, 2007)

Focusing primarily on examples in southern Africa, Tooth and McCarthy (2007) argue that wetlands that exist in drylands (as opposed to those existing in humid regions) can be shown to impart distinctive features in sedimentology and geomorphology. It is

argued that wetlands in drylands differ from humid (tropical and temperate) wetlands in that they have more frequent and/or longer periods of desiccation, channels that often reduce in size and sometimes disappear downstream, higher levels of chemical sedimentation, more frequent fires (reducing the potential for thick organic deposits and promoting aeolian activity), and longer timescales of development (extending far back into the Pleistocene) (Tooth and McCarthy, 2007).

(3) Groundwater-Fed Wetland Sediments and Paleosols: It's All About the Water Table (Ashley et al., 2013)

Ashley et al. (2013) argue that palustrine wetlands (including a range of semi-permanently to permanently inundate nontidal environments) are likely to leave a permanent paleosol record. Their premise was that groundwater provides a consistent, persistent water source to palustrine wetlands during short-term and long-term climate fluctuations. This sustained water supply renders them most likely to create permanently saturated or flooded environments where hydric soils and hydrophytic vegetation are most likely to develop, and thus, most likely to be preserved in the geologic record. Aqueous geochemical features and biota reflective of waterlogged environments are indicated to be distinctive among groundwater-fed wetland deposits. Furthermore, a combination of the sedimentological (old to young) as well as pedological approach (from the surface downwards) to viewing wetland deposits is argued to lead to a better understanding of wetlands records.

(4) Desert Wetlands in the Geologic Record (Pigati et al., 2014)

Based on their experience working in desert wetlands in the American Southwest and the Atacama Desert of northern Chile, Pigati et al. (2014) argue that desert wetlands

create distinct depositional environments which can be identified in the geologic record as groundwater discharge (GWD) deposits. Although GWD deposits were first identified by Quade et al. (1995) in the southern Great Basin of Nevada, Pigati et al. (2014) built upon that by arguing that such deposits can be identified as a facies model for desert wetlands. Such GWD deposits are argued to have distinct physical characteristics, sedimentology, and biota (Pigati et al., 2014). The deposition of clastic sediments, groundwater precipitates, and organic matter as well as the preservation of ostracods and gastropods are the fundamental signatures of such deposits that are unique to the depositional environment of a desert wetland.

STUDY SITES & METHODS

Modern and ancient wetland deposits from across the world were identified in published documents. Study sites were chosen from each biome of the world including tundra, subarctic taiga, temperate forest, temperate grassland, temperate desert, tropical rainforest, tropical savanna, and tropical desert (**Figure 4**). Information was compiled for each wetland site including wetland type and formation, local climatic setting, lithology/sedimentology, paleontology/biology, geochemistry, and wetland age.

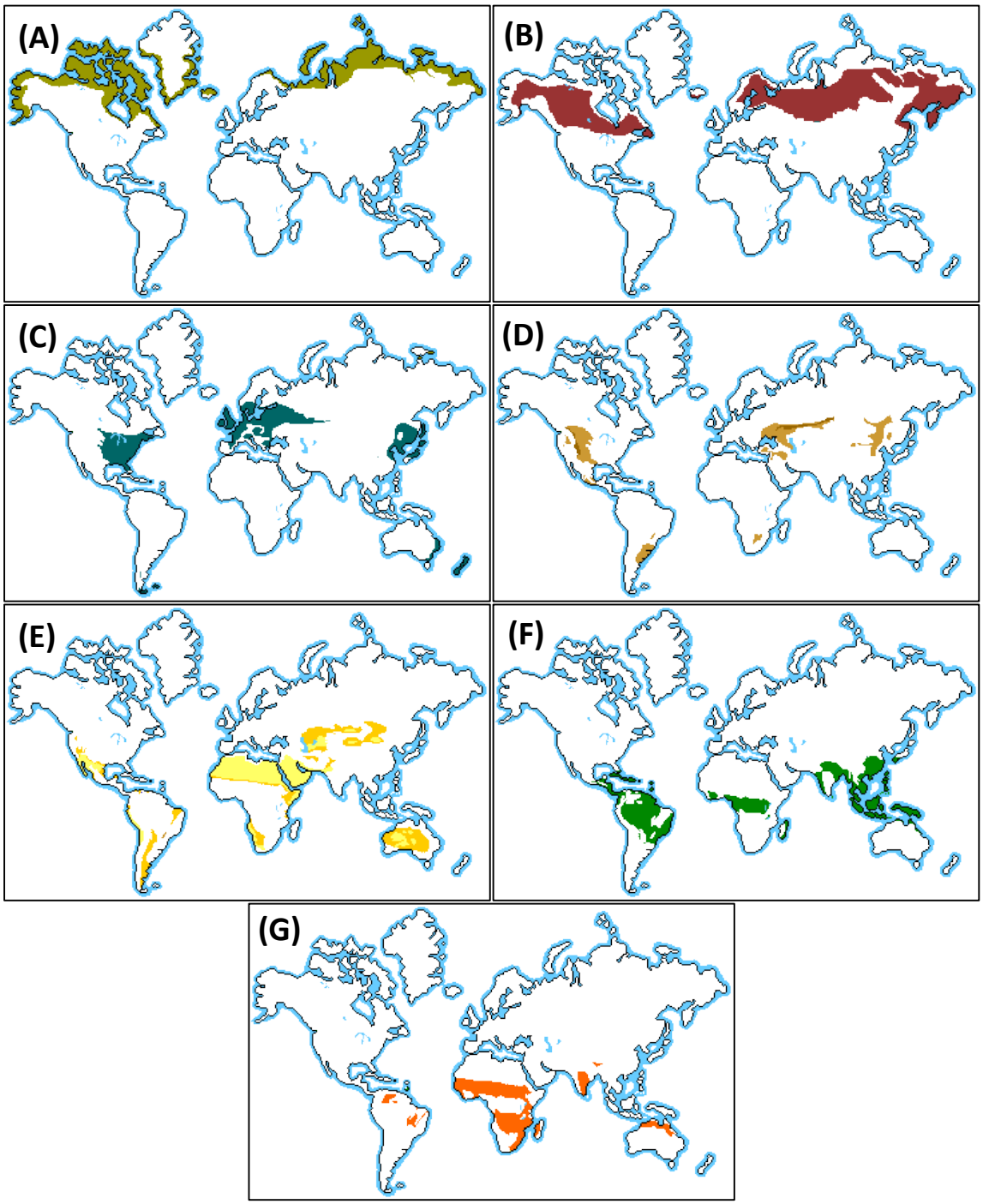

Figure 4. Location of biomes on a world map. (**A**) Tundra. (**B**) Taiga. (**C**) Temperate forest. (**D**) Temperate grassland. (**E**) Desert. (**F**) Tropical rainforest. (**G**) Tropical savanna. Modified from ISC-Audubon (2018).

RESULTS & INTERPRETRATIONS

Observations and Interpretations of Study Sites by Biome

While earlier studies (Quade et al., 1995; Tooth and McCarthy, 2007; Ashley et al., 2013; Pigati et al., 2014) provide a examples of previous attempts at distinguishing wetlands by climate, they focus primarily on wet versus dry wetlands and neglect to include the effects of temperature. By examining wetlands across all biomes (the objectives of this study) comparisons and distinctions can be made not only between wet and dry wetlands, but also between hot and cold wetlands (**Figure 2**).

The paleowetland/ wetland data collected for this paper are provided as a summary in **Table 1**. The complete list of the paleowetland/ wetland data, including information such as biome characterization, wetland type and formation, local climatic setting, lithology/sedimentology, paleontology/biology, geochemistry, and wetland age is provided in **Appendix VIII**. The following sub-sections describe the observations of the collected data for each wetland by biome and the interpretations that were drawn for each biome.

Table 1. Summary table of distinguishing features of wetland deposits based on referenced literature.

Biome	Reference	Study Site	Distinguishing Feature(s)?
Tundra	Pendea et al., 2017	Kamchatka Peninsula, NW Pacific seaboard, Russia	*Sphagnum* peat; lack of trees or deep roots, Peat-rich permafrost, low mineral percentages, many microfossil mosses
	Ellis and Rochefort, 2006	Simirlik National Park, part of the Canadian Arctic Archipelago	
Subarctic Taiga	Spooner et al., 2017	Baltzer Bog, Annapolis Valley, Coldbrook, Nova Scotia, Canada	*Sphagnum* peat; intermediate woodland layers (Black Spruce)
	Spooner et al., 2017	Big Meadow Bog, Briar Island, SW Nova Scotia, Canada	
	Lamentowicz et al., 2015	Baltic Bog, N Poland	
Temperate Forest	Coon, 1997	Ellison Park wetland, mouth of Irondequoit Creek, Rochester, New York	Organic material (**?**)
	Woodward et al., 2014	Little Llangothlin, New England Tablelands, E Australia	
Temperate Grassland	Norström et al., 2009	Braamhoek wetland, E Free State, South Africa	**?**
Temperate Desert	Sivan et al., 2011	Carmel coast, N Israel	Groundwater discharge (GWD) deposits: clastic sediment, groundwater precipitates, "black mats", and biota including ostracods, gastropods, foraminifera
	Pigati et al., 2014	Cerros Negros, Arizona Dove Springs, California Murray Springs, California Salar de Punta Negra, Chile Rio Salado, Chile	
	Li et al., 2015	Ulan Buh Desert, SW Inner Mongolia	
Tropical Rain Forest	Beach et al., 2009	Maya lowlands, Yucatan Peninsula and adjacent lowlands in Mexico, Belize, & Guatemala	Calcareous clayey sediments with high amounts of gypsum and organic matter; smectite clays (**?**)
Tropical Savana	Ashley et al., 2004	Loboi Swamp, Kenya, Africa	Redoximorphic features in clay; vegetation typical of semi-arid environment with a fluctuating water table (**?**)
	Irion et al., 2016	Araguaia River floodplain, S Amazon basin	
Tropical Desert	Quade et al., 2008	Salar de Punta Negra, central Atacama Desert, northern Chile, W slope of Andes	Groundwater discharge (GWD) deposits: clastic sediment, groundwater precipitates, less organic material, and biota including gastropods, sponges & diatoms; chemical sedimentation; evidence of frequent fires resulting in thin organic accumulations; desiccation features; redoximorphic features in clay
	Tooth and McCarthy, 2007	Okavango Delta, Botswana, Africa	
	O'Brien and Burne, 1994	The Great Cumbung Swamp, E Australia	

Tundra

The tundra biome (**Figure 4A**) is the world's coldest and driest biome. According to the Köppen Climate Classification (ISC-Audubon, 2018), this biome is located between latitudes 55° to 70° North, has an average annual temperature of -28°C, and receives only about 15 to 25 cm of precipitation a year, mostly in the form of snow. The picture below of a modern tundra wetland in Greenland depicts the typical landscape of a tundra wetland where mosses are present, but diversity in vegetation is limited (**Figure 5A**).

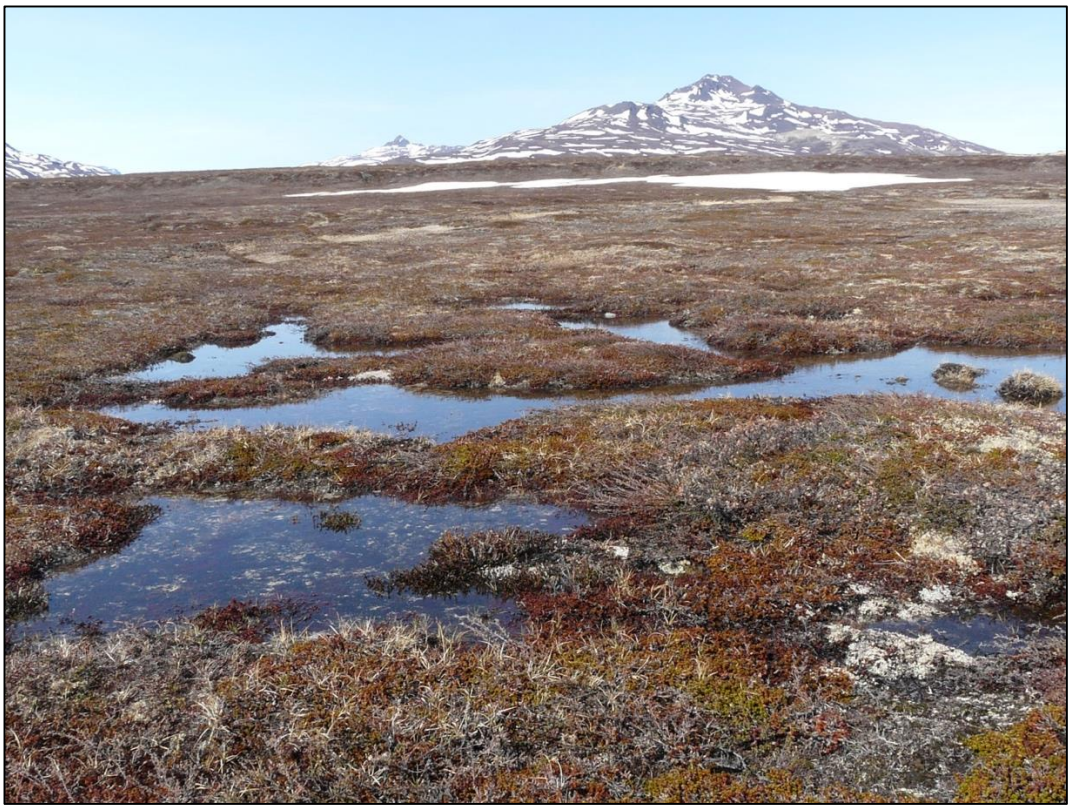

Figure 5A. Tundra wetland; photo taken at the Aqajarua and Sullorsuaq Ramsar Site in Greenland. Image credit: Tobias Salathé ("Ramsar focuses on Arctic wetlands," 2014).

Two paleowetland sites were examined from the tundra biome (**Table 1** and **Appendix VIII**). One modern wetland, located in the Kamchatka Peninsula in Russia, is a small coastal fen peatland nested in a former kettle basin that has existed for multiple periods over the past ~9000 years (Pendea et al., 2017). A fen, defined by Mitsch and

Gosselink (2007), is a “peat-accumulating wetland that receives some drainage from surrounding mineral soil and usually supports marshlike vegetation”. Presently, the peatland is dominated by sedges from the Cyperaceae family with a bryophyte understory consisting of Bryidae mosses and *Sphagnum* species. The wetland has been identified as an intermediate shrub-fen with *Sphagnum*-sedge peat, a rich fen with Bryidae-sedge peat, and a rich shrub fen with sedge-carr peat. Layers of tephra were deposited between these wetland sequences (Pendea et al., 2017). The tephra layers are associated with increased fire activity. Thick tephra air-fall deposits caused forest die-out leading to increased fire activity (Pendea et al., 2017). The other wetland, located in the Simirlik National Park in the Canadian Arctic Archipelago, is described as low-lying terraces (referred to as “tundra polygon complexes”) and has existed for multiple periods with the last ~3500 years (Ellis and Rochefort, 2006). Presently, the wetland consists of peat-rich permafrost soils dominated by sedges, grasses, and fen mosses. Wetland sequences are identified by the presence of macrofossil mosses and lower mineral percentages (Ellis and Rochefort, 2006).

The presence of moss-rich peat in these deposits has the potential to be a distinct characteristic for northern wetlands. Of the many types of soils that exist in wetlands, organic soil, particularly undecomposed organic soil (i.e., peat), is most commonly found in northern wetlands (i.e., peatlands) (Mitsch and Gosselink, 2007). Organic soils tend to have lower bulk densities and a greater cation exchange capacity than mineral soils. *Sphagnum* moss can be very light with bulk densities as low as 0.04 g/cm^3 and *Sphagnum* moss peat has a high cation capacity (Mitsch and Gosselink, 2007). Additionally, the lack

of evidence of trees or deep roots (which cannot be supported in tundra environment conditions) can further provide evidence of the tundra biome (ISC-Audubon, 2018) (**Table 1**).

Subarctic Taiga

The subarctic taiga biome (**Figure 4B**) is located near the top of the world, just south of the tundra biome. The average annual temperature is below freezing for half of the year. In the winter, the temperature ranges from -54°C to -1°C and in the summer the temperatures range from -7°C to 21°C. The annual precipitation is about 30 to 85 cm (ISC-Audubon, 2018). The picture below of a modern taiga wetland in Canada depicts a typical landscape of a taiga wetland where grasses and shrubs exist at the margin of open water and evergreen forest stands surround the wetland (**Figure 5B**).

Figure 5B. Taiga Wetland; photo taken along the shoreline of Long Lake, near Yellowknife in the Northwest Territories of Canada. Photography by Michael John Brown (Brown, 2011).

Data from four paleowetland sites from the subarctic taiga biome were examined (**Table 1** and **Appendix VIII**). Three wetlands are identified as bogs; two bogs are located in Nova Scotia, Canada (Spooner et al., 2017) and one in northern Poland (Lamentowicz et al., 2015). One of the wetlands is identified as a paleo-pingo depression located in the Sanjiang Plain in northeast China (Zhang et al., 2017). A bog, defined by Mitsch and Gosselink (2007), is a "peat accumulating wetland that has no significant inflows or outflows and supports acidophilic mosses, particularly *Sphagnum*". A pingo is a "perennial frost mound consisting of a core of massive ice, produced by injection of water, and covered with soil and vegetation" (Harris et al., 1998). A depression is created when the ice cone melts.

The three modern bogs have existed for multiple periods throughout at least the last ~1000 years; the paleo-pingo depression exists presently and has existed for multiple periods throughout the last ~4500 years. For the most part, the wetland deposits from these four localities consisted of peat containing various *Sphagnum* species (Lamentowicz et al., 2015; Spooner et al., 2017; Zhang et al., 2017). Intermediate woodland deposits occur between the wetland deposits at the two Canadian localities (Spooner et al., 2017). These intermediate woodland layers consisted of single wood layers within a *Sphagnum*-peat matrix with upright Black Spruce trunks (Spooner et al., 2017). Wetland sequences for the Chinese locality were identified by an increase in peat content (Zhang et al., 2017).

Similar to the tundra biome listed above, *Sphagnum* peat found in wetland deposits provides evidence for a northern wetland environment (Mitsch and Gosselink, 2007). The intermediate woodland layers containing Black Spruce trunks provide

additional context for the environment of deposition, as spruce trees are commonly found in the taiga biome (ISC-Audubon, 2018) (**Table 1**).

Temperate Forest

The temperate forest biome (**Figure 4C**) is also known as the deciduous forest biome or moist continental climate. The average annual temperature is 10°C and the average annual rainfall is approximately 75 to 155 cm (ISC-Audubon, 2018). The picture below of a modern temperate forest wetland in New York state shows the typical landscape of a temperate forest wetland and deciduous trees (i.e., swamp oak) (**Figure 5C**).

Figure 5C. Temperate Forest Wetland; photo taken at the Blueberry Patch Swamp in Schuyler County, New York (U.S. Forest Service, 2017).

Data from two wetland sites from the temperate forest biome were examined (**Table 1** and **Appendix VIII**): Ellison Park located in Rochester, New York (Coon, 1997) and

Little Llangothlin in eastern Australia (Woodward et al., 2014). The Ellison Park wetland is a modern wetland but has a sedimentary record. The deposits consist of silt and clay with high organic matter (Coon, 1997). The Little Llangothlin wetland is present today and has existed for multiple periods throughout at least the last ~1000 years. The deposits consist of varying amounts of dark brown organic sediment, peat, and charcoal (Woodward et al., 2014). The dominant plant species in the Ellison Park wetland is cattail (*Typha glauca*) whereas various plants ranging from *Myriophyllum varifolium* at the lagoon margin, *Potamogeton crispus* (pondweed) within the shallow portion of the lagoon, *Eleocharis sphacelata* (Cyperaceae-sedge) at the lagoon basin, to *Eucalyptus*, at the forest stands were documented (Coon, 1997; Woodward et al., 2014).

While wetland deposits from the two temperate forest sites both contain organic soils and hydrophytic vegetation, they do not appear to have characteristics in common that could provide evidence for a distinct facies model for temperate forest wetlands. However, it may be possible to rule out certain biomes by the existence of surrounding forest stands (e.g., tundra cannot support the growth of forests). Further research is needed to determine if a facies model for this biome could be generated (**Table 1**).

Temperate Grassland

The temperate grassland biome (**Figure 4D**) is located at mid-latitudes and in the interior of continents. In the winter, the temperature can be as low as -40°C and in the summer as high as 21°C. Temperate grasslands receive an average annual rainfall of 25 to 75 cm a year; the precipitation is erratic enough that drought and fire prevent large forests from growing, but it is enough precipitation to support grasses (ISC-Audubon,

2018). The picture below of a modern temperate grassland wetland in the prairie pothole region of the United States reveals the typical landscape of a temperate grassland wetland where lush grasses surrounding pools of water can be seen (**Figure 5D**).

Figure 5D. Temperate Grassland Wetland; photo taken from the Prairie Pothole Region of the United States (USDA Natural Resource Conservation Services).

One paleowetland site was examined from the temperate grassland biome (**Table 1** and **Appendix VIII**). The wetland is identified as Braamhoek wetland and is located in South Africa (Norström et al., 2009). The Braamhoek wetland is thriving under the present climate and has existed over multiple intervals throughout at least the past ~16,000 years. The deposits consist of variously colored organic “sandy peat”, “clayey peat”, and “tussock peat” containing minerogenic particles (Norström et al., 2009). The dominant species associated with the Braamhoek wetland include Poaceae grasses (*Phragmites*

australis and *Poa binata*) and Cyperaceae sedge (*Carex acutiformis*) (Norström et al., 2009).

These deposits do not contain any features that appear to be unique to this biome. Further research is needed to determine if a facies model for this biome could be generated (**Table 1**).

Temperate Desert

The temperate desert biome (**Figure 4E**) has an annual average temperature of 10°C and receives less than 100 cm of precipitation a year (ISC-Audubon, 2018; Cain et al., 2014). The picture below of a modern temperate desert wetland in Chile depicts typical landscape of a temperate desert wetland where lush vegetation is dependent on wetland water to persist (**Figure 5E**).

Figure 5E. Temperate Desert Wetland; photo taken in the Arcoiris Valley in Rio Salado, Chile (Explore-Share, 2019).

Seven paleowetland sites were examined from the temperate desert biome (**Table 1** and **Appendix VIII**) including: the Carmel Coast in northern Israel; Cerros Negros in Arizona; the Dove Springs in California; the Murray Springs in Arizona; Salar de Punta Negra in Chile; Rio Salado in Chile; and the Ulan Buh Desert in southwestern Inner Mongolia (Sivan et al., 2011; Pigati et al., 2014; Li et al., 2015). The wetland deposits from the American Southwest and Atacama Desert consisted of clastic sediments, groundwater precipitates (such as spring travertine, water-table carbonate, wetland marl, and wetland tufa, etc.), and organic matter ("black mats") (Pigati et al., 2014). The wetland deposits from the Carmel Coast and Ulan Buh Desert consisted mostly of dark brown silty clays (Sivan et al., 2011; Li et al., 2015). Ostracods and foraminifera were observed in all wetland deposits, except for those in the Ulan Buh Desert (Sivan et al., 2011; Pigati et al., 2014; Li et al., 2015). In the deposits of the American Southwest and Atacama Desert, biota such as gastropods, sponges, chironomids, ostracods, and algae were also observed (Pigati et al., 2014).

As already noted by Pigati et al. (2014), GWD deposits (i.e., clastic sediment, groundwater precipitates, and "black mats") were identified in all wetland deposits from the American Southwest and the Atacama Desert. Ostracods and foraminifera, identified as signature biota in GWD deposits of desert wetlands (Pigati et al., 2014), were observed not only in the deposits of the American Southwest and Atacama Desert, but also in the deposits from the Carmel Coast in Israel. This suite of characteristics provides evidence for a temperate desert wetlands facies model (**Table 1**).

Tropical Rainforest

The tropical rainforest biome (**Figure 4F**) has a moist climate with temperatures that rarely exceed 34°C or drop below 20°C (ISC-Audubon, 2018). The average humidity in this biome is between 77 and 88 percent with an average annual rainfall between 125 to 550 cm (ISC-Audubon, 2018). The picture below of a modern tropical rainforest wetland in the Amazon rainforest region of Brazil depicts the diverse flora typically seen in tropical rainforest wetlands (**Figure 5F**).

Figure 5F. Tropical Rainforest Wetland; photo taken in the Amazon rainforest region of Brazil. Image credit: James Davis Photography/ Alamy Stock Photo (Davis).

Wetlands located in the Maya lowlands of the Yucatán Peninsula and adjacent lowlands in Mexico, Belize, and Guatemala were examined from the tropical rainforest biome (**Table 1** and **Appendix VIII**). The wetlands in these localities ranged from upland and intermittent "bajos" to coastal plain's floodplains, depressions, and submerged

sinkholes (Beach et al., 2009). The wetlands exist presently and existed at multiple intervals throughout the Holocene. The deposits consist of thick calcareous clayey sediments with high amounts of gypsum and organic matter. Alternating wet-dry hydrology conditions are indicated by the expansion and contraction of smectite clays, and the uneven distribution of accumulating masses of sediment and argilliturbation (breakage of horizons, heaving, and slickensides throughout the soil profile) (Beach et al., 2009). The wetlands are characterized as forested and herbaceous including red mangrove (*Rhizophora mangle*), hardwood swamps, sawgrass (*Cladium jamaicense*) marsh, marl flats dominated by *Cyperaceae*, sedge marshes dominated by a few *Cyperus* species, and calabash marsh dominated by *Eleocharis interstincta* (Beach et al., 2009).

Evidence of these biota in the sedimentary record may indicate what biome the deposit did *not* form in (e.g., taiga, tundra, desert), but does not necessarily indicate a tropical rainforest depositional environment. However, the sedimentology of the deposits from this biome (i.e., calcareous clayey sediments, high amounts of gypsum and organic matter, smectite clays, etc.) prove to be distinctive; however, further research is needed to determine if a facies model for this biome could be generated (**Table 1**).

Tropical Savanna

The tropical savanna biome (**Figure 4G**) has a wet-dry tropical climate which is found between the tropical rainforest and desert biome. This biome does not receive enough rainfall to support forests, but typically has shrubs and isolated trees. Savannas have warm temperatures year-round, with two different seasons (a dry season in the winter and a wet season in summer). Only about 10 cm of rain falls during the dry season

and the temperatures are cooler at about 21°C. During the wet season, there is about 38 to 63 cm of rainfall and the temperatures get very hot and humid (ISC-Audubon, 2018). The picture below of a modern tropical savanna wetland in Australia depicts the typical landscape of a tropical savanna wetland (**Figure 5G**).

Figure 5G. Tropical Savanna Wetland; photo taken at Mareeba Wetlands in Queensland, Australia (Mapdata).

Two paleowetland sites were examined from the tropical savanna biome (**Table 1** and **Appendix VIII**). One wetland is identified as Loboi Swamp, located in Kenya, Africa (Ashley et al., 2004) and the other wetland is located in the Araguaia River floodplain in the southern Amazon basin (Irion et al., 2016). Loboi Swamp has existed for the past ~700 years and the deposits consist of peat capping organic-rich clay with redoximorphic features (Ashley et al., 2004). Presently, Loboi Swamp contains cattail *Typha domingensis Pers.* (80%) and *Cyperus papyrus L.* (20%), wetland pollen species (50%), and abundant

diatoms (*R. gibberula*) (Muasya et al., 2004). The surrounding floodplain consists of montane pollen and scarce diatoms; the uplands consist of *Acacia* scrubland; and the plains consist of salt-tolerant grasses such as *Sporoblous spicatus* (Ashley et al., 2004). The Araguaia River floodplain wetland has existed throughout multiple periods during the past ~240 ka years and the deposits consists of sequences of smectite, illite, kaolinite, and other clay minerals. Presently, 60% of the wetland area is covered in termite savannas, single-tree savannas, and savanna forests (Irion et al., 2016).

The abundant redoximorphic features observed with the clay deposits can be indicative of an environment that has a wet and dry season (Mitsch and Gosselink, 2007); however, this does not necessarily limit the deposits to the tropical savanna biome. Additionally, the biota present in these wetland deposits do not limit the wetland deposits to be from one particular biome either, but they do suggest a semi-arid environment where the plants have adapted to survive in long periods of drought (Ashley et al., 2004). Further research is needed to determine if a facies model for this biome could be generated (**Table 1**).

Tropical Desert

The tropical desert biome (**Figure 4E**) is hot and dry and located near the Tropic of Cancer or Tropic of Capricorn. The temperature ranges from 20 to 25°C and about 15 cm of precipitation is received annually on average (ISC-Audubon, 2018). The picture below of a modern tropical desert wetland in the Okavanga “Delta” shows the typical landscape of a tropical desert wetland (**Figure 5H**).

Figure 5H. Tropical Desert Wetland; photo taken at the Okavango Delta in Botswana (Mackay and Davidson, 2014).

Three paleowetland sites were examined from the tropical desert biome (**Table 1** and **Appendix VIII**) including older deposits from Salar de Punta Negra in the central Atacama Desert of northern Chile (Quade et al., 2008); deposits from the Okavango Delta in Botswana, Africa (Tooth and McCarthy, 2007);and deposits from the Great Cumbung Swamp in eastern Australia (O'Brien and Burne, 1994). At all three localities have modern wetlands which have existed at various times throughout the Holocene. Deposits from the Atacama Desert salt-pan consist of organic matter, greenish silt (from sustained reduction in locally-saturated/ oxygen-deficient conditions), and layered diatomite with evidence of wet sediment deformation; deposits from the Okavango delta wetlands consist of accumulations of chemical sediments in substrates (salt crusts) with peat that has burned off during natural fires; the deposits from the Great Cumbung Swamp consist of dark-colored clays composed of silt-sized quartz and smectite which show evidence of

dry conditions such as deep cracks, color mottling, granular structures, and less organic matter (O'Brien and Burne, 1994; Tooth and McCarthy, 2007; Quade et al., 2008). The biota in the deposits consist of gastropods, diatoms, sponge spicules, and various levels of salt-tolerant shrubs (i.e., *Tessaria* and *Atriplex*), grasses (*sporobolus spicatus* and *cunodon dactylon*), reeds (*Phragmites australis* and *Typha orientalis*), and trees. (O'Brien and Burne, 1994; Tooth and McCarthy, 2007; Quade et al., 2008).

As already noted by Pigati et al. (2014) and Tooth and McCarthy (2007), the wetland deposits from this biome can be distinguished by the presence of GWD deposits (i.e., clastic sediments, groundwater precipitates, gastropods), indications of higher levels of chemical sedimentation, frequent fires resulting in thin organic accumulations, and long periods of desiccation. In comparison with the deposits of the temperate desert biome, the deposits from the tropical desert biome appear to have less organic matter; however, more data is needed to confirm if this is a common pattern. Additionally, evidence of redoximorphic features were observed which indicate that the mineral soil is exposed to alternating wet and dry conditions (O'Brien and Burne, 1994; Tooth and McCarthy, 2007; Quade et al., 2008). However, further research is needed to support the facies model for this biome (**Table 1**).

DISCUSSION

Discussion of Differences and Similarities across Biomes

Similarities among Wetland Deposits

Although the data collected are limited, some inferences can be drawn in regard to the similarities and differences of the wetland deposits examined. It is much easier to find similarities among wetland deposits than differences. They all consist of hydric soils and support some forms of hydrophytic vegetation, distinct from the adjacent deposits (National Research Council, 1995). Hydric soils are soils that have been saturated, flooded, or ponded long enough during the growing season to develop anaerobic conditions that support hydrophytic vegetation (National Research Council, 1995). Hydric soils can be either organic or mineral. In mineral soils, biochemical processes causing iron and manganese to reduce have a big impact on the color and morphology of the soil, which acts as an indicator as to whether a soil is hydric or not (National Research Council, 1995). Moisture content plays a large role in driving such oxidation-reduction and acid-base reactions to occur (**Figure 6**). The substrates examined consist of a wide range of mineralogies (representing various geochemical settings) reflected in the various colors of fine-grained sediments forming either mineral or organic soil, with varying amounts of charcoal, and precipitates (**Appendix VIII**). The flora/fauna consists of various grasses, sedges, reeds, and mosses, diatoms, ostracods, gastropods, algae, sponges, foraminifera, teeth/bones of macro and micro vertebrates, and more (**Appendix VIII**). All of these features give wetland deposits a unique characterization, one worthy of its own facies model.

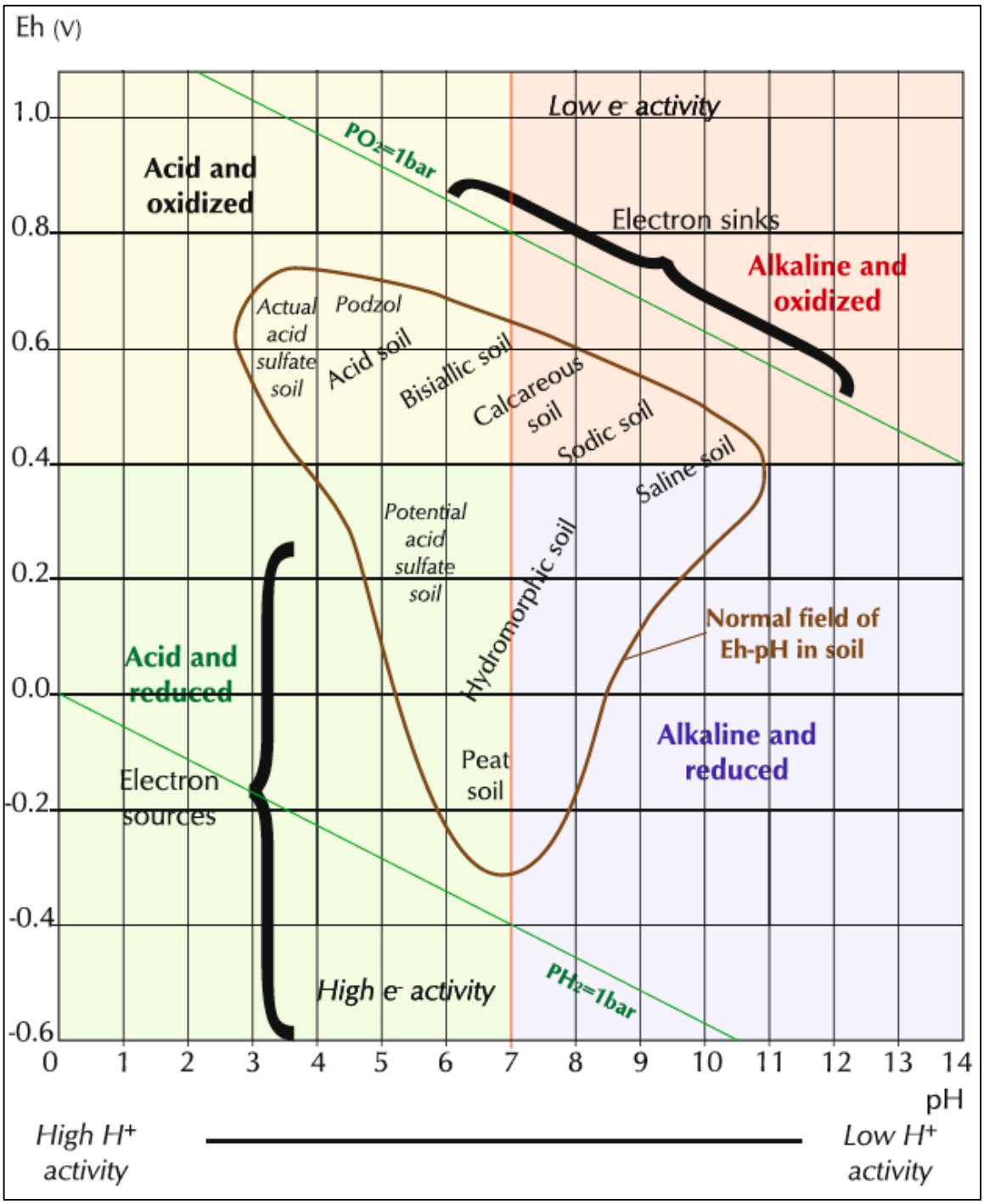

Figure 6. Pourbaix diagram. Soil distribution type in relation to pH and redox potential (Eh) (Tiner, 2017).

<u>Differences among Wetland Deposits</u>

Differences among wetland deposits, although quite often subtle, were discerned from the data collected for this study. Although distinctive features were not determined

for each biome, some patterns among a few biomes were recognized and with further research, there is a likelihood that wetland facies models can be created for each biome.

Distinguishing characteristics for the most arid endmembers (the tundra and desert biomes) as well as for the taiga were evident from the data collected. The tundra and taiga deposits both contained *Sphagnum* or other moss-rich peat (high in organic content) which is associated with northern wetlands (**Table 1**). These two biomes could be further distinguished by their deposits due to the lack of trees in the tundra deposits and the presence of trees in the taiga deposits (**Table 1**). In agreement with Husson (2013), Pigati et al. (2014), and Tooth and McCarthy (2007), desert wetland deposits, for the most part, can be distinguished by the presence of GWD deposits (clastic sediment, precipitates, “black mats”, and biota including ostracods, gastropods, foraminifera, sponges, and diatoms), charcoal, and desiccation features (**Table 1**). The main difference between temperate and tropical desert deposits was that tropical deposits contained less organic matter, likely due to more frequent fires (**Table 1**).

Some features found in the temperate forest deposits (i.e., high amount of organic material), the tropical rainforest deposits (i.e., calcareous clayey sediments with high amounts of gypsum and organic material and as well as the presence of smectite), and the tropical savanna deposits (i.e., redoximorphic features in clay indicative of a wet and dry season as well as the presence of vegetation typical of semi-arid environment with a fluctuating water table) could be distinguished (**Table 1**). The deposits from the temperate grassland were not indicative of any features that would be unique to that environment of deposition. While evidence from deposits of these three biomes may not

warrant individual facies models at this juncture, it is possible that together they have commonalities that are not seen in the other biomes (**Appendix VIII**).

Proposed Wetland Facies Model: Tundra/Taiga, Desert, & Grasslands/Forests Wetlands

Based on the differences outline above, a new wetland facies model is proposed (**Figure 7**). Although wetland deposits cannot be categorized into eight distinct categories by biome at this time, they can be categorized into three distinct groups, each with their own distinctive sediment "fingerprint": (1) Tundra/Taiga Wetlands; (2) Desert Wetlands; and (3) Grassland/Forest Wetlands (**Figure 7**).

The Tundra/Taiga Wetland type includes Tundra and Subarctic Taiga wetland deposits, the Desert Wetland type includes temperate and tropical desert wetland deposits, and the Grassland and Forest Wetland type includes temperate grassland, temperate forest, tropical savanna, and tropical rainforest deposits. The Tundra/Taiga and Desert Wetlands receive the lowest amounts of precipitation while the Grassland/Forest Wetlands receive the highest. The Tundra/Taiga Wetlands consist of the coldest temperatures while the Desert and Grassland/Forest Wetland consist of higher temperatures (temperate and tropical). Distinctive lithologic and biological features for each type are outlined in **Figure 6**. In general, there is an increase in organic content seen in wetlands located in wetter conditions (i.e., Grassland/Forest Wetlands) and an increase in mineral sediments and specified biota (i.e, *Spagnum*, Ostracods, gastropods, etc.) seen in wetlands located in drier conditions (i.e., Tundra/Taiga and Desert Wetlands).

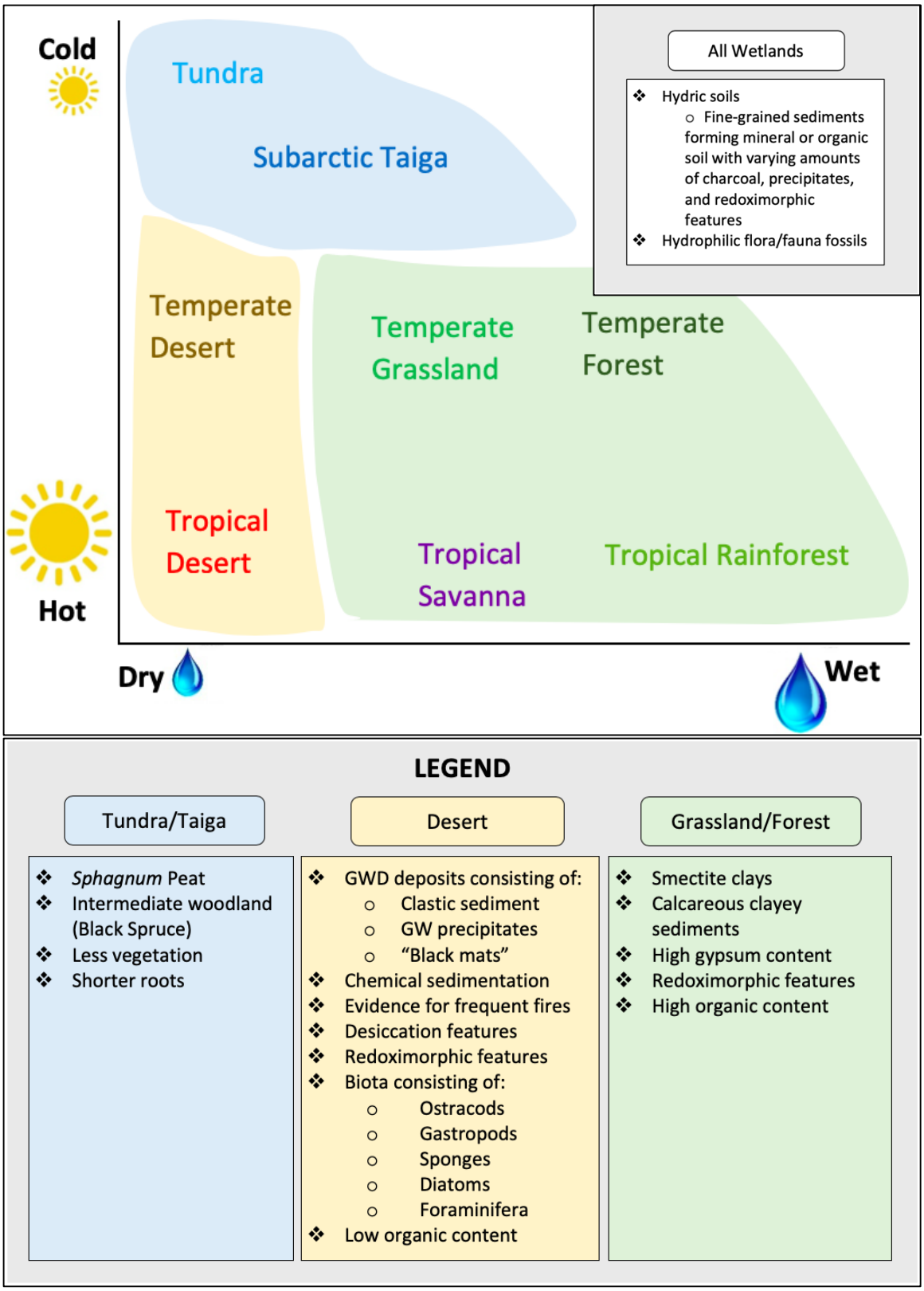

Figure 7. Wetland Facies Model. Wetland deposits from each biome are categorized into three types, each with distinct sedimentological and/or biological characteristics: (1) Tundra/Taiga Wetlands; (2) Desert Wetlands; and (3) Grassland and Forest Wetlands.

Limitations

Wetland biomes can be confidently grouped into three broad but distinctive types. With an expanded data set it is likely that more types will emerge. The following limitations of this paper must be taken into account: (1) the number of study sites per biome were not equal; some contained several deposits to draw inferences from, while others only contained one; (2) many of the paleowetland studies are biased in that they focus most heavily on the paleontology of the deposits, rather than the sedimentology; (3) the MAT and MAP for some study sites were not explicitly stated so inferences were made as to which biome those particular study sites were deposited in; (4) wetland types, soil, and vegetation were documented as reported in each paper, however these names can sometimes differ in meaning internationally as the classifications vary across the world; (5) various wetland types with various hydrologic sources (e.g., palustrine, lacustrine, riverine, estuarine, etc.) were examined as a part of this study; and (6) the facies model was based on the inclusion of clastic, biological, and chemical features in the sedimentary record, but these features were not considered alone. Future work could consider the creation of a wetland lithologic facies model, a wetland biologic facies model, and/or wetland chemical facies model.

CONCLUSIONS

Despite the fact that wetlands are among the most important ecosystems in the world and are recognized today as such, they are poorly understood (Mitsch and Gosselink, 2007). While they have been extensively studied by biologists, paleontologists, and hydrologists— they have been rather neglected by geologists (Tooth and McCarthy, 2007). The ability to understand the future of wetlands under global climate change is highly dependent on the empirical data collected from modern wetlands and wetland sedimentary records (LePage et al., 2012).

In an effort to fill this knowledge gap, this study examined modern wetland deposits from across the world. Through the collection and compilation of lithological/ sedimentological, paleontological/biological, and geochemical data of wetland deposits from every biome of the world, wetland deposits were identified to have unique facies in the lithologic record.

Similarities among all wetland deposits were identified and include the presence of hydric soils (fine-grained sediments forming either mineral or organic soil with varying amounts of charcoal, precipitates, and redoximorphic features) and fossils of hydrophytic flora/ fauna (**Figure 6**).

While there were not enough distinguishing characteristics to categorize wetland deposits into eight distinct categories by biome (**Table 1**), there were enough differences among the deposits to warrant a new facies model that categorizes wetlands into three distinct types by climate: (1) Tundra/Taiga Wetlands; (2) Desert Wetlands; and (3) Grassland/Forest Wetlands (**Figure 7**). Tundra/Taiga wetland deposits consist of

Sphagnum and moss-rich peats (specific to northern wetlands), intermediate woodland layers, less vegetation, and shorter roots. Desert wetland deposits consist of GWD deposits (with the distinct components of containing clastic sediment, precipitates, organic matter, and specific biota), chemical sedimentation, charcoal, and desiccation features, in agreement with Quade et al. (1995), Pigati et al. (2014), and Tooth and McCarthy (2007). Grassland/Forest wetland deposits consist of high organic content, calcareous clayey sediments with high gypsum content, redoximorphic features, and smectite clays. In general, there is an increase in organic content seen in wetlands located in wetter conditions such as the Grassland/Forest Wetlands and an increase in specified biota seen in wetlands located in drier conditions such as the Tundra/Taiga and Desert Wetlands. These results suggest that climate (MAT and MAP) plays an important role wetland deposition.

Wetland biomes can be confidently grouped into three broad but distinctive types based on climate. With an expanded data set it is likely that more types will emerge, therefore, further research and data collection is needed to support this wetland facies model and further fil the knowledge gap. Such studies will provide understanding and clarity to the wetland systems of the present, which can be used to constrain and understand how these important, yet fragile, ecosystems will behave in the future.

REFERENCES FOR CHAPTER TWO

Ashley, G.M., Deocampo, D.M., Kahmann-Robinson, J., and Driese, S.G., 2013, Groundwater-fed wetland sediments and paleosols: it's all about water table: New Frontiers in Paleopedology and Terrestrial Paleoclimatology: Paleosols and Soil Surface Analog Systems, p. 47–61, doi:10.2110/sepmsp.104.03.

Ashley, G.M., Mworia, J.M., Muasya, A.M., Owen, R.B., Driese, S.G., Hover, V.C., Renaut, R.W., Goman, M.F., Mathai, S., and Blatt, S.H., 2004, Sedimentation and recent history of a freshwater wetland in a semi-arid environment: Loboi Swamp, Kenya, East Africa: Sedimentology, v. 51, p. 1301–1321, doi:10.1111/j.1365-3091.2004.00671.x.

Beach, T., Luzzadder-Beach, S., Dunning, N., Jones, J., Lohse, J., Guderjan, T., Bozarth, S., Millspaugh, S., and Bhattacharya, T., 2009, A review of human and natural changes in Maya Lowland wetlands over the Holocene: Quaternary Science Reviews, v. 28, p. 1710–1724, doi:10.1016/j.quascirev.2009.02.004.

Brown, M.J., 2011, Lakes and Wetlands of the Taiga biome: PhotosNorth, http://www.photosnorth.ca/LakesWetlands/LakeWetlands-A2.html (accessed April 2019).

Cain, M.L., Bowman, W.D., and Hacker, S.D., 2014, Ecology: advance of the tree lines: biome boundaries and climate change: Sinauer Associates, https://ecology3e.sinauer.com/problem03.html.

Coon, W.F., 1997, Hydrology, sedimentology, and biology of Ellison Park wetland at the mouth of Irondequoit Creek near Rochester, New York: U.S. Geological Survey Water-Resources Investigations Report 96-4269,.

CZO, 2012, The critical zone: National Science Foundation, http://criticalzone.org/national/research/the-critical-zone-1national/.

Davis, J. Giant green water lilies float on the surface of a wetland area in the Amazon rainforest of Brazil: Alamy Stock Photography,.

Ellis, C.J., and Rochefort, L., 2006, Long-term sensitivity of a High Arctic wetland to Holocene climate change: Journal of Ecology, v. 94, p. 441–454, doi:10.1111/j.1365-2745.2005.01085.x.

Explore-Share, 2019, Valle del Arcoiris - Rio Salado full day hiking trip:, https://www.explore-share.com/trip/arcoiris-rio-salado-full-day-hiking/ (accessed April 2019).

Harris, S.A., French, H.M., Heginbottom, J.A., Johnston, G.H., Ladanyi, B., Sego, D.C., and Everdingen, R.O. van, 1998, Glossary of permafrost and related ground-ice terms.

Husson, O., 2013, Redox potential (Eh) and pH as drivers of soil/plant/microorganism systems: A transdisciplinary overview pointing to integrative opportunities for agronomy: Plant and Soil, v. 362, p. 389–417, doi:10.1007/s11104-012-1429-7.

Irion, G., Nunes, G.M., Nunes-da-Cunha, C., de Arruda, E.C., Santos-Tambelini, M., Dias, A.P., Morais, J.O., and Junk, W.J., 2016, Araguaia River floodplain: size, age, and mineral composition of a large tropical savanna wetland: Wetlands, v. 36, p. 945–956, doi:10.1007/s13157-016-0807-y.

ISC-Audubon, 2018, Köppen Climate Classification:, http://www.thesustainabilitycouncil.org/desert-biome.html.

James, N.P., and Dalrymple, R.W., 2010, Facies models 4: Geological Association of Canada, 3–18 p.

Lamentowicz, M., Gałka, M., Lamentowicz, T., Obremska, M., Kühl, N., Lücke, A., and Jassey, V.E.J., 2015, Reconstructing climate change and ombrotrophic bog development during the last 4000 years in northern Poland using biotic proxies, stable isotopes and trait-based approach: Palaeogeography, Palaeoclimatology, Palaeoecology, v. 418, p. 261–277, doi:10.1016/j.palaeo.2014.11.015.

LePage, B.A., Jacobs, B.F., and Williams, C.J., 2012, Insights from paleohistory illuminate future climate change effects on wetlands, *in* Global Change and the Function and Distribution of Wetlands, p. 1–151, doi:10.1007/978-94-007-4494-3.

Li, G., Jin, M., Chen, X., Wen, L., Zhang, J., Madsen, D., Zhao, H., Wang, X., Fan, T., Duan, Y., Liu, X., Wu, D., Li, F., and Chen, F., 2015, Environmental changes in the Ulan Buh Desert, southern Inner Mongolia, China since the middle Pleistocene based on sedimentology, chronology and proxy indexes: Quaternary Science Reviews, v. 128, p. 69–80, doi:10.1016/j.quascirev.2015.09.010.

Mackay, A., and Davidson, T., 2014, Botswana's Okavango Delta: a unique desert that's wet, and a worthy UNESCO addition: The Conversation US, Inc, https://theconversation.com/botswanas-okavango-delta-a-unique-desert-thats-wet-and-a-worthy-unesco-addition-28476 (accessed April 2019).

Mapdata Mareeba Tropical Savanna & Wetland Reserve:, https://mapio.net/place/40869108/ (accessed April 2019).

Mitsch, W.J., and Gosselink, J.G., 2007, Wetlands: John Wiley & Sons, Inc., Hoboken, New Jersey, 582 p.

Muasya, A.M., Hover, V.C., Ashley, G.M., Owen, R.B., Goman, M.F., and Kimeli, M., 2004, Diversity and distribution of marcrophytes in a freshwater wetland, Loboi swamp (Rift valley), Kenya: Journal of the East African Natural History Society, v. 93, p. 39–47, doi:10.2982/0012-8317(2004)93[39:DADOMI]2.0.CO;2.

National Research Council, 1995, Wetlands: Characteristics and Boundaries: Washington, D.C., National Academy Press.

Norström, E., Scott, L., Partridge, T.C., Risberg, J., and Holmgren, K., 2009, Reconstruction of environmental and climate changes at Braamhoek wetland, eastern escarpment South Africa, during the last 16,000 years with emphasis on the Pleistocene-Holocene transition: Palaeogeography, Palaeoclimatology, Palaeoecology, v. 271, p. 240–258, doi:10.1016/j.palaeo.2008.10.018.

O'Brien, P.E., and Burne, R.V., 1994, The Great Cumbung Swamp - terminus of the low-gradient Lachlan River, Eastern Australia: Journal of Australian Geology & Geophysics, v. 15, p. 223–233.

Pendea, I.F., Ponomareva, V., Bourgeois, J., Zubrow, E.B.W., Portnyagin, M., Ponkratova, I., Harmsen, H., and Korosec, G., 2017, Late Glacial to Holocene paleoenvironmental change on the northwestern Pacific seaboard, Kamchatka Peninsula (Russia): Quaternary Science Reviews, v. 157, p. 14–28, doi:10.1016/j.quascirev.2016.11.035.

Pigati, J.S., Rech, J.A., Quade, J., and Bright, J., 2014, Desert wetlands in the geologic record: Earth-Science Reviews, v. 132, p. 67–81, doi:10.1016/j.earscirev.2014.02.001.

Quade, J., Mifflin, M.D., Pratt, W.L., McCoy, W., and Burckle, L., 1995, Fossil spring deposits in the southern Great Basin and their implications for changes in water-table levels near Yucca Mountain, Nevada, during Quaternary time: GSA Bulletin, v. 107, p. 213–230.

Quade, J., Rech, J.A., Betancourt, J.L., Latorre, C., Quade, B., Rylander, K.A., and Fisher, T., 2008, Paleowetlands and regional climate change in the central Atacama Desert, northern Chile: Quaternary Research, v. 69, p. 343–360, doi:10.1016/j.yqres.2008.01.003.

Ramsar focuses on Arctic wetlands, 2014, The Ramsar convention, https://www.ramsar.org/news/ramsar-focuses-on-arctic-wetlands (accessed April 2019).

Sivan, D., Greenbaum, N., Cohen-Seffer, R., Sisma-Ventura, G., and Almogi-Labin, A., 2011, The origin and disappearance of the late Pleistocene-early Holocene short-lived coastal wetlands along the Carmel coast, Israel: Quaternary Research, v. 76, p. 83–92, doi:10.1016/j.yqres.2011.04.006.

Spooner, I., Principato, S., Hill, N., White, H., Dunnington, D., Neily, T., and Stolze, S., 2017, Late Holocene records of changing moisture regime from wetlands in southwestern Nova Scotia, Canada: implications for wetland conservation and restoration: Northeastern Naturalist, v. 24, p. 331–348, doi:10.1656/045.024.0310.

Tiner, R., 2017, Wetland Indicators: A Guide to Wetland Formation, Identification, Delineation, Classification, and Mapping: Boca Raton, CRC Press: Taylor & Francis Group, doi:10.1201/9781420048612.

Tooth, S., and McCarthy, T.S., 2007, Wetlands in drylands: geomorphological and sedimentological characteristics, with emphasis on examples from southern Africa: Progress in Physical Geography, v. 31, p. 3–41, doi:10.1177/0309133307073879.

U.S. Forest Service, 2017, Sustain our nation's forests and grasslands: restored wetland improves upland stream habitat of Lake Ontario tributary: United States Department of Agriculture, https://www.fs.fed.us/inside-fs/restored-wetland-improves-upland-stream-habitat-lake-ontario-tributary (accessed April 2019).

USDA, 2003, Major biomes map:, https://www.nrcs.usda.gov/wps/portal/nrcs/detail/soils/use/?cid=nrcs142p2_054002.

USDA Natural Resource Conservation Services USDA to invest in prairie pothole landscape effort: United States Department of Agriculture, https://www.nrcs.usda.gov/wps/portal/nrcs/detail/national/home/?cid=stelprdb1245728 (accessed April 2019).

Vnaya, 2016, Meaning and Classification of Biomes:, https://www.vnaya.com/meaning-and-classification-of-biomes/.

Walker, R.G., 1984, Facies Models: St. Johns, Geological Association of Canada, Business and Economic Service, 317 p.

Woodward, C., Shulmeister, J., Bell, D., Haworth, R., Jacobsen, G., and Zawadzki, A., 2014, A Holocene record of climate and hydrological changes from Little Llangothlin Lagoon, south eastern Australia: Holocene, v. 24, p. 1665–1674, doi:10.1177/0959683614551218.

Zhang, Z., Liu, K.B., Bianchette, T.A., and Wang, G., 2017, The mid-Holocene decline of the East Asian summer monsoon indicated by a lake-to-wetland transition in the Sanjiang Plain, Northeast China: Holocene, v. 28, p. 246–253, doi:10.1177/0959683617721321.

THESIS CONCLUSION

Springs and wetlands exist all over the world and it is unlikely for one to have never encountered or benefited from one of these hydrogeological features at some point in time. Yet, this thesis has unveiled how our understanding of such features can be so cloudy. The purpose of this thesis in its entirety is to bring science a step closer toward elucidating the uncertainties of what is occurring below the surface of these features from a geologist's perspective. Chapter One focused building a framework for understanding the modern spring systems of the NVH in Tanzania while Chapter Two zoomed out and attempted to generate a facies model for wetlands across biomes of the world. Both chapters have provided novel information on these hydrogeological features where knowledge is sparse.

Chapter One

Chapter One examined the groundwater system associated with the NVH as well as the spatiotemporal availability of water in the region. Through the amalgamation of several resources of data, it was found that distinct temporal and spatial rainfall patterns were determined for the study area and three schematic conceptual models were developed to determine modes of spring formation for the study area.

Findings from the rainfall analysis include the following: on a yearly basis, there are two wet seasons from October-November and March-May forced by the seasonal migration of the ITCZ; on an interannual basis, peak rainfall years occur nearly every 5 and can be partially attributed to the ENSO or the IOD; and the orography of the study area highly impacts the spatial distribution of rainfall. Extreme, episodic rainfall events, such

as the biannual monsoons and interannual peak rainfall years at the study region, likely recharge the local groundwater system. Additionally, recharge likely occurs at higher elevations such as the NVH.

The three schematic conceptual models developed are as follows: (1) Groundwater intersects the surface at local base level; (2) Permeable rock (aquifer) intersects the surface along slope; and (3) Artesian flow up fractures under hydraulic head. Moreover, a novel approach of measuring river stage was introduced.

These data help to describe the hydrological inputs and physical framework of the groundwater system at the NVH which, prior to this research, has not been done. In addition, this study provides the first step toward making quantitative groundwater models. The rainfall analysis provides necessary insights for estimating groundwater recharge, a highly important parameter used in groundwater modeling. The spring settings provide a qualitative, first-order, conceptualization of the physical framework of the groundwater system. These data lay the groundwork for future groundwater modeling and a more quantitative understanding of the hydrogeology of this region in the future. If more resources and time were allotted in the future, borehole drilling to obtain subsurface geological information for the region, as well as conducting additional rainfall and flow rate studies, would allow for more robust data to make more accurate groundwater models.

Chapter Two

Chapter Two explored modern and ancient wetland deposits from across the world to determine whether a facies model for wetlands could be developed. Lithological/

sedimentological, paleontological/ biological, and geochemical data mined from published documents where wetlands were identified in were compiled for each wetland site and analyzed for commonalities among all deposits as well as among deposits of the same biome.

Similarities among all wetland deposits were identified and include the presence of hydric soils (fine-grained sediments forming either mineral or organic soil with varying amounts of charcoal, precipitates, and redoximorphic features) and hydrophytic flora/fauna fossils.

While there were not enough distinguishing characteristics to categorize wetland deposits into six distinct categories by biome, there were enough differences among the deposits to propose a novel facies model that characterized wetlands into three distinct types by climate: (1) Tundra/Taiga Wetlands; (2) Desert Wetlands; and (3) Grassland/Forest Wetlands. These results suggest that MAT and MAP play an important role in wetland deposition.

The study was the first step in determining if a unique set of characteristics can be attributed to wetland deposits distinguishing them from all other depositional environments. Further research and data collection are needed to support this initial wetland facies model and further fill the knowledge gap. In doing so, more clarity will be obtained as to the wetland systems of the present and past, which will pave the way to obtaining more accurate data to constrain how future wetlands may behave as the environment changes.

APPENDICES

CHAPTER ONE

APPENDICES I-VII

APPENDIX I

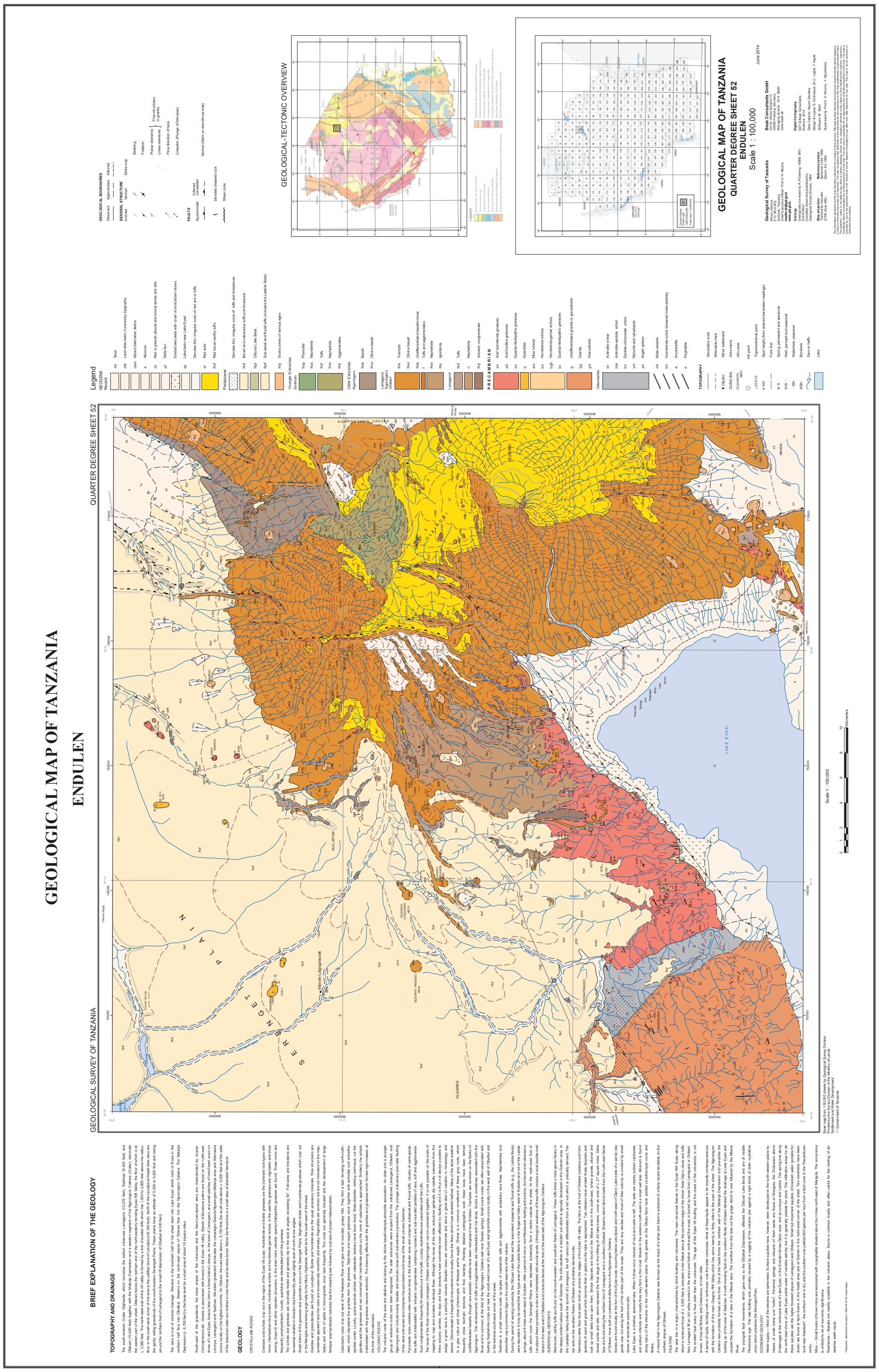
GEOLOGICAL MAP OF TANZANIA
ENDULEN
GEOLOGICAL SURVEY OF TANZANIA
QUARTER DEGREE SHEET 52
BRIEF EXPLANATION OF THE GEOLOGY
Legend
GEOLOGICAL-TECTONIC OVERVIEW
LAKE EYASI
SERENGETI PLAIN
GEOLOGICAL MAP OF TANZANIA
QUARTER DEGREE SHEET 52
ENDULEN
Scale 1 : 100,000
June 2014

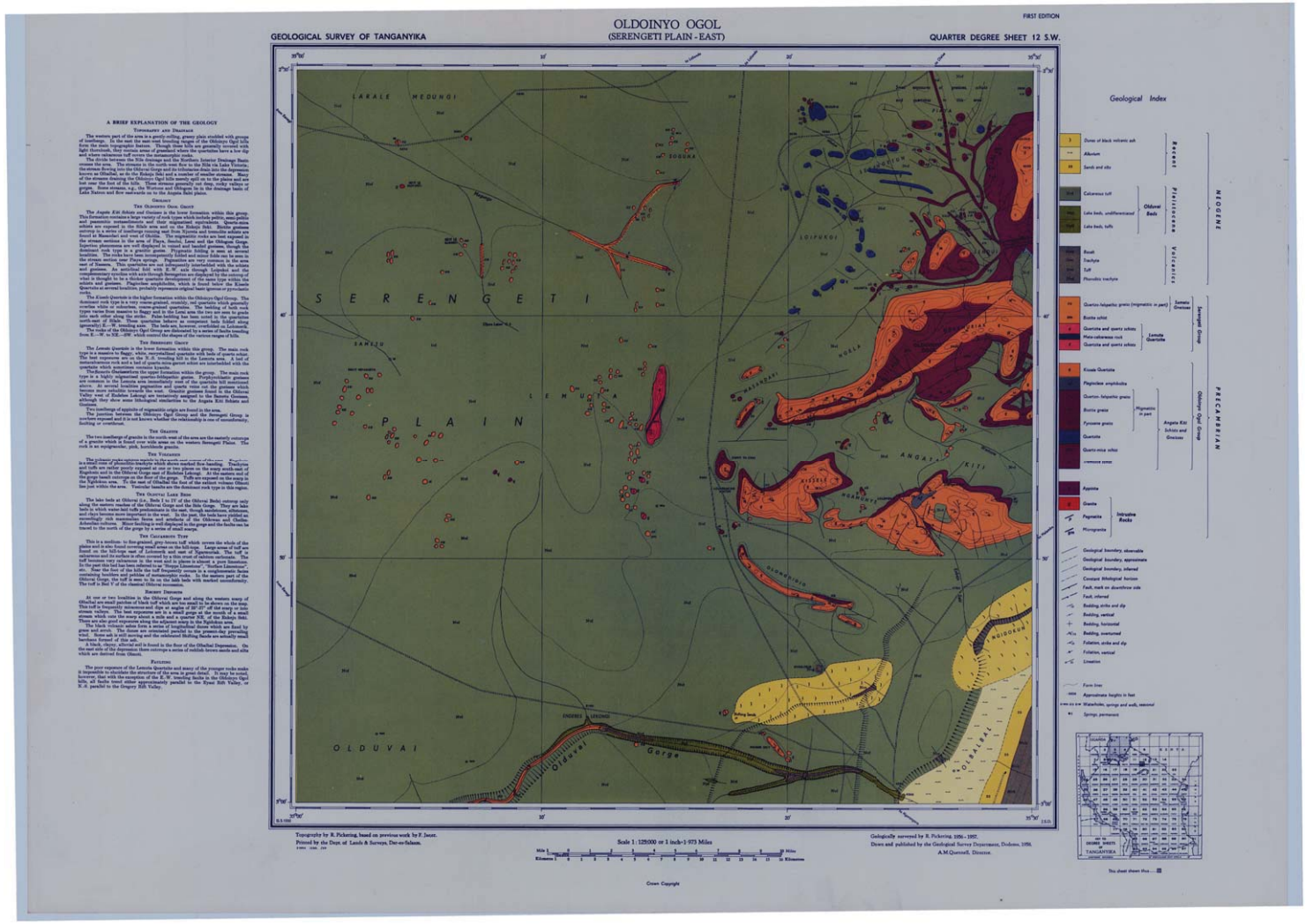

0.0 km 2.5 km 5.0 km 7.5 km 12.5 km

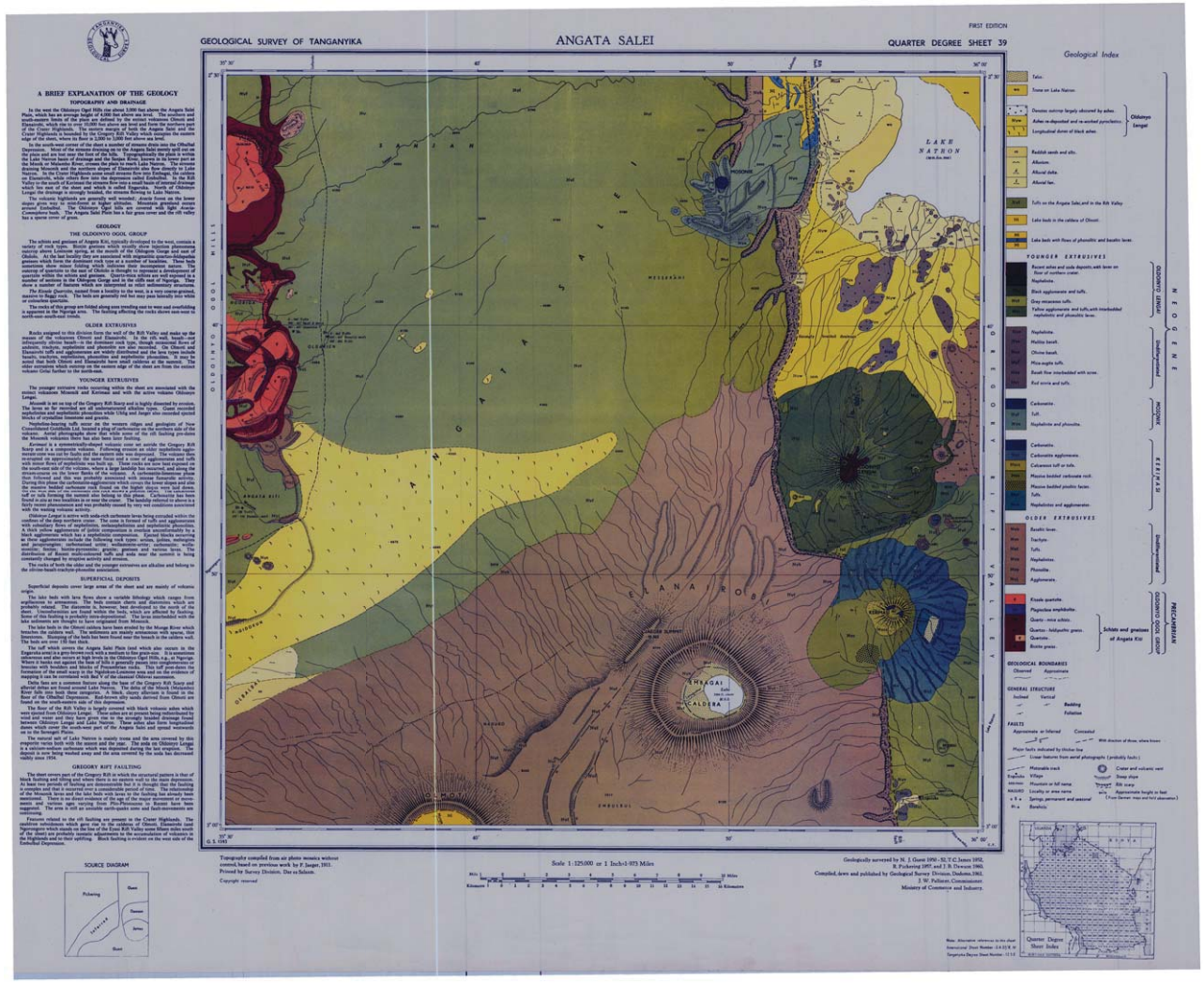

0.0 km 2.5 km 5.0 km 7.5 km 12.5 km

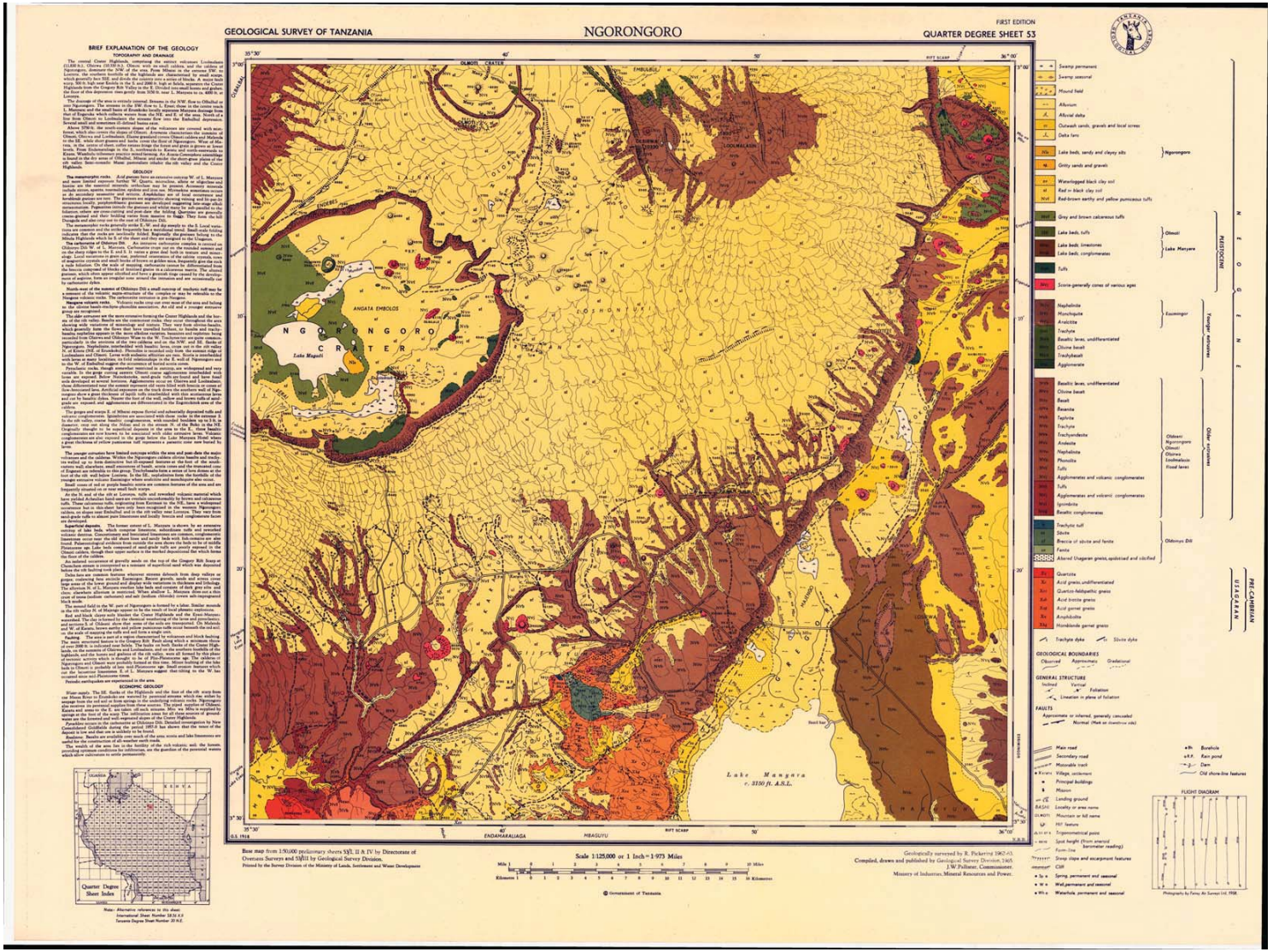
GEOLOGICAL SURVEY OF TANZANIA
NGORONGORO
FIRST EDITION
QUARTER DEGREE SHEET 53
BRIEF EXPLANATION OF THE GEOLOGY
TOPOGRAPHY AND DRAINAGE
GEOLOGY
ECONOMIC GEOLOGY
NGORONGORO CRATER
Lake Magadi
Lake Manyara
c. 3150 ft. A.S.L.
ANGATA EMBOLOS
OLMOTI CRATER
EMBULELI
LOLDIMALASIN
LOLOIMUTI
LOLOIMAIGA
LOLOHONUKI
ENDAMARAUGA
MBAGUTU
RIFT SCARP
Base map from 1:50,000 preliminary sheets 53/I, II & IV by Directorate of Overseas Surveys and 53/III by Geological Survey Division.
Printed by the Survey Division of the Ministry of Lands, Settlement and Water Development
Scale 1:125,000 or 1 Inch = 1·973 Miles
© Government of Tanzania
Geologically surveyed by R. Pickering 1967-69.
Compiled, drawn and published by Geological Survey Division, 1965.
J.W. Pallister, Commissioner.
Ministry of Industries, Mineral Resources and Power.
NEOGENE
PLEISTOCENE
Ngorongoro
Olmoti
Lake Manyara
Ngorongoro
Olmoti
Olduvai
Ngorongoro
Olmoti
Olduvai
Endikesh
Road lava
Olduvai Dill
PRE-CAMBRIAN
UJAGAAN
Swamp permanent
Swamp seasonal
Mound field
Alluvium
Alluvial delta
Outwash sands, gravels and local screes
Delta fans
Lake beds, sandy and clayey silts
Gritty sands and gravels
Waterlogged black clay soil
Red to black clay soil
Red-brown earthy and yellow pumiceous tuffs
Grey and brown calcareous tuffs
Lake beds, tuffs
Lake beds: limestones
Lake beds, conglomerates
Tuffs
Scoria-generally cones of various ages
Nephelinite
Monchiquite
Analcitite
Trachyte
Basaltic lavas, undifferentiated
Olivine basalt
Trachybasalt
Agglomerate
Basaltic lavas, undifferentiated
Olivine basalt
Basalt
Basanite
Tephrite
Trachyte
Trachyandesite
Andesite
Nephelinite
Phonolite
Tuffs
Agglomerates and volcanic conglomerates
Tuffs
Agglomerates and volcanic conglomerates
Ignimbrite
Basaltic conglomerates
Trachytic tuff
Silcrete
Breccia of silcrete and fenite
Fenite
Altered Ungaran gneiss, epidotised and silicified
Quartzite
Acid gneiss, undifferentiated
Quartzo-feldspathic gneiss
Acid biotite gneiss
Acid garnet gneiss
Amphibolite
Hornblende garnet gneiss
Trachyte dyke
Silcrete dyke
GEOLOGICAL BOUNDARIES
Observed
Approximate
Gradational
GENERAL STRUCTURE
Inclined
Vertical
Foliation
Lineation in plane of foliation
FAULTS
Approximate or inferred, generally concealed
Normal (Hach on downthrow side)
Main road
Secondary road
Motorable track
Village, settlement
Principal buildings
Mission
Landing ground
Locality or area name
Mountain or hill name
Hill feature
Trigonometrical point
Spot height (from aneroid barometer reading)
Steep slope and escarpment features
Cliff
Spring, permanent and seasonal
Well, permanent and seasonal
Waterhole, permanent and seasonal
Borehole
Rain pond
Dam
Old shore-line features
FLIGHT DIAGRAM
Photography by Fairey Air Surveys Ltd. 1958.
Quarter Degree Sheet Index
Note: Alternative references to this sheet:
International Sheet Number 3836 A.S.
Tanzania Degree Sheet Number 37 N.E.

APPENDIX II

ENDULEN

Photo 1. View of spring seepage area at headwaters of stream. Fig tree observed on the left.

Photo 2. View of headwaters of spring-fed river, looking upstream.

Photo 3. View spring-fed river, looking downstream.

Photo 4. View of concrete structure used to dam river water.

Photo 5. View of locals' clothing washed in river and hung out to dry.

Photo 6. View of local herding cows to stream to drink.

Photo 7. River channel located in lower topography/more vegetated area in center of picture.

ENGINA

Photo 1. View of spring site. Small spring-fed wetland can be observed in the far portion of the picture behind people where tall vegetation is observed.

Photo 2. View of small spring pool that supports tall wetland vegetation.

Photo 3. Additional photo of wetland vegetation. Change in vegetation is interpreted to represent extent of spring seepage area.

Photo 4. View of flowing water coming from highly vegetated spring seepage area. Water is flowing toward photographer.

Photo 5. View spring seepage area on left and concrete drinking structure on left. Water flows from seepage area into the concrete drinking area.

Photo 6. Close-up view donkey's drinking from concrete drinking area.

MTANE

Photo 1. View of Mtane River channel surrounded by vegetation and Yellow Fever trees. Locals' clothes are observed hanging on shrubs to dry after washing them in the river.

Photo 2. View of the river headwaters where groundwater is seeping out.

Photo 3. View of groundwater discharging into the river.

Photo 4. Close-up view of spring discharge area/ spring boils.

Photo 5. Downstream view of spring discharge area.

Photo 6. View of dry river bed located upstream of spring discharge area.

Photo 7. View of flood deposits in river bank.

Photo 8. View of downstream portion of river.

KISIMA NGEDA

Photo 1. View of small portion of extensive wetland system at Kisima Ngeda.

Photo 2. View of one of the spring pools surrounded by wetlands at Kisima Ngeda.

Photo 3. View of basalt outcrop located immediately adjacent upslope of the springs.

Photo 4. Close-up view of basalt outcrop.

Photo 5. View from basalt outcrop looking north. Wetlands observed along the fringes of Lake Eyasi to the west.

Photo 6. View from basalt outcrop, looking west toward Lake Eyasi. Wetlands are observed to extend up to the lake.

Photo 7. View from basalt outcrop, looking south. Wetlands observed along the fringes of Lake Eyasi to the west.

Photo 8. View from basalt outcrop, looking east. Landscape appears to be less vegetated upslope.

Photo 9. View of Mt. Oldeani from the Kisima Ngeda area. Evidence of streams can be seen on the slope of the mountain.

GARAFANI

Photo 1. View of spring seeping from rock into spring pool surrounded by wetland vegetation, looking downslope.

Photo 2. Additional view of spring pool surrounded by wetland vegetation.

Photo 3. View water seeping out of rock (left).

Photo 4. Close-up view of water seeping from rock.

Photo 5. View of spring sampling.

Photo 6. View of 5-gallon buckets that the local people bring to the spring to fill with water.

ESERE

Photo 1. View wetland vegetation surrounding spring area.

Photo 2. Additional view of wetland.

Photo 3. View of water pump located within wetland.

Photo 4. View of tufa deposit located in the area. Person on right is ~1.6 meters tall, for scale.

Photo 5 Tree growing out of tufa deposit.

Photo 6. View of local bringing goats to spring to drink.

Photo 7. View of man-made concrete dam.

Photo 8. View of highly fractured tuff deposits.

Photo 9. Additional view of highly fractured tuff deposits.

Photo 10. View of dry riverbed located near wetlands.

EREMET

Photo 1. View looking into pale lake basin where springs discharge, looking west.

Photo 2. View of the western edge of the paleo lake basin, looking north. Wetlands form within the basin.

Photo 3. View of reworked tuff along paleo lake bed wall where groundwater was observed to discharge from.

Photo 4. View of spring pool and surrounding wetland vegetation.

Photo 5. Additional view of wetlands along the western rim of the paleo-lake basin, looking west. Water flows from east to west.

MIDDLE & UPPER GARUSI RIVER

Photo 1. Dry channel bed of the Middle Garusi River.

Photo 2. Mud cracks on floor of Middle Garusi River.

Photo 3. Additional photo of dry Middle Garusi River bed.

Photo 4. Middle Garusi River photograph. Retrieved DIVER from river by Joseph Masoy and Gail Ashley. DIVER was secured to root of tree with cable ties and buried under boulders on July 2, 2016.

Photo 5. View of dry Upper Garusi River channel. The DIVER installed in this channel was not recovered.

Photo 6. Additional photo of dry Upper Garusi River channel.

BONUS PHOTO. Giraffe tongue. You're welcome.

APPENDIX III

Site	Latitude	Longitude	Elevation	$\delta^{18}O$_Picarro (‰)	δD_Picarro (‰)	Country	IPL_Sample_ID	Date	Type
Ngoile Spring	-3.0397	35.4834	1345	-4.86	-20.97	TZ	IPL_18W_101	6/18/2018	Spring
Misilli Spring	-2.9835	35.5066	1335	-4.38	-17.92	TZ	IPL_18W_102	6/18/2018	Spring
Olbalbal Lake	-2.9749	35.4328	1358	-3.58	-26.59	TZ	IPL_18W_103	6/18/2018	Lake
Endulen Spring	-3.2156	35.2690	1815	-4.05	-18.61	TZ	IPL_18W_104	6/24/2018	Spring
Esere Well	-3.3014	35.1873	1593	-4.75	-26.32	TZ	IPL_18W_105	6/22/2018	Ground
Engina Spring	-3.2165	35.2607	1784	-4.08	-18.50	TZ	IPL_18W_106	6/23/2018	Spring
Mtane River	-3.0264	35.2758	1532	-3.29	-15.42	TZ	IPL_18W_107	6/23/2018	River_or_stream
Eremet Spring	-3.0255	35.0749	1596	-4.49	-26.17	TZ	IPL_18W_108	6/24/2018	Spring
Lake Eyasi Lodge Well	-3.4877	35.3606	1057	-4.98	-20.86	TZ	IPL_18W_109	6/27/2018	Ground
Namiri Spring	-2.5511	35.0970	1668	-3.82	-17.93	TZ	IPL_18W_110	6/30/2018	Spring
Klein Spring	-1.8534	35.2237	1747	-3.38	-15.08	TZ	IPL_18W_111	6/30/2018	Spring

APPENDIX IV

2005													
Month	**JAN**	**FEB**	**MAR**	**APR**	**MAY**	**JUN**	**JUL**	**AUG**	**SEP**	**OCT**	**NOV**	**DEC**	**TOTAL**
Head quarter	7.7	125.5	219.4	154	55.5	30.5	11	5	43	35	22	48	819.4
Mokilal	113	57.5	169.2	114	12	0	16	0	4	20	28	0	537.7
Esirwa	32	26.5	32.7	74	22	16	12	0	0	0	10	8	233.2
Endulen	150	54.6	131.6	102	32	26	0	0	0	0	0	0	496.2
Esere	38.5	44	65.2	50.9	0	0	0	0	0	15	59.1	0	272.7
Kakesio	0	11	12	10	8	4	0	0	0	0	0	0	45.1
Angaengati	78	86	96	36	101	118	41	22	12.8	58	52	26	726.8
Old east gate	19.7	32	38	46	32	47	35	23	13	-8	0	8	298.7
Ndutu	404	369	108.5	753	112	202	0	60	86	54	1765	171.2	2496.2
Oldupai	212	32	90	36	22	0	0	0	0	0	28	0	410
Nasera	24	30	32	32	16	17	14	0	0	11	0	16	192
Olbalbal	16.8	18.5	30	16	12	0	9	6	0	0	0	6	114.3
seneto	11	16.9	18	16	12	11	11	4	4	0	8	0	111.9
Lerai	16	18.2	40	12	14	16	22	10	12	0	12	4	174.2
Ngoitokitok	18	20	22	9	6	11	7	0	6	0	6	0	105
Munge	22	32	38	11	8	12	0	12	0	3	0	0	138
Nainokanoka	142	79	107.4	14	132	4	0	4	0	0	0	155	637.4
Alailelai	114	83	181	145.9	67	25	0	12	8.2	54.7	45.4	120	857.2
Naiyobi	202.5	38.5	86	12	8	0	0	0	0	36	183	187	752.5
Endamagha	8.5	16	30	9.5	13	12	0	0	3	0	0	0	92
Mbulumbulu	46	62	75.8	42.9	31.8	32.4	0	0	11	4	129	0	435
2006													
Month	**JAN**	**FEB**	**MAR**	**APR**	**MAY**	**JUN**	**JUL**	**AUG**	**SEP**	**OCT**	**NOV**	**DEC**	**TOTAL**
Head quarter	101	70.8	201.8	307.5	10	41	18.4	7.6	8.6	0	10	37	813.7
Mokilal	68.2	87	227	170	73	0	0	7.3	0	13	177	291	1113.5
Esirwa	18	32	38	68	32	0	0	4.2	0	14.2	144.9	74.3	225.6
Endulen	95.5	156.4	201.8	126.4	88	0	0	0	0	26	227.6	273.2	1194.9
Esere	54.8	38.9	96.6	75.6	0	0	0	0	0	0	46	152.8	464.7
Kakesio	54.8	38.5	96.6	22	13	0	0	0	0	0	46	152	422.9
Angaengati	39	23	128	132	89	0	0	0	0	0	112	0	523
Ndutu	82	38	93	34	32	0	0	0	0	12	56	71	418
Old east gate	85.8	98.4	103	190.9	119	0	0	6.3	2.3	0	229.5	223.5	1158.7
Oldupai	40	64	91	38	113	0	0	0	0	0	10.2	81.6	437.8
Nasera	20	38	0	56	0	0	0	0	0	29	118	78	339
Olbalbal	40	64	91.5	42	12	0	0	0	0	28	42	56	375.5
seneto	5	0	18	16	9	0	0	0	0	38	11	36	133
Lerai	12	28.6	30.5	23	16	0	0	0	9.4	14.6	38.2	72	257.3
Ngoitokitok	18	0	30	10	7	0	0	0	0	22	28.6	46.5	162.1
Munge	12	28	30.5	0	0	0	0	0	0	16	37	71	194.5
Nainokanoka	18	59	88	250.5	130	0	0	28	26	68.9	0	0	668.4
Alailelai	97.2	50.1	152.6	133.7	109.8	0	4	7.6	0	88	208	257	1107.8
Naiyobi	56.1	46	156	153	65	0	0	45.3	58	176	172	275	1202.4
Endamagha	12	28	15	13	7	0	0	0	0	0	28	52.7	155.7
Mbulumbulu	65.6	45.7	145.9	163	61.4	0	0	0	0	80.6	227.8	346	1136
2007													
Month	**JAN**	**FEB**	**MAR**	**APR**	**MAY**	**JUN**	**JUL**	**AUG**	**SEP**	**OCT**	**NOV**	**DEC**	**TOTAL**
Head quarter	193.1	236	219	196	213.8	51.2	22.6	7.5	5.4	16.3	189	133.4	1413.2
Mokilal	165	124	98	81	84	49	15	0	0	24	92	137.4	869.4

Esirwa	42	56	29	39	13	0	11	0	6.7	11.3	18.7	19.3	246
Endulen	154.7	118.2	73.1	64	53	18.2	0	12	0	12.2	58.2	0	563.6
Esere	86	113.2	41	10	0	0	0	0	0	12	43.2	136	441.4
Kakesio	28	36	29	37	9	0	2.3	0	7.3	9	10.3	22.1	190
Angaengati	56	112	68	53	44	16	21	11	39.2	21.8	32.5	68.5	543
Ndutu	26	28	48.5	28	58	19.1	17.6	51	0	0	0	0	230.3
Old east gate	131.1	87.1	153.2	85	46.8	19.8	17	12.2	9.1	0	27.8	103.3	692.4
Oldupai	13	110	38	0	0	0	0	0	0	0	0	52	213
Nasera	78	18	26	26	31	10.1	10.1	0	0	0	0	0	199.2
Olbalbal	16	27	21	35	34	0	9	0	15.5	11	17.8	42.8	229.1
seneto	13	18	16	21	22	0	11.1	0	0	6.1	23	13	142.2
Lerai	35	28	16	51	21	18	14.2	8	16	17.1	25.2	18.1	267.6
Ngoitokitok	52	46.4	14.2	77	16	13	16.2	12.7	5	13.1	18.6	16.5	300.7
Munge	64	56	18.2	61	225	26	20	7.8	10.6	20.5	26.1	36.1	571.3
Nainokanoka	116.8	121.6	78	205.4	46.8	0	12	25	15.1	10.7	50.3	189.7	881..4
Alailelai	179	112	110	146	86	2	26	13.8	2	15	32	145	845.4
Naiyobi	232.1	112.8	50	160.5	15.5	0	8.6	11.4	0	11.7	91.5	211	905.1
Endamagha	18.6	26.6	9	30	34	4.3	0	9	32	35	13.1	49	260.6
Mbulumbulu	114.6	201.9	74.1	139.1	123.6	0	12.7	0	16.8	19.3	24.1	165	891.2
2008													
Month	**JAN**	**FEB**	**MAR**	**APR**	**MAY**	**JUN**	**JUL**	**AUG**	**SEP**	**OCT**	**NOV**	**DEC**	**TOTAL**
Head quarter	92.5	141	175.5	214.1	20.1	48.5	0	2.3	6.3	113	128	138	1079.3
Mokilal	87	131	264	54	49.8	33.2	9	0	0.2	86	157	123	994.2
Esirwa	22	38	77.9	17	13	11	9.2	31	11.6	68	118	112	528.7
Endulen	30	47.2	207	113	23.1	19.6	0	0	10.3	56	119.6	132.9	758.7
Esere	22	70	75	12.5	0	0	0	0	5.6	8	50.3	29	272.4
Kakesio	18.8	28.8	11.2	3.2	0	0	0	0	0	31	43.9	59.7	196.6
Angaengati	63.1	89	92	15.3	0	45.2	0	7	25.1	33	81.2	74.3	525.2
Ndutu	30	34	11	13	5.2	0	0	9	10.5	72.6	41.9	93.2	320.4
Old east gate	46.3	77.8	117.2	56.8	0	31.5	0	1.6	27.1	31.5	136.4	68.7	594.9
Oldupai	0	0	131.3	21.4	0	0	0	0	0	0	46.6	23.2	222.5
Nasera	17	23	25	28	18	0	0	0	0	19.7	31.5	49.2	211.4
Olbalbal	32	31	32	23	11.3	0	0	0	0	11.4	29	22.7	192.4
seneto	23	32.8	29.3	4	4.2	0	0	0	11	28.8	33.8	41.6	208.5
Lerai	43	52	33.2	43.1	18.2	12.5	0	9	18	37.2	91	22.1	379.3
Ngoitokitok	29.5	47	31	12	7	5.2	0	0	0	37	51.2	67.3	287.2
Munge	36	49	32.8	11	17	15.2	0	0	23	62	84.3	74	404.3
Nainokanoka	133.7	96.5	65.8	107.2	49.1	21.8	0	0	39.5	128	110	133	884.6
Alailelai	68	85	116.7	61.8	22	19.9	0	20.1	89.7	115.4	123.8	149.3	871.7
Naiyobi	0	0	0	88	0	0	0	0	0	168.4	0	0	256.4
Endamagha	31	22	31	16	21	0	0	0	24.7	41	21.8	18.6	227.1
Mbulumbulu	118.7	199.5	70.1	204.2	0	13.1	0	0.4	0.7	81.6	74.8	31.3	794.4
2009													
Month	**JAN**	**FEB**	**MAR**	**APR**	**MAY**	**JUN**	**JUL**	**AUG**	**SEP**	**OCT**	**NOV**	**DEC**	**TOTAL**
Head quarter	99.5	113.2	99.9	264.5	52.8	18	0	4	0	47	83.7	115.2	897.8
Mokilal	112	58	168	183.5	35	0	0	0	0	22.2	308	0	886.7
Esirwa	30	12	3	4.5	25	0	0	0	1	12	20	0	107.5
Endulen	3.8	0	177.3	169.7	96.6	0	0	0	0	111	127.5	221.6	907.5
Esere	46	31	63	48	11	0	0	0	6	7	200	233	645
Kakesio	27	17	3	24	6	0	0	0	0	11	15	0	103

Angaengati	38	11	12	13	13	0	0	9	5	8	4	0	113
Ndutu	15	8	4	3	15	20	0	0	0	0	4	0	69
Old east gate	50.1	18	88	123	10.7	0	0	0	0	0	115	213.4	618.2
Oldupai	9.8	9.8	9.8	9.8	9.8	9.8	9.8	9.8	9.8	9.8	9.8	9.8	117.6
Nasera	14	11	1	1	14	0	0	0	0	0	0	0	41
Olbalbal	40	29	7	4	6	0	0	0	0	0	0	0	86
seneto	17	3	6	7	7	0	0	0	2	1	16	0	59
Lerai	100	6	9	19	34	0	0	0	3	2	10	0	183
Ngoitokitok	39	9.5	6	29	19	0	0	0	0	5	17	0	124.5
Munge	41	9	4	11	24	0	0	0	15.3	4	3	0	111.3
Nainokanoka	131.1	96.5	144	135.5	54.4	0	0	0	15.3	42.5	205.6	254.6	1079.5
Alailelai	15	29	85	158	34	0	0	0	12	15	91	181	620
Naiyobi	105.5	161	0	180.5	166.5	0	0	0	0	55	115	0	783.5
Endamagha	19	7	8	17	13	0	0	15	0	12	20	0	111
Mbulumbulu	68	81	89.2	292.5	39	0	0	0	0	43.5	89.9	0	703.1
2010													
Month	**JAN**	**FEB**	**MAR**	**APR**	**MAY**	**JUN**	**JUL**	**AUG**	**SEP**	**OCT**	**NOV**	**DEC**	**TOTAL**
Head quarter	333.9	201.2	245.2	115.3	67.4	20.3	0	1.7	0	0	44	112.1	1141.1
Mokilal	67	160.6	120.5	134	78	13	0	0	0	113	77	529	1292.1
Esirwa	71	9	0	35.5	0	0	0	0	0	0	19.2	7	141.7
Endulen	86.4	129.9	219.1	126.9	0	0	0	0	0	2.1	101.3	140.9	806.6
Esere	0	87	135.2	37.5	22	0	0	0	0	2.2	56.4	82	422.3
Kakesio	0	88	0	0	0	45	0	0	0	0	0	4.5	137.5
Angaengati	0	86	0	0	0.5	0	0	0	0	0	0	7.4	93.9
Ndutu	0	53	0	31.6	3.9	0	0	0	0	2	0	24	114.5
Old east gate	68.7	54	156	68.7	68.4	0	0	0	0	2.1	16	147.3	581.2
Oldupai	363	45	10	0	0	0	0	0	0	0	0	8.5	426.5
Nasera	0	4	0	24	11	0	0	0	0	0	0	0	39
Olbalbal	0	2	0	27	3.6	0	0	0	2.7	3.3	2.5	11	52.1
seneto	56	55	0	9	55	0	0	0	0	0	0	0.5	175.5
Lerai	49	59	0	35.5	51	0	0	0	0	0	0.5	0	195
Ngoitokitok	99	10	0	20.5	10	0	0	0	0	0.7	1.3	5.7	147.2
Munge	52	0	0	0	1	0	0	0	0	2	0.5	0.5	56
Nainokanoka	169	245	171	169	35	0	0	0	0	43.7	102.8	129.3	1064.8
Alailelai	191	271	215	52	35	0	0	0	0	68	47	134	1013
Naiyobi	191	0	215	20	0	0	0	0	0	0	120.5	0	546.5
Endamagha	0	40	5.8	0	0	0	0	0	0	0	0	129.5	175.3
Mbulumbulu	65.7	155.8	288.7	65.7	72.2	2	0	0	72.2	0	119.1	80	921.4
2011													
Month	**JAN**	**FEB**	**MAR**	**APR**	**MAY**	**JUN**	**JUL**	**AUG**	**SEP**	**OCT**	**NOV**	**DEC**	**TOTAL**
Head quarter	84.6	115.5	193	52.2	139.2	34.8	13.7	7.2	13.4	113.5	133.3	112.2	1012.6
Mokilal	229.5	179	95	27	14	67	0	15	44	113	85	275	1143.5
Esirwa	0	8	8.7	0.5	0	0	0	0	4.1	1	17.7	16.7	56.7
Endulen	116.5	59	297.3	74	10.4	46	9.5	0	21	72.5	124.2	198.3	1028.7
Esere	0	53.5	93	1.6	15.6	18	0	118	14	19	75	54	461.7
Kakesio	3	4	8.3	0	0	0	0	0	0	3	3.7	20.7	42.7
Angaengati	8.1	0	19.6	0	0	2.5	0	0	1.4	2.3	9.2	13.3	56.4
Ndutu	94.6	0	78.2	28.7	0	40.9	7.1	0	26.7	81.2	92.5	76.9	526.8
Old east gate	0	0	0	0	15	8	6.1	9.2	0	1	12.5	26.5	78.3
Oldupai	6.5	0	120	0	0	15	0	0	0	0	44	0	185.5

Nasera	3	2.5	15.5	0	0	5.3	0	0	0	0	3.8	6.5	36.6
Olbalbal	0	4	11.5	0	0	4.5	3.9	5	6.2	4	9.2	9	57.3
seneto	0	0.5	8	0	0	0	13	2.1	1.2	0	7	5	36.8
Lerai	0	0	17.2	2.8	1	1.5	0	0	2.4	1.4	5.6	11.1	43
Ngoitokitok	6.8	4.5	12	3.5	0.5	0.7	0	0	2.3	2.1	7.9	13.7	54
Munge	0	1.5	8.5	0	0	2.7	0	0.4	6.6	0	5.6	10.2	35.5
Nainokanoka	70.2	30.8	108.6	34	126	12	0	10.5	44.9	117.2	248	122.5	924.7
Alailelai	89	37	115	9	11	4	2	7	19	45	98	131	567
Naiyobi	70.5	75	188.5	93	15	0	0	0	0	25.5	186.2	223.7	877.4
Endamagha	16	7	11.7	13	0.2	4.8	0	0	0.5	2.1	10.7	10.6	76.6
Mbulumbulu	8.5	14.8	126.5	140.6	59.6	2	0	0	0	44.1	201.2	92	689.3
2015													
Month	**JAN**	**FEB**	**MAR**	**APR**	**MAY**	**JUN**	**JUL**	**AUG**	**SEP**	**OCT**	**NOV**	**DEC**	**TOTAL**
HQ													
seneto	20	21.5	24.5	24.8	7.2	29	26.2	0	18.6	13.1	9.5	10.8	205.2
lerai	78	84.9	94.9	100	0	80	32	0	47.1	15.6	6	12.9	551.4
Munge	95	80	62	55	12.2	63.5	27.1	0	57.2	59.7	52.1	61.9	625.7
Ngoitoki	64	64.1	85.2	74	5	74	69.5	24	0	49.6	33.5	34.5	577.4
Olbalbal	49.2	42	23.1	37	1.5	25.5	67.1	26	20.9	7.5	19	70.1	388.9
Nasera	15	17	80.3	15.8	17.5	104.3	5	19	19.9	18.6	8.5	56.3	377.2
Old gate	27.5	23	47.2	7	9.5	47.9	23.5	6	6.5	7	16.2	19.7	241
Kakesio	47.1	46	26	11.2	0	45.2	6	35.6	22	16	16	25.5	296.6
Esirwa	42.3	39.1	16	18.5	13.8	26.2	39	18	13.1	13.7	18.6	32.5	290.8
Endamag	34	29	0	91.2	9.4	31.5	20.7	5	5.5	12	8.7	16.1	263.1
Angata	8	72	33	48.5	0		6.5	0	6	9	10		193
Mbulumbul			44.1										
2016													
Month	**JAN**	**FEB**	**MAR**	**APR**	**MAY**	**JUN**	**JUL**	**AUG**	**SEP**	**OCT**	**NOV**	**DEC**	**TOTAL**
HQ							0	0	0	0	7	7.2	
seneto	8.6	16	19.5	22.1	31.5	28	0	0	0	28	64	8.5	226.2
lerai	21	32	75.9	51	39	72	2	0.5	0	12.5	5.5	46.8	358.2
Munge	65.7	32.7	33.4	24	81	38	0	7	3	9.3	41	54	389.1
Ngoitoki	39.5	75.6	40	77.2	72	72	6	0	0	4	5.5	70	461.8
Olbalbal	23	17.8	0	9.5	30.5	3	1	0	0	5.5	0	20	110.3
Nasera	19 .5	38.5	30.2	32.5	32	0	2.5	0	5	15.2	0	32.8	188.7
Old gate	34	32	39.6	38.1	43.5	45	0	0	4	26.2	2.5	21.5	286.4
Kakesio	30	50	26.2	48	48.1	0	1	0	4.7	23	16	18.5	265.5
Esirwa	13.2	36	63.7	61.1	74	0	0	3	0	7	3	33.5	294.5
Endamag	50.5	36	50.1	37.3	35.5	0	3	0	0	3	0	11.6	227
Angata			62.4	79.1	81.5	84	4	3	0	31.4	85	40.9	471.3
Mbulumbul		NIL	NIL	NIL			0	0	0	45	6.7	60.5	112.2

Notes:

Rainfall Measurements collected by NCAA

NCAA = Ngorongoro Conservation Area Authority

NCA = Ngorongoro Conservation Area

NCAA HQ Rainfall Data from 1963-2014

YEAR	JAN	FEB	MAR	APR	MAY	JUN	JUL	AUG	SEP	OCT	NOV	DEC	TOTAL
1963	140.7	80.1	170.3	240.3	130.8	50.6	10.0	2.7	8.1	NIL	310.3	200.9	1344.8
1964	40.6	140.4	190.4	290.2	30.1	10.0	20.0	10.0	5.5	6.3	30.0	150.1	923.6
1965	100.7	70.1	120.9	150.4	70.1	NIL	NIL	2.5	50.0	10.8	2.5	50.5	628.5
1966	20.2	70.6	140.3	30.7	50.8	50.1	NIL	1.0	4.5	10.7	10.5	60.0	449.4
1967	50.0	80.6	60.8	250.7	260.1	70.6	100.0	50.1	50.5	70.8	170.7	200.3	1415.2
1968	120.1	80.9	100.7	160.3	260.6	4.3	4.5	0.5	0.5	8.6	100.2	200.8	1042.0
1969	94.9	129.6	13.9	16.5	11.4	5.4	22.8	NIL	46.2	160.0	245.3	76.2	822.2
1970	251.3	88.1	191.2	115.7	94.7	22.5	NIL	NIL	5.5	6.0	105.4	177.9	1058.3
1971	55.9	69.5	37.3	224.3	47.4	18.8	15.8	15.1	NIL	NIL	28.6	97.8	610.5
1972	104.6	128.7	108.7	84.2	108.8	31.3	5.8	NIL	0.9	121.7	154.4	181.4	1030.5
1973	303.8	278.8	5.4	181.4	39.1	13.1	NIL	NIL	8.0	10.0	34.4	38.8	912.8
1974	51.6	56.6	308.4	39.5	48.9	41.5	72.0	10.4	10.4	2.7	42.1	82.1	766.2
1975	66.1	32.2	142.8	121.2	118.2	3.6	28.9	NIL	8.7	15.0	4.5	117.9	659.0
1976	54.0	90.8	112.0	206.2	42.0	27.3	3.5	6.2	15.5	16.5	57.3	81.8	713.1
1977	133.1	173.2	103.1	300.8	85.6	85.6	2.3	1.9	10.0	14.4	112.8	145.5	1130.7
1978	160.0	61.3	228.1	197.4	58.7	12.1	2.7	NIL	NIL	40.1	51.8	131.5	943.7
1979	140.4	103.7	136.6	227.8	26.5	10.1	34.4	3.0	3.0	7.0	3.0	110.0	805.5
1980	73.1	22.6	10.4	69.5	93.7	12.7	7.0	58.4	12.7	10.1	80.7	57.1	508.0
1981	73.0	60.5	183.8	137.6	NIL	NIL	2.5	28.4	6.0	35.0	23.3	121.1	671.2
1982	90.2	62.3	48.5	152.1	137.6	49.7	15.5	30.0	30.6	102.3	167.8	156.4	1043.0
1983	352.8	75.3	287.2	329.1	299.4	80.5	13.7	4.9	14.4	16.0	45.9	87.9	1607.1
1984	103.3	39.7	97.3	178.3	29.2	20.3	25.2	NIL	1.1	105.7	110.4	105.2	816.2
1985	28.8	96.5	282.4	203.9	79.4	5.7	5.3	2.5	NIL	15.0	129.5	71.4	920.4
1986	86.0	20.0	189.7	191.1	139.5	11.1	NIL	2.0	1.0	81.5	99.5	179.5	1000.9
1987	135.3	99.0	141.1	71.0	141.5	4.5	NIL	11.1	NIL	NIL	37.7	72.2	713.4
1988	215.2	56.7	93.7	176.3	10.5	28.0	0.5	17.3	6.1	23.4	29.9	87.2	744.8
1989	117.6	122.4	203.3	318.0	180.0	21.1	NIL	10.0	20.0	118.3	NIL	187.4	1298.1
1990	76.3	167.4	167.8	179.0	128.0	4.0	NIL	NIL	2.5	NIL	NIL	160.0	885.0
1991	97.9	40.0	83.0	128.2	94.8	7.7	2.2	NIL	NIL	43.0	38.2	284.0	819.0
1992	NIL	91.0	67.0	330.0	14.0	NIL	NIL	NIL	NIL	10.4	7.0	188.4	707.8
1993	128.0	108.0	104.0	NIL	103.0	NIL	NIL	NIL	NIL	NIL	6.0	NIL	449.0
1994	130.0	170.0	320.0	270.0	210.0	45.0	32.0	NIL	NIL	66.0	87.0	76.0	1406.0
1995	2.0	20.0	67.0	109.0	98.0	NIL	NIL	NIL	NIL	NIL	NIL	NIL	296.0
1996	NIL	91.0	NIL	284.0	128.8	35.1	NIL	NIL	NIL	NIL	15.0	204.4	758.3
1997	NIL	NIL	274.9	428.6	258.4	47.0	15.0	NIL	NIL	35.0	206.0	440.1	1705.0
1998	292.3	NIL	NIL	NIL	NIL	37.0	NIL	NIL	NIL	17.0	51.0	26.5	423.8
1999	107.5	10.5	167.0	85.1	6.0	NIL	NIL	32.0	8.0	0.5	35.5	51.0	503.1
2000	38.0	89.7	79.0	78.8	73.2	16.5	1.0	33.0	NIL	NIL	122.0	155.0	686.2
2001	369.0	88.5	171.2	181.2	99.3	5.9	25.0	6.0	NIL	1.0	41.0	63.9	1050.4
2002	145.4	113.9	142.0	234.0	147.1	NIL	20.0	16.0	NIL	60.5	56.0	216.6	1150.9
2003	146.0	64.0	67.1	157.5	207.5	22.0	10.2	1.0	4.5	44.7	96.4	54.8	724.5
2004	46.7	75.8	141.4	198.0	55.6	9.3	1.5	NIL	19.5	29.7	92.7	217.8	897.0
2005	70.7	125.5	219.4	154.0	55.5	30.4	10.3	11.0	5.0	43.0	75.2	52.2	852.2
2006	91.2	60.8	202.1	307.5	162.0	41.0	18.4	8.6	NIL	52.1	203.4	321.6	1468.7
2007	293.1	236.0	219.0	196.0	213.8	51.2	22.6	75.5	5.4	16.3	18.9	133.4	1413.2
2008	92.5	141.0	175.5	214.1	20.1	48.5	0.0	2.3	6.3	113.0	128.0	138.0	1079.3
2009	99.5	113.2	99.9	264.5	52.8	18.0	0.0	4.0	0.0	47.0	83.7	115.2	897.8
2010	7.7	125.5	219.4	154.0	55.5	30.5	11.0	5.0	43.0	35.0	22.0	48.0	819.4
2011	333.9	201.2	245.2	115.3	67.4	20.3	0.0	1.7	0.0	0.0	44.0	112.1	1141.1
2012	56.6	45.8	131.7	271.7	126.8	2.2	NIL	17.8	4.7	18.7	48.1	146.7	870.8
2013	231.1	98.9	156.4	271.5	126.8	2.2	0.0	10.1	23.1	11.7	15.4	198.2	1145.4
2014	5.1	83.2	209.1	83.1	44.4	30.7	0.3	NIL	29.7	28.3	35.2	146.7	695.8
Average	122.9	95.0	148.7	187.2	102.9	26.6	15.2	14.5	13.1	38.2	75.8	135.6	912.0

Notes:
Rainfall measurements tajeb by **NCAA HQ** in milimeters
NCAA HQ = Ngorongoro Conservation Area Authority Head Quarters

Kisima Ngeda Rainfall Data from 1995-2015

Longitude 35.22 E ; Latitude 3.30 S

	JAN	FEB	MAR	APR	MAY	JUN	JUL	AUG	SEP	OCT	NOV	DEC	TOTAL
1995	31	102	47	16								6	202
1996	95	133	49	18								79	374
1997	35	18	55	125						3	75	222	533
1998	245	158	57	171	75						11		717
1999	205	20	296	67								16	604
2000	12	35	161	6							116	189	519
2001	188	25	131	23									367
2002	262	74	75	23	134					7	42	150	767
2003	57	72	52	17									198
2004	58	20	25	99	10				3		18	207	440
2005	66	95	105	15						3	11		295
2006	107	57	165	66						5	117	263	780
2007	42	173	45	2	6	12	15					185	480
2008	33	69	197	14							58	20	391
2009	64	60	75	196	3						88	58	544
2010	125	83	153	28							2	66	457
2011	86	96	96	9					2	8	105	58	460
2012	36	9	47	97	6						79	107	381
2013	53	86	74	156	6						5	62	442
2014	73	73	85	57	1			12	3	22	19	79	424
2015	42	14	20	176	2		2						256
Average	91	70	96	66	12	1	1	1	0	2	36	84	459

Notes:

Rainfall measurements taken by Chris Schmelling in milimeters

APPENDIX V

Groundwater Modeling in the Lake Eyasi Basin Tanzania, Africa

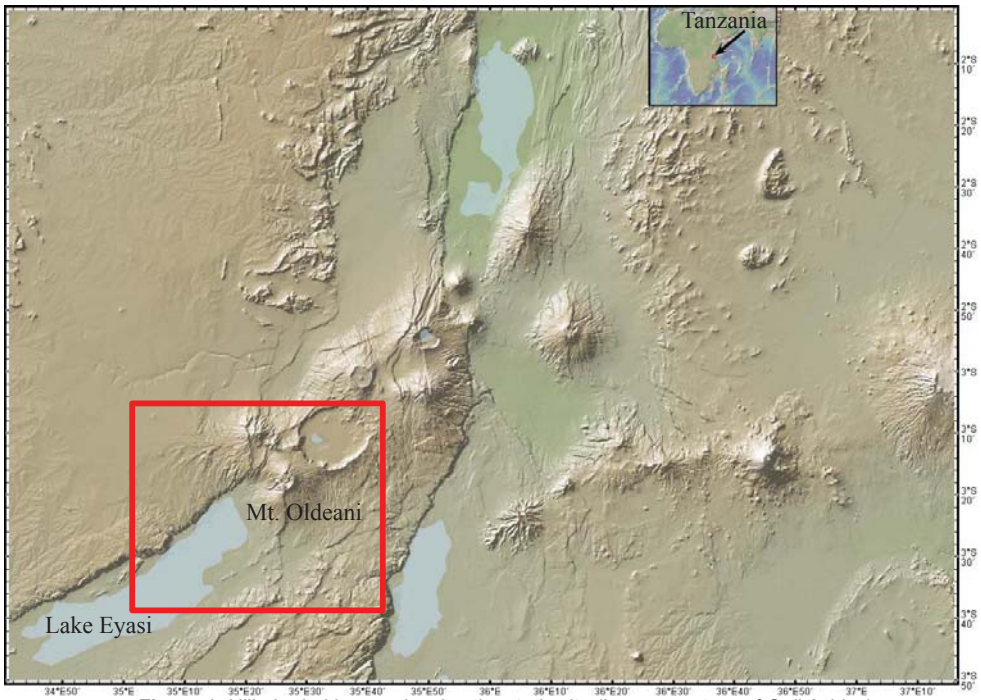

Figure 1: *Hill-shaded image showing the study site (Image courtesy of Gail Ashley)*

Elizabeth Miller
Groundwater Modeling
Fall 2012

Abstract: In this paper, I will document how I made a model to estimate the rate of groundwater flow into the wetlands surrounding Lake Eyasi in Tanzania, Africa. The geology and hydrology of Tanzania is not well understood due to lack of data and low abundance of research. I have made a general model with some educated assumptions to try and simulate the flow of groundwater in the Lake Eyasi watershed by using regional geologic maps and digital elevation maps of the region. The conductivities used are based on the bedrock and general principles of eroded materials. My specific area of study is the wetlands surrounding Lake Eyasi. Groundwater is assumed to flow down the slopes of Mt. Oldeani and feed into the wetland. The travel times ranged from an 1100 year average to a 700 year average, with differing water table recharge values. More refined research of this time period would ideally correlate with the wet and dry periods shown in the wetland stratigraphy and verify how long the wet period response is to feeding the wetland.

Introduction

The Lake Eyasi basin in located in northern Tanzania, Africa. The Lake rests at the base of Mt. Oldeani, a large stratovolcano and part of a large volcanic highland. Groundwater seeps out year-round at the base, feeding a wetland surrounding the mostly dry Lake Eyasi. The wetland is about a meter wide and encircles the Lake.

Figure 2: *The size of the wetland is estimated from Google Earth*

My model was created to estimate the rate of groundwater flow into the wetland. Cores taken in the wetland show that this area was not always fed by groundwater, and that it was dry before groundwater springs formed. East Africa is thought to be affected by cyclic changes in climate influenced by solar radiation. The question is how long it takes for groundwater to start feeding the wetland springs, and how long these springs can sustain the wetland after the rainy period has ceased.

I created a watershed-scale model with the intention of catching all of the potential rivers feeding into the basin and possibly affecting the groundwater interactions with Lake Eyasi. Later research revealed that the aridity of the region does not allow for long-standing rivers and lakes, so only a local-scale model might be necessary. Most of my model analysis is done around the lake margin.

Hydrologic Setting and Conceptual Model

Tanzanian Climate:

There is evidence that the little ice age spawned a wet climate in east Africa (Verschuren, 2000). The little ice age is a large-scale event of a relatively wetter climate, but it is sub-divided by smaller, decade-scale climate fluctuations due to periods of high and low solar radiation, producing drier and wetter climates respectively. This explains the fluctuating water availability in Lake Eyasi and the surrounding rivers, but the wetland exists even when the lake is dry. The wetland's springs must be fed by groundwater slowly permeating through the alluvium on Mt.Oldeani. It would follow that the springs will dry up once the rainy period ends and groundwater completely discharges, a time period inferred by the model.

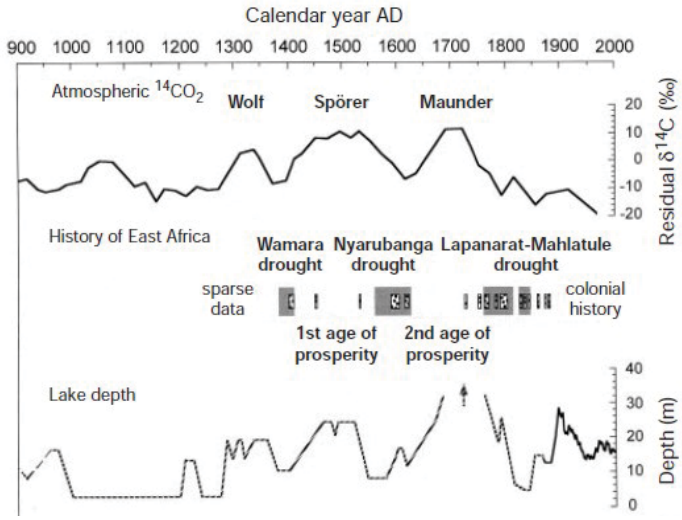

Figure 3: *Graphs showing climate change and corresponding lake level variations recorded in lake cores. Modified from Verschuren, 2000.*

Tanzanian Tectonics:

Northern Tanzania has an extensive record of tectonic activity. My study area is heavily faulted as part of the eastern branch of the East African Rift system, a system which is still currently active. The nearby volcanoes, such as Mt.Oldeani, were formed from crustal thinning and mantle plumes as the Somali micro-plate drifts from the more stationary Nubian plate. This eastern branch of the rift system is associated with higher magmatism and rift-associated volcanism (Dawson, 2008). A result of the extension fracturing is the regions various elongate basins, such as the Lake Eyasi basin I am studying. Lake Eyasi is a saline lake surrounded by volcanic rocks and alluvium sediments. The basin sits on the Tanzanian Craton.

Regional Conductivity:

Resulting from extensive the faulting and fracturing in the basin, the surfacial layer of the region is heavily eroded. Many faults are visible on the surface and die out with unknown depth. Because of this, I have tried to tailor the conductivities in my model to reconstruct a highly permeable top layer, with decreasing permeability with depth. I used Freeze and Cherry's 1997 conductivity chart, and modified the units for use in my model (m/day).

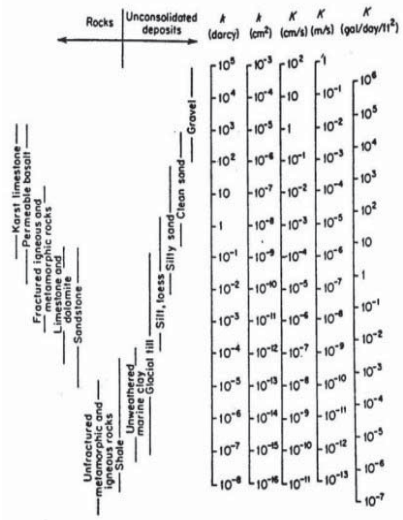

Figure 4: *Table of conductivites from Freeze and Cherry 1979.*

My surface layer represents all of the lithologies and corresponding conductivities for the geologic units shown in figure x. I assume that most of the surface sediments range from sand to gravel, and that permeability gradually decreases with depth. My conductivities are litholigically specific for the first layer of my model (accounting for about 220 m depth) and exist as a homogenous units downward to the bottom of my model (-1000 m).

I have not included any fractures or faults in my model. There are many tiny fractures that would be nearly impossible to input, and the large-scale faulting was not included so as to make a simple representation of flow down the slopes of Mt.Oldeani, which is parallel to the faults, seen in figure 5. If my study was on the flow perpendicular to the faults, I should have included them. In order to somewhat incorporate the presence of faulting and fracturing into my conductivity, I have made units more permeable in the z direction than the x or y directions.

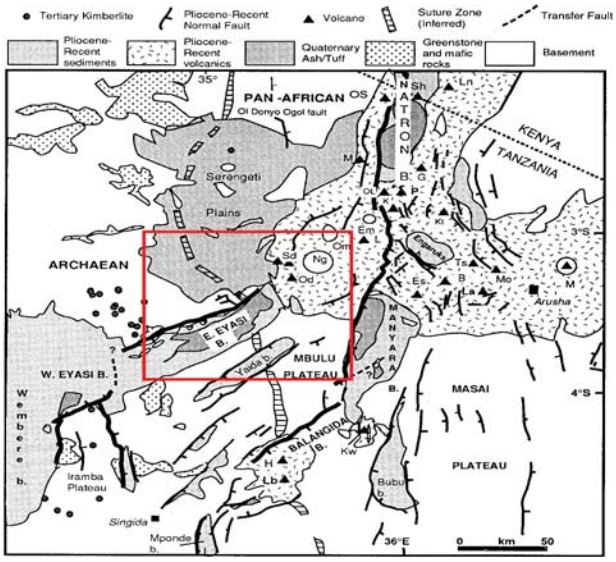

Figure 5: *Map showing major faults in northern Tanzania. Area of interest in outlined in red, Mt.Oldeani is in the NE corner of the box, with Lake Eyasi at it's base.*

Groundwater Source:

The source of my water is groundwater recharge in the high volcanic regions of my study area, with the highest recharge occurring only in areas of high elevation. I have identified the lakes as sinks for the water by making them constant heads. This way, the water will flow from areas of high recharge into the lakes, though they are sometimes, and maybe often, dry saline lakes. Originally I had the major rivers leading into the lakes set as constant heads, but seeing as they are most often dry rivers, unless there is a period of heavy rain, I omitted them from the model. I have included many surrounding rivers as drains, but my model does not incorporate them into groundwater flow. I have not omitted them from the model, but I do not feel like they have an effect on my results. This may be a result of using steady-state flow to run my model, and not a transient flow that may show wet and dry periods.

Groundwater Flow Model

Setting up the model:

The basemap I used for my model is adapted from a regional geology map of Tanzania published in 1959 (figure 6).

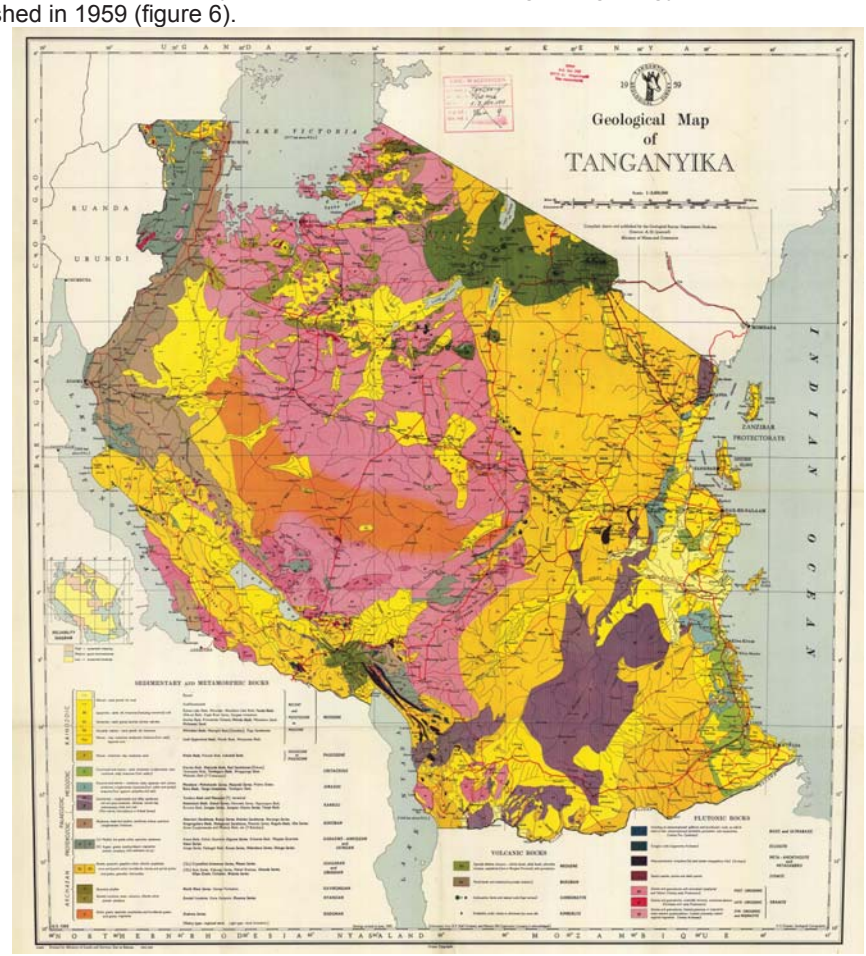

Figure 6: *Regional geology map, Tanganyika Geological Survey, 1959.*

I cut the area roughly into the shape of the internal drainage basin in which my area of interest sits (figure 7).

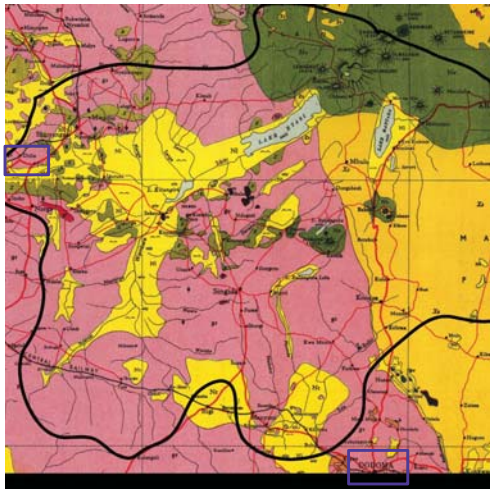

Figure 7: *Basemap image used for my groundwater model. Registration points are highlighted in blue boxes.*

The image was registered by locating a road intersection in the NE region of the image and locating the city of Dodoma in the SW region of the image (highlighted in figure 7). I used GPS coordinates from Google Earth to register this image into visualMODFLOW. I made the boundaries an even 400km^2 for easier calculations, and started the grids as 100km^2 (40 rows and 40 columns). I set the max elevation as 14,000m (an overestimate) and min elevation as -1000m. I have 10 layers in my model, each layer is about 220m. I then refined the grid around my area of interest so that the grids are 1.25km^2 (seen in figure 8).

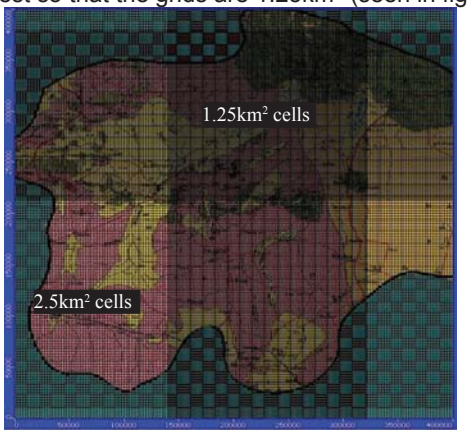

Figure 8: *Grid system of my model, refined in the area surrounding Lake Eyasi*

For my model elevation, I downloaded DEM data from the USGS earth explorer web database and converted it for use in visualMODFLOW by using Global Mapper software. The DEM file I imported into visualMODFLOW is a 1km^2 grid, which is slightly more refined than my model grid.

Boundaries:

The boundaries of my model are set by the drainage basin, a physical boundary of the rainfall catchment area. The way I set up my unit conductivities allows water to flow easier in the z direction than in x or y directions. Flow also decreases with depth. The flow is direction to the intermittent lakes, as I have set them as constant heads.

Model Conductivities:

The conductivities I have used for my model are adapted from Freeze and Cherry's 1997 conductivity chart (figure 4). The top two layers of the model are specific to the lithology seen in the geologic map (figure 6,9), and the lower layers are homogenous, showing decreasing conductivity with depth (figure 10). The high conductivity of the top layers reflects the highly weathered and fractured surface features.

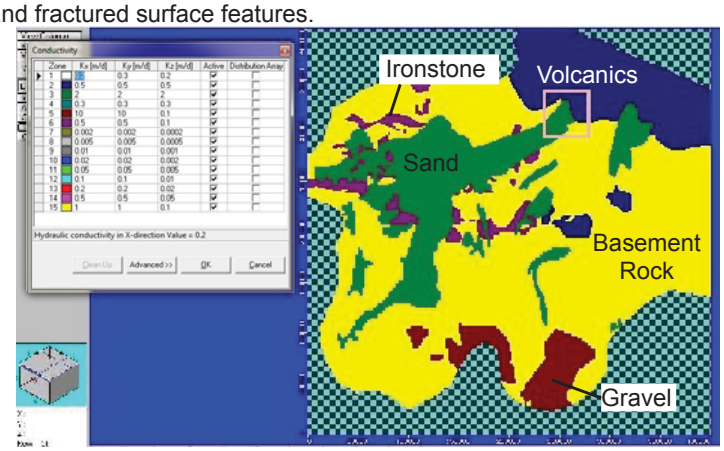

Figure 9: *Basic lithologies for the first layer of my model. Associated conductivity values shown in chart to the left. Area of interest in highlighted in pink.*

The gravel has the highest conductivity, at 10m/day in the x/y direction and 0.1 m/day in the z direction. The rest of the conductivities follow the same pattern of decreasing the conductivity in the z direction by a factor of 100, so I will henceforth only mention the x/y conductivities, which are always the same. Sand is one other anomaly, I have given it a conductivity value of 2 m/day in the x,y, and z direction. The idea is that this is unfractured basin fill, and will have the same conductivity in all directions. The basement rock was given a conductivity value of 1 m/day, which is less than the sand layer because it is older and more weathered. Ironstone and volcanics were given the same value of 0.5 m/day, but the volcanics layer has the same conductivity value in the x,y, and z direction. These volcanic deposits are part of an alluvial fan coming down Mt.Oldeani, are fairly recent, and shouldn't be as affected by fracturing.

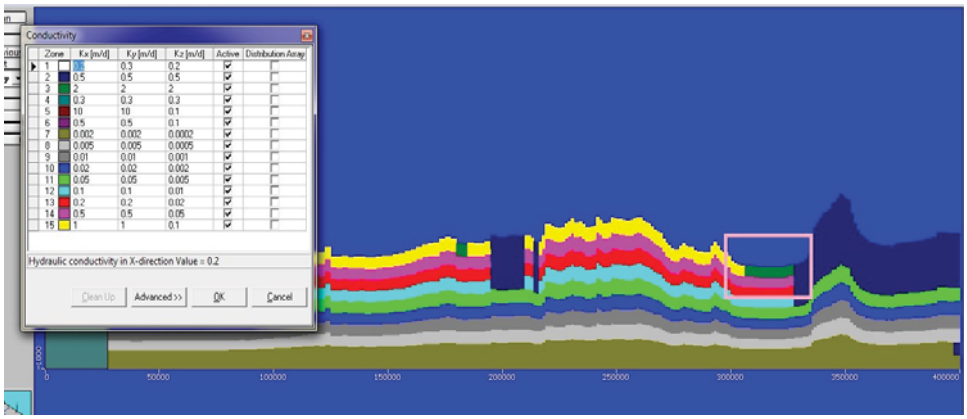

Figure 10: *Cross section showing conductivity layers. Associated values in chart to left.*

The first layer is the most lithologically varied. The volcanic layers carry through until the fourth layer, and then die out. The major conductivity of the second layer is 0.5 m/day in the x/y direction and 0.05 m/day in the z direction. The following layers follow the same pattern of decreasing the conductivity in the z direction by a factor of 100. The next layer is 0.2 m/day, followed by 0.1 m/day, 0.05 m/day, 0.02 m/day, 0.01 m/day, 0.005 m/day, and finally the last two layers which are 0.002 m/day.

Sources of Water:

Recharge zones are based on elevation. The highest recharge is in an area surrounding the peaks of these volcanoes, and a lesser recharge area surrounds the high area (figure 11). The low areas of the model do not receive groundwater recharge. I have conducted several tests of the model's sensitivity to different recharge values. Groundwater recharge is the only source of water into my model.

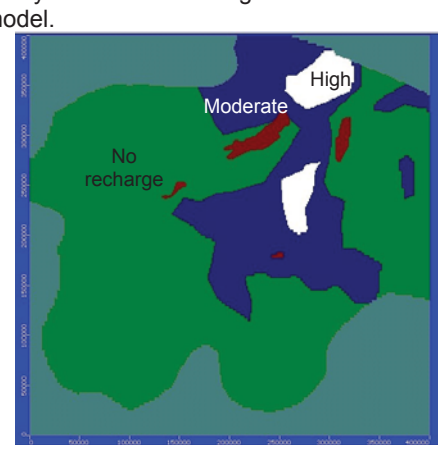

Figure 11: *Recharge zones shown in white, blue, and green. Lakes in red for reference.*

Sinks of Water:

The lakes shown on the geologic map (figure 6) are represented as areas of constant head in my model (figure 12). This way, water is directed from the highlands into the lakes. Though the lakes are often dry, they are permanent features that will fill with water when there is a period of heavy rainfall. The lakes are mostly fed by groundwater, as the surrounding rivers are only present during heavy rainfall. For this reason, they are not modeled as constant heads.

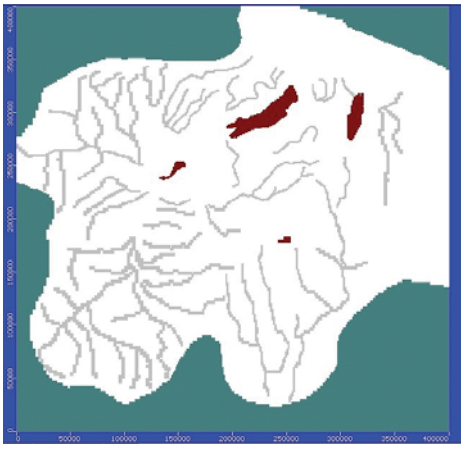

Figure 12: *Constant heads are shown in red. The gray lines are drains.*

I have created a 1km zone surrounding Lake Eyasi to represent the wetland (figure 13). This allows me to monitor how much groundwater is received in the wetland when I vary recharge and conductivity values. I do this by checking the zone budget feature after conducting a model run. This 1km zone is an estimation of the actual wetland size, and was determined using Google Maps (figure 2).

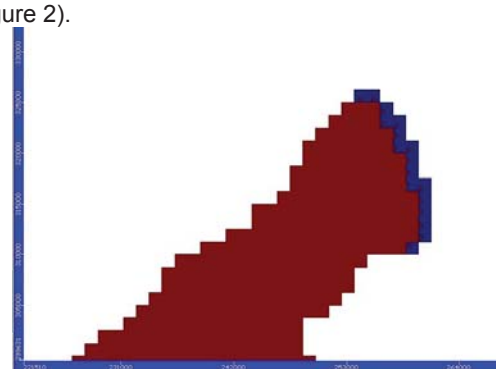

Figure 13: *Wetland zone shown in blue, on edge of Lake Eyasi (shown in red) and at base of Mt.Oldeani (not pictured, but to the north-east of the lake). The red dots are particles used in travel time analysis.*

Model Calibration:

Because there is not much data to calibrate my model to, I have made a variety of broad assumptions. I know that there is a shallow water table and the existence of springs at the base of Mt.Oldeani as well as other local sites. I have an idea of the conductivity values to use based on experiments of unconsolidated and fractured materials done by Freeze and Cherry. The biggest guess in my model is the exact value of groundwater recharge. For this reason, I have conducted several runs with varying recharge values. Every time, the lower value is half of the higher value, and the regions of low elevation receive no recharge. This halving is also a guess, as well as where exactly the boundaries should be set.

Sensitivity:

The particle flow rates are sensitive to changes in recharge on a 50-100 year scale. For example, when I changed the high recharge value from 50 mm/yr to 60 mm/yr, the average travel time changed from 1000 years to 1100 years. When I changed it to 70 mm/yr, the average travel time was 950 years.

Results and Conclusions

Simulations:

As seen in figure 13, I put several particles in the wetland zone to track. I used a backwards tracking method to calculate travel time from the upland area into the wetland springs. To simulate particle travel time and its sensitivity to changes in recharge, I ran my model several times with varying recharge values.

The first run was 100 mm/yr upland and 50 mm/yr on the slopes. This resulted in an average travel time on 700 years (min 400 years, max 1000 years).

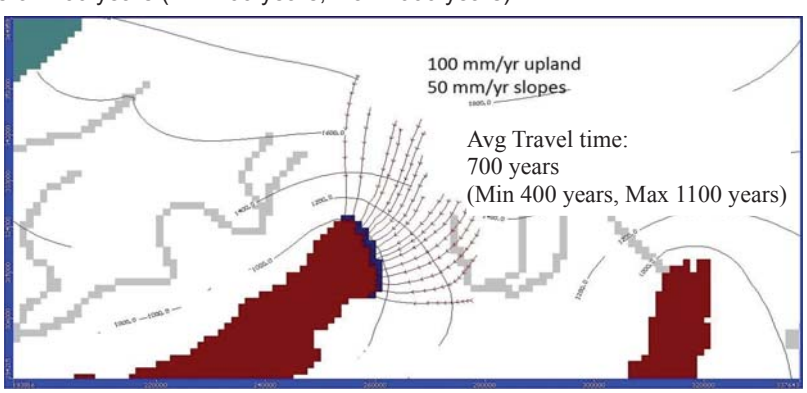

Figure 14: *Particle tracking for first run.*

For the second run, I tried a lower recharge value. This time I used 50 mm/yr upland and 25

mm/yr for slopes. The average travel time was 1100 years (min 700, max 1900). I thought this would be my minimum recharge value, and used increasing values for the next runs.

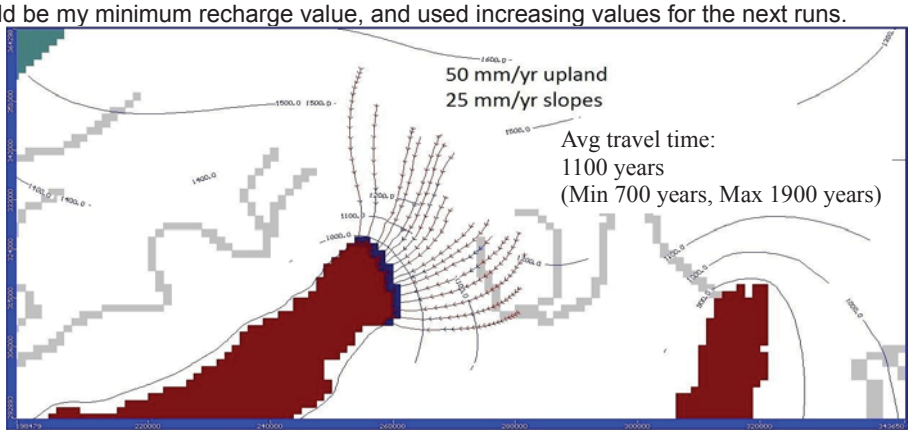

Figure 15: *Particle tracking for the second run.*

The following images show the next three runs I did, with their corresponding recharge and travel time values.

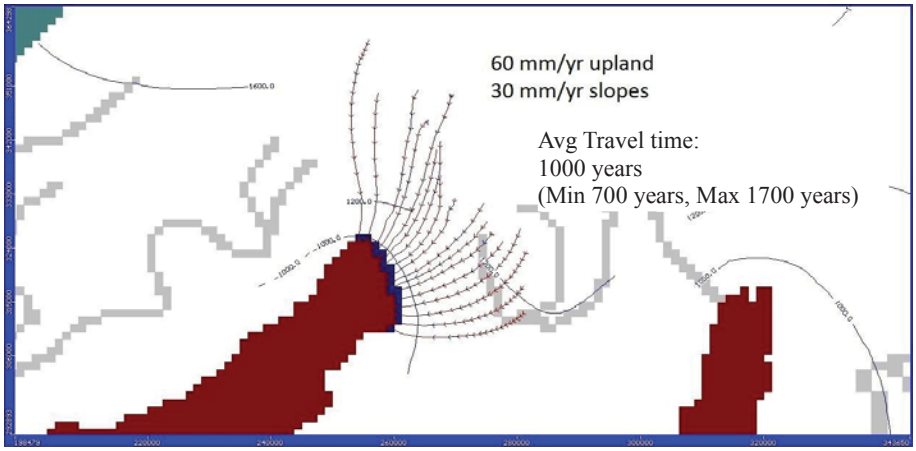

Figure 16: *Particle tracking for the third run.*

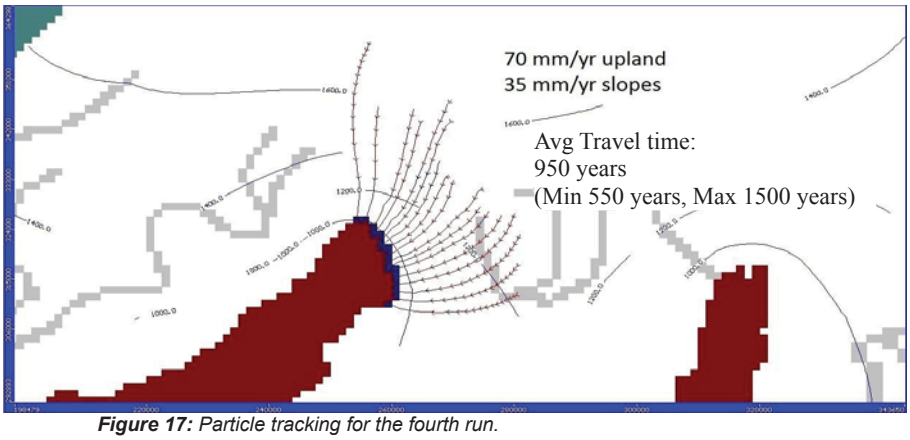

Figure 17: *Particle tracking for the fourth run.*

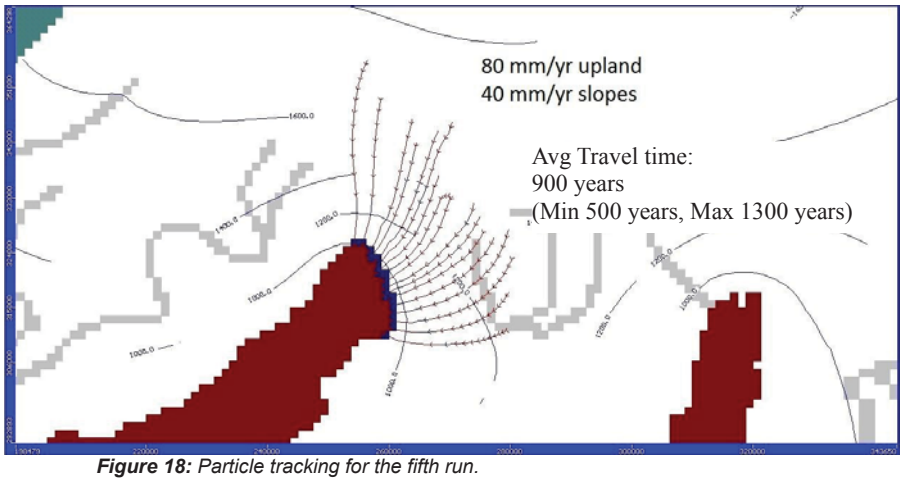

Figure 18: *Particle tracking for the fifth run.*

The minimum travel time achieved was 700 years, with a high 100 mm/yr recharge.

According to figure 3, the graph by Verschuren, the last rainy period was 300 years ago, and the one preceding that was 500 years ago. According to the models I made, the rain from those events would not have reached the wetland springs by the present time. So, either the water coming out of the springs is from a rainy period over 700 years ago (there is one inferred on the graph, and possibly more before), or the model is missing something, and the time it takes for a particle to travel to the springs is less than 700 years.

Water Budget:

Max Recharge for Run	Recharge to Wetland Zone	Groundwater Flux into Zone
50	1177	127510
60	1413	158330
70	1648	179980
80	1884	199220
100	2355	233940

My model faces several limitations. The grid is very coarse and covers a very large area; features are seen on a kilometer scale. Another issue is calibration. There is not a lot of data to calibrate my model to, such as wells and cores. Conductivity values are inferred and could probably use some refining. Looking back, I wonder why I picked each specific value for the first layer when the sediments might not vary by much, and I have no specific data on grain size. The biggest assumption, and perhaps most essential variable, is the recharge value. It has the largest impact on travel time and is the least understood.

Understanding what the actual recharge value is would be a great improvement to my model, and make it a lot more accurate and meaningful. Right now, I feel as though I can only guess at what might be going on. Refining conductivity values and recharge zones might also be good improvements. I would also try to make a smaller, more local model, with a more refined grid. Even a $10m^2$ grid would be better to show detail.

APPENDIX VI

ENDULEN

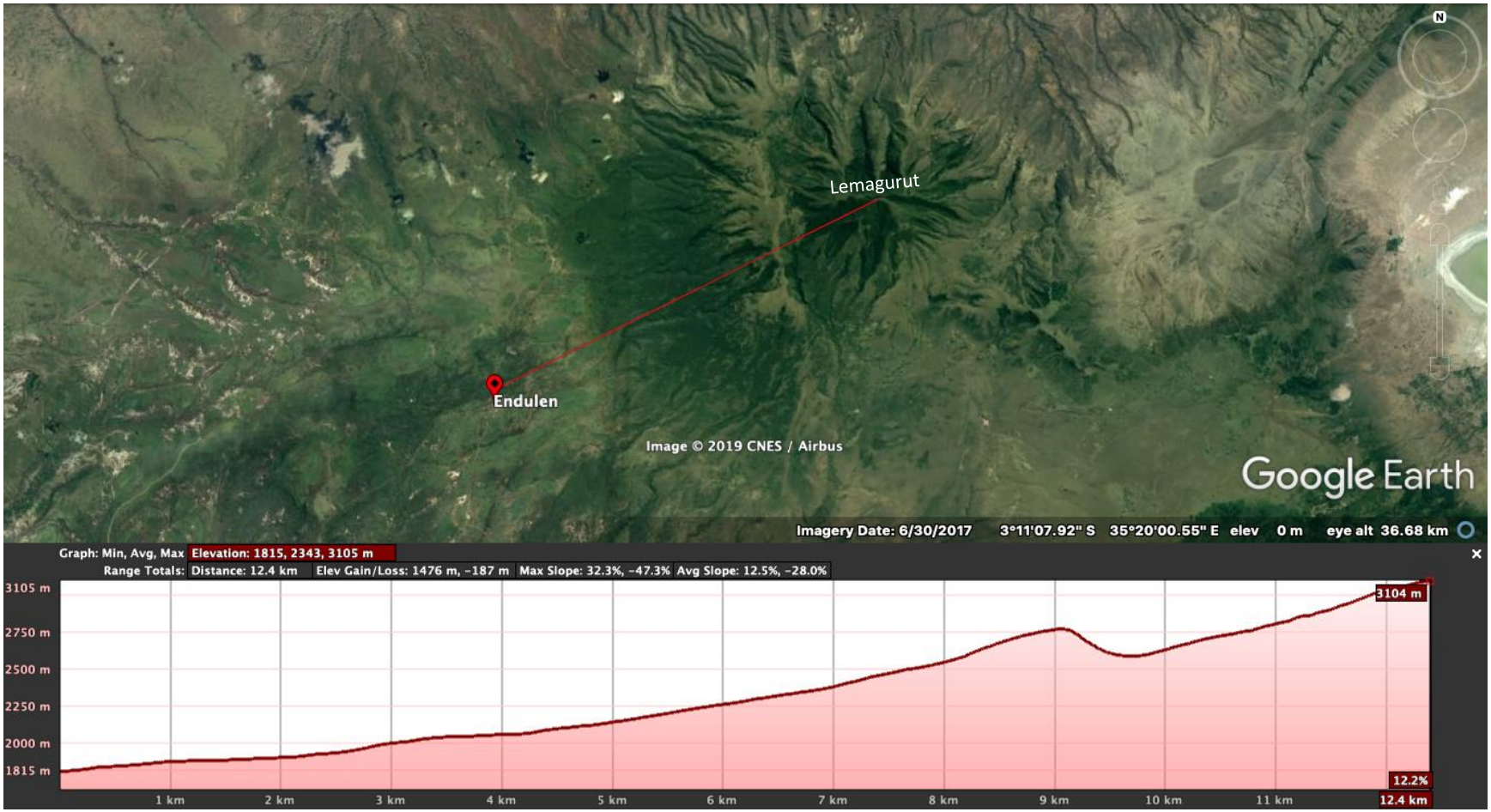

Elevation Profile from Endulen Spring to Mt. Lemagurut
Distance between spring and recharge area: **12.4 km**
Elevation between spring and recharge area: **1,287 m**
Average slope between spring and recharge area: **10.38%**

ENGINA

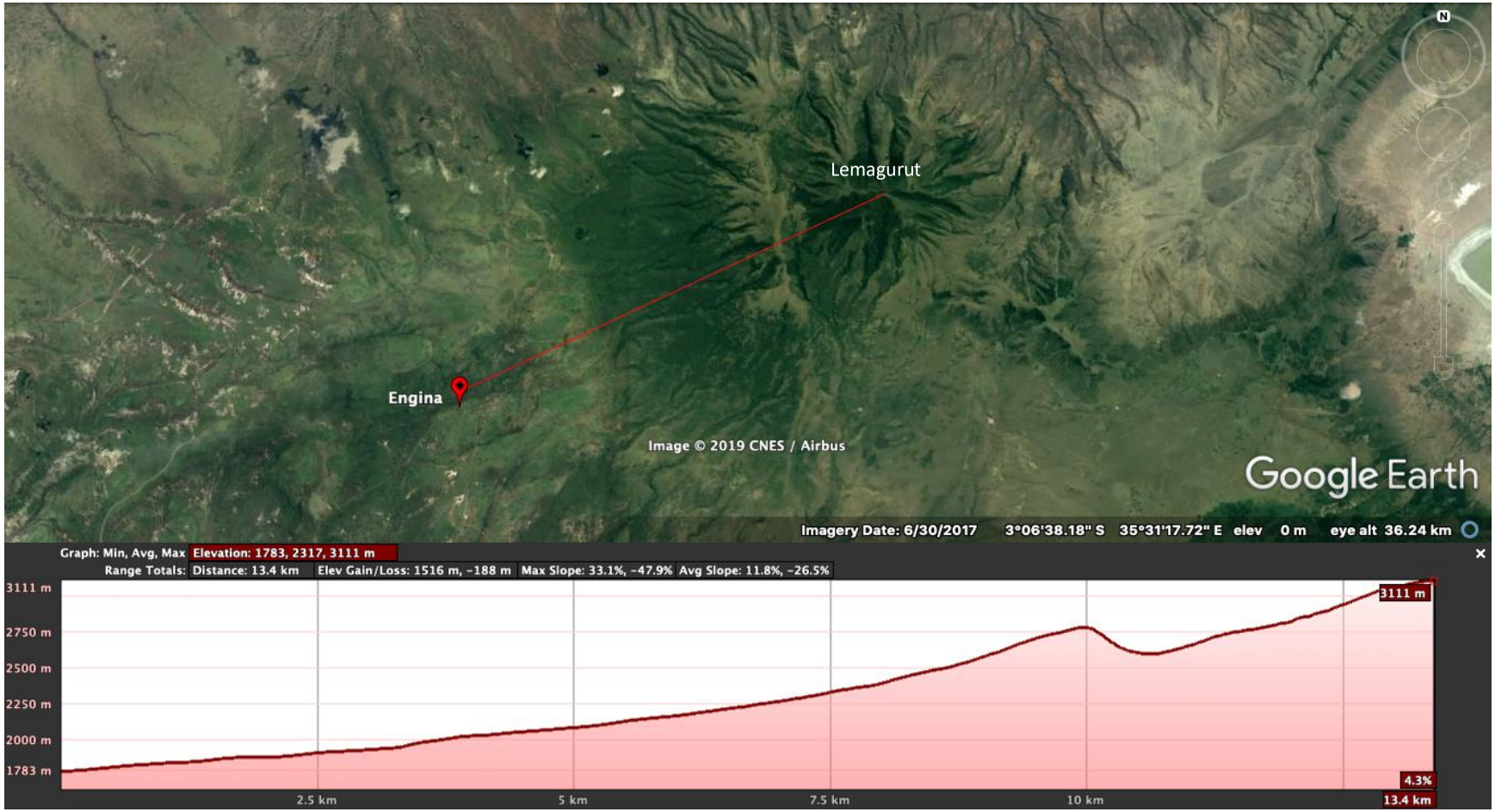

Elevation Profile from Engina Spring to Mt. Lemagurut
Distance between spring and recharge area: **13.4 km**
Elevation between spring and recharge area: **1,327 m**
Average slope between spring and recharge area: **9.90%**

MTANE

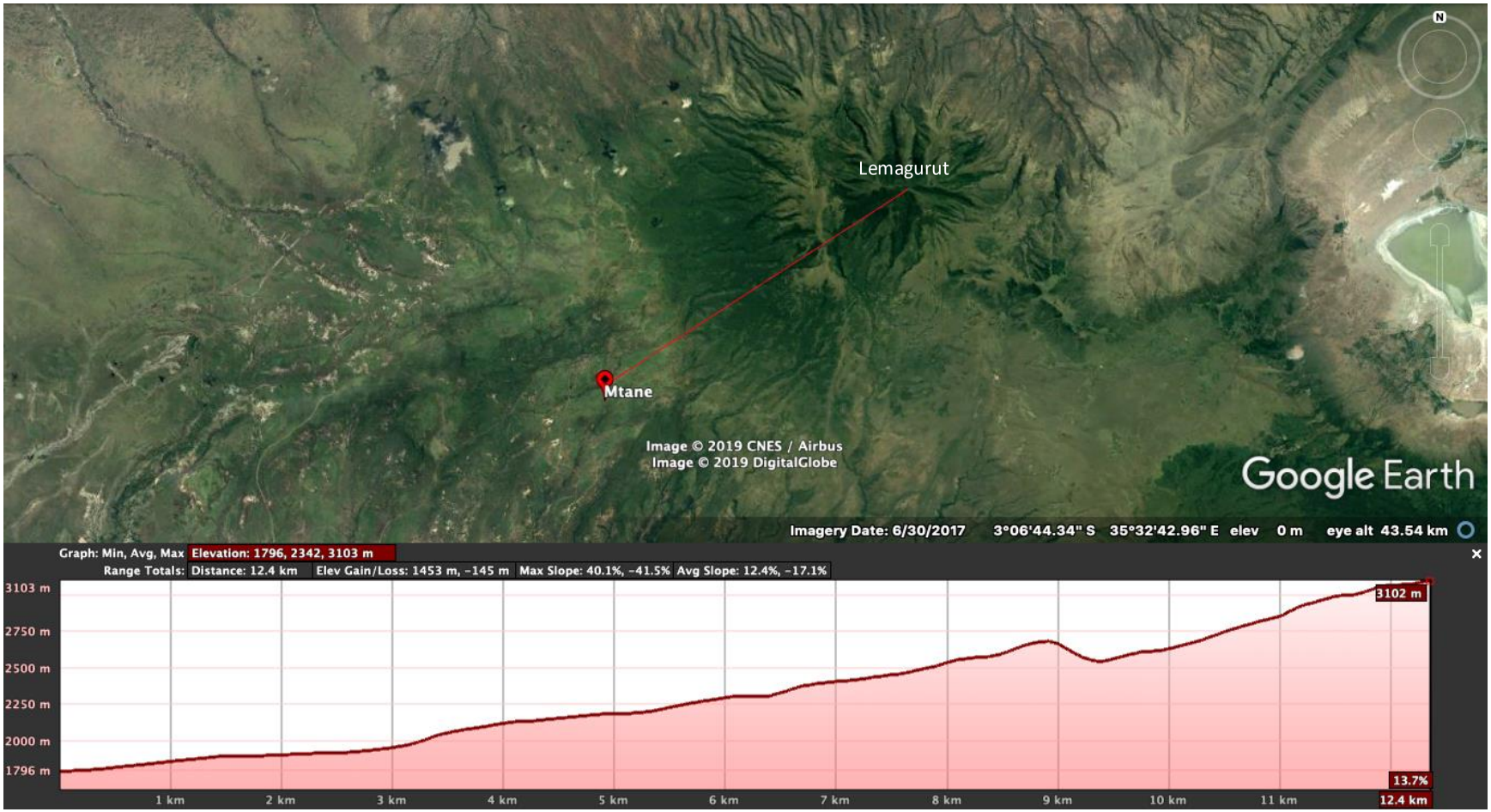

Elevation Profile from Mtane Spring to Mt. Lemagurut

Distance between spring and recharge area: **12.4 km**

Elevation between spring and recharge area: **1,304 m**

Average slope between spring and recharge area: **10.52%**

MISILLI

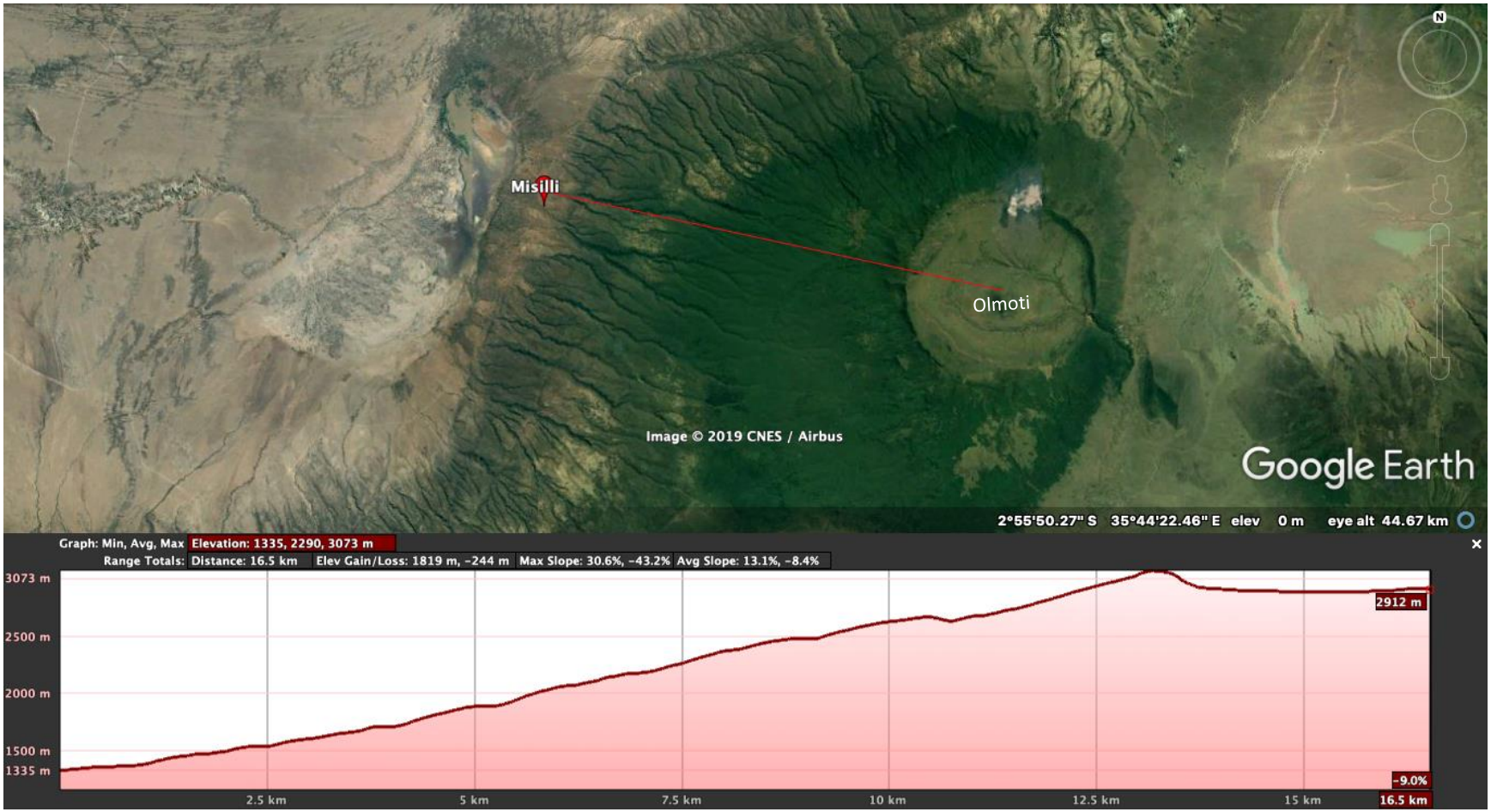

Elevation Profile from Misilli Spring to Mt. Olmoti
Distance between spring and recharge area: **16.5 km**
Elevation between spring and recharge area: **1,578 m**
Average slope between spring and recharge area: **9.56%**

NGOILE

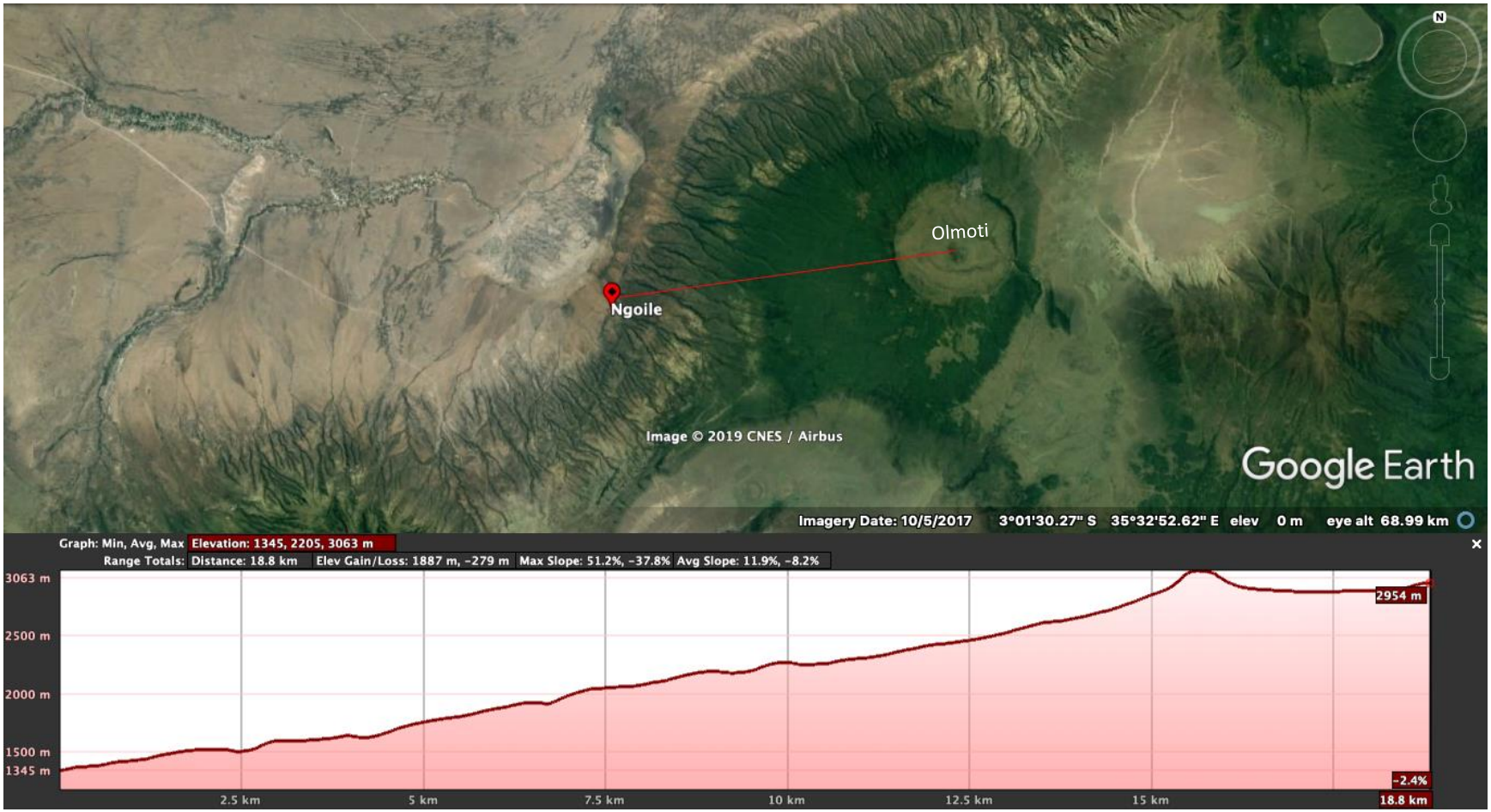

Elevation Profile from Ngoile Spring to Mt. Olmoti
Distance between spring and recharge area: **18.8 km**
Elevation between spring and recharge area: **1,610 m**
Average slope between spring and recharge area: **8.56%**

KISIMA NGEDA

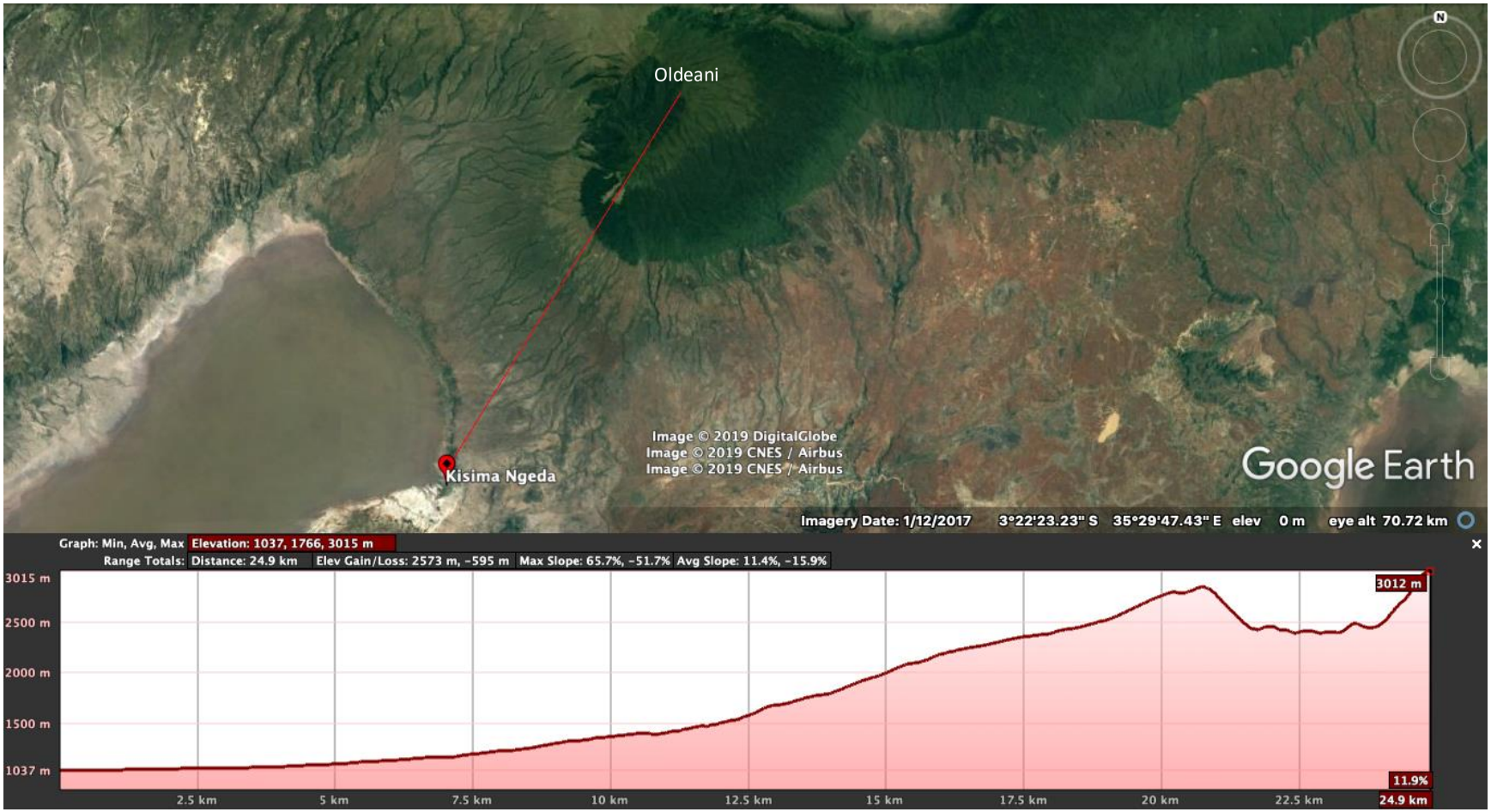

Elevation Profile from Kisima Ngeda Spring to Mt. Oldeani

Distance between spring and recharge area: **24.9 km**

Elevation between spring and recharge area: **1,973 m**

Average slope between spring and recharge area: **7.92%**

GARAFANI

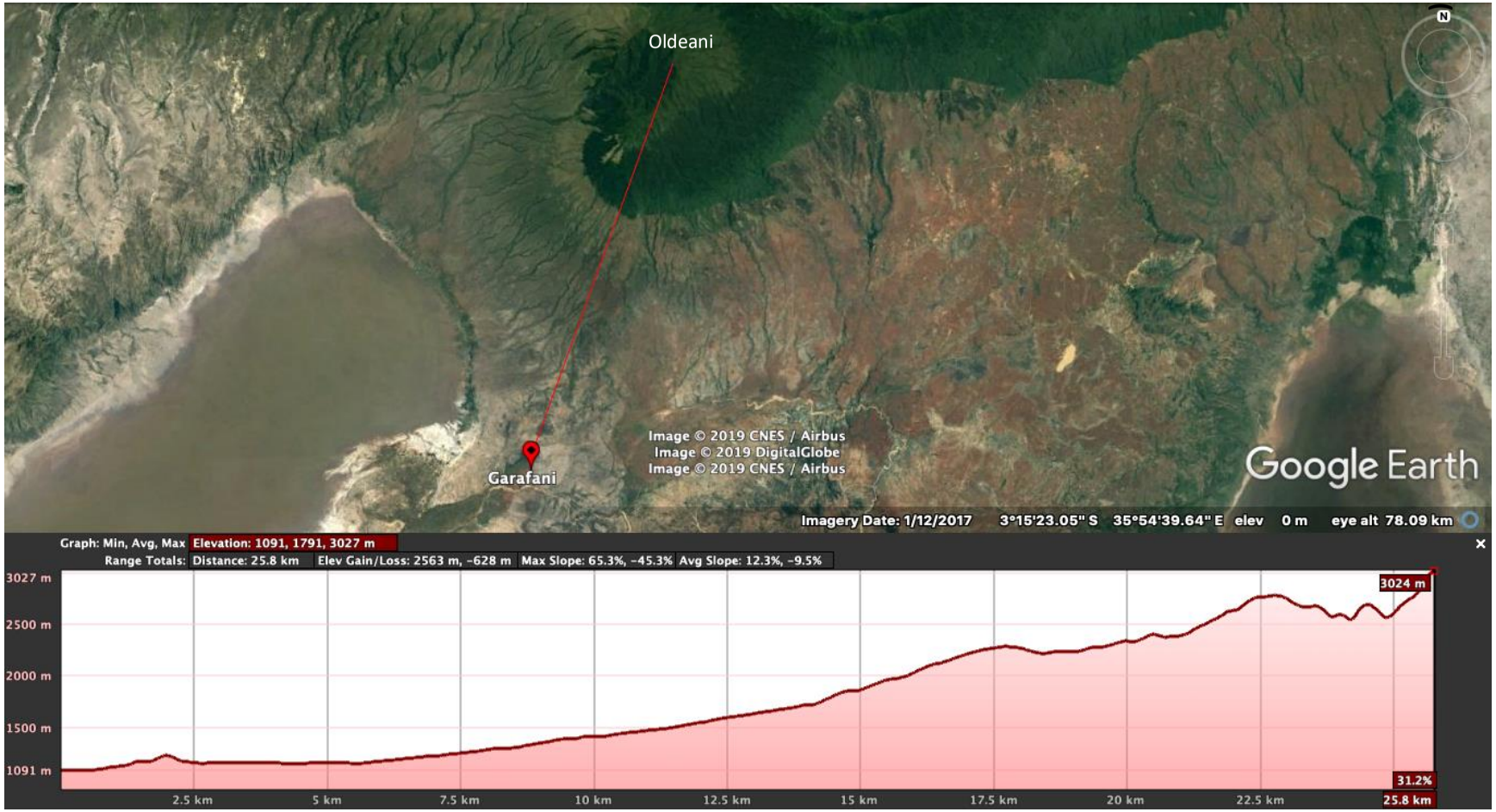

Elevation Profile from Garafani Spring to Mt. Oldeani
Distance between spring and recharge area: **25.8 km**
Elevation between spring and recharge area: **1,922 m**
Average slope between spring and recharge area: **7.45%**

ESERE

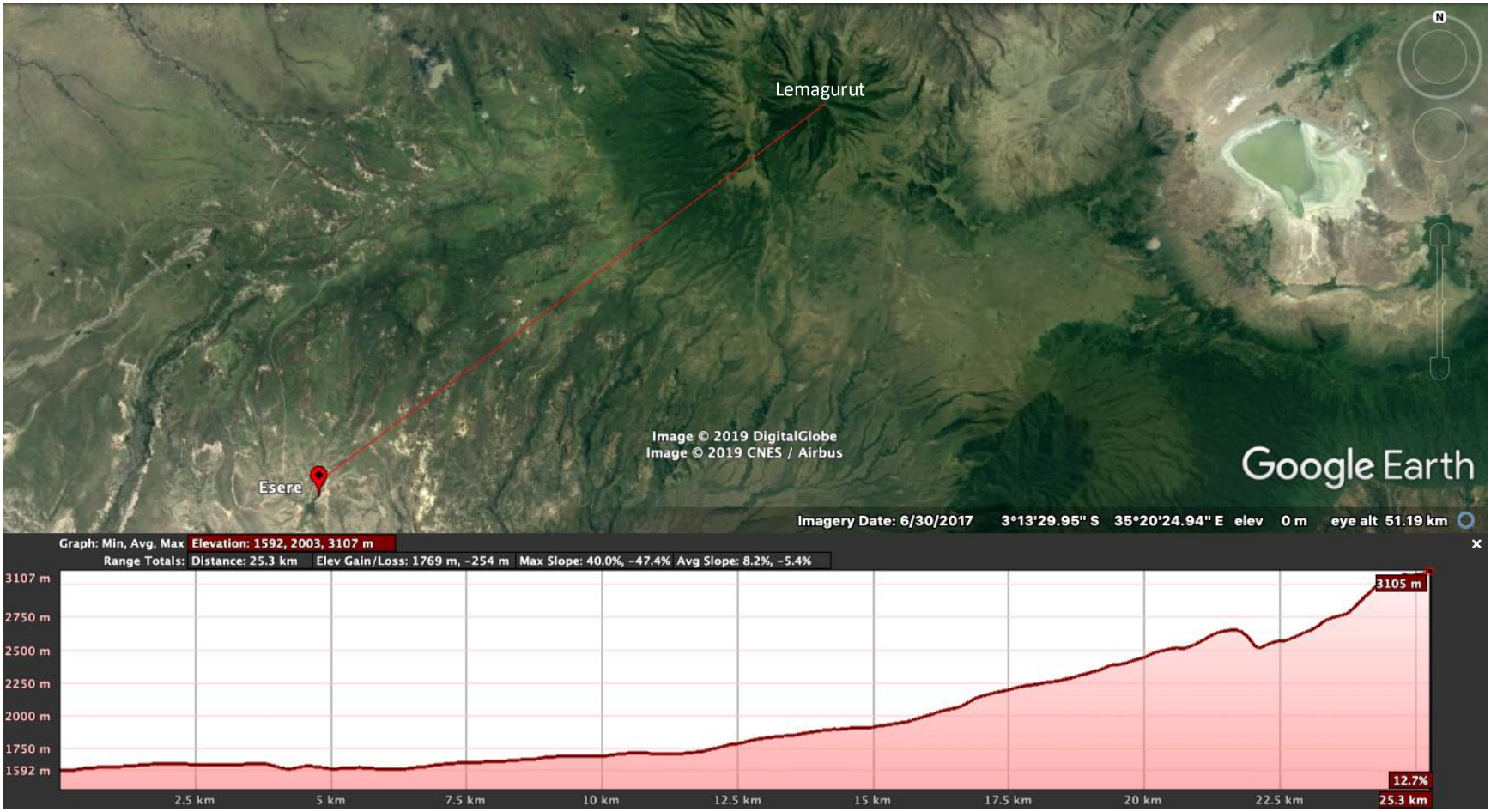

Elevation Profile from Esere Spring to Mt. Lemagurut

Distance between spring and recharge area: **25.3 km**

Elevation between spring and recharge area: **1,509 m**

Average slope between spring and recharge area: **5.96%**

EREMET

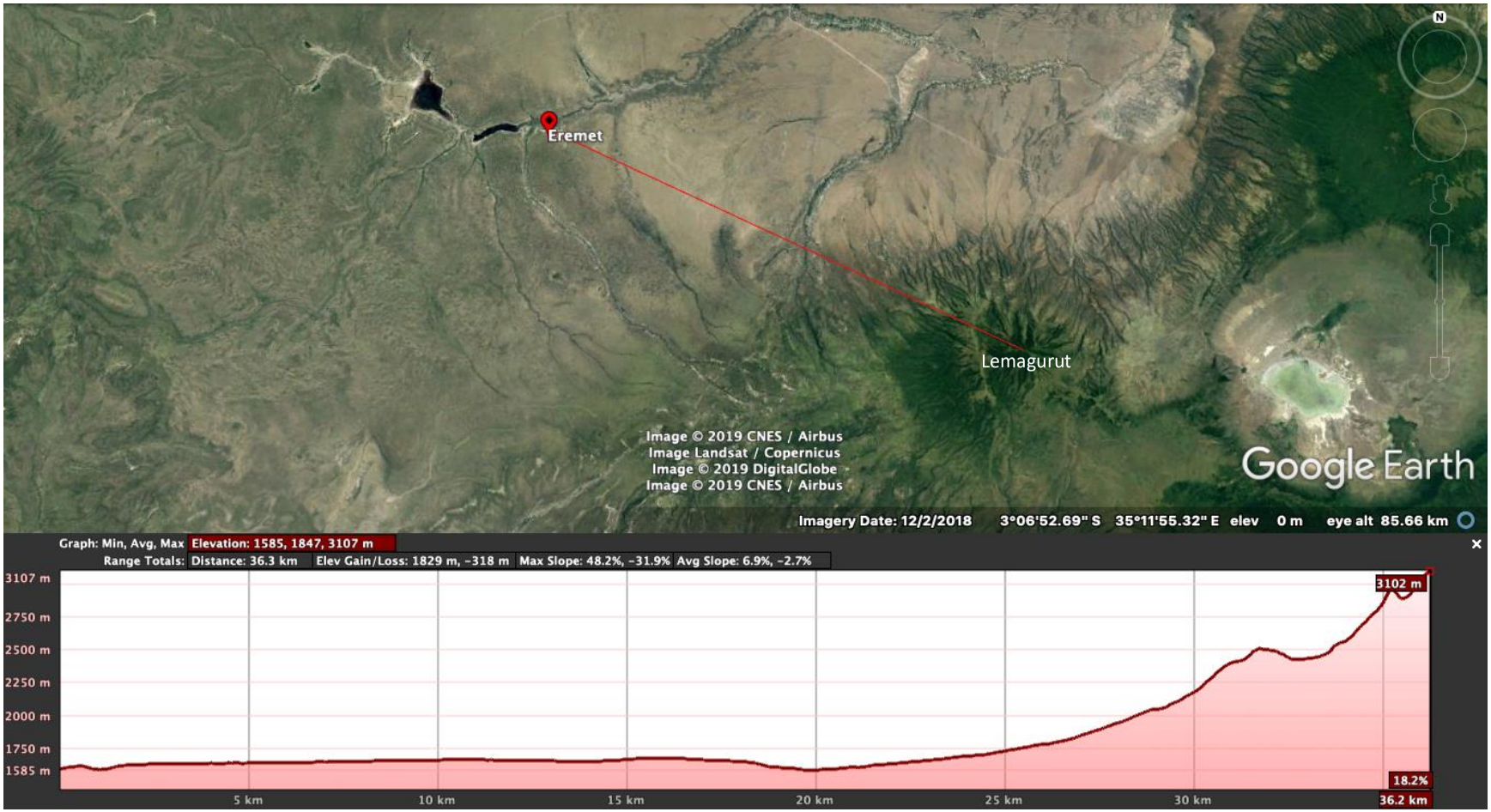

Elevation Profile from Eremet Spring to Mt. Lemagurut
Distance between spring and recharge area: **36.3 km**
Elevation between spring and recharge area: **1,499 m**
Average slope between spring and recharge area: **4.13%**

APPENDIX VII

ENDULEN

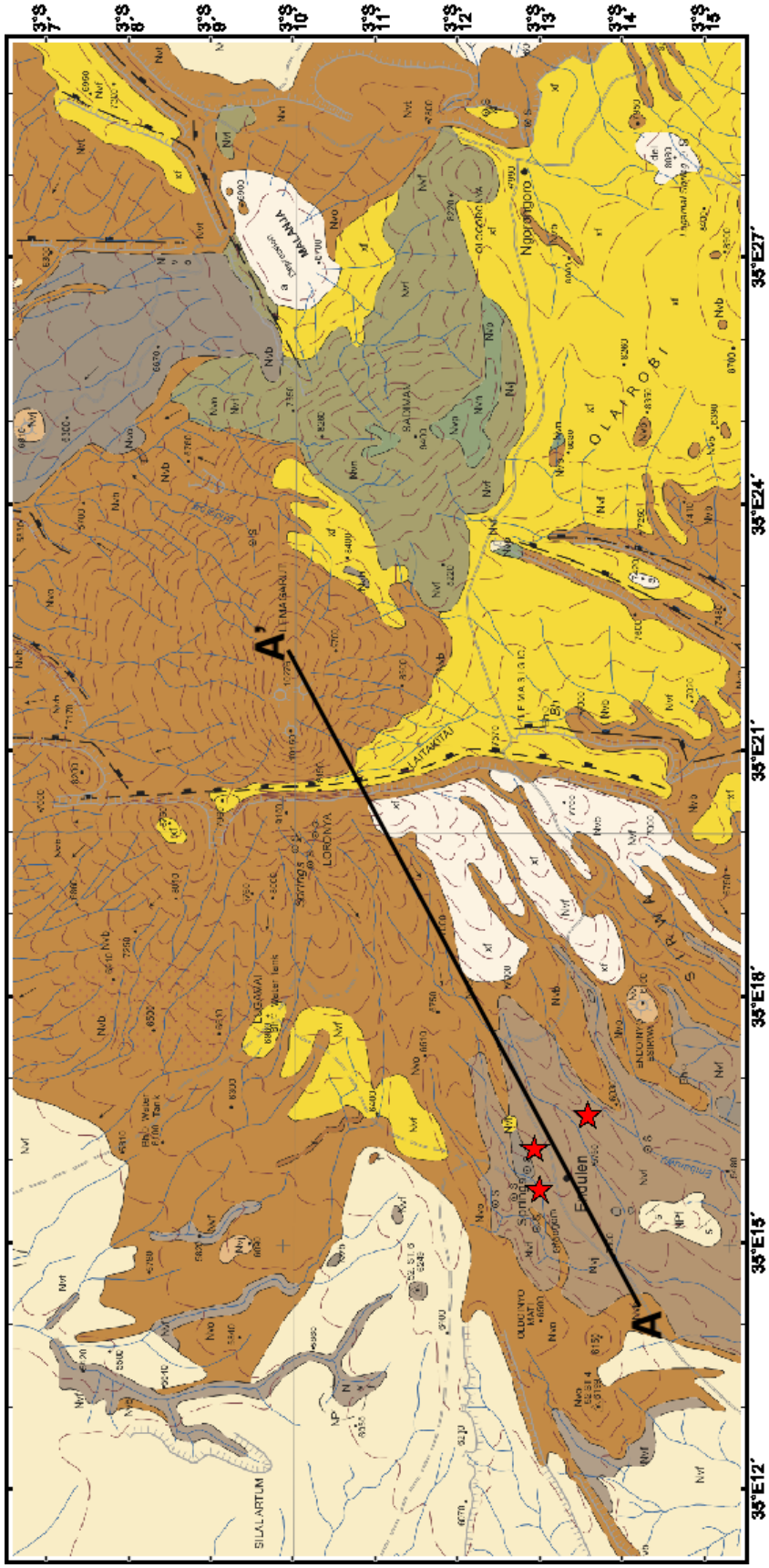
3°S 7'
3°S 8'
3°S 9'
3°S 10'
3°S 11'
3°S 12'
3°S 13'
3°S 14'
3°S 15'
35°E12'
35°E15'
35°E18'
35°E21'
35°E24'
35°E27'
A
A'
Endulen
Ngorongoro
SILALARTUM
LOGOMAI
LORONYA
LITAKITAI
MALAMA
SAIGIWAU
OLARO SI
Nvf
Nvb
Nvt
Nvn
Nvo
Nvj
Nvk
Nvl
Nvm
Nvp
Nvq
Nvr
Nvs
Nvu
Nvv
Nvw
Nvx
Nvy
Nvz
Nvaa
Nvab
Nvac
Nvad
Nvae
Nvaf
Nvag
Nvah
Nvai
Nvaj
Nvak
Nval
Nvam
Nvan
Nvao
Nvap
Nvaq
Nvar
Nvas
Nvat
Nvau
Nvav
Nvaw
Nvax
Nvay
Nvaz
Nvba
Nvbb
Nvbc
Nvbd
Nvbe
Nvbf
Nvbg
Nvbh
Nvbi
Nvbj
Nvbk
Nvbl
Nvbm
Nvbn
Nvbo
Nvbp
Nvbq
Nvbr
Nvbs
Nvbt
Nvbu
Nvbv
Nvbw
Nvbx
Nvby
Nvbz
Nvca
Nvcb
Nvcc
Nvcd
Nvce
Nvcf
Nvcg
Nvch
Nvci
Nvcj
Nvck
Nvcl
Nvcm
Nvcn
Nvco
Nvcp
Nvcq
Nvcr
Nvcs
Nvct
Nvcu
Nvcv
Nvcw
Nvcx
Nvcy
Nvcz
Nvda
Nvdb
Nvdc
Nvdd
Nvde
Nvdf
Nvdg
Nvdh
Nvdi
Nvdj
Nvdk
Nvdl
Nvdm
Nvdn
Nvdo
Nvdp
Nvdq
Nvdr
Nvds
Nvdt
Nvdu
Nvdv
Nvdw
Nvdx
Nvdy
Nvdz
Nvea
Nveb
Nvec
Nved
Nvee
Nvef
Nveg
Nveh
Nvei
Nvej
Nvek
Nvel
Nvem
Nven
Nveo
Nvep
Nveq
Nver
Nves
Nvet
Nveu
Nvev
Nvew
Nvex
Nvey
Nvez
Nvfa
Nvfb
Nvfc
Nvfd
Nvfe
Nvff
Nvfg
Nvfh
Nvfi
Nvfj
Nvfk
Nvfl
Nvfm
Nvfn
Nvfo
Nvfp
Nvfq
Nvfr
Nvfs
Nvft
Nvfu
Nvfv
Nvfw
Nvfx
Nvfy
Nvfz
Nvga
Nvgb
Nvgc
Nvgd
Nvge
Nvgf
Nvgg
Nvgh
Nvgi
Nvgj
Nvgk
Nvgl
Nvgm
Nvgn
Nvgo
Nvgp
Nvgq
Nvgr
Nvgs
Nvgt
Nvgu
Nvgv
Nvgw
Nvgx
Nvgy
Nvgz
Nvha
Nvhb
Nvhc
Nvhd
Nvhe
Nvhf
Nvhg
Nvhh
Nvhi
Nvhj
Nvhk
Nvhl
Nvhm
Nvhn
Nvho
Nvhp
Nvhq
Nvhr
Nvhs
Nvht
Nvhu
Nvhv
Nvhw
Nvhx
Nvhy
Nvhz
Nvia
Nvib
Nvic
Nvid
Nvie
Nvif
Nvig
Nvih
Nvii
Nvij
Nvik
Nvil
Nvim
Nvin
Nvio
Nvip
Nviq
Nvir
Nvis
Nvit
Nviu
Nviv
Nviw
Nvix
Nviy
Nviz
Nvja
Nvjb
Nvjc
Nvjd
Nvje
Nvjf
Nvjg
Nvjh
Nvji
Nvjj
Nvjk
Nvjl
Nvjm
Nvjn
Nvjo
Nvjp
Nvjq
Nvjr
Nvjs
Nvjt
Nvju
Nvjv
Nvjw
Nvjx
Nvjy
Nvjz
Nvka
Nvkb
Nvkc
Nvkd
Nvke
Nvkf
Nvkg
Nvkh
Nvki
Nvkj
Nvkk
Nvkl
Nvkm
Nvkn
Nvko
Nvkp
Nvkq
Nvkr
Nvks
Nvkt
Nvku
Nvkv
Nvkw
Nvkx
Nvky
Nvkz
Nvla
Nvlb
Nvlc
Nvld
Nvle
Nvlf
Nvlg
Nvlh
Nvli
Nvlj
Nvlk
Nvll
Nvlm
Nvln
Nvlo
Nvlp
Nvlq
Nvlr
Nvls
Nvlt
Nvlu
Nvlv
Nvlw
Nvlx
Nvly
Nvlz
Nvma
Nvmb
Nvmc
Nvmd
Nvme
Nvmf
Nvmg
Nvmh
Nvmi
Nvmj
Nvmk
Nvml
Nvmm
Nvmn
Nvmo
Nvmp
Nvmq
Nvmr
Nvms
Nvmt
Nvmu
Nvmv
Nvmw
Nvmx
Nvmy
Nvmz
Nvna
Nvnb
Nvnc
Nvnd
Nvne
Nvnf
Nvng
Nvnh
Nvni
Nvnj
Nvnk
Nvnl
Nvnm
Nvnn
Nvno
Nvnp
Nvnq
Nvnr
Nvns
Nvnt
Nvnu
Nvnv
Nvnw
Nvnx
Nvny
Nvnz
Nvoa
Nvob
Nvoc
Nvod
Nvoe
Nvof
Nvog
Nvoh
Nvoi
Nvoj
Nvok
Nvol
Nvom
Nvon
Nvoo
Nvop
Nvoq
Nvor
Nvos
Nvot
Nvou
Nvov
Nvow
Nvox
Nvoy
Nvoz
Nvpa
Nvpb
Nvpc
Nvpd
Nvpe
Nvpf
Nvpg
Nvph
Nvpi
Nvpj
Nvpk
Nvpl
Nvpm
Nvpn
Nvpo
Nvpp
Nvpq
Nvpr
Nvps
Nvpt
Nvpu
Nvpv
Nvpw
Nvpx
Nvpy
Nvpz
Nvqa
Nvqb
Nvqc
Nvqd
Nvqe
Nvqf
Nvqg
Nvqh
Nvqi
Nvqj
Nvqk
Nvql
Nvqm
Nvqn
Nvqo
Nvqp
Nvqq
Nvqr
Nvqs
Nvqt
Nvqu
Nvqv
Nvqw
Nvqx
Nvqy
Nvqz
Nvra
Nvrb
Nvrc
Nvrd
Nvre
Nvrf
Nvrg
Nvrh
Nvri
Nvrj
Nvrk
Nvrl
Nvrm
Nvrn
Nvro
Nvrp
Nvrq
Nvrr
Nvrs
Nvrt
Nvru
Nvrv
Nvrw
Nvrx
Nvry
Nvrz
Nvsa
Nvsb
Nvsc
Nvsd
Nvse
Nvsf
Nvsg
Nvsh
Nvsi
Nvsj
Nvsk
Nvsl
Nvsm
Nvsn
Nvso
Nvsp
Nvsq
Nvsr
Nvss
Nvst
Nvsu
Nvsv
Nvsw
Nvsx
Nvsy
Nvsz
Nvta
Nvtb
Nvtc
Nvtd
Nvte
Nvtf
Nvtg
Nvth
Nvti
Nvtj
Nvtk
Nvtl
Nvtm
Nvtn
Nvto
Nvtp
Nvtq
Nvtr
Nvts
Nvtt
Nvtu
Nvtv
Nvtw
Nvtx
Nvty
Nvtz
Nvua
Nvub
Nvuc
Nvud
Nvue
Nvuf
Nvug
Nvuh
Nvui
Nvuj
Nvuk
Nvul
Nvum
Nvun
Nvuo
Nvup
Nvuq
Nvur
Nvus
Nvut
Nvuu
Nvuv
Nvuw
Nvux
Nvuy
Nvuz
Nvva
Nvvb
Nvvc
Nvvd
Nvve
Nvvf
Nvvg
Nvvh
Nvvi
Nvvj
Nvvk
Nvvl
Nvvm
Nvvn
Nvvo
Nvvp
Nvvq
Nvvr
Nvvs
Nvvt
Nvvu
Nvvv
Nvvw
Nvvx
Nvvy
Nvvz
Nvwa
Nvwb
Nvwc
Nvwd
Nvwe
Nvwf
Nvwg
Nvwh
Nvwi
Nvwj
Nvwk
Nvwl
Nvwm
Nvwn
Nvwo
Nvwp
Nvwq
Nvwr
Nvws
Nvwt
Nvwu
Nvwv
Nvww
Nvwx
Nvwy
Nvwz
Nvxa
Nvxb
Nvxc
Nvxd
Nvxe
Nvxf
Nvxg
Nvxh
Nvxi
Nvxj
Nvxk
Nvxl
Nvxm
Nvxn
Nvxo
Nvxp
Nvxq
Nvxr
Nvxs
Nvxt
Nvxu
Nvxv
Nvxw
Nvxx
Nvxy
Nvxz
Nvya
Nvyb
Nvyc
Nvyd
Nvye
Nvyf
Nvyg
Nvyh
Nvyi
Nvyj
Nvyk
Nvyl
Nvym
Nvyn
Nvyo
Nvyp
Nvyq
Nvyr
Nvys
Nvyt
Nvyu
Nvyv
Nvyw
Nvyx
Nvyy
Nvyz
Nvza
Nvzb
Nvzc
Nvzd
Nvze
Nvzf
Nvzg
Nvzh
Nvzi
Nvzj
Nvzk
Nvzl
Nvzm
Nvzn
Nvzo
Nvzp
Nvzq
Nvzr
Nvzs
Nvzt
Nvzu
Nvzv
Nvzw
Nvzx
Nvzy
Nvzz

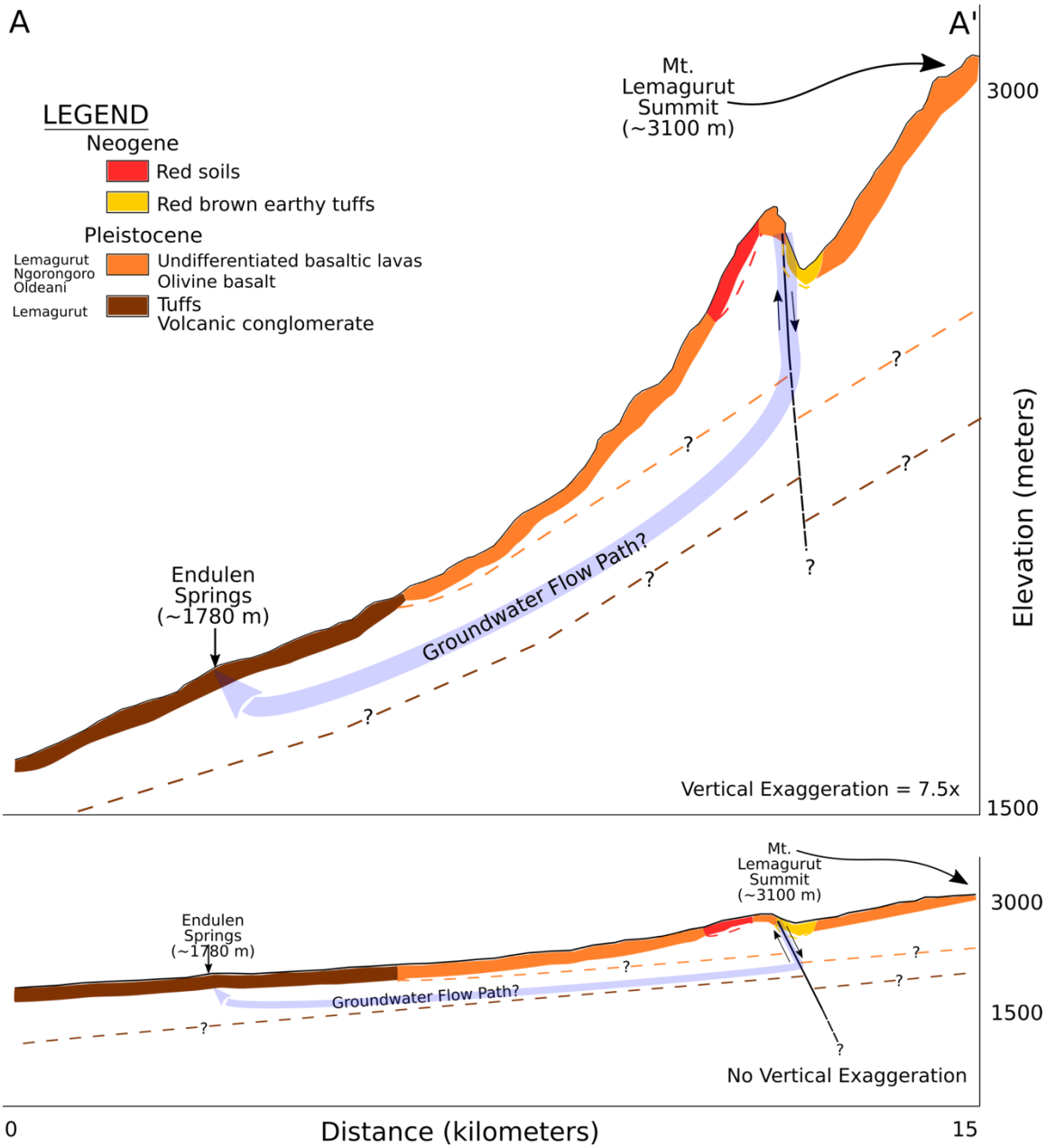
A
A'
LEGEND
Neogene
Red soils
Red brown earthy tuffs
Pleistocene
Lemagurut
Ngorongoro
Oldeani
Undifferentiated basaltic lavas
Olivine basalt
Lemagurut
Tuffs
Volcanic conglomerate
Mt. Lemagurut Summit (~3100 m)
3000
Elevation (meters)
Endulen Springs (~1780 m)
Groundwater Flow Path?
?
Vertical Exaggeration = 7.5x
1500
Mt. Lemagurut Summit (~3100 m)
3000
Endulen Springs (~1780 m)
Groundwater Flow Path?
1500
No Vertical Exaggeration
0
Distance (kilometers)
15

MISILLI

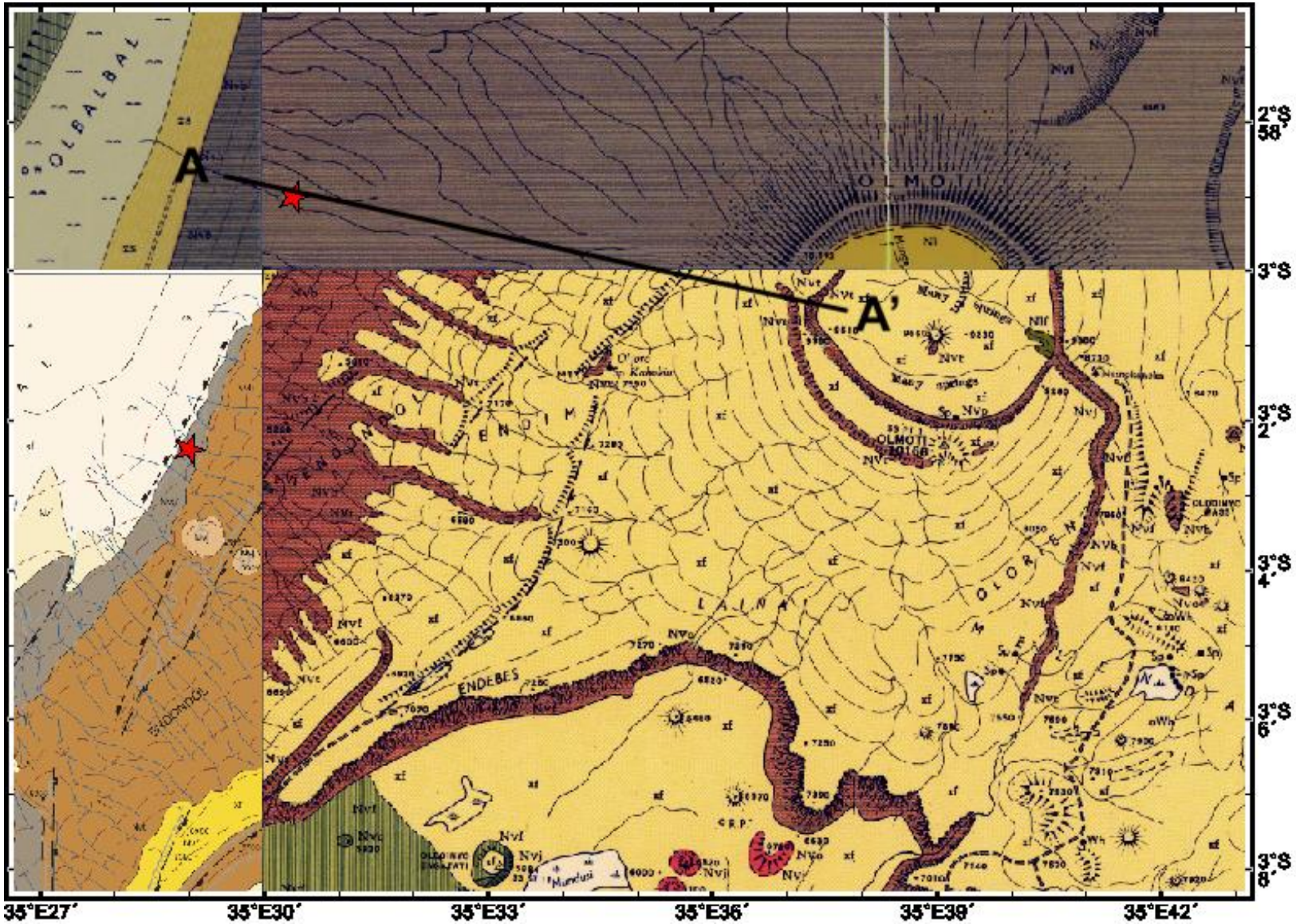
A
A'
OLMOTI
ENDEBES
35°E27′
35°E30′
35°E33′
35°E36′
35°E39′
35°E42′
2°S 58′
3°S
3°S 2′
3°S 4′
3°S 6′
3°S 8′

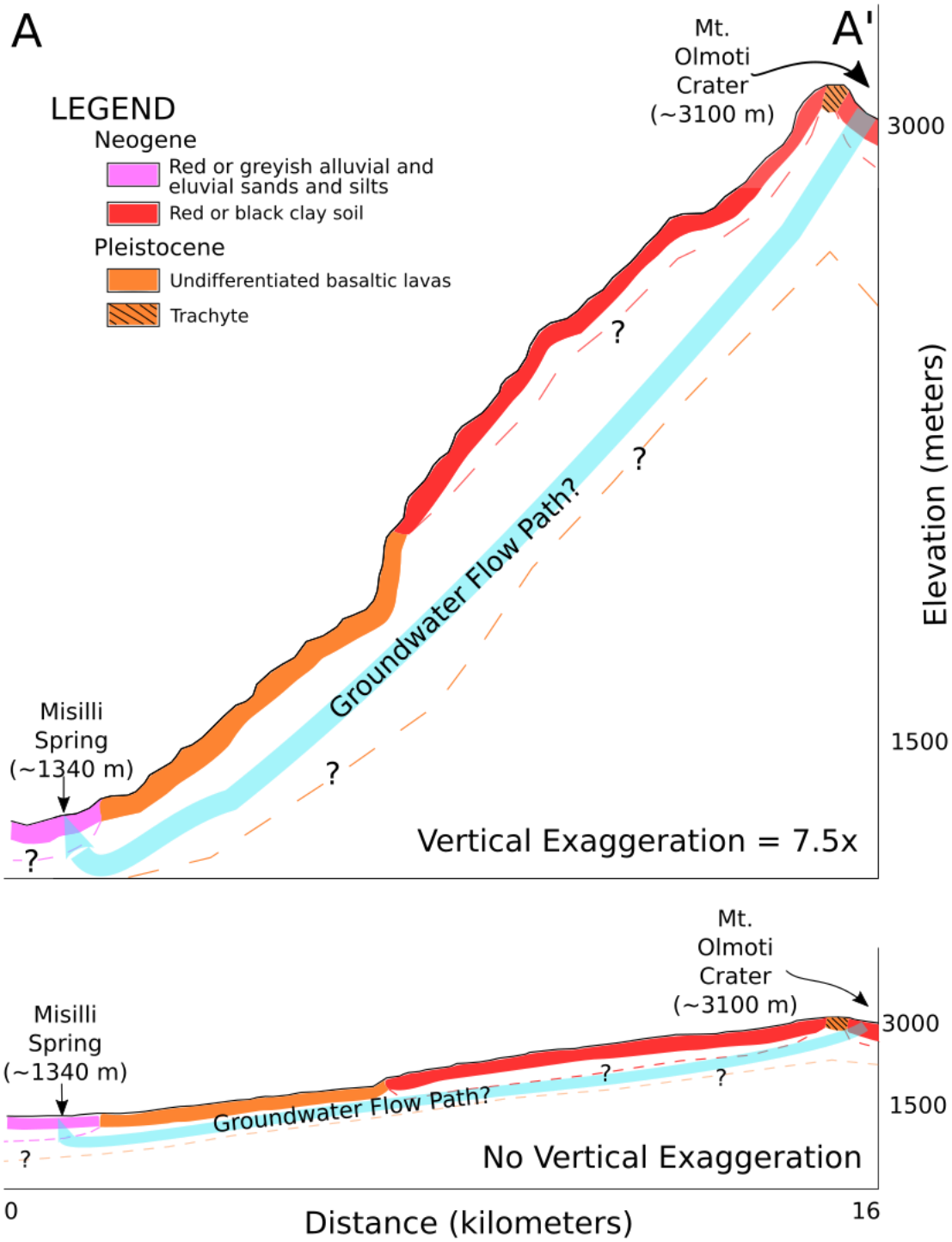
A
A'
Mt.
Olmoti
Crater
(~3100 m)
LEGEND
Neogene
Red or greyish alluvial and eluvial sands and silts
Red or black clay soil
Pleistocene
Undifferentiated basaltic lavas
Trachyte
3000
1500
Elevation (meters)
Groundwater Flow Path?
Misilli
Spring
(~1340 m)
Vertical Exaggeration = 7.5x
Mt.
Olmoti
Crater
(~3100 m)
Misilli
Spring
(~1340 m)
3000
1500
Groundwater Flow Path?
No Vertical Exaggeration
0
16
Distance (kilometers)

KISIMA NGEDA

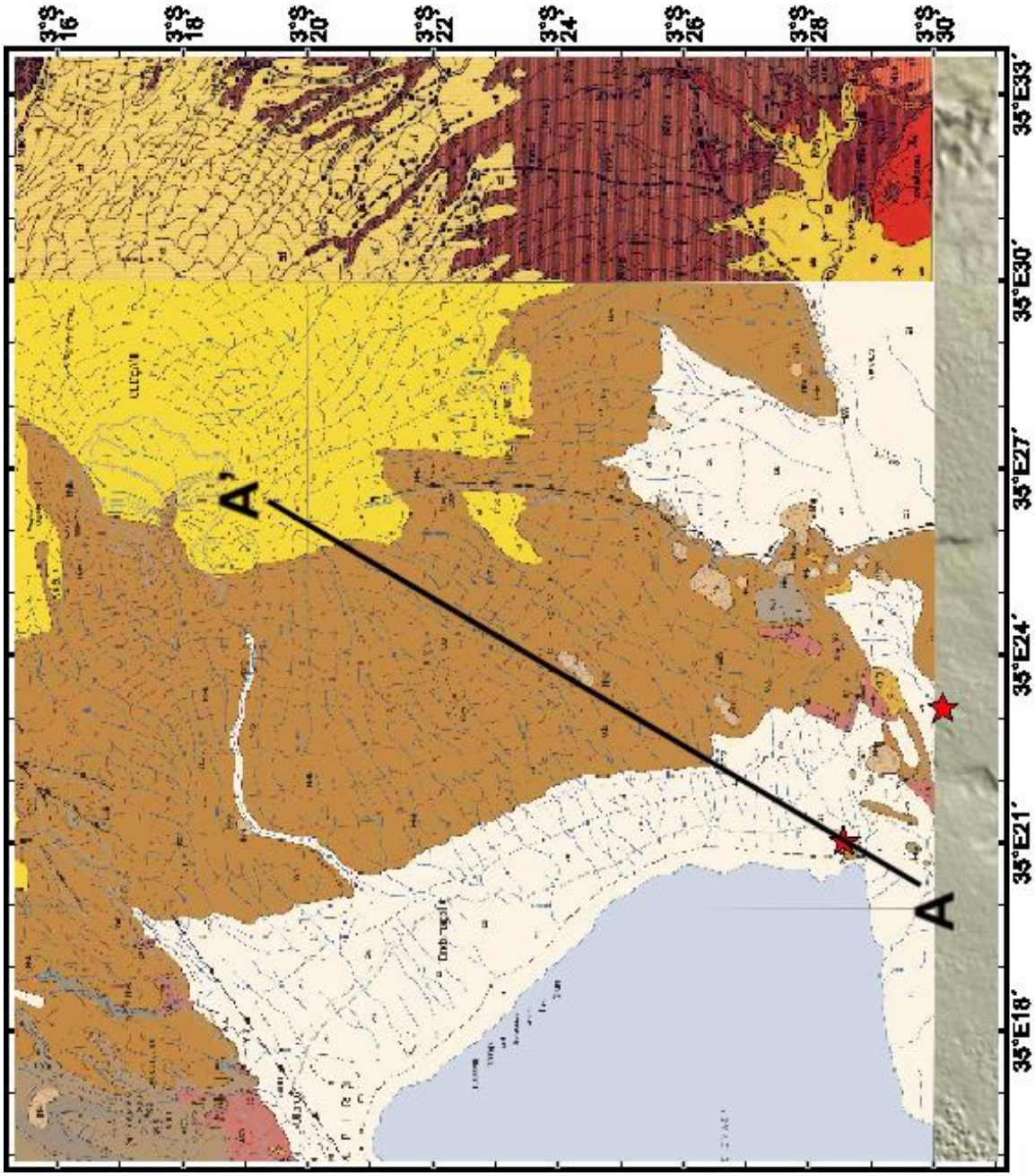
3°S 16'
3°S 18'
3°S 20'
3°S 22'
3°S 24'
3°S 26'
3°S 28'
3°S 30'
35°E18'
35°E21'
35°E24'
35°E27'
35°E30'
35°E33'
A
A'

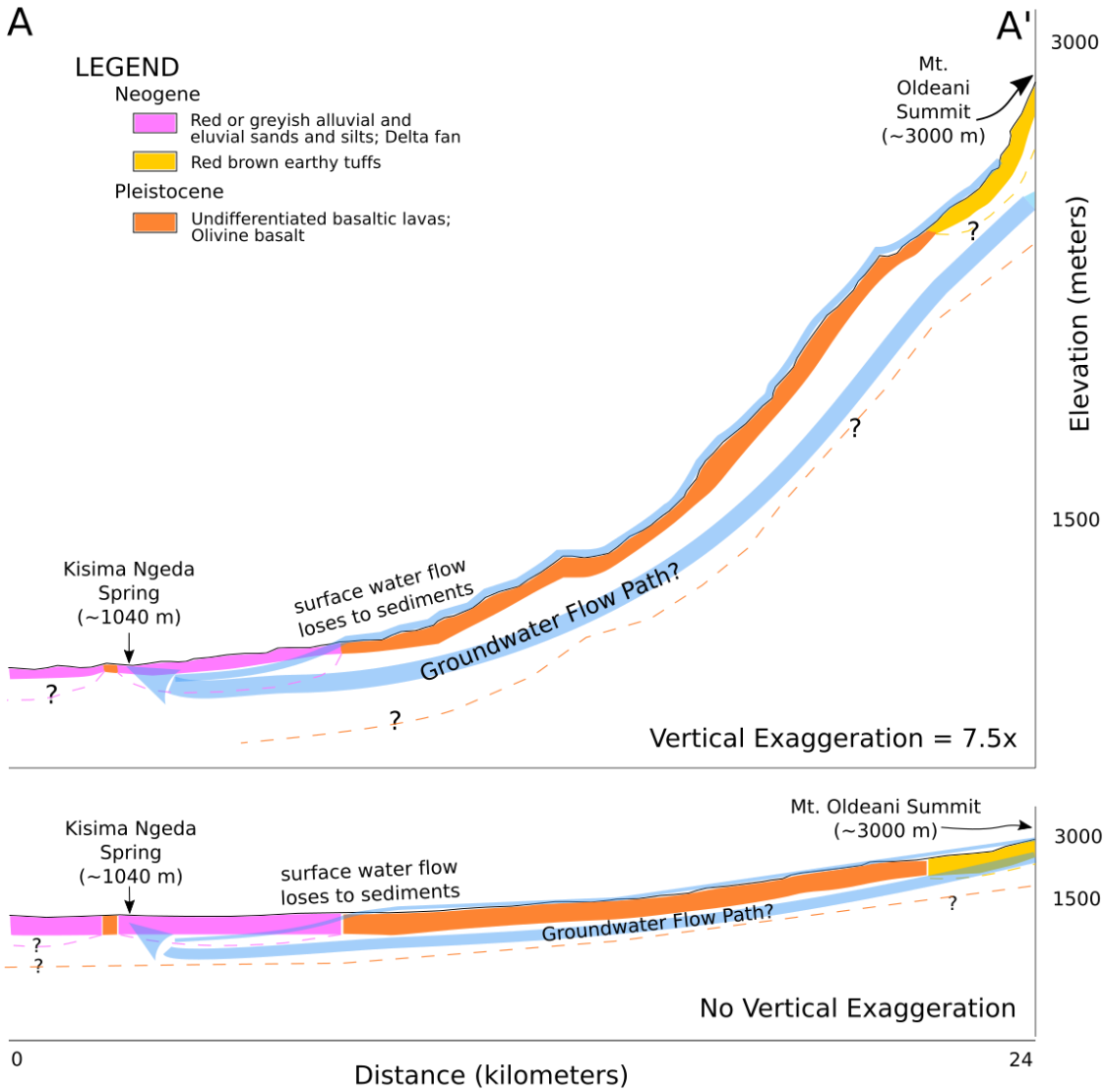
A
A'
LEGEND
Neogene
Red or greyish alluvial and eluvial sands and silts; Delta fan
Red brown earthy tuffs
Pleistocene
Undifferentiated basaltic lavas; Olivine basalt
Mt. Oldeani Summit (~3000 m)
Kisima Ngeda Spring (~1040 m)
surface water flow loses to sediments
Groundwater Flow Path?
Vertical Exaggeration = 7.5x
Mt. Oldeani Summit (~3000 m)
Kisima Ngeda Spring (~1040 m)
surface water flow loses to sediments
Groundwater Flow Path?
No Vertical Exaggeration
3000
1500
Elevation (meters)
0
24
Distance (kilometers)

ESERE

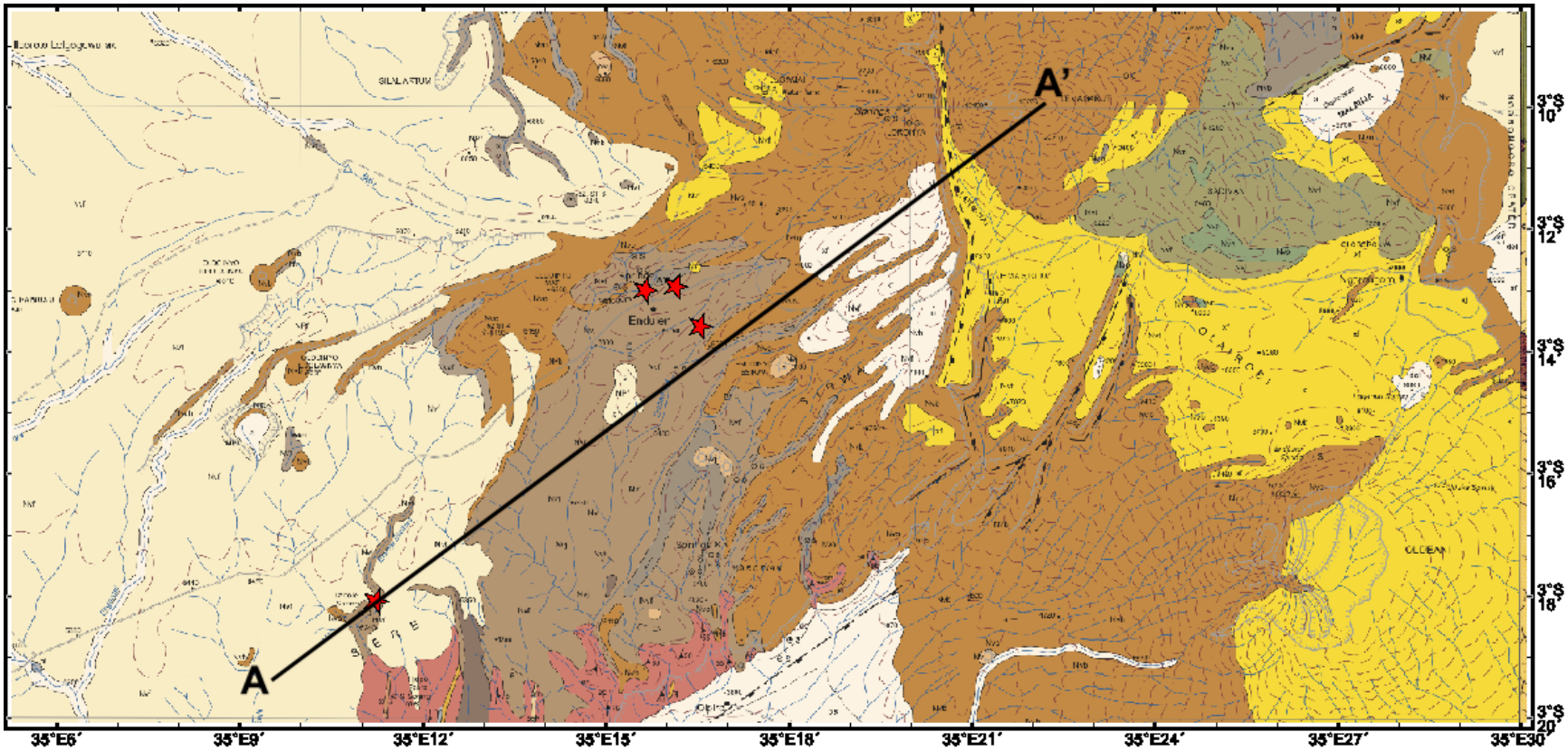
A
A'
Enduer
3°S 10'
3°S 12'
3°S 14'
3°S 16'
3°S 18'
3°S 20'
35°E6'
35°E9'
35°E12'
35°E15'
35°E18'
35°E21'
35°E24'
35°E27'
35°E30'

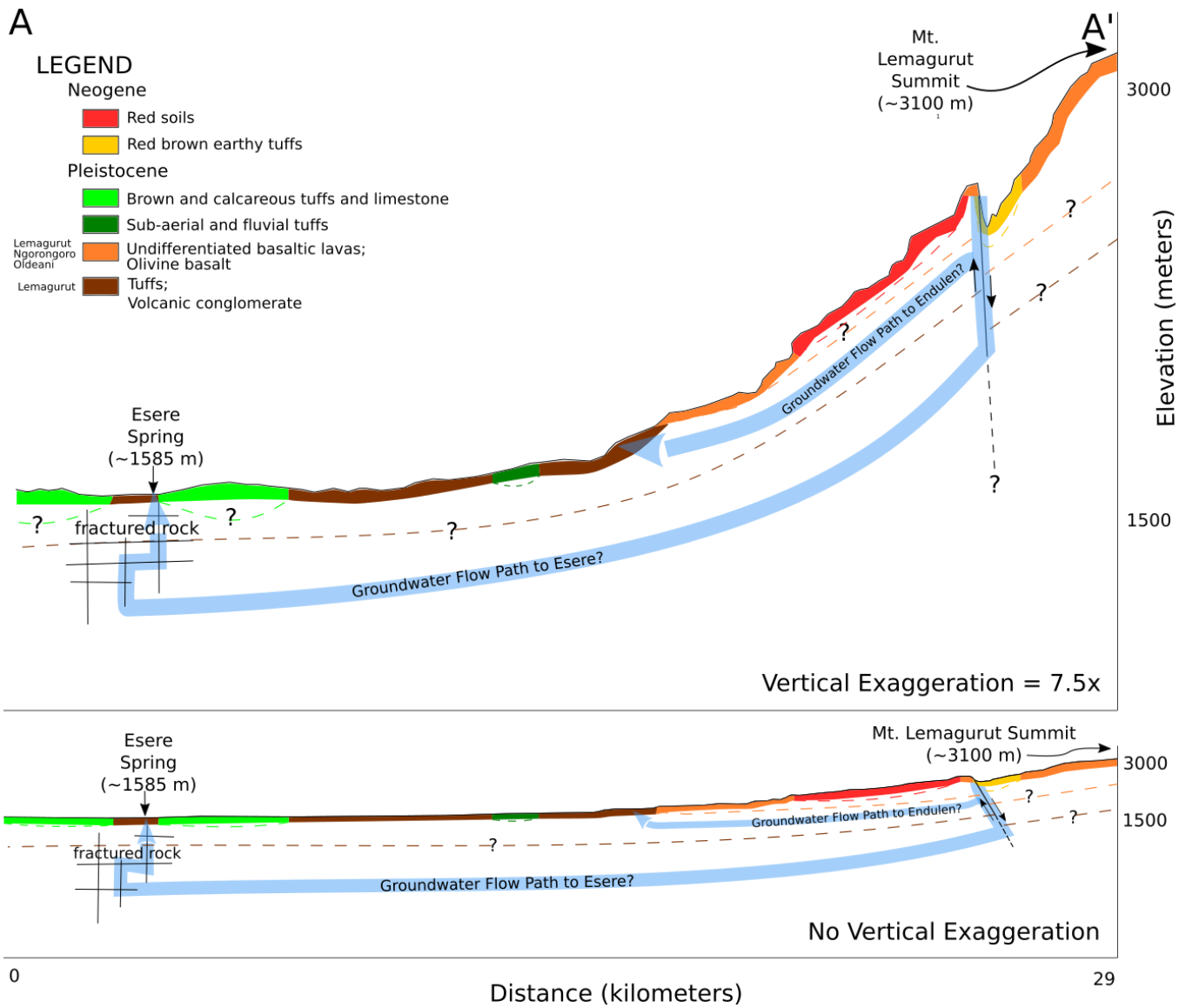
A
A'
LEGEND
Neogene
Red soils
Red brown earthy tuffs
Pleistocene
Brown and calcareous tuffs and limestone
Sub-aerial and fluvial tuffs
Lemagurut Ngorongoro Oldeani
Undifferentiated basaltic lavas; Olivine basalt
Lemagurut
Tuffs; Volcanic conglomerate
Mt. Lemagurut Summit (~3100 m)
Esere Spring (~1585 m)
fractured rock
Groundwater Flow Path to Endulen?
Groundwater Flow Path to Esere?
Vertical Exaggeration = 7.5x
No Vertical Exaggeration
3000
1500
Elevation (meters)
0
29
Distance (kilometers)

EREMET

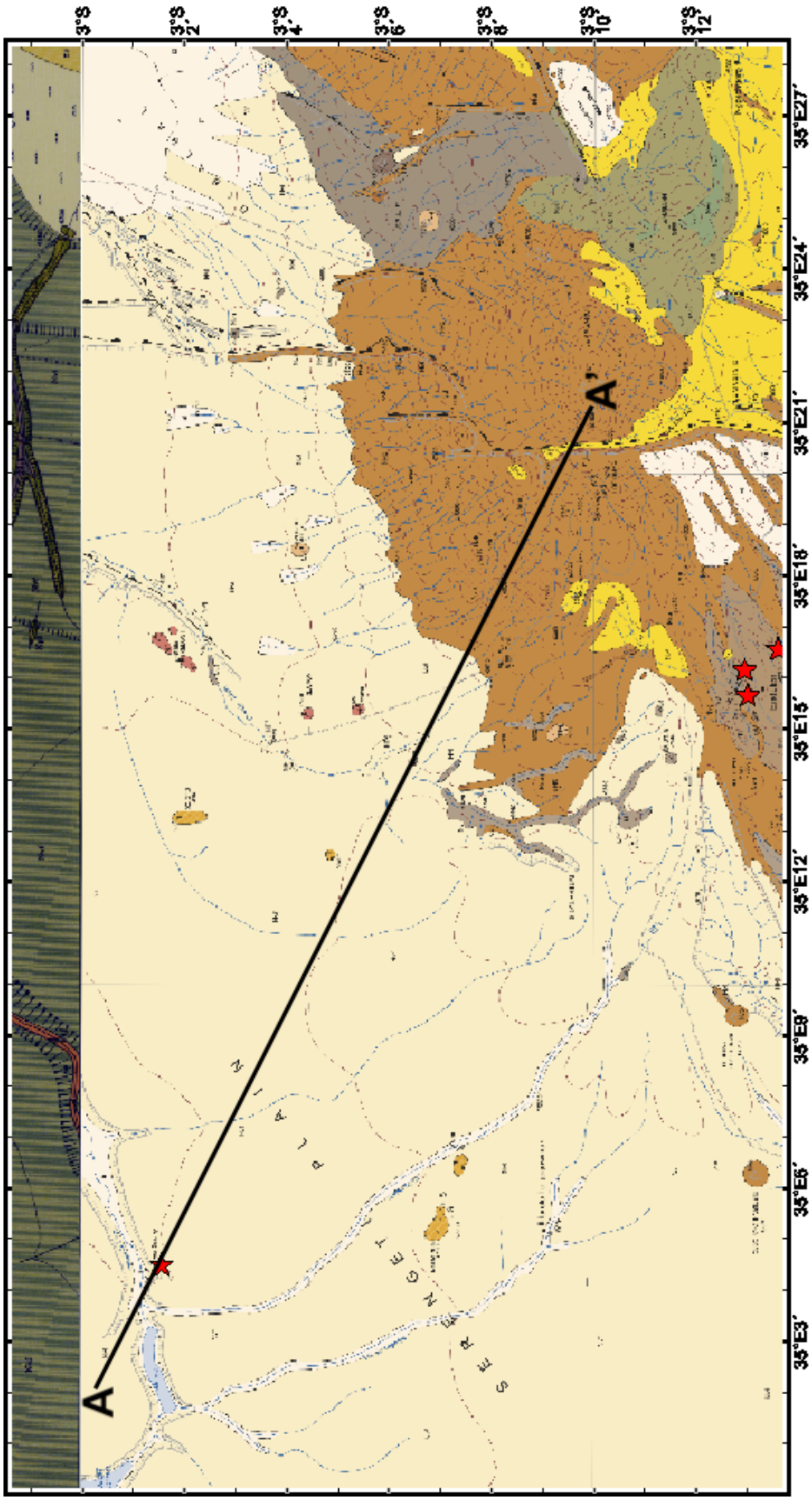
3°S
3°S 2'
3°S 4'
3°S 6'
3°S 8'
3°S 10'
3°S 12'
35°E3'
35°E6'
35°E9'
35°E12'
35°E15'
35°E18'
35°E21'
35°E24'
35°E27'
A
A'

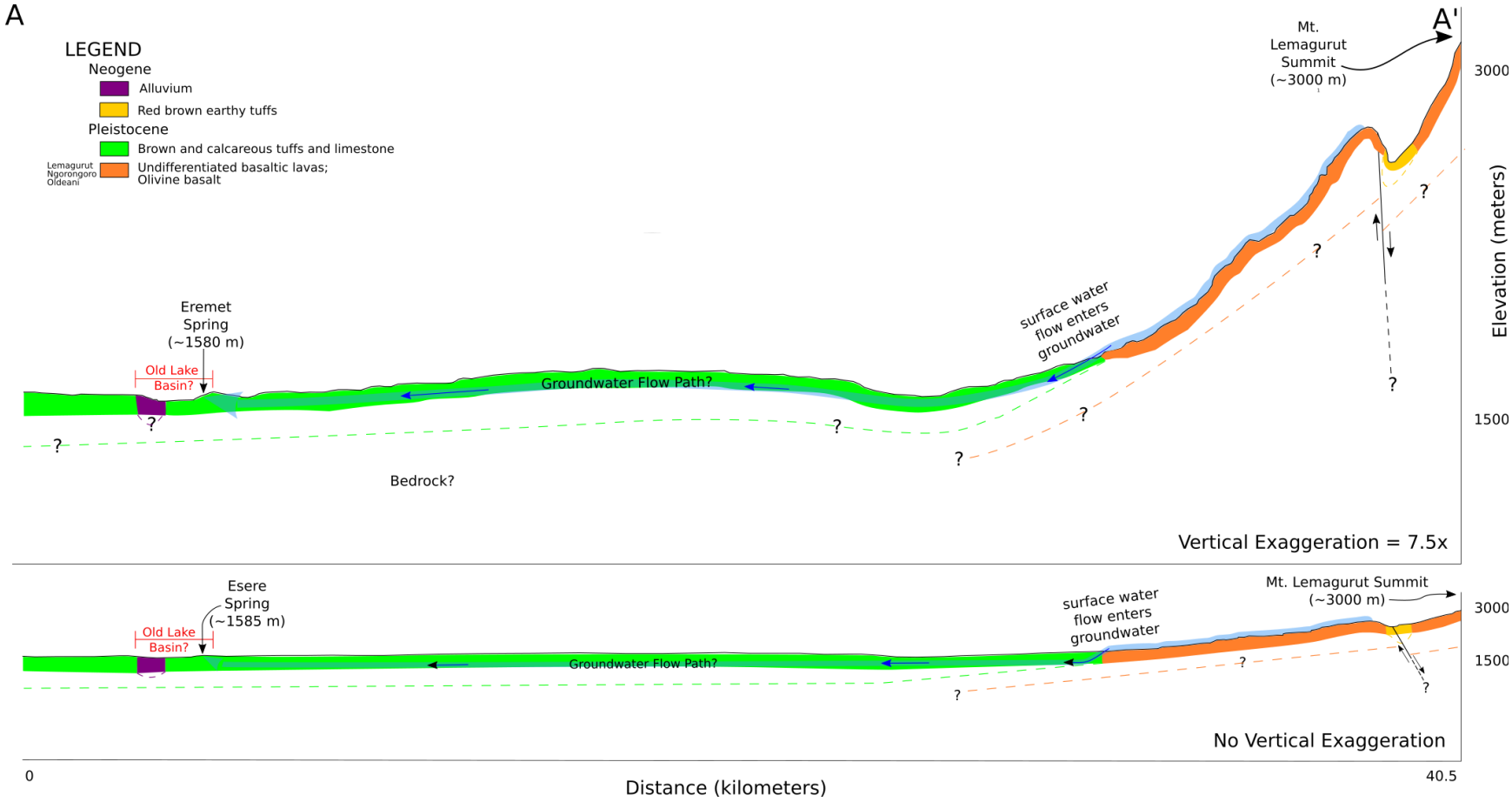
A
A'
LEGEND
Neogene
Alluvium
Red brown earthy tuffs
Pleistocene
Brown and calcareous tuffs and limestone
Lemagurut Ngorongoro Oldeani
Undifferentiated basaltic lavas; Olivine basalt
Mt. Lemagurut Summit (~3000 m)
3000
1500
Elevation (meters)
Eremet Spring (~1580 m)
Old Lake Basin?
Groundwater Flow Path?
surface water flow enters groundwater
Bedrock?
Vertical Exaggeration = 7.5x
Esere Spring (~1585 m)
Old Lake Basin?
Groundwater Flow Path?
surface water flow enters groundwater
Mt. Lemagurut Summit (~3000 m)
3000
1500
No Vertical Exaggeration
0
40.5
Distance (kilometers)

CHAPTER TWO

APPENDIX VIII

APPENDIX VIII

Reference	Biome Classification	Wetland Location	Wetland Type and Formation	Local Climatic Setting **T** = mean annual temperature **P** = mean annual precipitation **ET** = annual potential evapotranspiration	Distinctive Lithological Features	Distinctive Biological/ Chemcial Features	Wetland Age **yrs BP** = Years Before Present **P** = Present
Pendea et al. 2016	Tundra	Kamchatka Peninsula, northwestern Pacific seaboard, Russia	Type: small coastal fen peatland nested in a former kettle basin Size: ~250 m in diameter Source: the basin is exclusively rain-fed, no apparent surface drainage	Tundra T: -0.33°C P: 71.8 cm	Present Day and IV wetland phases: Present Day: peatland Phase I (0-225 cm depth): Intermediate shrub-fen with *Sphagnum*-sedge peat Phase II (225-405 cm depth) & Phase III (445-555 cm depth): rich fen with Bryidae-sedge peat Phase IV (555-620 cm depth): rich shrub fen with sedge-carr peat Layers of tephra in sequence may indicate prior forest fires, followed by soil erosion, and then wetland vegetation emergence	Present Day and IV wetland phases: Present Day: Myrica tomentosa-Cyperaceae peatland community with a bryophyte understory dominated by Bryidae mosses and *Sphagnum teres* Phase I (0-225 cm depth): intermediate shrub-fen with *Sphagnum* mosses and *Myrica tomentosa* and *Ericaceae* remains and Filipendula Phase II (225-405 cm depth) & Phase III (445-555 cm depth): rich fen with Bryidae-sedge peat, increase in aquatic and wetland taxa (e.g., *Potamogeton/Triglochin, Equisetum, Bryidae*) and *Filipendula* Phase IV (555-620 cm depth): rich shrub fen with *Almus fructicosa*	?-P Phase I: 60-3,118 yrs BP Phase II: 3,118-5,717 yrs BP Phase III: 6,153-7,815 yrs BP Phase IV: 7,815-8,910 yrs BP
Ellis and Rochefort 2006	Tundra	Simirlik National Park (73.08°N; 80.00°W), part of the Canadian Arctic Archipelago	Type: low-lying terraces formed via glacial retreat "tundra polygon complex" Size: n/a Source: fed by meltwater from hills	High-Arctic T: -32.7 to -4.9°C (mean min-max) P: 15.9 cm	3500 yrs BP-P: peat-rich permafrost soils; wetter periods showed lower mineral percentages (~40-80%) whereas dryer periods showed higher mineral percentages (~80-100%)	Present Day: dominated by sedges (e.g. Carex aquatilis var. stans, Eriophorum scheuchzeri), grasses (e.g. Arctagrostis latifolium, Dupontia fischeri, Pleuropogon sabinei) and fen mosses (e.g. Drepanocladus spp., Aulocomnium spp.). 3500 yrs BP-P: wetter periods had much higher microfossil moss abundances; wetter periods had lower percent melt	3500 yrs BP-P (various wet and dry periods within this time frame)
Spooner et al. 2017	Taiga	Baltzer Bog, Annapolis Valley, Coldbrook, Nova Scotia, Canada	Type: shrub bog, kettle-lake bog (elevated, closed basin wetland) Size: 28 ha Source: kettle-lake bog on top of kame deposit, water table elevation/ perched water table	Moist continental climate T: 4-11°C (mean min-max) P: 100 cm	3 woodland-wetland transitions in the record: Wetland: deposits consisted of organic sediment and red-hued *Sphagnum* peat containing very little woody material or minerogenic sediment. Intermediate Woodland: deposits observed at 3 positions between the *Sphagnum* peat and consisted of terrestrial organic with some aquatic material, wood, and upright stumps	3 woodland-wetland transitions in the record: Wetland: deposits consisted of organic sediment and red-hued Sphagnum peat and *Sphagnum* leaves and stems Intermediate Woodland: deposits observed at 3 positions between the Sphagnum peat and consisted of terrestrial organic with some aquatic material, wood, and upright stumps	3260 yrs BP-P (with intermittent woodland dated at 1,640 and 1,045 yrs BP)
Spooner et al. 2017	Taiga	Big Meadow Bog, Briar Island, southwestern Nova Scotia, Canada	Type: oval-shaped peatland with a central raised bog Size: 2 km in length Source: surrounded by basalt ridges; groundwater-fed	Boreal T: 2-12°C (mean min-max) P: 140 cm	Wetland: deposits consisted of a Sphagnum peat moss layer dominated by *Sphagnum affine* (fen species). Bog surface wetness data records increases indicative of high decomposition. Intermediate Woodland deposits: single wood layer occurred in peat matrix dominated by *Sphagnum megallanicum* with *Sphagnum* Section *Acutifolia* with upright trunks of Black Spruce and consisted of terrestrial organic with some aquatic material	Wetland: deposits consisted of a *Sphagnum* peat moss layer dominated by *Sphagnum affine* (fen species) Intermediate Woodland deposits: single wood layer occurred in peat matrix dominated by *Sphagnum megallanicum* with *Sphagnum* Section *Acutifolia* with upright trunks of Black Spruce	3260 yrs BP-P (with intermittent woodland dated at 1,760 yrs BP)
Lamentowicz et al. 2014	Taiga	Baltic Bog, northern Poland	Type: bog Size: 318.82 ha Source: formed by activity of last Scandinavian ice sheet that retreated	T: -3-17°C (mean min-max) P: 65 cm	Sedimentology during Present Day and ~755-3,460 yrs BP Present Day: peat (86-795 cm depth): constant and rapid peat accumulation	Paleontology during Present Day and ~755-3,460 yrs BP: Present Day: *Sphagnum magellanicum, S. cuspidatum, Sphagnum capillifolium, Baeothryon caepitosum, Scheuchzeria palustris, Drosera rotundifolia,* and *Oxycoccus palustris* (86-795 cm depth): *Sphagnum fuscum*/rubellum stems	?-P ~755-3,460 yrs BP

Reference	Biome Classification	Wetland Location	Wetland Type and Formation	Local Climatic Setting **T** = mean annual temperature **P** = mean annual precipitation **ET** = annual potential evapotranspiration	Distinctive Lithological Features	Distinctive Biological/ Chemcial Features	Wetland Age **yrs BP** = Years Before Present **P** = Present
Zhang et al. 2017	Taiga	Sanjiang Plain, northeast China Paleo-pingo depression: 47°35.096'N, 133°30.006'E, 71 m asl	Type: paleo-pingo depressions Size: ~400 mm diameter, water depth 0.5 m Source: fluvial control nonexistent, water level controlled by atmospheric precipitation	T: 1.4-4.3°C Avg Max (July): 22°C Avg Min (Jan): -18°C P: 50-65 cm	Present Day: meadow, swamp, and black soils blackish-gray mud with apparent laminar structures at the bottom, overlain by brownish peat with high plant residue contents 5,500-4,500 yrs BP: at mud-peat boundaries, increase in accumulation rate variability, organic matter content. Peat sections high in silt and clay. Peat accumulation high organic matter contents (~70%, mostly plant residuals). Shift from low to high peat initiation as paleolake transitions to wetland	Present day: characterized by marsh plants and dominated by *Carex pseudocuraica, Carex meyeriana, Carex lasiocarpa, Alnus sibirica, Betula fruticosa, Salix brachypoda, Lythrum salicaria, Calamagrostis anagustifolia, Pedicularis grandiflora, Glyceria spiculosa, Phragmites australis, and Sphagnum pseudocymbifolium* 5,500-4,500 yrs BP: *Sphagnum pseudocymbifolium* and *Carex* plant residues dominant in peat (oligotrophic with water supply largely from atmospheric precipitation).	4,500 yrs BP-P Lake to Wetland Transition Period: 5,500-4,500 yrs BP
Coon 1997	Temperate Forest	Ellison Park wetland, mouth of Irondequoit Creek, Rochester, New York	Type: riverine/ lacustrine wetland Size: 423 acres Source: fed mainly by groundwater discharge and also rivers which run through the wetland	T: 9°C P: 80.01 cm (rain and snow)	Wetland: deposits consist of silt and clay with high organic matter Irondequiot Creek: sand makes up the predominant bed material in the main channel throughout the wetland. Where there is erosion of underlying glacial deposits, coarse bed material is deposited	Wetland: dominant plant species: *Typha glauca* (cattail). Several other plant species indicate a diverse and highly productive floral ecosystem. Provides spawning/ rearing habitat for at least 16 species. Primary fish food source are chironomids (midges) and corixids (true water bugs). 11 other species of aquatic insects, crustaceans, worms, and crayfish identified in fish-stomach contents. Painted turtles, snapping turtles. 95 species of birds in/around wetland.	?-P
Woodward et al. 2014	Temperate Forest	Little Llangothlin, New England Tablelands, eastern Australia	Type: semi-permanent to permanent freshwater wetland Size: 1.2 km^2 Source: wetting and drying of depressions on the surface of the Tertiary basalt flows or impeded drainage by the basalt flows in paleovalleys	Sub-Tropics, but cool Temperate climate because of elevation T: -0.6-10.2°C (mean min-max) P: ~88 cm E: 126.2 cm	Sedimentology of various wetland phases (young to old): More frequent wet phases: dark brown organic sediment, increased charcoal flux Dry phase with possible wet interval: end of peat preservation, low charcoal Permanent wetland: peat and low charcoal flux Semi-permanent wetland: start of peat formation Ephemeral wetland: high macrosporic charcoal flux	Paleontology of various wetland phases (young to old): More frequent wet phases: increase in charophyte oospores, *Myriophyllum varifolium* (lagoon margin), *Potamogeton crispus* (shallow lagoon), *Eleocharis sphacelata* (lagoon basin), *Eucalyptus* (forest stands) Dry phase with possible wet interval: low abundance of wetland macrofossils Permanent wetland: *E. schreberi* expansion Semi-permanent wetland: switch to dominance of perennial plant (*M. variifoliu* m) and then to *E. sphacelata* Ephemeral wetland: *N. sonderi* and *C. muelleri* (charophyte) oospores	More frequent wet phases: 1,000 yrs BP-P Dry phase with possible wet interval: 6,100-1,000 yrs BP Permanent wetland: 8,000-6,100 yrs BP Semi-permanent wetland: 9,300-8,800 yrs BP Ephemeral wetland: 9,800-9,300 yrs BP
Norstrom et al. 2008	Temperate Grassland	Braamhoek wetland, Eastern Free State, South Africa	Type: permanent wetland Source: wetland are fed by both upper catchment draining of main inlet river and shallow groundwater springs	South African Grassland Biome T: 27 to -2°C (max and min) P: 140 cm	Present Day: dark brown to dark gray to black organic "sandy peat, "clayey peat", "tussock peat" containing minerogenic particles ranging from clay to sand and roots and well-preserved macrofossils	Present Day: Associated with the tussocks: *Phragmites australis* (Poaceae), *Carex acutiformis* (Cyperaceae), and *Poa binata* (Poaceae). Near the drier fringes of the wetland: *Cyperus fastigiatus, Juncus effuses* , and species of *Crassula* , *Ericocaulon, Scripus* , *Limosella* , and *Polygonum*	16,000 yrs BP-P (constant peat accumulation throughout this time frame, but local climate varies along with the sedimentology and paleontology)

Reference	Biome Classification	Wetland Location	Wetland Type and Formation	Local Climatic Setting **T** = mean annual temperature **P** = mean annual precipitation **ET** = annual potential evapotranspiration	Distinctive Lithological Features	Distinctive Biological/ Chemcial Features	Wetland Age **yrs BP** = Years Before Present **P** = Present
Sivan et al. 2011	Temperate Desert ?	Carmel coast, northern Israel	Type: shallow-water bodies fed by groundwater (fresh-brackish water) Source: fed by groundwater mainly (upper Pleistocene coastal aquifer)	T: 14-20°C ? P: ?	Wetland: deposits consist of thick layers of dark silty-clay with low organic matter content	Wetland: Calcareous micro- and macrofauna typical of low brackish environments, abundance of benthic foraminifera (many hyalines - *Ammonia tepida/ Ammonia parkinsoniana*), ostracods (*Cyprideis torosa* and some *Candona neglecta*), 12 species of mulluscs (most abundant *Cerastoderma glaucum*)	9,340-10,000 yrs BP
Pigati et al. 2014	Temperate Desert	American Southwest: Cerros Negros, AZ, Dove Springs, CA, and Murray Springs, AZ	Various wetland types and sources in the American Southwest	Cerros Negros: T:10°C, P: 36 cm Dove Springs: T: 16°C, P: 18.3 cm Murray Springs T: 17.5°C, P: 36 cm	Wetlands: deposits consist clastic sediments, carbonate-rich groundwater precipitates, and organic matter ("black mats")	Wetland: megafuana (i.e., teeth and bones of mammoth, horse, bison, and camel), ostracods, gastropods, chironomids, sponges, forams, and algae (mainly diatoms)	?-P
Pigati et al. 2014	Temperate Desert	Atacama Desert of northern Chile: Salar de Punta Negra and Rio Salado	Various wetland types and sources in the Atacama Desert of northern Chile	Salar de Punta Negra and Rio Salado: T: 17.9°C, P: 0.1 cm	Wetlands: deposits consist of clastic sediments, silica-rich groundwater precipitates, and organic matter ("black mats")	Wetland: ostracods, gastropods, chironomids, sponges, forams, and algae (mainly diatoms)	?-P
Li et al. 2015	Temperate Desert	Ulan Buh Desert, southwestern Inner Mongolia	Type: interdunal ponds/lacustrine wetland Source: rise in lake elevations	Arid to Semi-Arid Present P: 10.3 cm	Wetland: deposits consisted of a think silty clay layer, a thick layer of gray clayey sand and blue-gray clayey sand or sandy clays	Wetland: pollen assemblages indicate desert vegetation and an arid climate condition. No *Typha* pollen found, suggesting absence of permanent aquatic environment	Potential Wetland dated at: 20,000 and 52,000 yrs BP Wetland Phase between: 8,000-7,000 yrs BP
Beach et al. 2009	Tropical Rain Forest	Maya lowlands, Yucatan Peninsula and adjacent lowlands in Mexico, Belize, and Guatemala	Type: range from upland and intermittent "bajos" to coastal plain's floodplains, depressions, and submerged sinkholes Size: variable sizes Source: Holocene sea level rise inundating depressions in karst terrain	Tropical wet and dry climate P: 150 cm	Wetland: deposits consist of thick calcareous clayey sediments (high amounts of gypsum) and organic matter. Alternating wet-dry hydrologic conditions indicated by expansion and contraction of smectite clays, and the uneven distribution of accumulating masses of sediment and agrilloturbation (breakage of horizons, heaving, and slickensides throughout soil profile)	Forested and herbaceous wetlands including: red mangrove (*Rhizophora mangle*), hardwood swamps, sawgrass (*Cladium jamaicense*) marsh, marl flats dominated by *Cyperaceae* , sedge marshes dominated by a few *Cyperus* spp., and calabash marsh dominated by *Eleocharis interstincta* Prominent upland vegetation: broadleaf, semi-deciduous forest	?-P
Ashley et al. 2004	Tropical Savanna	Loboi Swamp, Kenya, Africa	Type: freshwater, fed by warm springs emanating from grid faults on the rift floor; low relief alluvial plain Size: 1.5 km^2 Source: shallow meteoric water	Semi-Arid T: 23-25°C P: ~70 cm ET: >250 cm	Swamp: deposits consist of peat capping organic-rich clay, increased C and N, low sed. rate, redoximorphic features (Fe reduction and precipitation of siderite and pyrite), shift from C4 to C3 vegetation Floodplain: deposits consist of silty clay to sandy silt (mostly smectite-rich, minor illite-rich clay, kaolinite, K-feldspar, some plag feldspar), increased magnetic susceptibility, montane pollen species	Swamp: Cattail - *Typha domingensis Pers.* (80%) and floating Papyrus - *Cyperus papyrus L.* (20%), wetland pollen species (50%), abundant diatoms (*R. gibberula* indicative of GW-fed warm springs) Floodplain: montane pollen, scarce diatoms (*Nitzschia*) Uplands: *Acacia* scrubland Plains: salt-tolerant grasses such as *Sporoblous spicatus*	~680 yrs BP-P
Irion et al. 2016	Tropical Savanna	Araguaia River floodplain, southern Amazon basin	Type: floodplain, riverine Size: 88,119 km^2 total floodplain area at max flood level Source: rise of river, saturated, rainy season	T: 22-26°C P: 120-190 cm	Active-recent floodplain: sequence of smectitie, illite, kaolinite Inactive paleo-floodplain: kaolinte, gibsite, geothite, and Al-chlorite (poor in Mg, Ca, and K). Indicates low soil fertility of the paleo-floodplain	Active-recent floodplain: termite savannas, single-tree savannas, and savanna forest (cover 60% of wetland) River and lake samples: "clear water" category, characterized by near-neutral pH, low electrical conductivity, relatively high transparency	Paelo-floodplain: Early Pleistocene (evidece for as early as 240 ka BP) - P

Reference	Biome Classification	Wetland Location	Wetland Type and Formation	Local Climatic Setting **T** = mean annual temperature **P** = mean annual precipitation **ET** = annual potential evapotranspiration	Distinctive Lithological Features	Distinctive Biological/ Chemcial Features	Wetland Age **yrs BP** = Years Before Present **P** = Present
Quade et al. 2008	**Tropical Desert?**	Salar de Punta Negra, central Atacama Desert, northern Chile, western slope of Andes	Type: salt-pan Size: 250 km^2 Source: elevated groundwater levels supported phreatic discharge into wetlands	Currently driest place on earth, but at the time observed in lithologic record, global temperature was lower and there were monsoons that made it wetter than today	Sedimentology of Present Day and in Lithologic Units Studied: Wetlands in Lithologic Units Studied: deposits consist of organic matter and greenish silt (sustained reduction in locally water-saturated, O_2-deficient conditions), lithic artifacts of paleoindians Phreatic Playas in Lithologic Units Studied: deposits consist of coarse blocky cementation by gypsum and minor carbonate (gypsum display vertical or radiating crystal growth) Ephemeral Stream and Dry Alluvial Fan in Lithologic Units Studied: deposits consist of reddish to green gravels and sands. Can be bioturbated by rootlets and iron-stained. Present Wetland: layered diatomite and wet-sediment deformation	Paleontology of Present Day and in Lithologic Units Studied: Present Wetland: extensive mats of plants, continuous carpets of sedges, grasses, and small salt-tolerant shrubs growing on margins of Tessaria and Atriplex. Wetlands in Lithologic Units Studied: deposits consisted of diatoms, sponge spicules, organic matter (especially grasses) abundant as a dense overprint of root channels, Succinds (semi-aquatic gastropod)	?-P 12,700-9,700 yrs BP 15,900-13,800 yrs BP
Tooth and McCarthy 2007	**Tropical Desert**	Okavango Delta, Botswana, Africa	Type: delta permanent and seasonal wetlands Size: >12,000 km^2 Source: supplied by perennial inflow (Okavango river) originating in humid area, depression wetlands	T: Arid to Semi-Arid P: 50 cm E: 220 cm	Wetland: deposits consist of accumulations of chemical sediments in substrates (salt crusts of sodium bicarbonate I middle of island) due to strong ET demand from floodplain trees and shrubs. Channel avulsion causes desiccation and peat burns off during natural fires	Floodplain Island (from middle to edge): grass (sporobolus spicatus), palm (hyphaene petersiana), deciduous trees, grass (cunodon dactylon), broad leaved evergreen species, palm (Phoenix reclinata), and floodplain vegetation. Species zonation by salt-tolerance is due to concentration of salt in groundwater, where middle is usually devoid of vegetation) and edges contain the most. Panhandle and Fan: sedges (e.g. *Cyperus papyrus*) and emergent grasses (e.g. *Phragmites* spp., *Miscanthus junceus*, *Pennisetum glaucocladum*) rooted in a 4m thick peat layer with low amounts of clay	?-P

Reference	Biome Classification	Wetland Location	Wetland Type and Formation	Local Climatic Setting **T** = mean annual temperature **P** = mean annual precipitation **ET** = annual potential evapotranspiration	Distinctive Lithological Features	Distinctive Biological/ Chemcial Features	Wetland Age **yrs BP** = Years Before Present **P** = Present
O'Brien and Burne 1994	**Tropical Desert**	The Great Cumbung Swamp, Eastern Australia	Type: freshwater riverine swamp Source: fed by the Lachlan River which is sourced in a sub-humid environment	Semi-Arid P: 28.2 cm E: 158 cm	Phragmites Marsh: deposits consist of black to grey clays composed mostly of clay to silt-sized quartz and smectite with minor kaolinite and illite present. When dry, these vertisols clays develop networks of deep cracks. There are subtle variations in texture, organic content, and color between the different depositional settings. Evidence of pedogenesis (block and granular structures, color mottling and less organic matter) result from cyclic volume changes due to repeated wetting and drying Lachlan Channel: dark-gray fluid clay which grades downward becoming very dark-gray to black, stiff and massive (scattered rootlets and fragments of fibrous plant matter) Marginal Lakes and Alluvial Plains: black to grey deep-cracking clays	Phragmites Marsh: Colonized by reeds *Phragmites australi* . Also by *cumbungi Typha orientalis* . The clay beds of the marsh and vegetated levees are both bioturbated by roots and have relatively high content of plant remains Lachlan Channel: Upstream *Typha* , downstream into the Swamp *Phragmites* Marginal Lakes and Alluvial Plains: colonized by bushy groundsel (*Senecio cunninghamii*) and river red glums (*Eucalyptus camaldulensis*)	Early Pliocene-P